CHAPTER ONE

Introduction

INTRODUCTION

The Intraosseous Transcutaneous Amputation Prosthesis (ITAP) is a titanium alloy implant that is anchored to bone (osseointegrated) and penetrates the skin (transcutaneous) to provide a means of direct skeletal attachment for artificial limbs. This device has the potential to improve the quality of life for amputees by avoiding many of the common soft tissue complications associated with conventional socket prostheses and by improving comfort, sensory feedback and overall function. The main complication associated with ITAP is infection due to a poor soft tissue seal at the skin-implant interface. This thesis explores approaches to enhance soft tissue integration while simultaneously reducing bacterial colonisation of ITAP. New surface modifications and functionalisation with coatings are investigated.

The following literature review evaluates published information relevant to ITAP and develops the rationale for further modification of ITAP using the surface modifications and coatings that have been investigated in this thesis.

1.1 THE CLINICAL PROBLEM

1.1.1 Epidemiology of Amputation

Amputation is a significant clinical problem worldwide. The incidence of extremity amputation varies depending on factors such as geography, age and gender (The Global Lower Extremity Amputation Study Group, 2000). The global incidence of lower extremity amputation has been reported to be between 0.5 and 49.5 per 100,000 people (The Global Lower Extremity Amputation Study Group, 2000). There are estimated to be approximately 1.9 million amputees in the United States (Limb Loss Research and Statistics Program, ACA). In the United Kingdom, the number of new referrals to prosthetic services made annually has increased from 4957 in 2006 to 2007 to 5988 in 2010 to 2011 (The Amputee Statistical Database for the United Kingdom, 2006/7; Limbless Statistics, United National Institute for Prosthetics & Orthotics Development, Annual Report 2010-2011). Data from Hospital Episode Statistics (HES) has shown that the total number of lower extremity

amputations performed in the National Health Service in England (both major (i.e. above ankle) and minor operations combined) was 34,109 between the years 2007 and 2010 (Holman et al 2012). The commonest indication for amputation in the developed world is peripheral vascular disease, whereas in developing countries the major indications are trauma and bone tumours (Yinusa et al 2003; Thanni et al 2007). The incidence of amputation is expected to increase over the next few decades due to the ageing population and associated increases in diabetes and peripheral vascular disease (Harker 2006; Vamos et al 2010). However, improved diabetic foot care and vascular surgical interventions such as bypass and angioplasty procedures have the potential to prevent amputations (Larsson et al 2008; Krishnan et al 2008; Canavan et al 2008; Gutacker et al 2010). In recent years there have been increases in the incidence of amputation due to the returning war wounded (Krueger et al 2012). Advances in body armour and trauma resuscitation techniques have increased survival rates for patients with blast wounds, leading to an increase in severe injuries (including amputation) of the unprotected extremities (Manring et al 2009; Kim et al 2010).

1.1.2 Problems Associated with Conventional Socket Prostheses

Rehabilitation following amputation is a significant challenge. Traditionally, amputees are fitted with socket prostheses that are attached to the stump via suction or straps. Socket prostheses may be associated with complications including discomfort or pain, excessive perspiration, contact dermatitis, recurrent skin infections and the need for repeated fittings due to changing stump shape and poor prosthetic fit. Ulceration and pressure sores caused by non-uniform pressure distribution over the stump may also occur (Hagberg et al 2001; Koc et al 2008; Meulenbelt et al 2011). A survey of non-vascular amputees with socket prostheses showed that health related quality of life was significantly lower than age and gender matched controls. A quarter of the patients experienced poor or extremely poor overall quality of life. This reduction in quality of life was attributed to the fact that 72% of patients were found to experience excessive heat and perspiration of the stump, 62% experienced sores and 59% experienced slow gait (Hagberg et al 2001). More recent improvements in the design of the socket have increased the quality of

life for some patients; however, a substantial number of patients still experience unacceptable function. A 2011 cross-sectional survey of 124 amputees with socket prostheses identified skin problems in 36% of patients, which is similar to results from earlier studies (Demet et al 2003; Dudek et al 2005; Meulenbelt et al 2011).

1.1.3 Osseointegrated Transcutaneous Amputation Prostheses

Osseointegrated transcutaneous prostheses such as ITAP have been designed in order to avoid the problems described above. These implants are able to avoid these problems because the forces that would be encountered by the soft tissues of the stump with the use of a socket prosthesis are transferred directly to the skeleton. Figure 1.1 is a schematic diagram of an osseointegrated transcutaneous prosthesis. Patients with osseointegrated transcutaneous implants experience increased proprioception and sensory feedback, which is known as 'osseoperception'. Osseoperception results in improved control of limb function and gait (Marks et al 2001; Abarca et al 2006). Although the exact mechanism responsible for osseoperception is unknown, hypothetically, transfer of tactile stimuli to endosteal nerves in the bone via the implant may play a role (Lundborg et al 1996). Other advantages include fixing the external prostheses to short residual limbs (where the use of conventional prostheses is problematic) and easier donning and doffing of the external prosthesis (Sullivan et al 2003; Kang et al 2010).

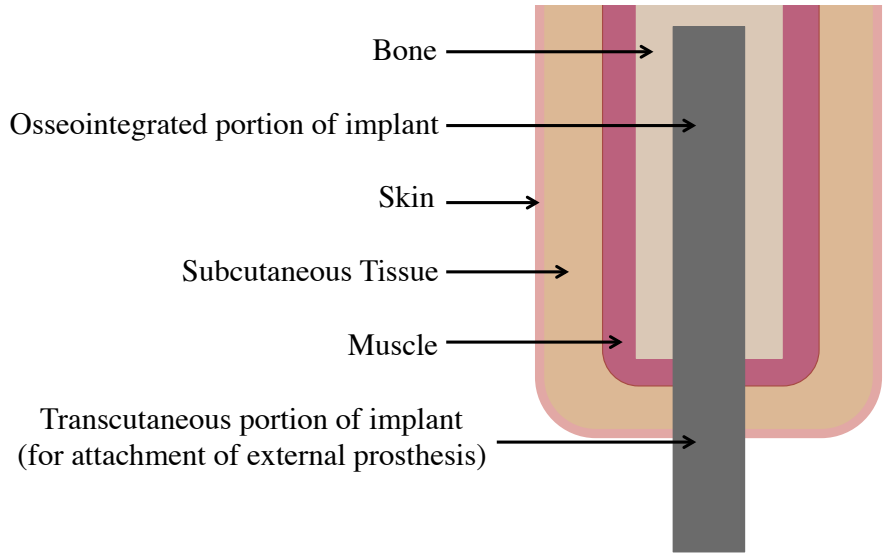

Figure 1.1 Schematic diagram of an osseointegrated transcutaneous prosthesis.

1.1.3.1 Use of Osseointegrated Implants Outside of Limb Reconstruction

Osseointegrated titanium implants have been used successfully in dental surgery for replacement of prosthetic teeth for over forty years (Adell et al 1981). The twenty-year survival rate has been reported to be 98.9% (Ekelund et al 2003). Osseointegrated implants have also been used in craniofacial and otorhinolaryngological surgery e.g. for bone-anchored hearing aids and auricular implants. Implant infection/failure rates of up to 10% have been reported (Nishimura et al 1995; Granstrom 2007; Hagr et al 2007). Failure rates have been found to be higher in older patients potentially due to reduced blood flow and osteoporosis (Drinias et al 2007; Granstrom 2007). Higher failure rates have also been reported in specific regions such as the frontal bone and the zygoma, which may be related to these regions being irradiated more than other bones (Granstrom 2007). Osseointegrated digital prostheses have been generally uncomplicated with good long-term functional and cosmetic outcomes as well as low infection rates (Lundborg et al 1996; Manurangsee et al 2000; Aydin et al 2007; Aydin et al 2008; Doppen et al 2009; Sierakowski et al 2011). In contrast, infection is a common complication associated with osseointegrated transcutaneous prostheses to treat limb amputations with reports of superficial infection rates varying between approximately 18 and 55% (Tillander et al 2010; Brånemark et al 2014). However, few deep intramedullary infections necessitating implant removal have been reported (Aschoff et al 2010; Brånemark et al 2014).

The reduced success rate associated with osseointegrated limb amputation prostheses compared with dental, craniofacial, otorhinolaryngological and digital implants may be related to the greater soft tissue mass and coverage around limb implants, which increases interfacial movement of the soft tissue relative to the stiffer less mobile bone-anchored implant. The particularly high success rates associated with dental osseointegrated implants is potentially partly due to the fact that oral mucosal fibroblasts exhibit more rapid proliferation, greater extracellular matrix reorganisational ability as well as increased matrix metalloproteinase expression and growth factor secretion compared with dermal fibroblasts (Stephens et al 2001; Gron et al 2002; Rodemann et al 2011). Furthermore, Pendegrass et al (2015) have shown

that oral gingival epithelial cells up-regulate focal adhesion and hemidesmosome expression at earlier time points compared with epidermal keratinocytes. Hemidesmosome expression in oral gingival cells was found to be three times greater compared with that of epidermal keratinocytes at four hours after seeding onto titanium alloy surfaces (Pendegrass et al 2015). It is postulated that this contributes to the formation of a more robust epithelial seal around dental implants compared with extra-oral transcutaneous implants.

1.1.3.2 Osseointegration, Bone Structure and Bone Biology

Osseointegration was first described by Brånemark in the 1950s. It was initially defined as a direct structural and functional connection between living bone and the surface of a load-carrying implant (Brånemark et al 2001). The definition nowadays considers osseointegration to have occurred if there is no progressive movement between the implant and the bone with which it has direct contact (Brånemark et al 2001; Nebergall et al 2012). Osseointegration is not the focus of this thesis as it has been studied extensively and is not the main factor limiting the success of osseointegrated transcutaneous prostheses. However, as osseointegration is a key component of osseointegrated transcutaneous prostheses, the following description of bone structure, biology and factors affecting the success of osseointegration has been included.

Bone Structure

Bone is a specialised form of connective tissue. Its basic functions include protection of internal organs, locomotion and mineral homeostasis (Buckwalter 1995; Downey and Siegel 2006). Macroscopically, the two main morphological types of bone are cortical (compact) or cancellous (spongy/trabecular) (Downey and Siegel 2006; Buck and Dumanian 2012). Cortical bone forms approximately 80% of the mature skeleton and surrounds the marrow and cancellous bone plates. Cortical bone forms the diaphysis of long bones. The metaphysis and epiphysis of long bones have thinner cortical walls. Cortical and cancellous bone have a similar matrix structure

and composition but the mass of cortical bone per unit volume is greater. Cortical bone has approximately 5 to 10% porosity and cancellous bone has 50 to 90% porosity. The modulus of elasticity and the ultimate compressive strength of cortical bone is up to ten times greater than cancellous bone. Cancellous bone has a higher rate of metabolic activity and remodelling than cortical bone (Buckwalter 1995; Downey and Siegel 2006; Buck and Dumanian 2012).

Histologically, bone consists of woven (primary) or lamellar (secondary) bone (Buck and Dumanian 2012). Woven bone is an immature form of bone that occurs in the embryonic skeleton and is later resorbed and replaced by lamellar bone (Buckwalter 1995; Burkitt et al 1997). Woven bone has a disorganised irregular appearance and a greater rate of metabolic activity compared with lamellar bone. Lamellar bone has a highly organised appearance consisting of layers appearing in parallel units or sheets with densely packed collagen fibrils. Concentric rings of lamellae form osteons (haversian systems). Osteons surround central canals (haversian canals), which are lined by endosteal cells and contain blood vessels, lymphatics and occasionally nerves (Buckwalter 1995; Buck and Dumanian 2012). Tunnel-like structures known as cannaliculi extend from the central canals and contain the cell processes of osteocytes. Obliquely orientated Volkmann canals allow the neurovascular bundles to interconnect with one another and with the endosteum and periosteum (Buckwalter 1995; Burkitt et al 1997).

Periosteum covers the external surface of long bones and consists of an outer fibrous layer and inner cellular cambial layers. The periosteum supplies nerves, blood vessels and lymphatics to bone and contains numerous osteoprogenitor cells (Burkitt et al 1997; Buck and Dumanian 2012).

Cellular Composition of Bone

The four cellular elements of bone are osteoblasts, osteocytes, bone lining cells and osteoclasts. Osteoblasts, osteocytes and bone lining cells originate from mesenchymal stem cells. Osteoclasts originate from haematopoeitic stem cells

(Buckwalter 1995). Osteoblasts are responsible for production and mineralisation of the organic matrix of bone (Freemont 1993). Osteoblasts play a role in regulating osteoclastic activity. They produce receptor activator of nuclear factor-κβ ligand (RANKL), which activates osteoclasts, as well as osteoprotegerin, which inhibits osteoclasts (Simonet et al 1997; Gori et al 2000). Osteoblasts may become surrounded by matrix and differentiate into osteocytes or they may become relatively inactive and form bone lining cells (Downey and Siegel 2006). Osteocytes have connecting cytoplasmic processes that project through the cannaliculi and are important in cellular communication and nutrition (Downey and Siegel 2006). Osteocytes also appear to be responsible for translating mechanical loading into biochemical signals that affect bone formation and resorption (Bonewald and Johnson 2008). The fourth cell type is the osteoclast. Osteoclasts are giant multinucleated cells responsible for resorption of bone (Freemont 1993; Väänänen et al 2000).

Extracellular Composition

The extracellular composition of bone comprises approximately 90% of its volume and is composed of both an organic component and an inorganic component. The organic matrix accounts for approximately 35% of the total weight of bone tissue and the inorganic part accounts for approximately 65%. The organic makeup of bone consists primarily of Type I collagen that is synthesised by osteoblasts, secreted and then assembled extracellularly. Small amounts of Type V, VI, VIII and XII are also present (Downey and Siegel 2006). Non-collagenous proteins and non-protein components that are involved in the structural integrity and/or control of bone cell function are also present. These include osteocalcin and osteonectin and transforming growth factor-β (Freemont 1993). The inorganic matrix of bone provides a major portion of the tensile yield strength. The mineral salts of bone contain 99% of the calcium, 85% of the phosphorus and 40 to 60% of the sodium and magnesium found in the body. The inorganic matrix of bone contains a salt of calcium and phosphate, which has a crystal structure that closely resembles hydroxyapatite (Freemont 1993). Bone mineral crystals are classified as apatite,

rather than pure hydroxyapatite as they contain both carbonate ions and acid phosphate groups (Buckwalter 1995).

Factors Affecting the Success of Osseointegration

Osseointegration is influenced by a number of factors. Firstly, the material of the implant is important. Titanium is a popular choice due to its excellent biocompatibility. It is bioinert. It has been proposed that the absence of negative tissue responses associated with titanium is responsible for its enhanced osseointegration (Stanford and Keller 1991). When titanium is exposed to air, a thin titanium oxide layer forms on the surface. A thickness of approximately 2-5 nm is often formed in a few seconds (Guo et al 2012). The oxide layer is known to increase corrosion resistance and may improve ingrowth of bone cells (depending on the surface preparation and thickness of the oxide layer formed) (Cunha et al 2014). It has been postulated that the interface between titanium and the living bone is a titanium peroxy matrix and that a chemical bond forms between the tightly adherent oxide layer and the tissue (Adell et al 1981, Brånemark et al 2001).

Intraoperatively, tissues should be handled carefully in order to minimise tissue damage, which could be detrimental to osseointegration (Adell et al 1981). Drilling temperatures should be kept as low as possible and irrigation may be used while drilling (Adell et al 1981). Handling the implant with only titanium instruments is more favourable for osseointegration (Granstrom 2007). The design of the implant is also relevant. A screw-shaped implant may show better primary stability than a cone-shaped implant. Roughened and microgrooved surfaces have been found to promote osseointegration (Adell et al 1981; Granstrom 2007, Mavrogenis et al 2009). Surface nanotopography has also been shown to influence osseointegration by promoting osteoblast adhesion and migration and by influencing cell differentiation (de Oliviera et al 2007; Feller et al 2015). For example, nanotextured surfaces produced by chemical treatment of titanium with a mixture of sulphuric acid and hydrogen peroxide have been found to upregulate the early expression of bone sialoprotein and osteopontin in osteogenic cell cultures, which leads to an increase in bone-like

nodule formation (de Oliviera and Nanci 2003; de Oliviera et al 2007). It has been shown that nanoscale features on titanium implants may direct the differentiation of mesenchymal stem cells towards an osteogenic lineage and stimulate osteoprogenitor cell differentiation towards an osteoblastic phenotype (Dalby et al 2006; Mendonca et al 2009; Tan et al 2014; Tsimbouri et al 2014). Nanotopography may lead to alterations in cell shape, which may affect cell differentiation by influencing cellular interaction with surface features via filopodia (McBeath et al 2004; de Oliviera et al 2007; Feller et al 2015). Furthermore, nanotopography may affect cell differentiation by influencing gene expression, e.g. higher gene expression of $\alpha 1\beta 1$ integrins in cells grown on nanotextured surfaces has been observed (Rosa et al 2014; Curtis and Tsimbouri 2014). Poor bone quality e.g. due to irradiation or primary osteoporosis is detrimental to osseointegration (Granstrom 2007).

1.1.3.3 Failure Mechanisms of Osseointegrated Transcutaneous Prostheses

Mechanisms that prevent the formation of a robust seal between the soft tissues and the implant result in failure of transcutaneous implants. Epithelial downgrowth is the main mechanism that prevents this seal forming. Epithelial downgrowth is the migration of epithelial cells downwards and parallel to the side of the implant (Figure 1.2 (a)). The presence of a transcutaneous implant prevents the wound margins from meeting. The epithelial cells are unable to form cell-cell adhesions as they would during normal wound healing. As a result, prevention of epithelial cell migration via contact inhibition does not occur (Zegers et al 2003; Pendegrass et al 2012a). This leads to epithelial downgrowth. The failure of the epithelium to unite with the surface of the implant and the subsequent space at the skin-implant interface provides a direct route for microorganisms to enter the underlying soft tissues (Von Recum et al 1984; Pendegrass et al 2006a). Marsupialisation is the formation of pockets between the implant and the surrounding epithelium that occurs as a result of epithelial downgrowth (Figure 1.2 (b)). The pockets are filled with cell detritus and exudate, which creates a favourable environment for bacterial colonisation (von Recum et al 1984). In some cases further epithelial downgrowth may lead to the cells re-establishing continuity beneath the implant resulting in the implant becoming extra-cutaneous. This rarely occurs with osseointegrated medical devices. Avulsion

is a mechanically induced failure mechanism in which the soft tissue-implant interface is disrupted. Small forces may cause avulsion when the prosthesis is poorly supported by the attachment of soft tissues. Avulsion has been shown to lead to haematoma formation, focal inflammatory areas and tissue necrosis, which predispose to infection (von Recum et al 1984).

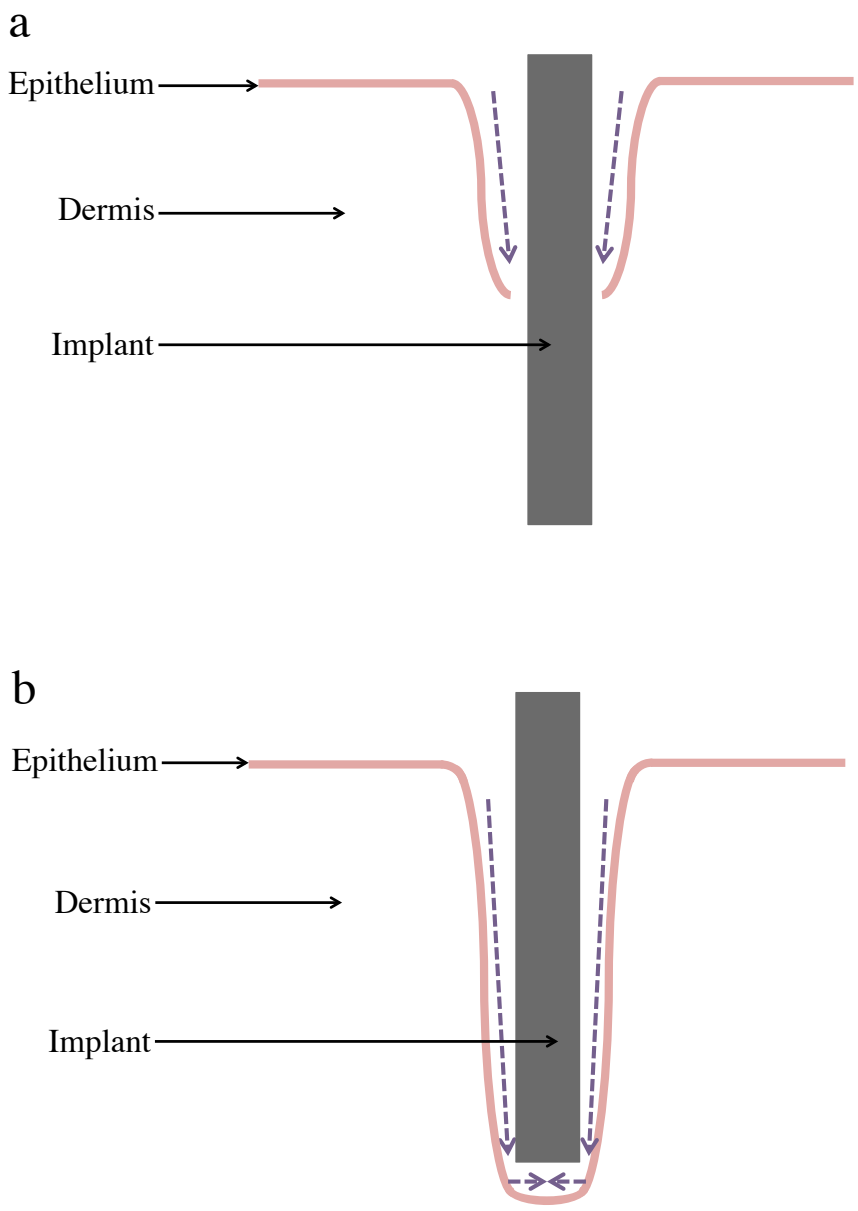

Figure 1.2 Diagram illustrating the process of (a) epithelial downgrowth and (b) marsupialisation.

1.2 CONSIDERATION OF SKIN HISTOLOGY AND WOUND HEALING

In order to increase the skin-implant seal and to improve the success of transcutaneous implants it is necessary to consider the histological features of skin and the process of wound healing.

1.2.1 Histological Features of Skin

The skin consists of three layers, namely the epidermis, dermis and hypodermis. The epidermis is a stratified squamous keratinising epithelium composed of 90 to 95% keratinocytes (Kanitakis 2002). Small numbers of other cells are also present, e.g. melanocytes, Langerhan's cells and Merkel cells. Mitotically active cells within the *stratum basale* (the deepest layer of the epidermis) give rise to other keratinocytes. There is progressive movement of cells from the *stratum basale* up through to the more superficial layers of the epidermis. These layers are the *stratum spinosum*, the *stratum granulosum*, the *stratum lucidum* (which is only present in very thick skin) and finally the *stratum corneum*. Cells are continuously shed from the outer *stratum corneum* and replaced by the progressive movement and maturation of cells from the deeper layers (Burkitt 1997). The epidermal appendages (sweat glands and pilosebaceous follicles) are specialised epithelial structures connected to the surface epidermis but located mainly within the dermis and hypodermis (Kanitakis 2002).

The cells of the *stratum basale* attach to the basement membrane that separates the epidermis from the underlying dermis by hemidesmosomes. The basement membrane is synthesised by the basal keratinocytes and dermal fibroblasts. It regulates the exchange of metabolic products between the dermis and epidermis and serves as a support for keratinocyte migration during wound healing (Kanitakis 2002; Woolf 1998). The basement membrane consists of four zones. The plasma membrane of keratinocytes contains the hemidesmosomes. The *lamina lucida* contains the bullous pemphigoid antigen and various isoforms of the protein laminin (laminin 5, 6 and 10). The *lamina densa* consists of type IV collagen. The sub-basal lamina filamentous zone mainly contains anchoring fibres (Kanitakis 2002).

The dermis is the supportive connective tissue underlying the epidermis that incorporates a generous vascular system to provide metabolic support for the avascular epidermis and for thermoregulation (Burkitt 1997). The thickness of dermis varies considerably depending on the anatomic location (Kanitakis 2002). The majority of dermal fibres consist of type I and type III collagen. Fibroblasts are the predominant cells of the dermis and all connective tissues. They produce and organise the extracellular matrix and play a crucial role in wound repair (Sorrell and Caplan 2004). The extracellular matrix of the dermis consists of fibrous proteins and proteoglycans. The fibrous proteins include structural proteins such as collagen and elastin as well as adhesive proteins such as fibronectin and laminin (Alberts 2002; Schultz et al 2005). The dermis consists of two zones. The upper papillary zone forms upright projections known as dermal papillae. These papillae are separated from each other by rete ridges (prolongations of the epidermis). This increases the surface of contact between the dermis and the epidermis, which allows better adhesion between these layers. The papillary dermis consists of collagen fibres arranged in loose bundles. It contains loops of blood vessels and nerve fibres. The deeper reticular dermis consists of coarser collagen bundles orientated approximately parallel to the overlying skin surface. It contains thick elastic fibres, vascular and nerve plexuses and the deep part of cutaneous appendages such as sweat glands, sebaceous glands and hair follicles (Burkitt 1997).

The deepest layer of the skin, the hypodermis, consists mainly of mature adipose tissue cells, which are arranged in lobules (Woolf 1998). Lobules are separated by connective septa containing fibroblasts and other cells e.g. dendrocytes and mast cells. Sweat glands, vessels and nerves are also present in the hypodermis (Woolf 1998; Kanitakis 2002). Figure 1.3 is a histological section of the skin.

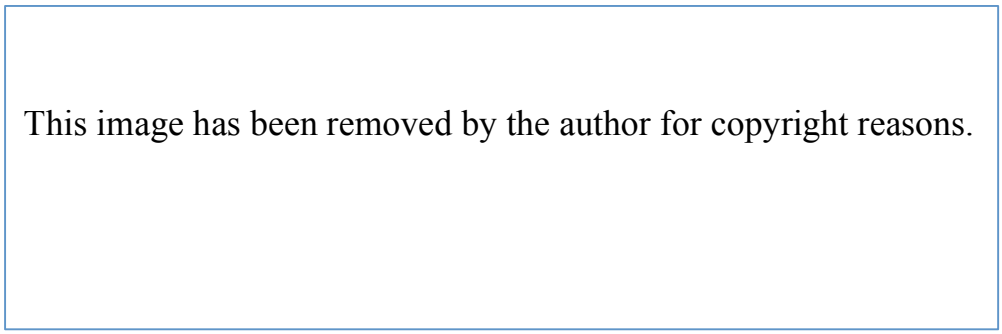

Figure 1.3 Histological section of the skin (Adapted from Slomianka 2009).

1.2.2 Wound Healing

Wound healing consists of four overlapping stages, which are haemostasis, inflammation, proliferation and maturation. Haemostasis starts immediately after the injury or incision. Platelets accumulate within the tissue defect (Reinke and Sorg 2012). Clotting mechanisms are activated leading to conversion of fibrinogen to polymerised fibrin. This is stabilised by fibronectin binding by means of a glutaminase bridge (Woolf 1998). The blood clot that forms is composed of cytokines, growth factors, fibrin molecules, fibronectin, vitronectin and thrombospondins (Reinke and Sorg 2012). In the case of incised wounds without a large tissue defect, the gel formed by fibrin and fibrinogen acts as a 'glue' to help

keep the wound edges apposed. The provisional wound matrix formed during the haemostasis stage acts as a scaffold for the migration of leucocytes, keratinocytes and endothelial cells as a reservoir of growth factors (Woolf 1998; Reinke and Sorg 2012).

The inflammatory phase of wound healing is activated by the haemostasis stage. The clot and surrounding wound tissue release pro-inflammatory cytokines and growth factors such as transforming growth factor-β, platelet-derived growth factor, fibroblast growth factor, and epidermal growth factor (Guo and DiPietro 2010). Within the first few hours after wounding neutrophils are recruited (Woolf 1998). Neutrophils release inflammatory mediators such as tumour necrosis factor α, interleukin-1β and interleukin-6 to amplify the inflammatory response and stimulate vascular endothelial growth factor and interleukin-8 to promote the repair response (Reinke and Sorg 2012). Another important function of neutrophils is to release proteolytic enzymes such as the broad specificity serine proteases (e.g. elastase) and metalloproteinase that specifically digests collagen. As a result, neutrophils digest bacteria and non-viable tissue (Broughton et al 2006). Macrophages migrate into the area approximately one to three days after injury (Woolf 1998; Reinke and Sorg 2012). Initially, they release cytokines and promote the inflammatory response. Macrophages phagocytose pathogens and cell debris. Additionally, they are responsible for inducing and clearing apoptotic cells including neutrophils, thus promoting the resolution of inflammation (Guo and DiPietro 2010).

The proliferation phase occurs approximately three to ten days after wounding. Fibroblasts migrate into the wound and lay down collagen type I and III. Collagen type III predominates initially but is later replaced by collagen type I (Reinke and Sorg 2012). Fibroblasts also produce fibronectin, glucosaminoglycans and proteoglycans, which are components of the extracellular matrix (Guo and DiPietro 2010). Angiogenesis is initiated when growth factors bind to their receptors on the endothelial cells of existing vessels. This activates intracellular signalling cascades. The activated endothelial cells secrete proteolytic enzymes, which degrade the basement membrane. The endothelial cells proliferate and migrate into the wound. New ‘sprouts’ form a vessel loop and differentiate into arteries and venules and

mature. Local keratinocytes at the wound edges and epithelial stem cells from hair follicles or sweat glands re-epithelialise the wound. The formation of granulation tissue is the last step in the proliferation phase. Granulation tissue is highly vascular and contains a high density of capillaries as well as fibroblasts, granulocytes, macrophages and loosely organised collagen bundles (Reinke and Sorg 2012).

The final stage of wound healing is maturation and involves the process of tissue remodelling and increasing wound strength (Gosain and DiPietro 2004). This stage can last for years after the initial wounding occurred. The formation of granulation tissue stops through apoptosis of the cells. The mature wound is acellular and avascular. Collagen type III is replaced by the stronger Collagen type I. Myofibroblasts result in wound contraction, which helps reduce the surface of the developing scar (Guo and DiPietro 2010; Reinke and Sorg 2012). Figure 1.4 summarises the process of wound healing.

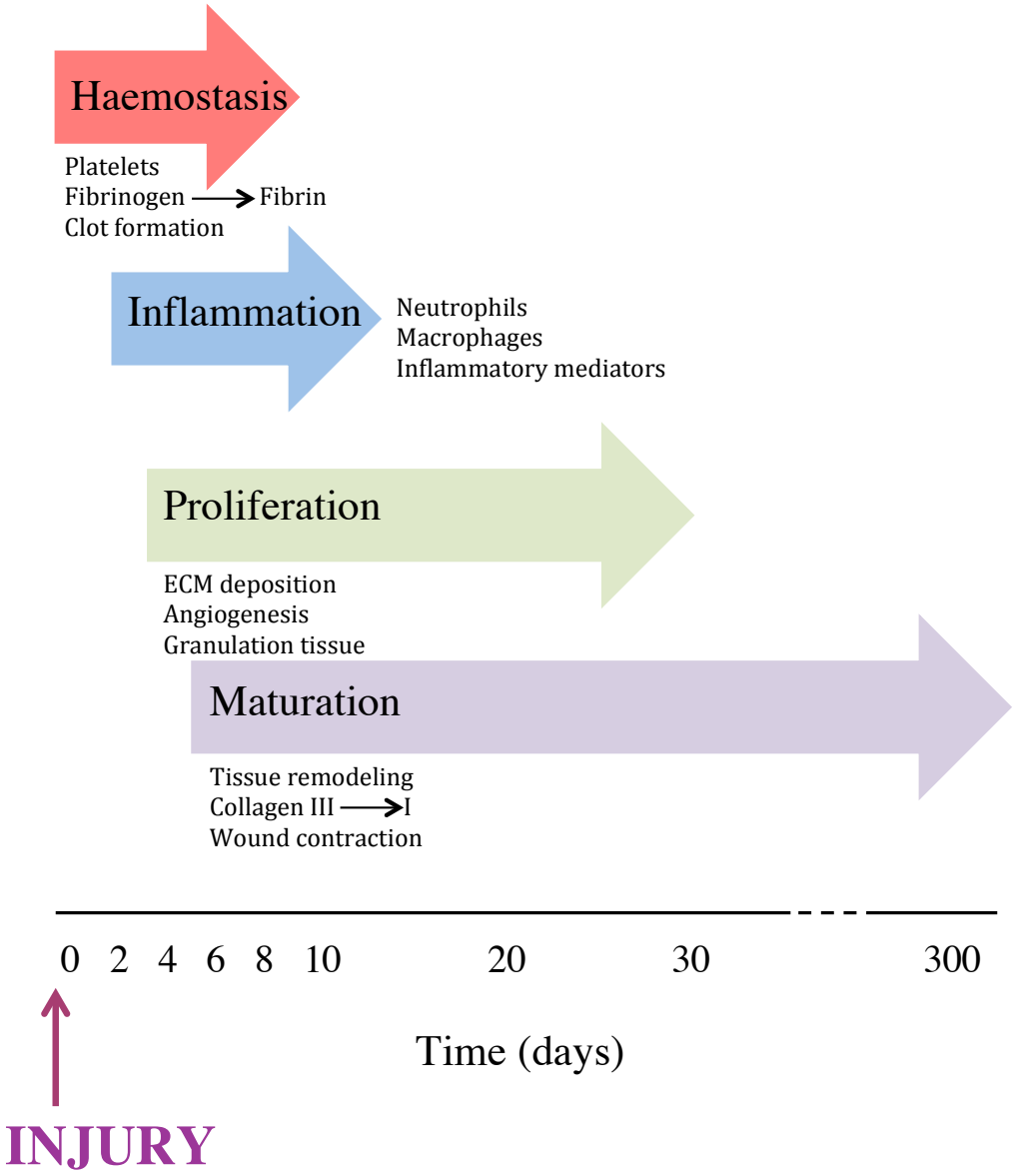

1.4 The four overlapping stages of wound healing (Adapted from Gendaszewska-Darmach and Kucharska 2011 and Akhundov et al 2012).

The soft tissue seal around transcutaneous implants could potentially be improved by modifying the surface of the implant to promote wound healing and increase fibroblast and/or keratinocyte adhesion.

1.3 BACTERIAL COLONISATION VERSUS TISSUE INTEGRATION

1.3.1 'Race for the surface'

In order to achieve tissue integration and prevent biomaterial-associated infections it is necessary for tissue cells to win the 'race for the surface' against bacteria. The term 'race for the surface' refers to the competition between eukaryotic cells and bacterial adhesion on the biomaterial surface (Gristina 1987). In the case of ITAP, ideally fibroblasts and keratinocytes need to adhere to the surface before bacteria do. If the fibroblasts win the 'race', the implant surface would be covered by a cellular layer, making the surface less available for bacterial attachment. This would lead to successful tissue integration. However, bacteria may win the 'race' establishing biofilm formation, which may be very difficult to eradicate. Furthermore, bacteria may be able to start the 'race' before tissue cells, because at the time of surgery, bacteria are frequently introduced despite aseptic technique (Gristina et al 1988; Subbiahdoss et al 2010a; Subbiahdoss et al 2010b). Approximately 270 bacteria/cm^2 are known to fall into wounds in theatre during a one-hour surgical procedure (Fitzgerald 1979; Busscher et al 2012). However, a number of factors may reduce bacterial colonisation. Adequate skin preparation is necessary, particularly as hair follicles and sebaceous glands, which may be disrupted during the skin incision, are a source of bacteria. Modern, better-ventilated operation theatres with conventional ventilation systems with 20 air-changes per hour and laminar air flow systems with up to 600 air-changes per hour, may also reduce the numbers of bacteria entering a wound (Ahl et al 1995; Verkkala et al 1998; Busscher et al 2012).

1.3.2 Biofilm Formation

If bacteria win the 'race for the surface' against tissue cells, they adhere to the surface and colonise it. This results in impairment of tissue cell functions by bacterial virulence factors and toxins (Gristina et al 1988; Subbiahdoss et al 2010a; Subbiahdoss et al 2010b). The bacteria produce a hydrated matrix consisting of polyssacharide, nucleic acids and protein known as extracellular polymeric substance (EPS) or the glycocalyx layer. They become encased in EPS and the implant becomes covered by a biofilm. The bacteria within biofilms act as a group rather

than autonomous individuals (Davies 2003). They communicate and respond to local cell density through a cell-to-cell signalling process known as quorum sensing. Quorum sensing is mediated by bacterial secretion and detection of low molecular weight highly diffusible signalling molecules known as autoinducers. When the concentration of autoinducers reaches a threshold level, it indicates that a sufficient level or 'quorum' of bacteria is present. This leads to regulation of gene expression. Bacteria may use quorum sensing to regulate the secretion of EPS and to control biofilm formation (Smith et al 2004; Nadell et al 2008). Quorum sensing has also been shown to be responsible for the release of degradative extracellular enzymes and cytotoxins in a number of bacterial species (Davies 2003).

It is generally accepted that biofilm formation proceeds in five stages, which are illustrated in Figure 1.5. Stage one is the process of initial attachment, which involves loose or transient bacterial adhesion to the surface. During stage two, robust, irreversible adhesion occurs and EPS is secreted. Stages three and four involve cell replication and aggregation of cells into microcolonies followed by growth and maturation. Stage five consists of detachment or dispersal of cells from the biofilm, which allows propagation and self-renewal of the biofilm (Hall-Stoodley et al 2004; Renner and Weibel 2011).

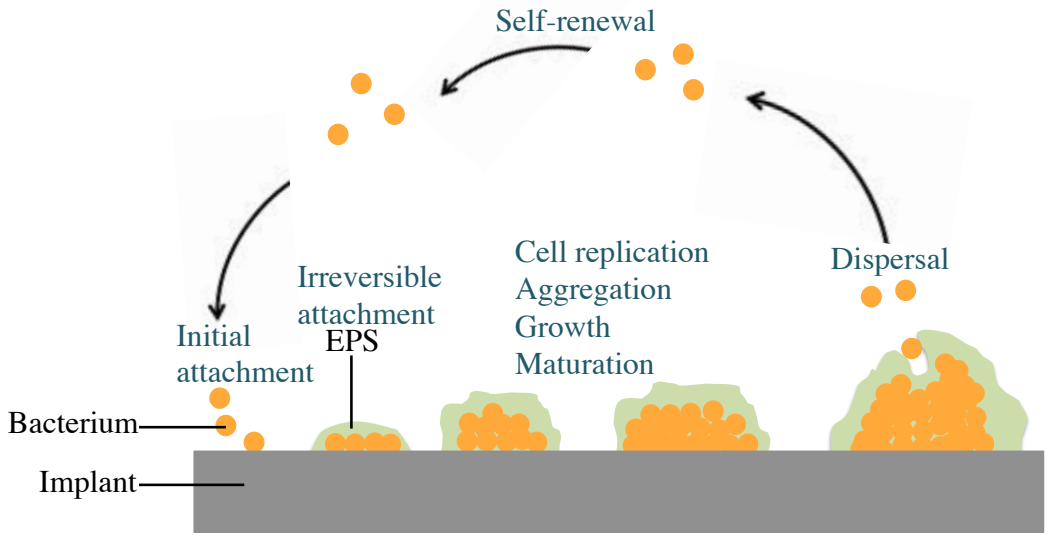

Figure 1.5 The stages of biofilm formation (Adapted from Park et al 2011).

1.3.3 Antibiotic Resistance in Biofilms

Bacteria within biofilms are known to be considerably less susceptible to antimicrobials than the same bacterium grown in planktonic culture (Davies 2003). *In vitro* biofilm models have shown the survival of bacterial biofilms after treatment with antibiotics at concentrations hundreds of times above the minimum inhibitory concentration of the bacteria (Ceri et al 1999). Antibiotics have also been shown to fail to eradicate bacteria within biofilms *in vivo* (Stewart and Costerton 2001). Several theories to explain mechanisms of resistance to antibiotics in bacterial biofilms exist.

It has been hypothesised that the inability of antibiotics to penetrate all areas of the biofilm may play a role in resistance. It has been suggested that the glycocalyx may act as a barrier to antibiotic diffusion (Donlan and Costerton 2002). However, as the biofilm matrix is predominantly water, it is unlikely that diffusion of solutes the size of antibiotics would be blocked (Stewart and Costerton 2001). In theory, the antibiotics may react with biofilm matrix components and be deactivated leading to a delay in the rate of penetration. Reduced penetration of some antibiotics through biofilms has been demonstrated *in vitro*, but other antibiotics have been shown to readily penetrate through biofilms. For example, Singh et al (2010) found that penetration of the glycopeptide vancomycin and the β-lactam antibiotics oxacillin and cefotaxim was significantly reduced through *Staphylococcus (S) aureus* and *S epidermidis* biofilms. Penetration of the aminoglycoside amikacin and the fluoroquinolone ciprofloxacin was unaffected (Singh et al 2010). There have been some conflicting results between studies. For example, a Fourier transform infrared spectrometry study showed delayed penetration of ciprofloxacin through *Pseudomonas (P) aeruginosa* biofilms (Suci et al 1994). In contrast, a diffusion cell bioassay showed that ciprofloxacin was able to penetrate *P aeruginosa* biofilms but failed to kill the bacteria effectively (Walters et al 2003). It is likely that differences in experimental conditions between studies and the heterogeneity of biofilms may explain the conflicting results (Mah 2012).

Another theory to explain antibiotic resistance of biofilms is that the chemical microenvironment is altered (Stewart and Costerton 2001; Stewart 2002). Bacteria

within biofilms are expected to experience some form of nutrient limitation. This results in slow growth of bacteria, which could account for the increase in resistance to antibiotics. It is known that the antibiotic sensitivity of both planktonic bacteria and bacteria within biofilms is dependent on the growth rate of the bacteria and decreases with reduced growth rate (Evans et al 1990; Duguid et al 1992; Costerton et al 1999; Donlan and Costerton 2002). Additionally, non-growing bacteria have been shown to be phenotypically tolerant to the killing activity of β-lactam antibiotics (Tuomanen et al 1986). Reduced oxygen availability within the deep layers of biofilms may affect antibiotic sensitivity. For example, minimum inhibitory concentrations of aminoglycosides are known to be increased under anaerobic conditions (Tack and Sabath 1985). Differences in pH within biofilms may also occur due to local accumulation of acidic waste products. This may affect the action of antibiotics (Stewart and Costerton 2001). Furthermore, the osmotic environment within a biofilm may be altered leading to a stress response. The stress response could change the relative proportion of porins (transmembrane proteins that selectively transport molecules through the outer cell membrane) and reduce permeability to antibiotics (Prigent-Combaret et al 1999; Stewart and Costerton 2001).

The presence of persister cells and small colony variants (SCVs) is also associated with the enhanced antibiotic resistance of many bacteria within biofilms (Singh et al 2009). Persister cells are a subpopulation of dormant, non-dividing cells. Cell metabolism is slowed or shut down and antibiotics cannot act because their targets are not active (Lewis 2007). SCVs are small slow-growing bacteria, which often show increased resistance to antibiotics. One SCV mutant was shown have a multifactorial resistance including overexpression of efflux mechanisms and alterations in genes affecting the outer membrane composition (Wei et al 2011; Mah 2012).

Another factor that may contribute to biofilm resistance is differences in gene expression profiles of biofilm cells compared with planktonic cells. A number of genes have been identified that exhibit a higher level of gene expression in biofilms than planktonic cultures and protect biofilm cells from antibiotics (Zhang et al 2013).

For example, the *ndvB* gene product of *P aeruginosa* sequesters antibiotic molecules before they reach their cellular target and affects the expression of several *P aeruginosa* genes (Beaudoin et al 2012). PA1875-1877 is thought to function as an efflux pump (Mah 2012). The function of other genes such as *tSSC1,* PA0756-0757, PA2070 and PA5033 is under investigation (Zhang et al 2011; Mah 2012; Zhang et al 2013).

The inherent resistance of bacteria within biofilms means that in clinical practice, once biofilms have formed they are very difficult to eradicate. As a result, biofilm formation may lead to chronic infection or the need for the implant to be surgically removed (Subbiahdoss et al 2010a; Subbiahdoss et al 2010b). The use of topical antimicrobial agents on implants may have the potential to be more effective than parenteral antibiotics by preventing initial bacterial adhesion.

1.4 BACKGROUND ON THE CLINICAL USE OF OSSEOINTEGRATED TRANSCUTANEOUS PROSTHESES

1.4.1 Early Direct Skeletal Attachment in Humans

The earliest published report of clinical application of transcutaneous prostheses in humans described use in above-knee and above-elbow amputees in 1977 (Mooney et al 1977). Three patients were fitted with a stainless steel implant cemented to the intramedullary canal with a carbon collar. Postoperatively the patients developed superficial wound infections that delayed fitting of the external prostheses. All three patients developed chronic infection aggravated by mechanical irritation leading to removal of the implants within six months postimplantation. Movement at the skin-implant interface was found to prevent maintenance of a good seal (Mooney et al 1977).

1.4.2 Modern Osseointegrated Transcutaneous Amputation Prostheses

A small number of osseointegrated transcutaneous amputation prosthesis systems are currently in clinical use worldwide. The specific design features of the ITAP model

will be discussed in Section 1.5. This section describes other systems that have been used in humans to date and have published clinical outcomes.

1.4.2.1 Osseointegrated Prostheses for Rehabilitation of Amputees (OPRA)

Brånemark's group have been carrying out treatment with osseointegrated transfemoral prostheses at the Centre for Orthopaedic Osseointegration, Gothenburg, Sweden since 1990. They have now treated over 100 patients. Initially, their rehabilitation protocol for osseointegrated transcutaneous implants was not standardised, but the OPRA protocol was introduced in 1999. The OPRA implant is made of commercially pure titanium and implantation involves a two-stage procedure. The procedure consists of screwing a threaded fixture into the intramedullary canal of the residual femur. The skin is closed and once the wound has healed, the use of a conventional socket prosthesis is an option until the second surgical procedure is performed. The second stage procedure is performed six months later once osseointegration has occurred. This procedure consists of inserting a skin-penetrating abutment into the distal end of the fixture onto which the external prosthetic limb is attached. Once the soft tissues have healed the rehabilitation process is commenced. This consists of using a short training prosthesis for the first three months and gradually increasing loading on the implant (Hagberg and Brånemark 2009).

The clinical outcomes of the 100 patients showed that 20 of the implants required explantation. Thirteen were revised, of which nine revisions were successful. They reported that proportionately more implants were removed from patients who had not been rehabilitated with the OPRA protocol. Fifty-one of the patients from this series (55 implants) were included in a prospective clinical investigation. At two years follow-up, promising results in terms of quality of life were reported. However, several complications occurred. The patients developed an average of one superficial infection every two years that required treatment with oral antibiotics. There were six deep infections in four patients necessitating removal of one implant. Additionally,

three implants were removed due to loosening (Berlin et al 2012; Brånemark et al 2014).

1.4.2.2 Endo-Exo-Femur Prosthesis

The Endo-Exo-Femur Prosthesis (EEFP) is a cobalt-chrome implant with a spongiosa metal surface (Pitkin 2013). The procedure consists of two stages. The first stage employs a press-fit technique to implant the stem into the bone followed by closing the soft tissue and skin. After six to eight weeks, a stoma is cut out and a transdermal coupler is connected for fixation of the external prosthesis (Aschoff et al 2011; Aschoff et al 2012). This system has been used to treat more than 50 patients in Lübeck, Germany over a period of ten years. In the earlier years, this implant was associated with a high rate of complications. In 2010, it was reported that 20 out of 37 patients who had undergone this procedure required one or more revisions. Four patients underwent removal of the implant due to failure. Two patients underwent successful reimplantation at a later date (Aschoff et al 2010). Design modifications such as the use of a smoothly polished coupler and a larger circular incision have lead to substantially improved results. Of 24 implants (in 23 patients) inserted between January 2009 and December 2011, no revisions were required (Aschoff et al 2012). However, long-term follow-up data including information about cases of infection that did not require revision are needed.

1.5 DEVELOPMENT OF ITAP

1.5.1 Basic Principles of ITAP

ITAP is different from other osseointegrated transcutaneous implants. Research on previous implant designs for direct skeletal attachment has focused on osseointegration and this has been achieved with excellent success rates (Brånemark et al 2014). In contrast to other osseointegrated transcutaneous implants, research into developing the ITAP design focuses on promoting the soft tissue seal. Additionally, the surgery is a single-stage procedure, which allows faster

rehabilitation. A failsafe device is included in the design to protect the bone from fracture if excessive loading occurs (Newcombe et al 2013).

1.5.2 Biomimickry and Specifics of the ITAP Design

ITAP is a biomimetic implant that is modelled on the deer antler. The deer antler is considered to be a natural analogue of ITAP because it is a bony skin-penetrating appendage that maintains an intact infection-free interface despite undergoing extreme loading during the rutting season (Pendegrass et al 2006a; Pendegrass et al 2006b). Histomorphological analysis has shown that deer antlers possess a highly porous pedicle structure beneath the skin. The pedicle contains pores with a significantly larger size and has a greater number of pores than the antler proper. Additionally, numerous thick Sharpey's fibres were seen to be spanning the dermal soft tissue-pedicle interface creating a seal between the dermal tissues and the pedicle bone. These fibres were found to emanate from the pores and were orientated perpendicular to the pedicle surface (Pendegrass et al 2006b). The dermal seal is considered to be the key to the success of ITAP. It is believed that this seal presents a physical barrier to epithelial cell migration, which prevents invasion by microorganisms and ultimately infection (Pendegrass et al 2006a; Pendegrass et al 2006b).

As a result of the study findings described above, ITAP has a flange incorporated into the design in order to promote soft tissue integration. The flange has 0.7 mm drilled holes which mimics the porous nature of the pedicle. Figure 1.6 is a schematic diagram of the ITAP model. In addition to this, the flange is coated with a plasma sprayed layer of hydroxyapatite. A goat model of ITAP demonstrated that epithelial downgrowth was reduced significantly around flanged implants. It was also found that if dermal attachment is achieved even without epithelial attachment, epithelial downgrowth is inhibited (Pendegrass et al 2006a; Pendegrass et al 2006b). It is postulated that once epithelial downgrowth is prevented and keratinocytes in the epithelium come into contact with the implant surface, they may attach via

hemidesmosomes and allow an epithelial seal to from in addition to the dermal seal (Pendegrass et al 2006a; Pendegrass et al 2006b; Gordon et al 2010).

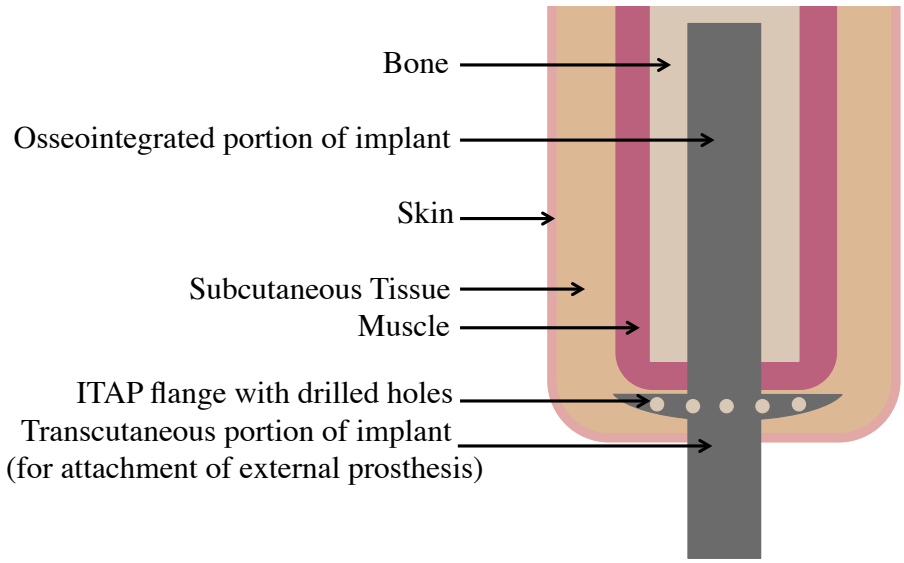

Figure 1.6 Schematic diagram of the ITAP design.

1.5.3 Choice of Titanium Alloy as a Biomaterial

In addition to the features of titanium that enhance osseointegration discussed above in Section 1.1.3.2 (i.e. biocompatibility, bioinertness and corrosion resistance due to the formation of an adhesive titanium oxide layer on the surface), titanium and its alloys possess favourable mechanical properties such as high strength and low density (Geetha et al 2009). Commercially pure titanium alloy is used most commonly for dental implants, but titanium alloys are used commonly for orthopaedic implants including ITAP due to enhanced mechanical properties necessary for load-bearing (Navarro et al 2008). Ti6Al4V is the most commonly used titanium alloy in orthopaedics. Aluminium and vanadium stabilise the microstructure and improve the mechanical structure in relation to commercially pure titanium. The elastic modulus of titanium alloys varies from 55 to 110 GPa which is closer to the elastic modulus of bone than some other metals including stainless steel and cobalt-chrome alloys which have elastic moduli of greater than 200 GPa (Geetha et al 2009). This has the potential to reduce the risk of stress shielding i.e. a reduction in mechanical stress in cortical bone adjacent to an

orthopaedic implant, due to the elastic modulus mismatch, leading to periprosthetic loss of bone stock (Sumner et al 1998). A less desirable feature of titanium and its alloys is its susceptibility to wear. It undergoes significant wear when it is rubbed with itself or most other metals (Miller and Holladay 1958). Titanium alloy wear may lead to the liberation of potentially toxic metal debris into the surrounding tissues (Agins et al 1988). Another disadvantage is the high cost of refining, processing and fabricating titanium (Seong et al 2009). The cost of titanium alloys varies according to the alloying elements used (Yoshimura et al 2009).

1.5.4 Clinical Application of ITAP

The ITAP model has been translated clinically in a relatively small number of patients to date. ITAP was first used clinically to treat veterinary cases. Favourable functional outcomes as well as robust dermal and osseous integration have been reported in the radius or tibia of four dogs (Fitzpatrick et al 2011). ITAP has been used to treat human transhumeral and transfemoral amputees. A patient who sustained a transhumeral amputation in the '7/7' London Underground Bombings was fitted with an ITAP device. At two years postoperatively, she was reported to have near-normal shoulder range of motion, without infection or pain (Figure 1.7) (Kang et al 2010). Ongoing Phase 1 clinical trials of transfemoral ITAPs at the Royal National Orthopaedic Hospital have yielded some promising results with patients anecdotally reporting improved function (O'Leary n.d.). However, the problem of infection has not been solved (Chimutengwende-Gordon et al 2010 unpublished audit).

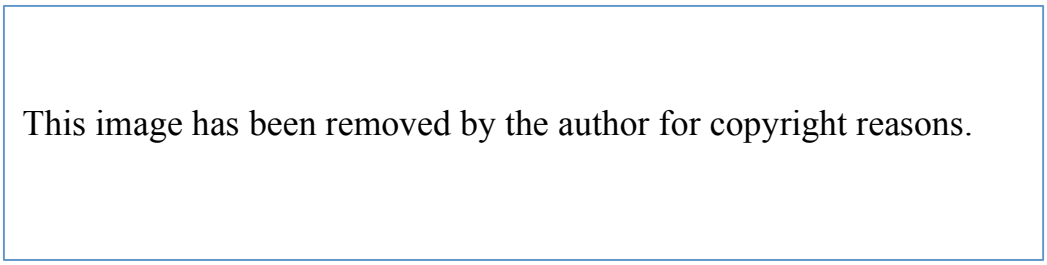

Figure 1.7 (a-c) Near-normal motion with a transhumeral ITAP. This patient was unable to use conventional prostheses due to restricted motion. (d) The skin-implant interface at 740 days. (e) A radiograph of the ITAP (Kang et al 2010).

1.6 APPLICATION OF THE 'RACE FOR THE SURFACE' TO RESEARCH ON PREVENTING INFECTION OF ITAP

To date, research on preventing infection of ITAP has focused on enhancing the soft tissue-implant seal. This thesis proposes that it may be beneficial to use a surface that possesses both soft tissue enhancing properties and antimicrobial activity. The antibacterial activity would need to be present during the early postoperative period until soft tissue attaches. This would mean that adhesion of any bacteria present before soft tissue integration has occurred would be prevented. Additionally an antimicrobial that is released from the implant surface into the surrounding tissues would be needed to kill bacteria present within the soft tissues. This would enable fibroblasts to win the 'race for surface' against bacteria.

1.6.1 Potential Strategies to Increase Soft Tissue Attachment to ITAP

1.6.1.1 Porous Titanium

A fully porous titanium alloy ITAP flange with interconnected pores is a design modification that has the potential to improve the soft tissue seal to a greater degree than the current drilled-hole flange. This may emulate the deer antler more closely than drilled holes, due to the larger number of pores and the interconnected porosity. A flange is necessary rather than a porous section of the implant shaft, as the porous section would not have adequate mechanical strength to be used for the implant

shaft. Pores allow migration and proliferation of cells as well as ingrowth of blood vessels and consequently tissue formation within the porous structure (Hulbert et al 1970; Kuboki et al 1998).

Additive layer manufacturing techniques such as Electron Beam Melting (EBM) and Direct Metal Laser Sintering (DMLS) processes allow fabrication of porous custom-designed titanium implants with a controlled porosity (Parthasarathy et al 2010). A laser or an electron beam melts a metal powder and portions rapidly solidify to produce a fully dense body according to a computer-aided design model. A layer-by-layer process is used to produce complex three-dimensional structures (as shown in Figure 1.8) that cannot be fabricated by traditional methods, such as metal casting or net-shape powder metallurgy (Parthasarathy et al 2010; Koike et al 2011a; Koike et al 2011b; Gong et al 2014).

Studies investigating the ability of porous biomaterials to induce tissue ingrowth have predominantly focused on bone tissue ingrowth with a view to using porous metals as a substrate for joint replacement prostheses. Bone ingrowth into porous materials results in mechanical interlocking between the implant and the surrounding bone (Story et al 1998). Open porous metallic structures with greater porosity, pore size and interconnectivity have been shown to result in increased bone ingrowth *in vivo* (Karageorgiou and Kaplan 2005). It is generally accepted that the minimum pore size required to allow ingrowth of cells, vascularisation, nutrient delivery and regeneration of mineralised bone, is approximately 100 μm and the optimum pore size is in the range of 100 to 400 μm (Hulbert et al 1970; Kuboki et al 1998; Karageorgiou and Kaplan 2005; Ryan et al 2006; Wang and Jain 2010).

The effect of porous titanium on promoting soft tissue attachment has been studied to a lesser degree. *In vivo* soft tissue ingrowth into transcutaneous porous titanium alloy implants ranging from 40 to 160 μm in size has shown incomplete soft tissue ingrowth (up to approximately 50% at four to six weeks) (Farrell et al 2014). There is a lack of quantitative data in the literature showing whether fully porous titanium

alloy structures with larger pore sizes (in the range of the drilled holes used in the current ITAP flange) increase soft tissue ingrowth and vascularisation. Studying the effect of functionalising porous titanium alloy structures with bioactive coatings to determine if this enhances soft tissue ingrowth further may also be of value. Bioactive materials are defined as 'materials that elicit a specific biological response at the interface of the materials which results in the formation of a bond between the tissues and the materials' (Cao and Hench 1996).

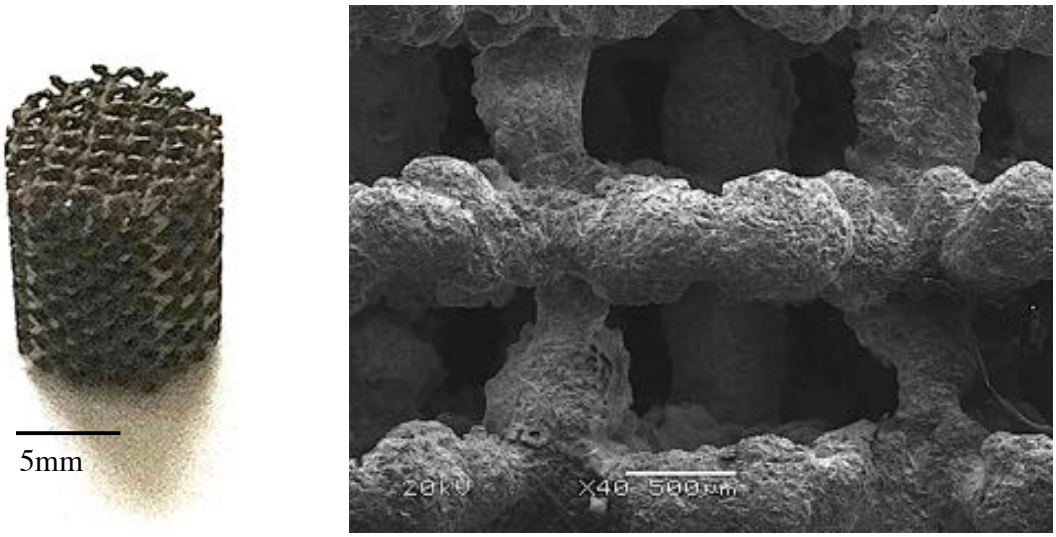

Figure 1.8 Photograph and scanning electron micrograph of porous titanium alloy.

1.6.1.2 Hydroxyapatite

Hydroxyapatite is a naturally occurring calcium phosphate mineral with the chemical formula $Ca_{10}(PO_4)_6(OH)_2$ (Kay et al 1964). It is one of the main constituents of bone comprising approximately 60 to 70% of bone (Piatelli et al 1993). Pure stoichiometric hydroxyapatite has a calcium/phosphorus (Ca/P) molar ratio of 1.67 (40 weight % Ca^{2+} and 18.5 weight % PO_4^{3-}) (Murugan and Ramakrishna 2005). Hydroxyapatite shows excellent biocompatibility and is primarily osseoconductive (promotes bone growth on its surface) rather than osseoinductive (promotes differentiation of stem cells into osteoblasts) (Albrektsson and Johansson 2001; Kalfas 2001; Hu and Miao 2004; Larsson et al 2012). It is also considered bioactive

as it forms a strong chemical bond with host bone tissue. Hydroxyapatite coatings may be derived from natural or synthetic sources and are commonly used to increase the bioactivity and promote osseointegration of biomaterials for dental implants, hip and knee arthroplasties and fracture fixation devices (Manley et al 1998; D'Antonio et al 2001, Murugan and Ramakrishna 2005). A disadvantage of hydroxyapatite is that it possesses poor mechanical strength, making it unsuitable for use on its own for load bearing applications. The fracture toughness of hydroxyapatite is approximately 1.0 MPa $m^{1/2}$, which is low compared with the fracture toughness of bone, which is approximately 2-12 MPa $m^{1/2}$ (Kitsugi et al 1993; Murugan and Ramakrishna 2005). Therefore, its use is restricted to non-loadbearing applications such as coatings for implants or to fill bone defects (Calori et al 2011).

The ITAP flange is coated with hydroxyapatite because hydroxyapatite has also been shown to enhance soft tissue integration (Piza et al 2004; Pendegrass et al 2006a; Larsson et al 2012). Larsson et al (2012) conducted a histological assessment of soft tissue integration of abutments for bone anchored hearing implants in an ovine model. The use of hydroxyapatite-coated titanium abutments resulted in greater dermal adherence and less epithelial downgrowth than non-coated abutments (Larsson et al 2012). Smith et al (2006) assessed soft tissue integration of external fixator pins. They found that dermal contact on fully coated external fixator pins was greater than on pins that were not coated with hydroxyapatite or on pins where only the threaded intraosseous portion was coated with hydroxyapatite. However, they also studied bacterial colonisation and showed that fully coated hydroxyapatite pins were associated with increased bacterial colonisation despite the increased soft tissue integration (Smith et al 2006). This indicates that although hydroxyapatite increases soft tissue integration, if the implant is exposed to bacteria before the seal has formed, hydroxyapatite may increase bacterial colonisation leading to an increased risk of infection. The increased bacterial colonisation associated with hydroxyapatite may be related to the chemical composition and the positive surface charge of the coatings (Laure et al 2008). Eukaryotic cells (such as human tissue cells) and prokaryotic cells (such as bacteria) are likely to be descended from a common primordial ancestor (Cooper 2000). The endosymbiotic theory hypothesises that

eukaryotes evolved from symbiotic association of prokaryotes (Cooper 2000). As a result, surfaces such as hydroxyapatite that promote human tissue cell adhesion and growth may also promote bacterial colonisation. It is necessary to achieve the correct balance between promoting eukaryotic cell and bacterial adhesion. The use of other coatings in combination with hydroxyapatite that further enhance soft tissue integration and/or coatings with antibacterial activity may have the potential to overcome any detrimental effects of hydroxyapatite on bacterial colonisation.

1.6.1.3 Fibronectin-Functionalised Coatings

Adsorption of fibronectin onto hydroxyapatite has the potential to enhance soft tissue integration further. Fibronectin is a glycoprotein that is present in the extracellular matrix and plasma that is produced by most mesenchymal cells (Mosher 1984; Sousa et al 2005). Fibronectin has multiple functions. Its main functions include promotion of cellular migration during wound healing, regulation of cell growth and differentiation, promotion of cell-to-cell adhesion, cell-to-basement membrane attachment and clot stabilisation (Sousa et al 2005; Proctor 1987).

Fibronectin usually exists as a dimer composed of two nearly identical subunits of approximately 250 kDa. The subunits are linked covalently by disulphide bonds near one end (Pankov and Yamada 2002). Each monomer consists of three types of repeating units, I, II and III. Types I and II consist of disulfide-bonded loops of approximately 50 amino acids long. Type III is approximately 90 amino acids long without any disulfide bonds. Fibronectin contains binding sites for heparin, collagen and fibrin (Odermatt et al 1985; Pankov and Yamada 2002). Fibronectin attaches fibroblasts and other cells via the tripeptide Arginine-Glycine-Aspartic acid (RGD) amino acid sequence. The RGD sequence is the cellular recognition site of a number of other extracellular and platelet adhesion proteins e.g. type I collagen, vitronectin, fibrinogen, von Willebrand factor and osteopontin (Ruoslahti and Perschbacher 1987). The RGD sequence binds integrins, which are a family of heterodimeric transmembrane glycoproteins that mediate cell-cell and cell-extracellular matrix interactions. Cellular attachment to extracellular matrix results in clustering of

integrins, which associate with a variety of cytoplasmic proteins to from focal complexes with the actin cytoskeleton (Hotchin and Hall 1995). Integrins are composed of two non-covalently associated subunits, denoted α and β. The combinations of α and β subunits determine the specificity for extracellular ligands. Fibronectin is recognised by at least ten cell surface receptors of the integrin family including α5β1, αIIbβ3 and α4β1 (Johansson et al 1997; Alberts 2002).

Several *in vitro* studies have demonstrated that fibronectin can enhance fibroblast adhesion and/or spreading on biomaterials (Grinell 1984; Cannas et al 1988; Dean et al 1995; Middleton et al 2007). Adsorption of fibronectin onto hydroxyapatite has been shown to result in greater increases in fibroblast focal adhesion formation and soft tissue attachment compared with fibronectin and hydroxyapatite individually (Pendegrass et al 2010a). The exact nature of the bonding between hydroxyapatite and proteins is not entirely clear (Dong et al 2007). However, it has been reported that strong adsorption of some proteins with hydroxyapatite is mediated by the acidic N-terminal (Shaw et al 2000; Stayton et al 2003). Electrostatic energy is reported to play a dominant role in the interaction between hydroxyapatite and proteins (Shen et al 2008). Proteins can interact with hydroxyapatite through functional groups such as -OH, $-NH_2$ and COO^-. Hydrogen bonding results in the adsorption of many interactive groups with no net charge (Dong et al 2007).

1.6.1.4 Approaches to Increase Epithelial Cell Attachment

Research into increasing keratinocyte attachment to ITAP has also been carried out. Covalent bonding of the basement membrane protein laminin to titanium alloy results in a 20-fold increase in the number of keratinocyte adhesion plaques compared with uncoated titanium alloy (Gordon et al 2010). Additionally, the formation of cell-cell adherens junction on titanium alloy by adsorbing E-cadherin has been shown to result in a four-fold increase in keratinocyte attachment (Pendegrass et al 2012a). Approaches such as these may be useful as an adjunct to increasing dermal attachment. However, as it has been shown that epithelial attachment by hemidesmosomes occurs if dermal attachment is achieved (Pendegrass

et al 2006a; Gordon et al 2010). This thesis has taken the approach of enhancing dermal attachment with the aim of achieving epithelial attachment secondary to this.

1.6.2 Antibacterial Coatings

In theory, using the strategies discussed above to promote soft tissue attachment should enable fibroblasts to win the 'race for the surface' and block bacterial attachment. However, bacteria often adhere to surfaces that promote tissue integration. Consequently, these strategies for promoting soft tissue integration could also potentially increase bacterial colonisation in the period before a robust seal has formed. Therefore, the addition of an antimicrobial agent may be valuable and is another approach that may help fibroblasts win the 'race for the surface' against bacteria. Antimicrobial agents may also be cytotoxic to eukaryotic cells. For example, dose-dependent impairment of osteoblast and fibroblast viability, proliferation and/or morphology has been demonstrated following exposure to a range of antibiotics including rifampicin, doxycycline, penicillin, gentamicin, ciprofloxacin, clindamycin and metronidazole (Isefuku et al 2001; Isefuku et al 2003; Antoci et al 2007a; Ferreira et al 2009; Rathbone et al 2011). Therefore, it is important to ensure that the toxicity to eukaryotic cells associated with antimicrobial agents is limited.

1.6.2.1 Antibiotic coatings

Antibiotic coatings have been applied to titanium and other orthopaedic implant materials and assessed both *in vitro* and *in vivo*. For example, the aminoglycoside gentamicin has been used to coat implants in several studies. Neut et al (2012) developed a gentamicin-releasing coating for cementless titanium hip prostheses that demonstrated a wide-spectrum of antibacterial efficacy (Neut et al 2012). Titanium implants coated with polyelectrolyte multilayers incorporating gentamicin have been shown to reduce *S aureus* bone infection (Moskowitz et al 2010). Gentamicin and gentamicin-RGD coatings with 99% release of gentamicin within 24 hours have been found to be biocompatible and associated with good bony integration (Alt et al 2011). A clinical prospective case series of 21 patients treated with a gentamicin-

coated tibial nail showed good clinical, laboratory and radiological outcomes after six months. These patients included complex tibial fractures and revision cases. No patients developed infections. However, this study was non-randomised and did not have a control group (Fuchs et al 2011). Covalent bonding of antibiotics to implant surfaces has been studied in order to confer long-term antibacterial activity. Antoci et al (2007) covalently bound antibiotics to titanium and showed that antibiotic activity against *S aureus* was maintained for at least six weeks (Antoci et al 2007b; Antoci et al 2007c). Vancomycin-modified titanium rods implanted into *S aureus* infected rat femora decreased clinical signs of infection and bacterial load and prevented osteolysis (Antoci et al 2007c). Other antibiotics that have had promising results include tobramycin, ciprofloxacin, cationic steroidal antimicrobial-13 (CSA-13), doxycycline, minocycline and rifampicin (Darouiche et al 2007; Moojen et al 2009; De Giglio et al 2011; Hickok et al 2012; Sinclair et al 2013). A potential drawback associated with the use of antibiotics is the emergence of antibiotic-resistant strains. As a result, alternatives to antibiotics such as antiseptics and inorganic antimicrobial agents (including metals with antimicrobial properties) are of interest (Darouiche et al 1998; Campbell et al 2000; Kalicke et al 2006; Zhao et al 2009).

1.6.2.3 Silver Coatings

Silver has been used to treat infections for centuries (Politano et al 2013). It has been considered attractive as an antimicrobial agent because it has a broad spectrum of antimicrobial activity against both bacteria and fungi (Guggenbichler et al 1999; Agarwal et al 2010). Importantly, silver resistance is considered rare and numerous antimicrobial resistant strains have been found to be susceptible to silver-based compounds (Wright et al 1998; Silver 2003; Alt et al 2004; Percival et al 2011; Jaiswal et al 2012). Metallic silver is inert, but when silver compounds come into contact with moisture or body fluids, biologically active silver cations are released (Lansdown 2010). The silver ion binds strongly to electron donor groups in biological molecules containing sulphur, oxygen or nitrogen (Schierholz et al 1998). This results in interference with bacterial DNA function, thus preventing bacterial replication (Modak and Fox 1973; Darouiche 1999; Feng et al 2000). Silver also

interacts with the sulphydryl groups of the metabolic enzymes of the electron transport chain and inactivates them (Petering 1976; Darouiche1999).

It is essential that the silver concentration used for medical applications is carefully selected because silver is known to have cytotoxic effects on eukaryotic cells. However, this cytotoxicity is dose-dependent. Studies have shown that when used at low concentrations, silver has antibacterial activity without being cytotoxic to eukaryotic cells (Bosetti et al 2002; Alt et al 2004; Chen et al 2006; Chen et al 2008; Agarwal et al 2010). A number of other metals also possess this property, which was termed the 'oligodynamic effect' by von Nägeli in 1893 (Clement and Jarrett 1994). Silver has received a great deal of interest and has been said to be the element with the highest toxicity for microorganisms and the least toxicity for animal cells (Guggenbichler et al 1999).

Silver has been used in medicine with varying results for applications such as wound dressings and coating of medical devices including urinary, vascular, central venous and peritoneal catheters, vascular grafts, prosthetic heart valves and sutures (Darouiche 1999; Ewald et al 2006). In orthopaedic research, as well as coating implants, silver has been used to confer antimicrobial activity to bone cement (Alt et al 2004; Oei et al 2012; Propokovich et al 2013; Prokopovich et al 2015).

Several *in vivo* studies of silver-coated orthopaedic implants have failed to show significant antimicrobial effectiveness of silver. Sheehan et al (2004) concluded that silver-coated wires inoculated with bacteria and inserted into rabbit femoral canals did not reduce biofilm formation compared with controls (Sheehan et al 2004). A trial of 106 silver-coated external fixation pins compared with 56 uncoated control pins in 24 patients showed a non-statistically significant reduced rate of positive microbiological cultures compared with uncoated screws (Masse et al 2000). In this study, silver coated pins were associated with a significant increase in silver serum levels, which resulted in the study being terminated prematurely for ethical reasons. Conversely, a number of other *in vivo* studies have shown promising results with silver-coated implants. Rodent models assessing silver-coated tibial intramedullary rods (Akiyama et al 2013) and implants inserted into back subcutaneous tissue

(Shimazaki et al 2010) have shown significant reductions in bacterial numbers with silver coated implants. Collinge et al (1994) inserted external fixation pins into the iliac crest of sheep and found that silver-coated pins were less frequently infected than stainless steel pins (Collinge et al 1994). In humans, silver-coated megaprostheses in patients with bone sarcomas reduced the infection rate from 17.6% to 5.9% (Hardes et al 2010).

The results of these studies on silver-coated orthopaedic implants indicate that silver has the potential to be an effective antimicrobial agent, but that the method of application and the concentration used must be optimised. In the case of ITAP, silver's antimicrobial properties could be investigated by combining it with soft tissue seal-enhancing coatings to prevent bacterial growth.

1.7 AIMS AND HYPOTHESES

The overall goal of this research is to develop a surface and coatings for the ITAP flange that reduces the infection risk by enabling fibroblasts to win the 'race for the surface' against bacteria. In order to meet this aim, I investigated the use of a fully porous titanium alloy flange coated with fibronectin-functionalised hydroxyapatite and silver (HAAgFn).

The specific aims of this research were:

1. To identify a porous titanium alloy structure that promotes soft tissue ingrowth.

2. To develop an antibacterial cytocompatible HAAgFn coating that can be applied to porous titanium alloy to reduce bacterial colonisation without being detrimental to soft tissue cell adhesion *in vitro*.

3. To assess the effect of using a porous titanium alloy flange for ITAP with and without HAAgFn coatings on soft tissue integration and bacterial colonisation in a transcutaneous pin model *in vivo*.

It was hypothesised that:

1. More open porous titanium alloy structures with larger pore sizes would increase soft tissue ingrowth more than less open porous structures.

2. HAAgFn would reduce bacterial colonisation while enabling viable fibroblast growth.

3. The use of a fully porous titanium alloy ITAP flange would increase soft tissue integration and reduce bacterial colonisation compared with the standard ITAP flange.

4. Coating the porous titanium alloy flange with HAAgFn would increase soft tissue integration and reduce bacterial colonisation further.

1.8 CHAPTER OVERVIEW

Chapter Two presents a study investigating the effect of altering pore and strut size combinations on soft tissue ingrowth into porous titanium alloy structures *in vivo*. This chapter aimed to explore the hypothesis that more open porous titanium alloy structures with larger pore sizes would increase soft tissue ingrowth more than less open porous structures. Porous titanium alloy cylinders were inserted into sheep paraspinal muscles and left *in situ* for four weeks. A histological assessment of soft tissue ingrowth was performed. The outcome of this chapter was that the porous structure that promoted soft tissue ingrowth to the greatest degree was identified and this was selected for further study in Chapters Six and Seven.

The aims of Chapters Three and Four were to investigate the hypothesis that HAAgFn would reduce bacterial colonisation while enabling viable fibroblast growth. In Chapter Three an *in vitro* assessment of dermal fibroblast viability, proliferation and morphology on HAAgFn was performed. In Chapter Four an *in vitro* assessment of the antibacterial activity of the cytocompatible surface identified from Chapter Three was carried out. The bactericidal activity of these surfaces was

investigated by challenging the surfaces with two bacterial species that have caused infection in clinical trials of ITAP.

Chapter Five presents the coating of porous titanium alloy ITAP flanges with the porous structure identified from Chapter Two with the HAAgFn coatings selected from Chapter Three and Four. The flange design, the surface characteristics of the coating and the release kinetics of silver are presented.

Chapters Six and Seven investigated the hypotheses that firstly, the use of a fully porous titanium alloy ITAP flange would increase soft tissue integration and reduce bacterial colonisation compared with the standard ITAP flange; and secondly, coating the porous titanium alloy flange with HAAgFn would increase soft tissue integration and reduce bacterial colonisation further. In these two chapters I assessed the *in vivo* performance of HAAgFn-coated porous titanium alloy. A histological assessment of *in vivo* soft tissue integration in an ovine transcutaneous pin model is presented in Chapter Six. Chapter Seven assessed *in vivo* bacterial colonisation on the same implant designs and coatings tested in Chapter Six.

Chapter Eight discusses the key findings of this thesis. It discusses the benefits and drawbacks of the research carried out. It highlights how the knowledge contributed from this thesis may be used to direct future clinical applications. Further areas of research are discussed.

It is hoped that the findings presented in this thesis will contribute to the further development of ITAP for clinical translation.

CHAPTER TWO

Soft Tissue Integration of Porous Titanium Alloy Cylinders: *In Vivo* Investigation of the Effect of Pore and Strut Size Combinations on Soft Tissue Ingrowth

2.1 INTRODUCTION

The current ITAP model employs a flange with drilled holes, which has been shown to reduce epithelial downgrowth and increase dermal attachment significantly compared with a solid pin without a flange (Pendegrass et al 2006a). Despite this, in clinical practice infection remains an issue with the use of this flange. A fully porous titanium alloy flange may be an alternative to the drilled-hole model and it is postulated that this may enhance soft tissue attachment to a greater degree. It is essential that pores of a sufficient size to promote successful soft tissue ingrowth are selected for the fully porous flange design. If pores are not of a sufficient size, poor vascularity leading to a lack of nutrients may inhibit fibroblast survival resulting in reduced tissue ingrowth (Pendegrass et al 2006a).

The effects of porous metals on soft tissue ingrowth have been investigated by several groups (although to a lesser extent than bone tissue ingrowth as discussed in Chapter One). The use of porous-coated metal implants has been studied. Bobyn et al (1982) used peel tests to study fibrous tissue attachment in a canine model. Stainless steel plates that were porous-coated with cobalt-based alloy powder were implanted into the dorsal subcutaneous tissues of mongrel dogs. They studied a range of pore sizes and found that the largest pore sizes tested (50 to 200 μm) were associated with the greatest tissue attachment strength (Bobyn et al 1982). LaBerge et al (1990) also used a canine model to study soft tissue bonding to porous-coated cobalt-chrome alloy implants with larger average pore sizes of 300 or 900 μm at two, four and six months after implantation. A non-vascularised fibrous membrane surrounded the implants with smaller pore sizes, without ingrowth or mechanical bonding. The implants with larger pore sizes resulted in the development of a vascularised membrane and increasing attachment strength and vascularity over time (LaBerge et al 1990). Hacking et al (2000) reported vascularised paraspinal fibrous tissue ingrowth into fully porous tantalum blocks inserted into the dorsal subcutaneous tissues of dogs with pore sizes of approximately 400 μm. They did not assess the effect of altering pore size or quantify the degree of vascularisation or tissue maturity (Hacking et al 2000). Reattachment of canine supraspinatus tendons to the greater tuberosity between porous tantalum washers resulted in tendon ingrowth into the

porous tantalum. Collagen density and tendon-implant strength increased with time (Reach et al 2007). These studies focused on applications to attach muscles and tendons to implants (LaBerge et al 1990; Hacking et al 2000; Reach et al 2007) and subcutaneous tissue attachment to implants (Bobyn et al 1982) rather than on soft tissue integration to enhance dermal attachment to transcutaneous implants.

Osseointegrated transcutaneous pin models to assess soft tissue ingrowth into porous titanium have been conducted. However, so far the effect of large pore sizes in the range of the size of the drilled holes used in the ITAP flange have not been investigated. Farrell et al (2014) inserted transcutaneous porous titanium pins with pore sizes of 40 to 100 μm and 100 to 160 μm into the subcutaneous tissue of the backs of rats. Histological analysis demonstrated incomplete soft tissue ingrowth of approximately 30% after three weeks and 50% at four to six weeks (Farrell et al 2014). Jeyapalina et al (2012) assessed the effect of transcutaneous pins with a subdermal barrier coated with a porous titanium coating. The pins were inserted into sheep metacarpals. After nine months, the porous-coated implants reduced infection and proximal skin migration compared with smooth titanium controls (Jeyapalina et al 2012).

This chapter aims to examine the effect of a range of porous titanium alloy structures, with pore sizes up to 1000 μm in diameter, on soft tissue ingrowth and revascularisation. The effect of different strut sizes will also be studied. The overall aim of this chapter is to select a pore and strut size combination that results in successful soft tissue ingrowth and can be used in future *in vivo* transcutaneous pin models of the ITAP.

It was hypothesised that more open structures with larger pore sizes would result in the most successful soft tissue ingrowth and revascularisation.

2.2 MATERIALS AND METHODS

The study was performed under a Project License and a Personal License according to the UK Home Office Scientific Procedures Act 1986.

2.2.1 Implants

10 mm x 20 mm porous titanium alloy cylinders with spherical pores and interconnecting struts of a constant diameter were implanted into the paraspinal muscles of skeletally mature female sheep (Mules) weighing between 60 and 80 kg. The implants were manufactured using Electron Beam Manufacturing (EOS, Germany). Nine groups (i.e. pore and strut size combinations) were studied (Table 2.1). Six machine finished implants for each pore and strut size combination were implanted (n=6).

Group	Pore size (µm)	Strut size (µm)	Abbreviation
1	1000	400	P1000 S400
2	1000	200	P1000 S200
3	700	400	P700 S400
4	700	300	P700 S300
5	700	200	P700 S200
6	500	400	P500 S400
7	500	300	P500 S300
8	500	200	P500 S200
9	250	300	P250 S300

Table 2.1 Pore and strut size combinations.

2.2.2 Surgical Procedure

2.2.2.1 Premedication and Anaesthesia

0.2 mg/kg of 2% xylazine (Bayer HealthCare, Berkshire, UK) was administered as premedication. Induction of anaesthesia was achieved with 2 mg/kg of intravenous ketamine hydrochloride (Fort Dodge Animal Health Ltd, Southampton UK) and 2.5 mg of intravenous midazolam (Roche Products Ltd, Hertfordshire, UK). Subjects underwent endotracheal intubation and 5 mL cephalexin (Schering-Plough Animal Health, Welwyn Garden City, UK) was administered as prophylactic antibiotic cover on induction. Anaesthesia was maintained with inhaled 2% isoflurane.

2.2.2.2 Operative Details

Animals were positioned lying prone. The spinal region was shaved approximately from the level of the twelfth thoracic (T12) vertebra to the sacrum. The width of the shaved area was approximately 15 cm positioned centrally over the spine. The shaved area was prepared with povidone iodine solution and then with antiseptic chlorhexidine solution. 2 cm longitudinal incisions were made through the skin, subcutaneous fat and fascia paraspinally and the cylinders were implanted within the paraspinal muscles. 3-0 vicryl sutures were used to close the fascia and subcutaneous tissues and a continuous subcuticular 3-0 vicryl suture was used to close the skin. Four implants were implanted through separate incisions on both sides of the spine.

2.2.2.3 Postoperative Course

Cefalexin was administered for three days postoperatively as further prophylactic antibiotic cover. Postoperative analgesia consisted of 2 mL buprenorphine (Alstoe Animal Health, Meton Mowbray, UK) administered intramuscularly twice daily. Animals were allowed to mobilise freely.

2.2.3 Removal of Implants

Four weeks postoperatively, euthanasia was performed with 0.7 mL/kg intravenous pentobarbitone (JM Loveridge Ltd, Southampton, UK). The implants were removed

en bloc with the surrounding soft tissues. Care was taken not to disrupt the attachment of the soft tissues to the implants.

2.2.4 Histological Procedure

Specimens were analysed with hard grade resin histology.

2.2.4.1 Histological Processing

The specimens were fixed in 10% formal saline. Following this, they underwent ascending graded alcohol dehydration in LR White Resin (London Resin Company Ltd, Reading UK). The histological processing protocol used is detailed in Appendix 1.1.

2.2.4.2 Preparation of Histological Sections

The resin-embedded samples were cut transversely through the middle of each implant. The resulting blocks were glued onto slides with cyanoacrylate glue. The upper surface (the middle section of each implant) was ground flat using an Exakt-Micro-Grinding System (Mederex, Frome, UK). This flat surface was then glued onto a second glass slide using Technovit glue (Kulzer, Exakt, Germany) under an ultraviolet light source. After allowing the specimen to cool, a 300 μm section was cut away from the Technovit glue surface using an Exakt E310 diamond-edged band saw (Mederex, Frome, UK). The resulting sections were ground to thickness of 70 μm using the Exakt-Micro-Grinding System with 400, 1200, 2500 and 4000 grit paper and polished with alpha-alumina suspension (Struers, Denmark). A micrometer was used to measure the thickness of specimens (Mitutoyo Ltd, UK).

Once a smooth surface was achieved, the sections were stained with toluidine blue for 25 minutes before proceeding onto analysis under a Zeiss microscope. Toluidine blue stains nucleic acids blue as it has a high affinity for acidic tissue components (Sridharan and Shankar 2012). Further analysis was carried out after secondary staining with paragon for 25 minutes. Paragon is a polychromatic stain that stains

cellular components dark blue and connective tissue such as collagen pink (Vydyanath et al 2012).

2.2.4.3 Histological Analysis

The resulting cross-sections were divided into three zones: Zones 1 and 2 being the outer sections and Zone 3 being the central section of the implant (Figure 2.1). The following outcomes were assessed for each pore in each zone:

1. Percentage soft tissue fill - A semi-quantitative assessment of soft tissue fill within pores was carried out. This was scored by two independent assessors. A percentage for soft tissue fill was assigned based on the percentage of the pore that was filled with soft tissue as well as taking into account the density of the tissue within the pore compared with the tissue outside the implant. Figure 2.2 shows examples of percentage soft tissue fill scores.

2. Cell nuclei density - The numbers of nuclei per mm^2 were quantified to assess recellularisation.

3. Blood vessel density - The numbers of blood vessels per mm^2 were quantified to assess revascularisation.

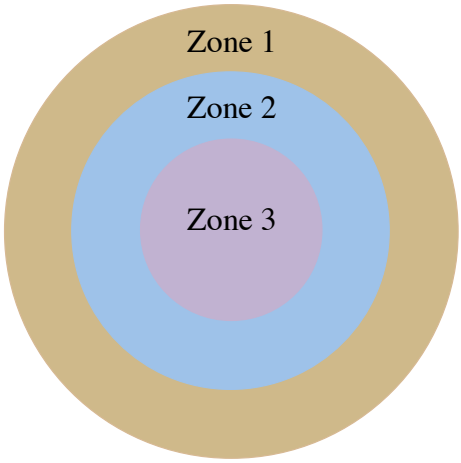

Figure 2.1 The three zones analysed for each histological section.

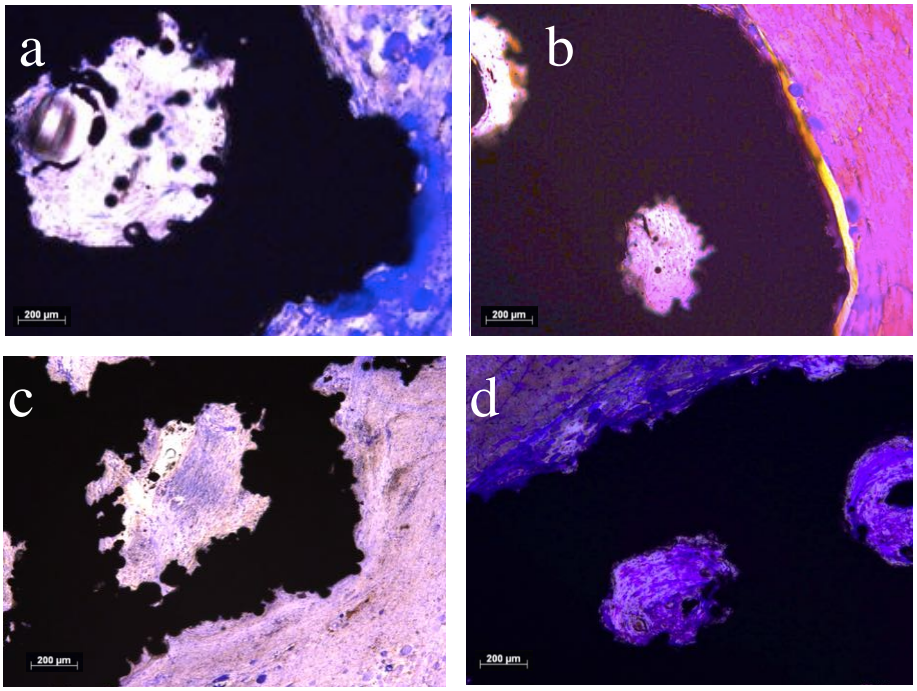

Figure 2.2 Semi-quantitative assessment of percentage soft tissue fill within pores (a) 25% (b) 50% (c) 75% (d) 100%.

2.2.5 Statistical Analysis

The data were analysed using SPSS, version 21.0 for Windows (Chicago, US). Non-parametric tests were performed. The Kruskall Wallis test was used to determine if differences existed between the groups. Pair-wise Mann-Whitney tests were used to determine differences between two porous structures. A p value of less than 0.05 was considered to be a statistically significant result. The Spearman's rho analysis was used to assess the correlation between variables. The intraclass correlation coefficient for agreement between the two assessors of the percentage soft tissue semi-quantitative score was calculated.

2.3 RESULTS

Soft tissue ingrowth was not seen in samples from group 9 (P250 S350); therefore, data were not collected for this group. Soft tissue was seen to penetrate through to the innermost pores in all other groups. The results from Zone 3, the innermost zone, are highlighted, as the quality of tissue that penetrates through to the centre of the implant is likely to be the best indicator of the overall success of soft tissue ingrowth.

2.3.1 Percentage Soft Tissue Fill

The intraclass correlation coefficient for agreement between the two independent assessors for the percentage soft tissue fill semi-quantitative score was 0.870 (95% confidence interval 0.822 to 0.906) (Appendix 2.4). The highest overall percentage fill scores were observed in the following pore/strut size combinations: P1000 S400, P1000 S200 and P700 S300. Soft tissue was present throughout all three zones of all implants from these groups. The ingrown tissue was dense and well organised displaying extensive collagen deposition with little open space and a well-ordered arrangement of collagen fibres. Intimate contact was observed both between the surrounding soft tissue and the implant surface and tissue within the pores and the struts. Increased collagen deposition was observed at the periphery of the pores and the struts. Very few gaps within the soft tissue were seen. Less densely organised tissue with more gaps within the tissue was present within the remaining pore and strut size combinations (i.e. P700 S400, P700 S200 and all three P500 groups) (Figure 2.3).

P1000 S400 was associated with significantly greater percentage fill than P700 S400 in all three zones ($p=0.010$). There were no significant differences between P1000 S200 and P700 S200 (Zone 1 $p=0.101$, Zone 2 $p=0.138$, Zone 3 $p=0.445$). There were no significant differences between P700 S300 and P700 S200 (Zone 1 $p=0.177$, Zone 2 $p=0.792$, Zone 3 $p=0.329$). Within Zone 3, P700 S300 was associated with greater percentage soft tissue fill than P500 S300 ($p=0.003$). No differences were observed between P700 S400 and P500 S400 ($p=0.484$) or between P700 S200 and P500 S200 ($p=0.101$) (Figures 2.4 to 2.6).

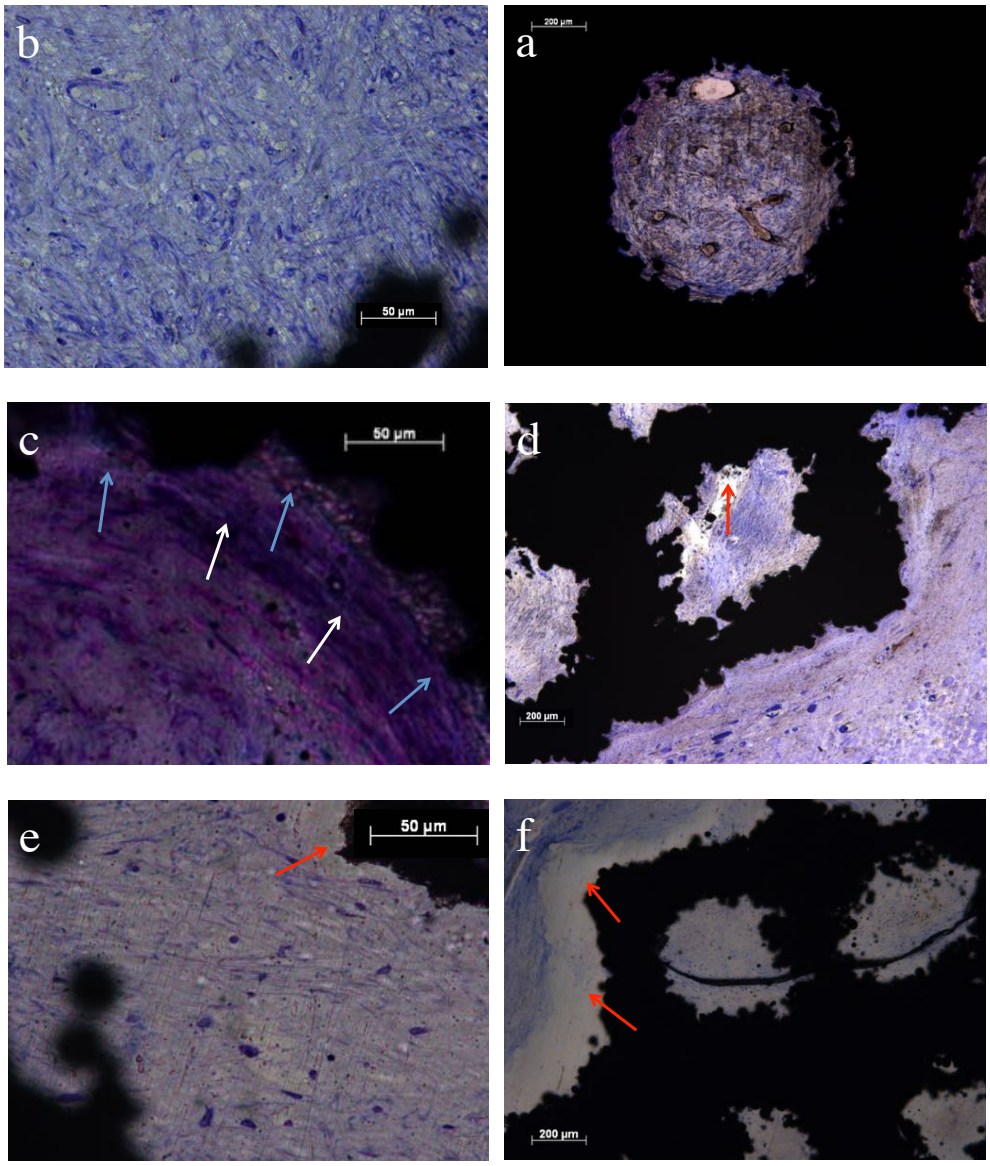

Figure 2.3 (a) and (b) P1000 S400 Zone 3 - densely ordered tissue filling pore. (c) P700 S300 Zone 3 - dense tissue with intimate contact between pore edges and soft tissue (blue arrows) and increased tissue density at the pore periphery (white arrows). (d) P700 S200 Zone 1 - gap in soft tissue (red arrow). (e) P500 S300 Zone 3 - less dense soft tissue infiltration with gap in soft tissue at pore periphery (red arrow). (f) P500 S200 Zone 1 - sparse soft tissue infiltration and lack of contact between soft tissue and periphery of implant (red arrows).

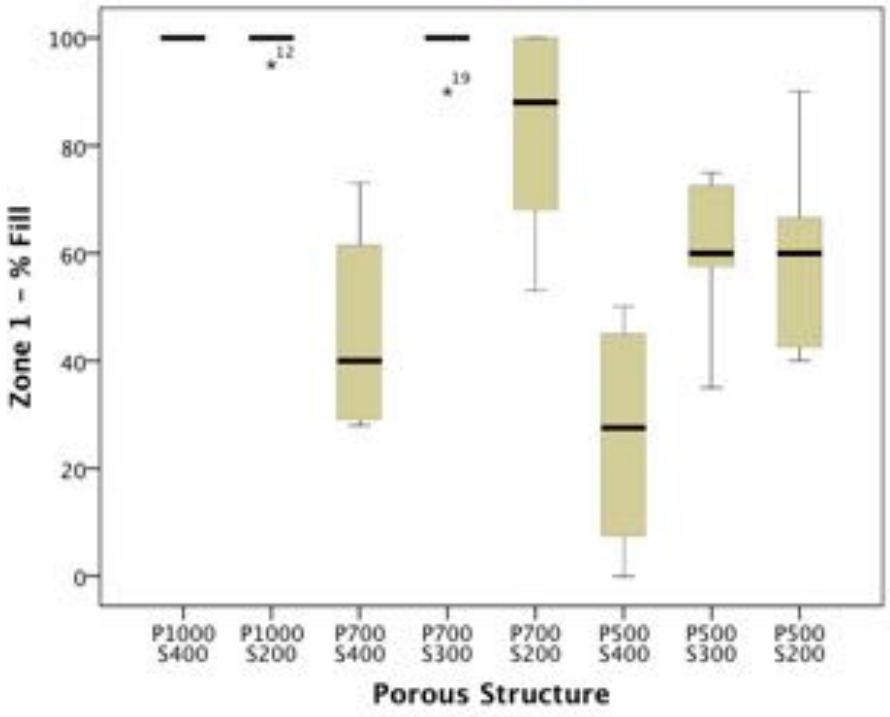

Figure 2.4 Box-and-whisker plot showing percentage fill in Zone 1.

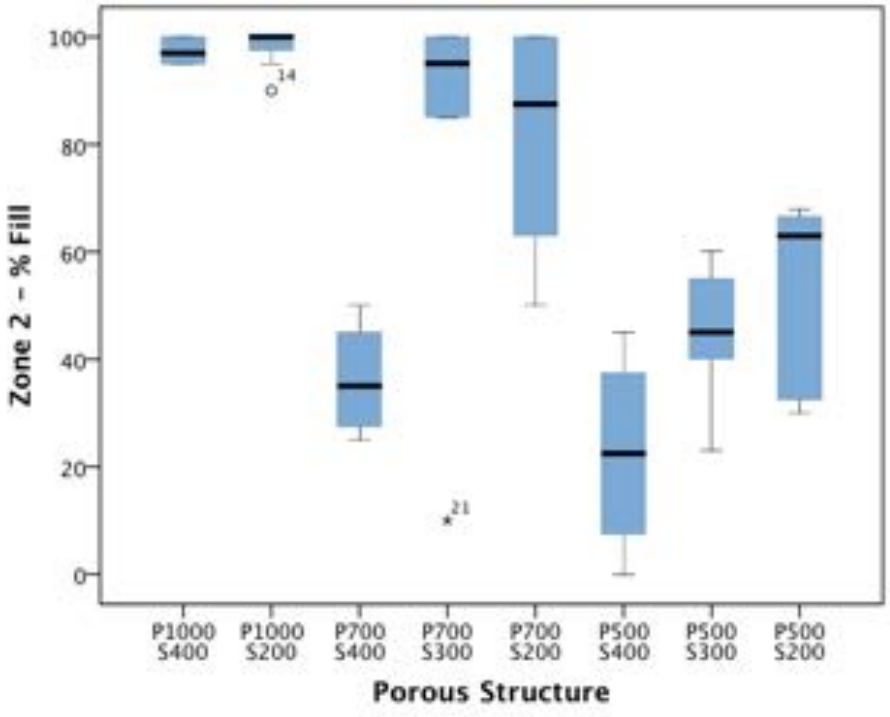

Figure 2.5 Box-and-whisker plot showing percentage fill in Zone 2.

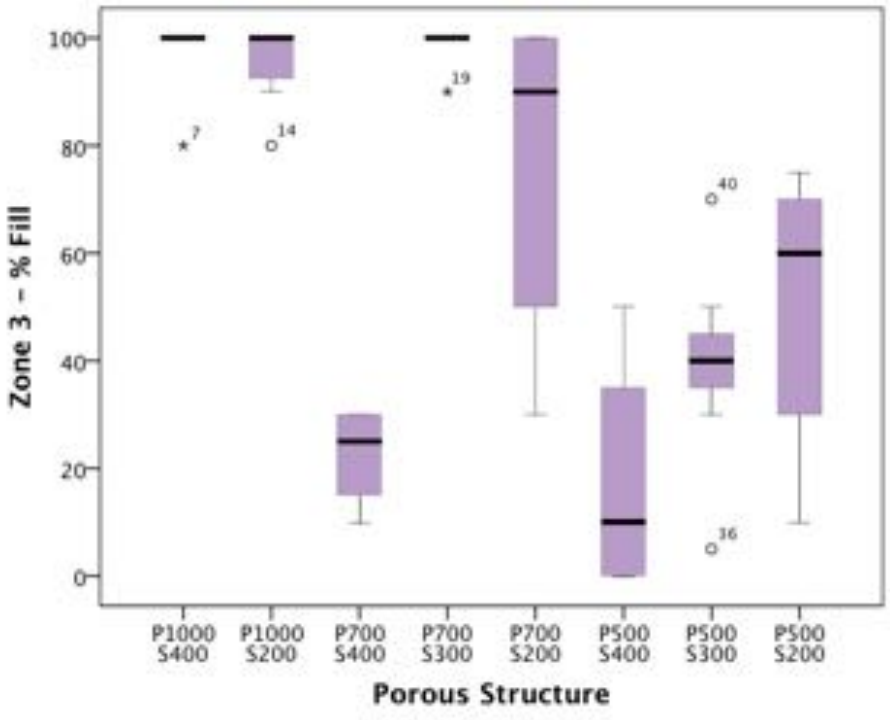

Figure 2.6 Box-and-whisker plot showing percentage fill in Zone 3.

2.3.2 Cell Nuclei Density

In keeping with the findings for percentage soft tissue fill, cell nuclei density was greatest for P1000 S400, P1000 S200 and P700 S300. Within Zone 3, although P1000 S200 had the highest cell nuclei numbers, there was no significant difference when compared with P1000 S400 ($p=0.073$). P1000 S200 was associated with greater cell nuclei density within Zone 3 than P700 S200 and P500 S200 ($p=0.006$ and 0.001 respectively). Cell nuclei density within Zone 3 was greater for P700 S300 than P700 S400 and P700 S200 ($p=0.016$ and 0.03 respectively) (Figures 2.7 to 2.10).

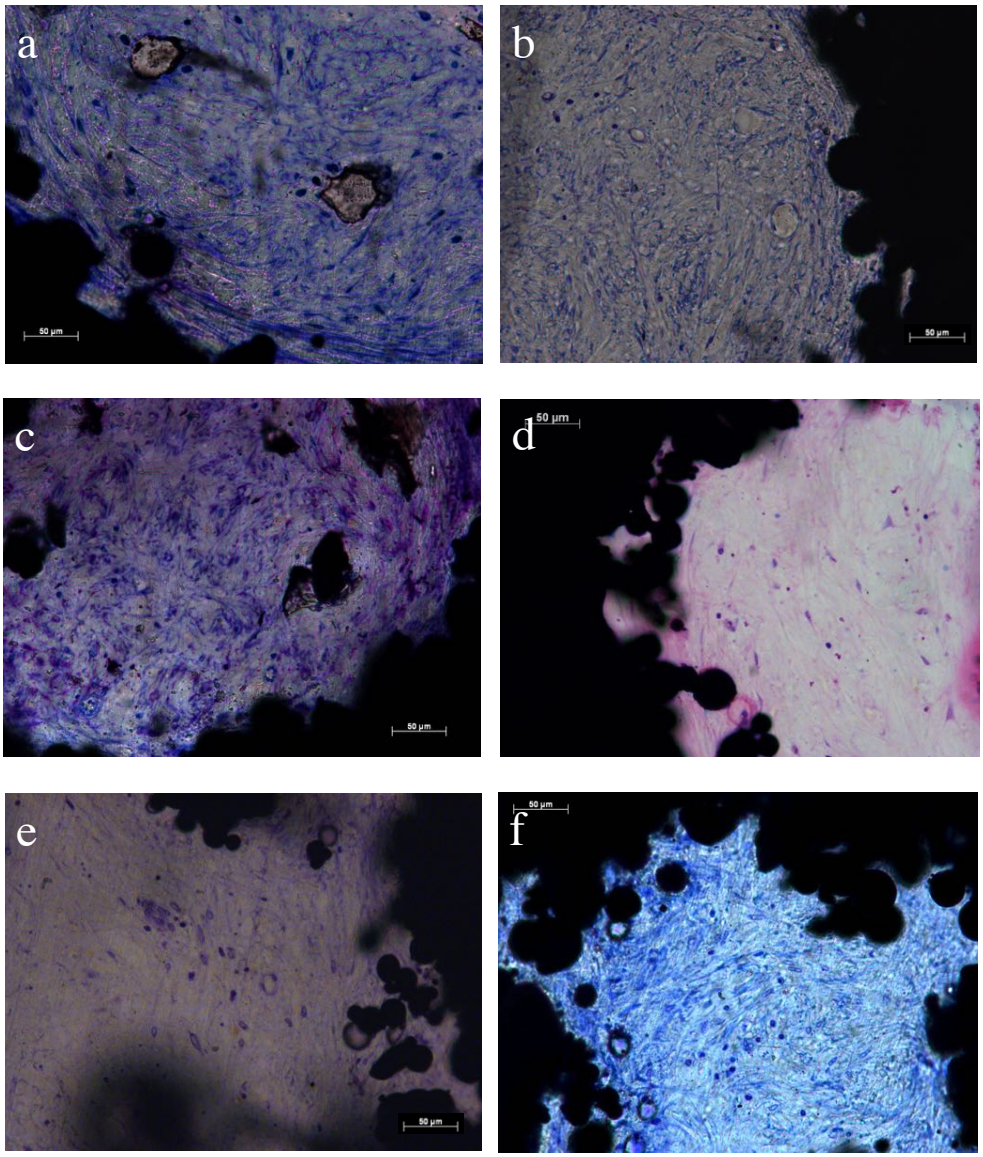

Figure 2.7 Histological sections demonstrating cell density in Zone 3 of the following implants: (a) P1000 S400 (b) P1000 S200 (c) P700 S300 (d) P700 400 (e) P500 S400 (f) P500 S300. Cell nuclei density is greatest in (a) to (c).

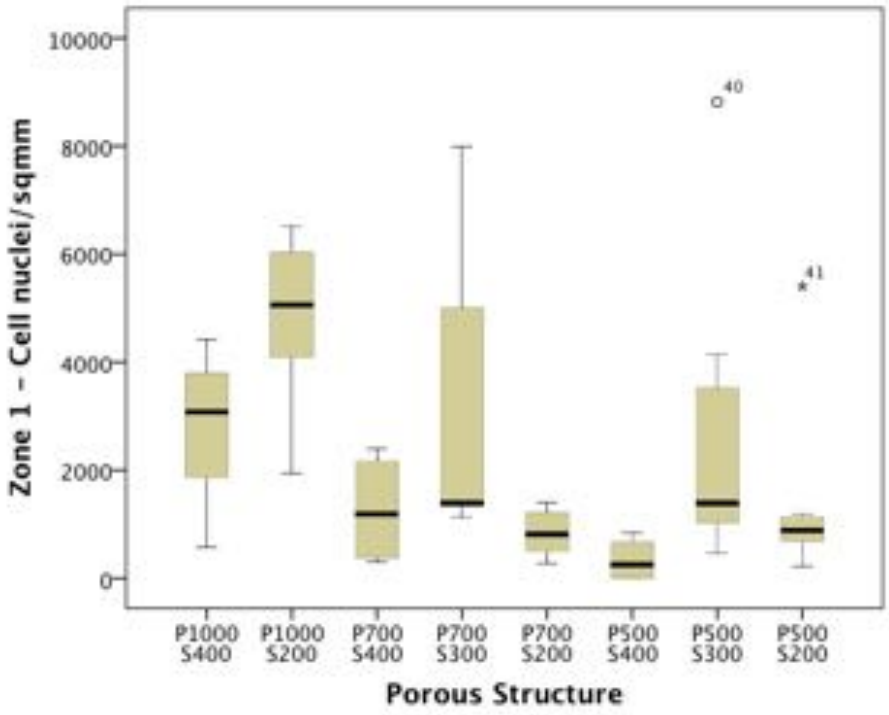

Figure 2.8 Box-and-whisker plot showing cell nuclei density in Zone 1.

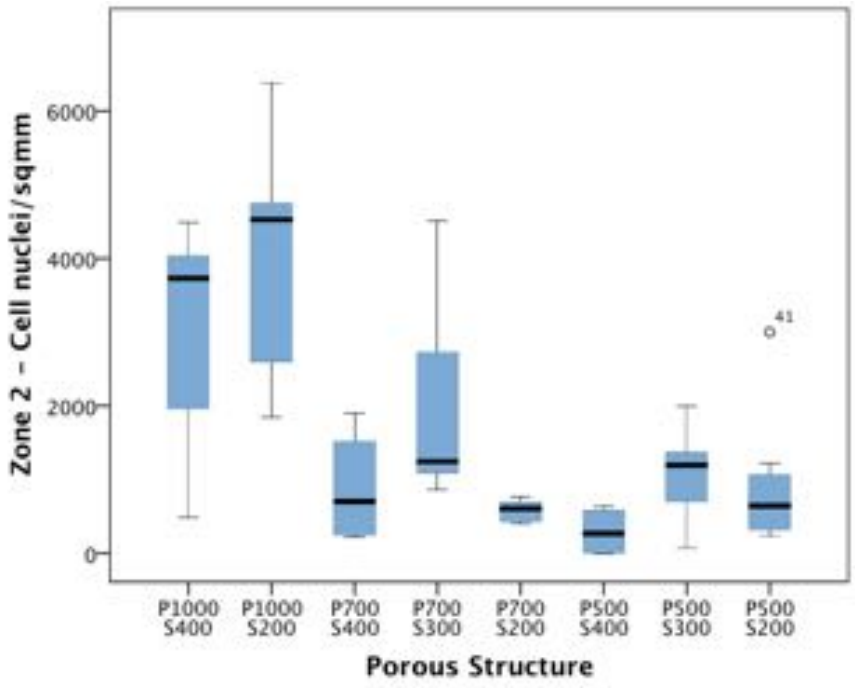

Figure 2.9 Box-and-whisker plot showing cell nuclei density in Zone 2.

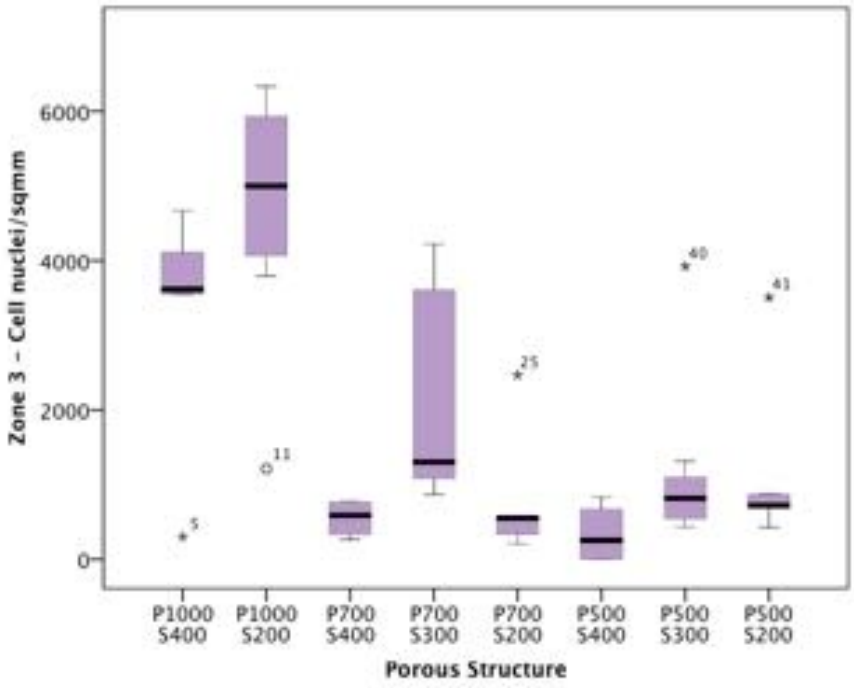

Figure 2.10 Box-and-whisker plot showing cell nuclei density in Zone 3.

2.3.3 Blood Vessel Density

The greatest blood vessel density was observed within P1000 S400, P1000 S200 and P700 S300 implants. This was the case within all three zones. Within Zone 3, P700 S300 was associated with the highest blood vessel density and was associated with a significantly greater blood vessel density than both P700 S200 and P500 S300 ($p=0.004$ and 0.005 respectively). P1000 S200 was associated with greater blood vessel density than P700 S200 ($p=0.001$), but there was no statistically significant difference between P1000 S200 and P500 S200 ($p=0.456$). There was no significant difference between P1000 400 and P700 S400 and P500 S400 ($p=0.914$ and 0.352 respectively). Very sparse blood vessel ingrowth was observed within Zone 3 for P700 200, P500 400 and P500 200. (Figures 2.11 to 2.14).

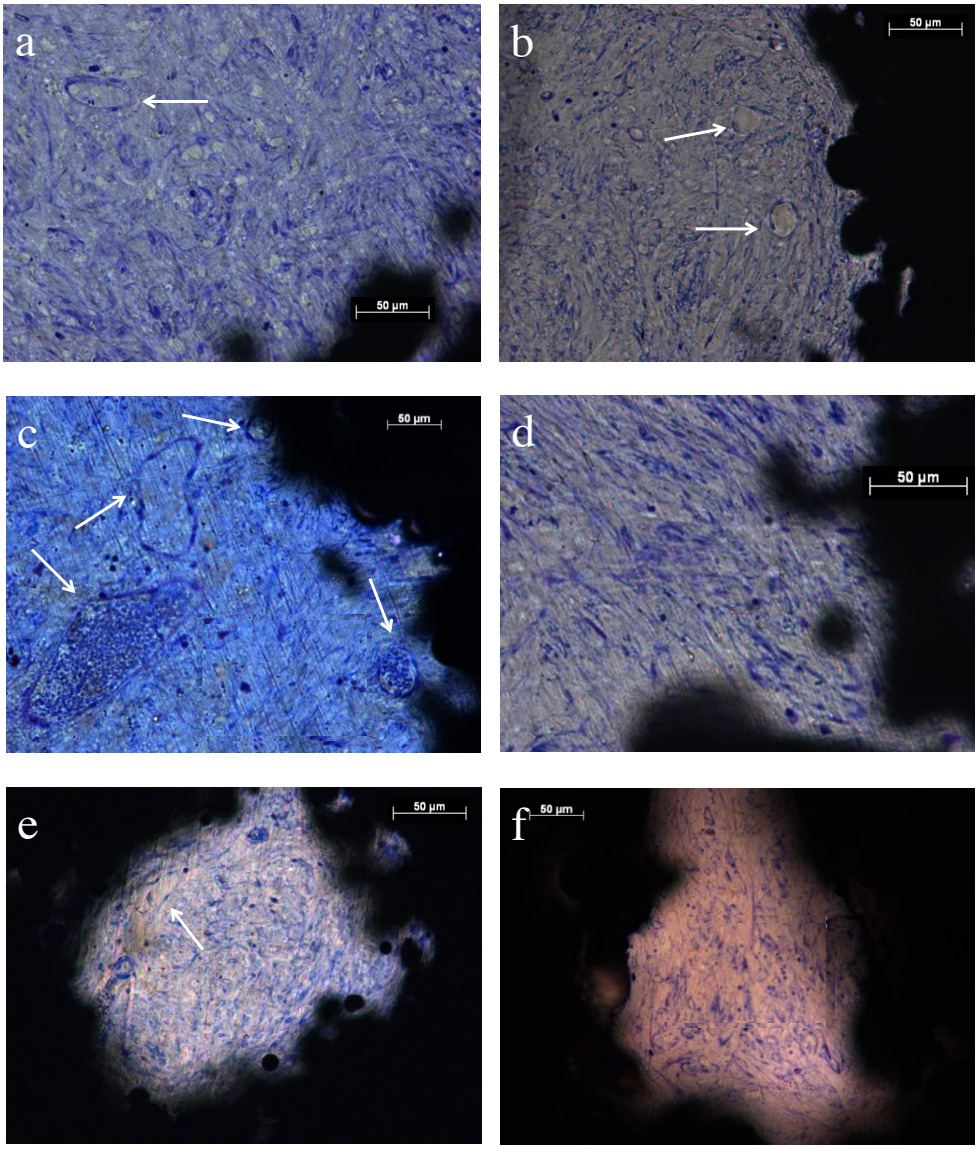

Figure 2.11 Histological sections demonstrating blood vessel ingrowth in Zone 3 of the following implants: (a) P1000 S400 (b) P1000 S200 (c) P700 S300 (d) P700 200 (e) P700 S400 (f) P500 S200. The arrows indicate blood vessels. In (a) to (c) higher numbers of blood vessels are present than in (d) to (f).

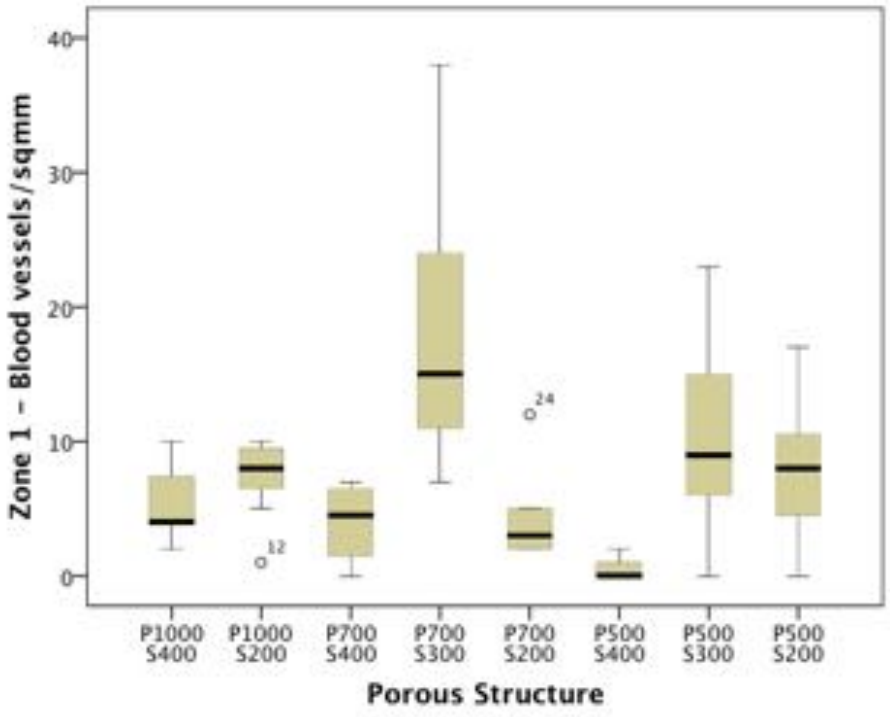

Figure 2.12 Box-and-whisker plot showing blood vessel density in Zone 1.

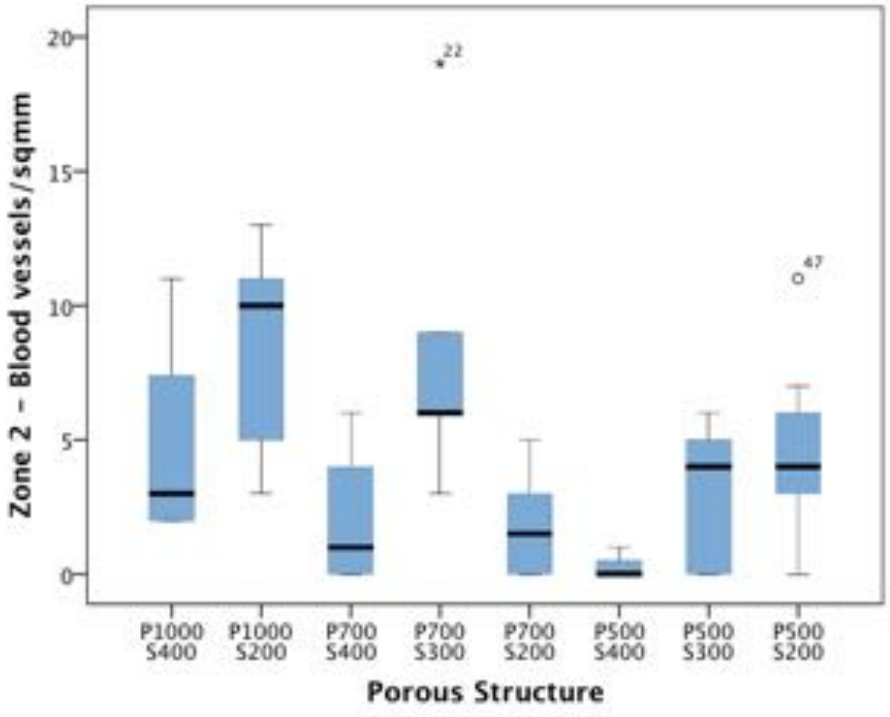

Figure 2.13 Box-and-whisker plot showing blood vessel density in Zone 2.

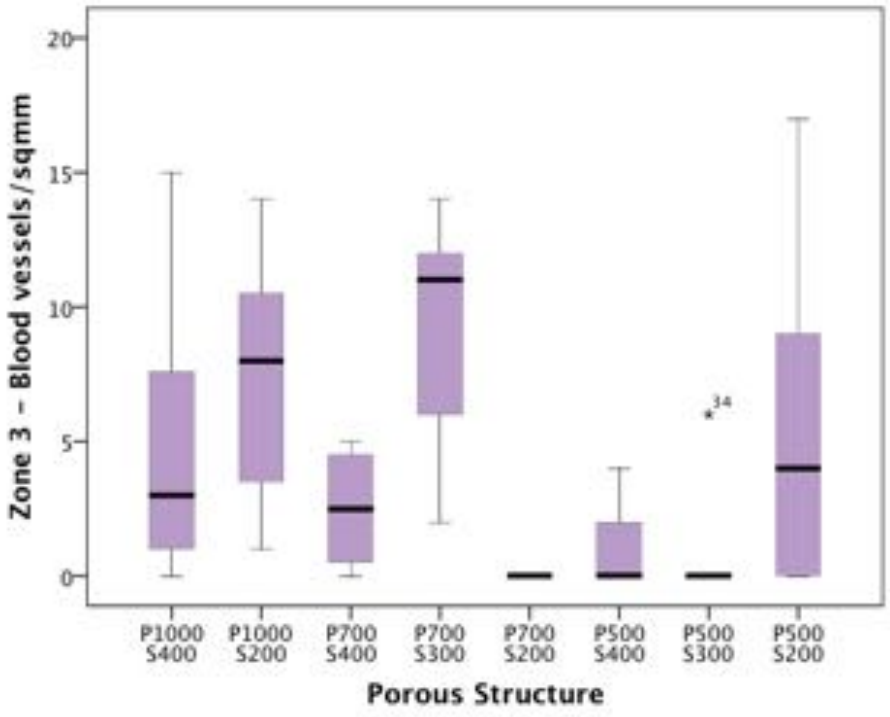

Figure 2.14 Box-and-whisker plot showing blood vessel density in Zone 3.

2.3.4 Correlation Analysis

The Spearman's rho analysis showed positive correlations between percentage soft tissue fill of pores and cell nuclei density, which were significant at the 0.01 level (Zone 3: p=0.000, Correlation coefficient=0.621). Weaker positive correlations were identified between percentage soft tissue fill and blood vessel density. These were significant at the 0.01 level (Zone 3: p=0.003, Correlation coefficient=0.432). Positive correlations were also identified between cell nuclei and blood vessel density. These were significant at the 0.01 level (Zone 3: p=0.000, Correlation coefficient=0.503). Strong positive correlations were observed between the three zones for percentage soft tissue fill, cell nuclei density and blood vessel density (Appendix 2.3). Figures 2.15 to 2.18 are graphs illustrating correlations between variables.

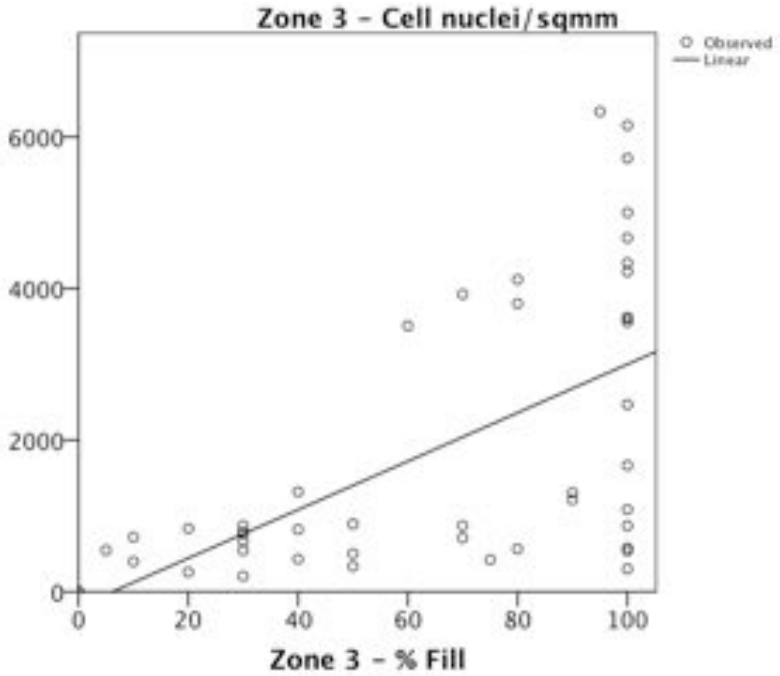

Figure 2.15 Graph showing the relationship between cell nuclei density and percentage soft tissue fill. There is an increase in cell nuclei density with increasing percentage soft tissue fill.

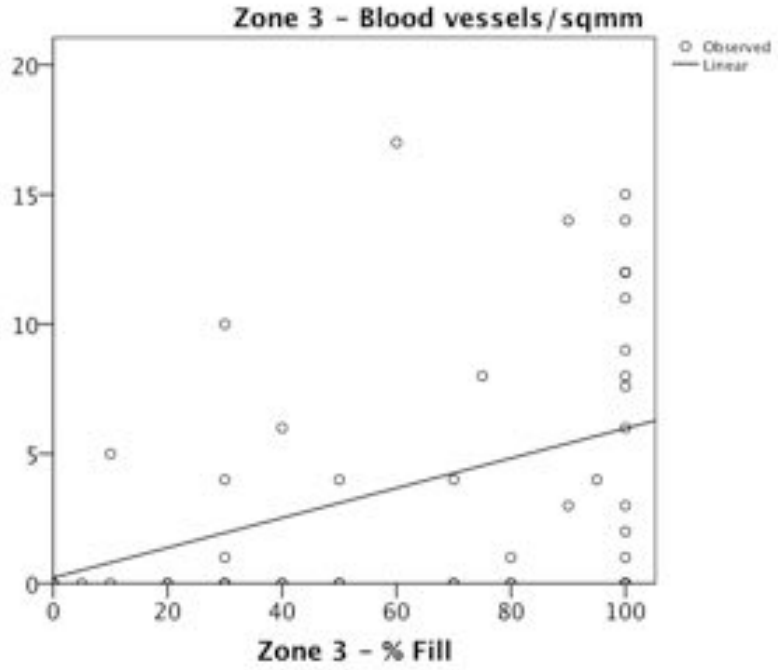

Figure 2.16 Graph showing positive correlation between percentage soft tissue fill and blood vessel density.

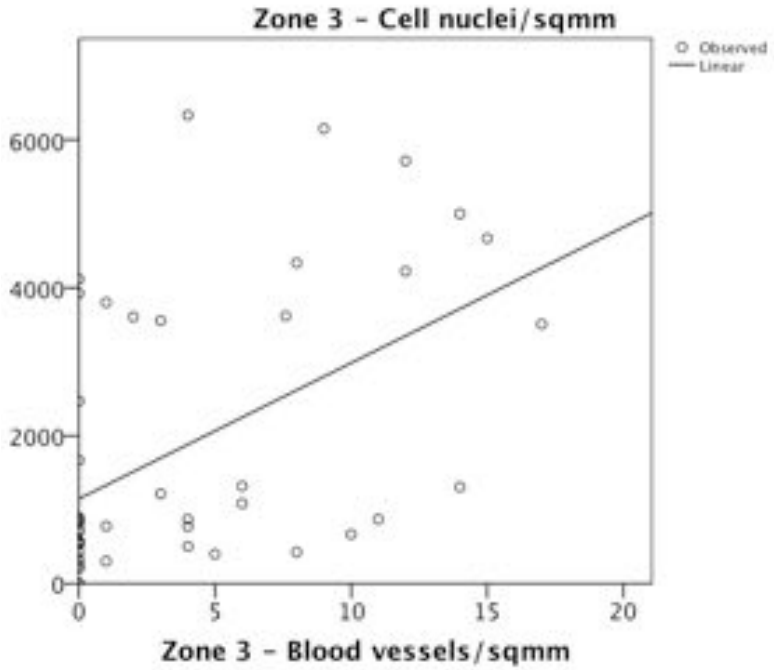

Figure 2.17 Graph showing the positive correlation between blood vessel and cell nuclei density.

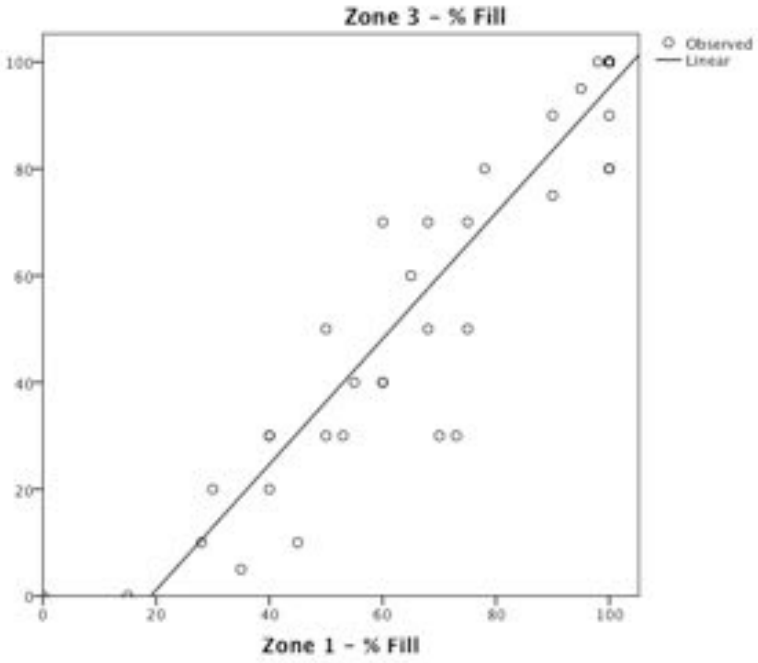

Figure 2.18 Graph showing the strong positive correlation between Zone 1 and Zone 3 for percentage soft tissue fill (p=0.000, Correlation coefficient= 0.941).

2.4 DISCUSSION

This study has contributed to the current literature by quantifying soft tissue ingrowth and by assessing the effects of a range of pore and strut size combinations. Three combinations resulted in the greatest soft tissue ingrowth and vascularisation: P1000 S400, P1000 S200 and P700 S300. In general, results for P500 were less favourable than results for the larger pore sizes. Furthermore, there was no soft tissue ingrowth into P250 implants. These findings support the hypothesis that open structures with larger pore sizes facilitate soft tissue ingrowth.

Reasons for Increased Soft Tissue Ingrowth into Larger Pore Sizes

The increased vascularisation associated with larger pore sizes is expected to play a role in increasing soft tissue ingrowth. Vascularisation promotes healthy tissue ingrowth as it results in oxygenation and provision of nutrients to tissues as well as removal of waste products (Jain et al 2005). Therefore, increased vascularisation is beneficial when aiming to enhance tissue attachment strength. It is also intuitive that the larger pores provide more space for healthy tissue to fill, which in turn may allow greater blood vessel ingrowth. However, the findings of Feng et al (2011) do not support this. They implanted β-tricalcium phosphate cylinders with pore sizes ranging from 300 to 700 μm into the lumbodorsal fascia in rabbits and found that pore sizes less than 400 μm limited blood vessel growth, which is in keeping with the results from this chapter. However, in contrast to this chapter they found that pore sizes above 400 μm did not produce further increases in vascularisation. Furthermore, in contrast to this chapter they found that the reduced vascularisation observed with pore sizes less than 400 μm was not associated with reduced tissue ingrowth. They demonstrated increases in percentage fibrous tissue ingrowth with decreasing pore size (Feng et al 2011). These results indicate that factors other than vascularisation are likely to contribute to increased tissue ingrowth. The strut sizes used may contribute to the differences in findings between this chapter and those of Feng et al. Feng et al used a constant interconnection size of 120 μm which is smaller than the sizes used in this chapter. However, despite this, the findings of this chapter do not completely contradict those of Feng et al. Although this chapter has

shown positive correlations between blood vessel density and percentage soft tissue fill, the fact that these correlations were not of high strength also suggests that other factors contribute to the increased tissue ingrowth.

Larger pore sizes promote cell migration. It is known that if pores are too small, cells are unable to migrate through scaffolds. Additionally a cellular capsule forms around the edges of the scaffold, which can limit diffusion of nutrients and removal of waste products (Yannas et al 1992; O'Brien et al 2007; Murphy et al 2010). Murphy et al (2010) studied *in vitro* adhesion and early proliferation of a pre-osteoblastic cell line on collagen-glycosaminoglycan scaffolds up to seven days post-seeding. Although, they studied a different cell type and scaffold type and a smaller range of pore sizes (85 to 325 μm), the findings are relevant to explaining some of the results of this chapter. They showed that larger pore sizes improve cellular infiltration into scaffolds with even cell distribution. They found that with larger pore sizes cells migrated from the edges into the centre of the scaffolds whereas with smaller pore sizes cell aggregation was seen along the edges of the scaffolds limiting the number of cells infiltrating the scaffolds. The aggregations found with smaller pore sizes at this early time-point formed a 'skin' around the outer surface of the scaffolds, which restricts the diffusion of nutrients and removal of waste from the cells colonising the centre of the scaffold. The authors did however identify an early additional peak in cell number in scaffolds with a mean pore size of 120 μm at time points up to 48 hours post-seeding. They showed that specific surface area is greater for smaller pore sizes. This explains this peak, as specific surface area increases cell infiltration and tissue ingrowth. However, they concluded that the effect of specific surface area is overcome by larger pores due to the importance of increased cell migration and proliferation and the reduced cell aggregations along the edges of the scaffold (Murphy et al 2010).

Selection of a Porous Structure for the ITAP Flange

Overall, there were few differences or clear advantages between the three structures found to promote the soft tissue ingrowth to the greatest degree in this chapter.

P1000 S200 resulted in the greatest cell nuclei density. Increased cell nuclei density is important as fibroblasts secrete collagen. P700 S300 produced the greatest vascularisation. These results provide three options for porous flange structures that would be suitable for use in further studies of ITAP. It was decided that P700 S300 would be used in further studies due to its effects on promoting vascularisation. Additionally, as overall P1000 S400 and P1000 S200 structures did not have a clear advantage over P700 S300, P700 S300 would be preferable as structurally it is likely to result in less risk of flange breakage. This is because the larger the pore size, the greater the void volume, which may compromise the mechanical properties of the scaffold (Karageorgiou and Kaplan 2005).

Differences in Minimum Pore Size for Soft Tissue Ingrowth with Other Studies

Although, it was hypothesised that smaller pore sizes would be associated with less favourable results, it is interesting that there was a complete absence of soft tissue ingrowth into the P250 S300 structure. Other studies have shown soft tissue ingrowth into pores of this size and smaller. For example, Farrell et al (2014) used small pore sizes (40 to 160 μm) but demonstrated soft tissue ingrowth. However, the degree of soft tissue fill of pores was 30 to 50% which is considerably less than that observed in the implants with pore sizes of 500 to 1000 μm studied in this chapter (Farrell et al 2014). Differences in tissue morphology may have contributed to the observation of soft tissue ingrowth into smaller pore sizes as Farrell et al's study was conducted in rodents. Furthermore, as mentioned earlier, the effect of strut size may also have contributed to differences in results between this chapter and other studies. It is possible that if smaller strut sizes were used in combination with pores sizes of 250 μm the results may have been different.

It is also interesting to note that the mean pore size of the deer antler pedicle is 217 μm, which is considerably smaller than the pore sizes that resulted in favourable results in this study (Pendegrass et al 2006b). Other factors such as the surface chemistry and the presence of proteins such as fibronectin may play a role in the fact that smaller pore sizes promote soft tissue ingrowth into the deer antler pedicle. The

use of biological coatings may have the potential to enhance soft tissue ingrowth into porous titanium alloy structures in general (including those with smaller pore sizes). Additionally, the deer antler pedicle protrudes from the frontal bones of the skull of the animal and is thus immobilised, resulting in less motion at the interface, which may promote better soft tissue infiltration. Similarly, a transcutaneous pin model with the implants fixed to bone would result in less motion at the soft tissue-implant interface and potentially better soft tissue ingrowth results in general, including for smaller pore sizes. In clinical practice, soft tissue infiltration results could potentially also be improved in general (i.e. for all pore sizes) due to the surgical technique. The surgical technique for implantation of ITAP (in humans) includes thinning of the soft tissues and suturing of the thinned skin flap to the drilled-hole flange providing further immobilisation of the tissues (Kang et al 2010). It would, however, be technically more difficult to suture through a fully porous implant due to the needle being obstructed by adjacent layers of pores. Therefore, separate dedicated pores for suture fixation (not obstructed by adjacent layers) could be added to the side of the implant to solve this problem. The theory that suturing the soft tissue could result in better soft tissue infiltration is supported by Bobyn et al's study (1982). Porous implants were implanted into dorsal flank subcutaneous tissue in a canine model. Soft tissue ingrowth was demonstrated with small pore sizes ranging from 5 to 200 μm. They had secured the implants in place with suture fixation at the time of implantation (Bobyn et al 1982).

Upper Limit for the Degree of Openness of Porous Structures for Promoting Soft Tissue Ingrowth

In keeping with the principle that open structures are beneficial, P700 S400 did not promote soft tissue ingrowth as much as P700 S300. It is expected that this is due to the fact that the larger strut size reduces the volumetric porosity and takes up free space. However, it is important to note that porosity does not explain all the results of this study. Firstly, when pore size was decreased but strut size also decreased proportionally there were differences and soft tissue ingrowth was impaired e.g. P1000 S400 was associated with significantly better soft tissue ingrowth than P500 S200. This suggests that pore size itself (separate to porosity) was a key factor

affecting soft tissue ingrowth. However, results for P700 S200 did not fit in with the principle that open structures were better or that pore size is the main factor. P700 S200 did not perform as well as P700 S300. This means that the relationship between pore size and soft tissue ingrowth is not linear. Open structures are needed for soft tissue ingrowth, but for a given pore reducing the strut size and hence increasing the degree of openness increases soft tissue ingrowth only up to a point. If a larger range of strut sizes had been studied for a given pore size it would have provided more information about what this point is. The results of this study suggest that the point at which reducing strut size for P700 structures reduces soft tissue ingrowth is when the strut size is between 300 and 200 μm.

The finding that there is an upper limit for a beneficial effect for openness of porous structures is in keeping with the findings of Pendegrass et al (2010) (Pendegrass et a 2010a). They studied pore sizes of 500, 700 and 1000 μm, but did not alter strut size. The implants had drilled holes and were not fully porous structures as used in this study; however, the findings are relevant. The implants were subcutaneous plates implanted onto the medial aspect of sheep tibiae. The implants were removed after four weeks and soft tissue attachment was examined histologically. Similarly to the findings of this chapter, it was found that a pore size of 700 μm resulted in better soft tissue ingrowth than 500 μm. Pores of 500 μm diameter resulted in a contracted band of dermis with a clear gap between the soft tissue and the internal pore margins. Often the tissue did not fully traverse the complete pore. Pores of 700 μm diameter resulted in greater contact and significantly more perpendicular cell nuclei indicating better soft tissue attachment. In contrast to the findings of this chapter, 1000 μm pores had a detrimental effect. Pores of 1000 μm diameter demonstrated pegs of dermis not completely traversing the pores with one-sided dermal attachment often noted. It is possible that a reason this chapter did not find this detrimental effect with 1000 μm pores is that the advantage of an interconnecting fully porous structure meant that any negative effect of a pore size of 1000 μm was overcome. However, if this is the case, it is unknown if in the long term the disadvantageous effects of 1000 μm pores will occur. This supports the choice of P700 S300 for future study rather than P1000 S400 or P1000 S200. It is expected that the reason Pendegrass et al found

that pores of 1000 μm produced less favourable results is because if pores are too large, the decrease in surface area limits cell adhesion as discussed earlier (Murphy et al 2010).

Pore Size and Bacterial Colonisation

This study has resulted in the selection of an open porous structure with a larger pore size (P700 S300) for further *in vivo* testing with the ultimate aim of encouraging fibroblasts to win the 'race for surface' and prevent bacterial colonisation. This study has not assessed bacterial colonisation but this will be studied in subsequent chapters of this thesis. Braem et al (2013) conducted quantitative analyses of *in vitro* bacterial colonisation on porous titanium and showed that increasing pore size is associated with an increase in roughness parameters leading to an increase in bacterial attachment (Braem et al 2013). Therefore, it will be interesting to determine if the soft tissue ingrowth promoted by the porous structure selected by this chapter will overcome the possible detrimental effects of large pore sizes on bacterial colonisation. Chemical modification of titanium surfaces to increase hydrophilicity reduces bacterial numbers suggesting that functionalisation to reduce the infection risk of porous coatings may be of value (Braem et al 2014). These previous studies have not assessed the bacterial colonisation in an *in vivo* model, when soft tissue attachment is also occurring. Further *in vivo* transcutaneous pin studies (Chapter Six and Seven) will study this gap in the current knowledge by assessing the *in vivo* effect of P700 S300 titanium alloy flanges with and without bioactive and antimicrobial coatings on both soft tissue attachment and bacterial colonisation.

Limitations of This Study

As discussed earlier a transcutaneous pin model would be more representative and would limit the mobility of the soft tissues at the interface, which is likely to affect the results. Additionally, the model used in this chapter did not specifically assess dermal tissue integration as the implants were inserted into the paraspinal muscles. A transcutaneous pin model will be used for further *in vivo* studies that will be presented in this thesis.

It could be argued that the use of a semiquantitative assessment of percentage soft tissue fill is another limitation as different assessors could potentially interpret findings differently. In order to estimate the likelihood of this, the assessment was carried out by two independent observers. The intraclass correlation coefficient of 0.870 for agreement between the two assessors indicated that the semi-quantitative score had a high level of interobserver reliability. Furthermore, quantitative assessments of cell nuclei density and blood vessel density were carried out. However, a limitation of the quantitative assessment is that the number of blood vessels was quantified, however, the size of blood vessels was not taken into account. The size of blood vessels may affect vascularisation.

This study did not perform mechanical testing. It is noted that other studies that have performed mechanical testing have shown that the histological findings support strength of attachment results (La Berge et al 1990; Hacking et al 2000). Mechanical testing by other researchers has shown that increased pore size is associated with increased soft tissue attachment strength (Bobyn et al 1982; La Berge et al 1990).

Finally, the time period of four weeks for this study was short. It is known that as time increases soft tissue attachment increases (Bobyn et al 1982; La Berge et al 1990). A study with a longer time period may have provided useful information. For example, it would have been possible to determine if the detrimental effects of pore sizes of 1000 μm identified by the study of drilled holes by Pendegrass et al (2010) become apparent with a fully porous structure over time. However, if significantly longer time periods were studied it would mean obtaining meaningful results for cell nuclei density would be unlikely. This is because it is likely that there would be too many cells present to see distinctly as separate nuclei that are quantifiable. Additionally, an assessment of early attachment is essential as early soft tissue attachment is the key factor affecting the outcome of the 'race for the surface.'

2.5 CONCLUSION

This chapter has quantified percentage soft tissue fill, cell nuclei and blood vessel density associated with a range of porous titanium alloy structures. The results show that larger pores sizes are supportive of soft tissue ingrowth. P1000 S400, P1000 S200 and P700 S300 resulted in the greatest soft tissue ingrowth. P700 S300 supported blood vessel ingrowth to the greatest degree and therefore a fully porous ITAP flange with this structure will be designed (Chapter Five). This flange will be assessed in future *in vivo* studies of ITAP (Chapters Six and Seven). The following chapters (Chapters Three and Four) will develop a fibronectin-functionalised hydroxyapatite coating with silver incorporated into it that will be used to coat the porous flange to determine if this has additional effects on soft tissue integration and bacterial colonisation.

CHAPTER THREE

In Vitro Assessment of the Effects of Hydroxyapatite, Silver and Fibronectin on Fibroblast Viability

3.1 INTRODUCTION

Bioactive coatings such as hydroxyapatite and fibronectin may be applied to porous titanium to further enhance soft tissue integration. Fibronectin-functionalised hydroxyapatite coatings have been found to improve *in vitro* fibroblast attachment compared with hydroxyapatite, uncoated titanium or titanium with adsorbed fibronectin (Pendegrass et al 2010a). Studies on other cell types including mesenchymal stem cells and osteoblasts have also shown that hydroxyapatite with fibronectin or the RGD sequence improves cellular responses such as cell spreading, proliferation and attachment (Sawyer et al 2005; Deligianni et al 2006; Sogo et al 2007; Dolatshahi-Pirouz et al 2011). A histological assessment of *in vivo* soft tissue attachment to subcutaneous plates with drilled holes and hydroxyapatite coatings has shown an improvement in dermal contact and ingrowth with fibronectin adsorption (Pendegrass et al 2010a). Another *in vivo* assessment has shown significantly more perpendicular dermal fibroblast alignment relative to the implant when fibronectin is adsorbed onto hydroxyapatite-coated solid subcutaneous plates compared with hydroxyapatite alone, indicating an improvement in ingrowth (Chimutengwende-Gordon et al 2011).

As discussed in Chapter One, a potential disadvantage of the use of fibronectin-functionalised hydroxyapatite coatings is that they could increase bacterial colonisation and the risk of peri-implant infection (Smith et al 2006; Laure et al 2008; Henderson et al 2010). Therefore, during the early postoperative period before the soft tissue seal has formed, the addition of an antimicrobial agent may be useful to prevent bacterial colonisation. This study explores the incorporation of silver into fibronectin-functionalised hydroxyapatite coatings. Silver was selected over other antimicrobials due to its broad spectrum of activity against both gram-positive and gram-negative bacteria as well as fungi. Additionally, silver's known action against numerous antibiotic-resistant strains e.g. methicillin resistant *Staphylococcus epidermidis*, methicillin resistant *Staphylococcus aureus* and antibiotic resistant *Pseudomonas*, *Acinetobacter* and *Enteroccoccus* species, could be beneficial clinically (Wright et al 1998; Alt et al 2004; Agarwal et al 2010; Percival et al 2011).

Electrochemical deposition is a technique that may be used to incorporate silver into hydroxyapatite coatings. The technique involves precipitation from an aqueous electrolyte solution containing calcium phosphate and silver nitrate. An electric current passed through the solution results in positively charged ions from the solution being attracted to the implant, which acts as a cathode and is consequently coated. Advantages of electrochemical deposition include that it takes place at low temperatures, allows control of coating composition and is economical. It is a non-line-of-sight technique that is capable of coating complex structures (Garcia-Gareta et al 2013). This is important because it would enable coating of the inner pores of an ITAP flange fabricated from porous titanium. Other more commonly commercially available methods such as plasma spraying are not able to do this (Garcia-Gareta et al 2014). Ghani et al (2012) modified Redepenning et al's technique of electrochemical deposition by impregnating hydroxyapatite with silver ions (Redepenning et al 1996; Ghani et al 2012). The silver-containing hydroxyapatite coating produced was uniform, crystalline, antibacterial and resulted in a sustained release of silver over 22 days (Ghani et al 2012).

It is essential that preliminary experiments are conducted *in vitro* to assess the effects of these silver-containing coatings on dermal fibroblast viability before use in an *in vivo* model. Silver is known to have dose-dependent cytotoxic effects (Agarwal et al 2010). If the concentration of silver used is too high, fibroblast viability will be impaired which would prevent or delay the formation of a soft tissue seal. However, when used at lower concentrations, silver has been shown to maintain its antibacterial activity without being cytotoxic (Bosetti et al 2002; Alt et al 2004; Chen et al 2006; Agarwal et al 2010). For example, Agarwal et al (2010) developed polymeric thin films with silver contents as low as 0.4 $\mu g/cm^2$. They found that these low silver content films were able to achieve a 99.9999% reduction in *Staphylococcus epidermidis* colonisation in suspensions incubated in contact with the films without being toxic to fibroblasts (Agarwal et al 2010).

The *in vitro* biocompatibility of antibacterial silver-containing hydroxyapatite coatings produced by a range of methods including magnetron co-sputtering (Chen et al 2006), ion-beam assisted deposition (Feng et al 1999; Bai et al 2011), the sol-gel technique (Jadalannagari et al 2014) and electrodeposition (Lu et al 2011) has shown a lack of cytotoxicity to cell types such as osteoblasts, osteoblast precursors and macrophages. Fibroblast viability has been assessed on plasma-sprayed silver-containing hydroxyapatite coatings and was found to be cytocompatible (Chen et al 2008). However, fibroblast viability on electrochemically deposited silver-containing hydroxyapatite coatings specifically needs to be determined. The effect of this coating in combination with fibronectin has also not been studied. Furthermore, the cytotoxic effects of the specific silver/HA electrochemical deposition method used in this study have not been studied for eukaryotic cells in general.

Preconditioning the surface with serum or simulated body fluids is a method that could be applied to reduce the cytotoxic effects of silver-containing hydroxyapatite coatings (Coathup et al 2012). This simulates the *in vivo* environment and removes some ionisable metals from biomaterials (Sandrucci et al 2005). In the case of serum-preconditioning, the proteinaceous layer that forms may provide attachment sites for cells (Ducheyne and Qui 1999). Furthermore, preconditioning has been shown to have effects on the pH and the crystallinity of the apatites formed (Foppiano et al 2007). It has also been postulated that the cytoprotective action of serum may be due to its trophic properties, which promote cell growth (Hidalgo and Dominguez 1998). It has been shown that detrimental effects of silver nitrate on human dermal fibroblast proliferation are reduced by increasing the concentration of fetal calf serum in the culture medium (Hidalgo and Dominguez 1998).

This study aimed to assess human dermal fibroblast viability on fibronectin-functionalised silver-containing hydroxyapatite (HAAgFn) with varying silver contents. The study also aimed to determine whether the cytotoxicity of these coatings can be reduced by serum-preconditioning. It was hoped that a cytocompatible HAAgFn coating would be identified that could then be assessed for antibacterial activity before applying it to porous titanium and implanting it *in vivo*.

It was hypothesised that firstly, HAAgFn coatings would support viable fibroblast growth. Secondly, reducing the silver content of coatings would increase the cytocompatibility. Thirdly, serum-preconditioning would increase the cytocompatibility.

3.2 MATERIALS AND METHODS

3.2.1 Surface Preparation

10 mm x 3 mm titanium alloy (Ti6Al4V) discs were used. The discs were ground with grinding paper in ascending order of grit sizes, (400, 1200, 2500 and 4000) (Struers Ltd, Solihull, UK). A Metopol 2000 grinder (Buehler, Coventry, UK) was used to polish the discs with MD polishing cloth (Struers Ltd, Solihull, UK), OP-S colloidal silica suspension (Struers, Denmark) and 30% hydrogen peroxide (H_2O_2) (BVD, VWR International Ltd, Poole, UK). The discs were washed with tap water, rinsed with distilled water and then ultrasonically cleaned in a 10% Decon 90 solution for 10 minutes (Decon Laboratories Ltd, East Sussex, UK). The discs were washed in distilled water prior to ultrasonic cleaning in acetone.

The following surface coatings were tested: Polished (uncoated) titanium alloy (Pol), hydroxyapatite (HA), hydroxyapatite with fibronectin (HAFn), hydroxyapatite with silver (HAAg) and hydroxyapatite with silver and fibronectin (HAAgFn). HA was electrochemically deposited onto the surface of the discs.

3.2.1.1 Electrochemical Deposition

The discs were immersed into a 0.13 M solution of calcium phosphate monobasic ($Ca(H_2P_4)_2$). The disc to be coated acted as a cathode and was attached to the negative terminal of a DC Dual Power Supply 6010D. A platinum (Pt) ring was used as the anode. An electrical current of 200 mA (current density 80 mA/cm^2) was applied for 10 minutes. The current was controlled using a FLUKE 867B Graphical Multimeter (Fluke Corporation, USA). To produce HAAg coatings, 100 mg of silver nitrate ($AgNO_3$) was added per litre of the $Ca(H_2P_4)_2$ solution as described by Ghani et al (2012). This coating was named HAAg100. Modifications of this coating named HAAg10 and HAAg50 were developed. These coatings were produced by adding 10 or 50 mg of $AgNO_3$ per litre of the $Ca(H_2P_4)_2$ solution respectively. An electrical current of 70 mA (current density 28 mA/cm^2) was applied for four minutes. The equipment used for electrochemical deposition is shown in Figure 3.1.

Electrochemical deposition of HAAg coatings was carried out in the dark to prevent precipitation of silver. The initial layer of brushite ($Ca(HPO_4)\cdot 2(H_2O)$) that formed (with or without silver incorporated) was converted to HA by immersion in 0.1 M sodium hydroxide for 72 hours (Ghani et al 2012; Garcia-Gareta et al 2013).

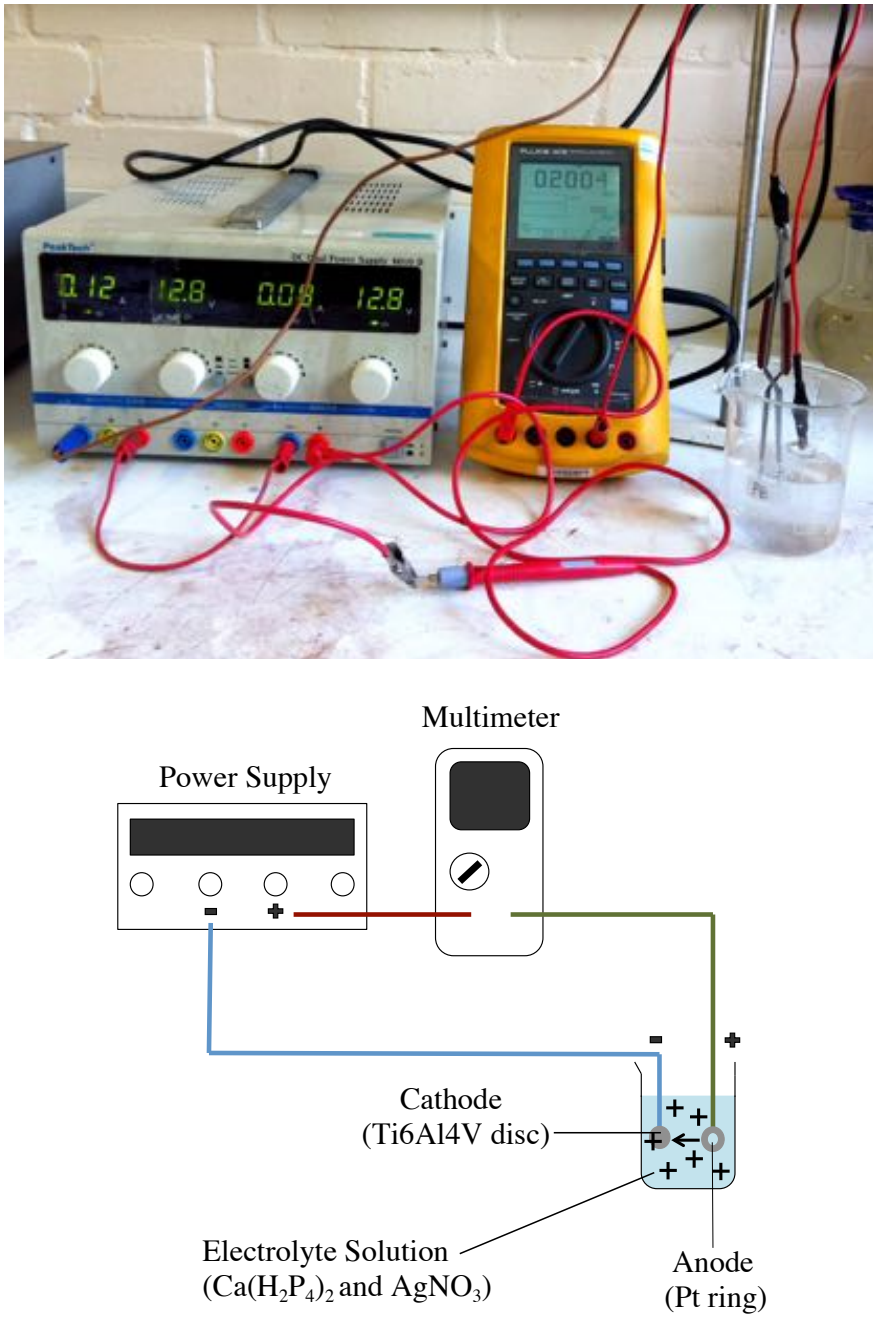

Figure 3.1 Photograph and schematic diagram of the equipment used for electrochemical deposition.

3.2.1.2 Sterilisation, Addition of Fibronectin and Preconditioning

Discs were sterilised with dry heat for one hour at 160°C. Filter sterilised fibronectin was added to surfaces as a 20 μL droplet containing 500 ng of human plasma fibronectin (F2006 Sigma-Aldrich, Dorset, UK). Additional sets of discs were preconditioned by immersing discs in fetal calf serum (First Link Ltd, UK). For surface characterisation experiments, all groups were preconditioned for 24 hours (P24). For experiments with fibroblasts, HAAg10 and HAAg50 groups were preconditioned for 4 hours (P4), 8 hours (P8) or 24 hours. HAAg100 surfaces were preconditioned or 24 hours or 48 hours (P48). (The longer preconditioning periods were chosen for HAAg100 surfaces because a scanning electron microscopy (SEM) pilot study of cell morphology on HAAg100 had shown poor results on these surfaces).

3.2.2 Surface Characterisation

Surface characterisation was carried out to determine if there were any differences in the morphology, the composition and roughness of the coatings as these factors may affect cell attachment and subsequently cytocompatibility. Six areas on three discs per group (P0 and P24) were analysed. SEM was used to visualise samples and assess the morphology of the coatings (JSM 5500LV, JOEL, UK). Energy Dispersive X-ray Analysis (EDX) Analysis (EDAX Genesis V5216 AMETEK, NJ, USA) was used to measure the percentage weight and atomic percentage of silver within coatings. Surface Roughness (R_a) was measured using a non-contact surface optical profilometer (Bruker Contour GT).

3.2.3 Cell Culture

Human dermal fibroblasts (1BR3G, ECACC) were cultured in 225cm^2 vented flasks (Corning Incorporated, New York, USA). The cells were cultured in Dulbecco's modified Eagle's Medium (DMEM) (Sigma-Aldrich, Dorset, UK) containing 4500 mg/L glucose, 1% penicillin/streptomycin (Invitrogen Corporation, Paisley, UK) and 10% fetal calf serum (First Link Ltd, UK). The cells were cultured at 37°C with 5% humidified carbon dioxide (CO_2).

3.2.4 Fibroblast Viability

Cells were seeded onto the disc surface at a density of 5000 cells per disc and cultured for 24 hours. The surfaces were rinsed with phosphate buffered saline (Sigma-Aldrich, Dorset, UK) for five minutes to remove weakly adherent cells from the surface. The cells remaining on the disc surface were incubated in a solution containing 2 μM calcein AM and 4 μM Ethidium homodimer-1 (Invitrogen Molecular Probes Live/Dead viability/cytotoxicity Kit L-3224) for 45 minutes in the dark. A Zeiss microscope was used to visualise cells using the FITC filter to view both live (green staining) and dead (red staining) cells and the DAPI filter to view any additional dead cells. Six areas on each disc were visualised. The experiment was repeated three times. The numbers of live cells and dead cells were counted and the percentage of live cells in each area was calculated.

3.2.5 Fibroblast Metabolism

Cells were seeded onto the disc surface at a density of 15,000 cells per disc. After 24 hours, the surfaces were rinsed with 1 mL of phenol red free DMEM (Sigma-Aldrich, Dorset, UK) for five minutes. 1 mL of 10% Alamar blue in phenol red free DMEM was then added. The cells were incubated at 37°C with 5% CO_2 for four hours. Six discs per coating were used and two 100μL aliquots from each sample were added to a white 96 well plate (FluoroNunc™). Absorbance was measured using an Ascent fluoroscan plate reader (Thermo Electron Corporation, MA).

3.2.6 Fibroblast Morphology

SEM was used to assess cell morphology. Fibroblasts were seeded at a density of 5000 cells per disc onto two discs from each group. After 24 hours the discs were washed with phosphate buffered saline to remove weakly adherent cells. The discs were fixed with 1.5% glutaraldehyde in 0.1 M sodium cacodylate buffer and serially dehydrated with ascending concentrations of industrial methylated spirits and ethanol. They were immersed in hexamethyldisilazane and then air-dried for 24

hours (Appendix 1.2). Following this, they were gold sputter coated using an Emitech K5500 (Emitech Ltd, Ashford, Kent) prior to imaging with the SEM (JSM 5500LV, JOEL, UK).

3.2.7 Statistical Analysis

The data were analysed using SPSS, version 21.0 for Windows (Chicago, US). The Kolmogorov-Smirnov test indicated that the data did not fit the assumptions for parametric testing ($p<0.05$). Therefore, non-parametric tests were performed. The Kruskall Wallis test was used to determine if differences existed between the groups. Mann-Whitney tests were used to perform pair-wise comparisons. A post hoc Benjamini-Hochberg test was carried out because a large number of comparisons were made. This was carried out because as the number of comparisons increases, the likelihood of a false-positive result increases. The Benjamini-Hochberg test controls the false discovery rate by adjusting the threshold for significance. A false discovery rate of 0.05 was used and the threshold for significance was reduced for each pair-wise comparison according to the rank of the p value and the number of comparisons. The p values and adjusted thresholds for significance are detailed in Appendix 3. The Benjamini-Hochberg test reduces the chance of a Type 1 error but increases the chance of a Type 2 error to a lesser extent than more simple tests such as Bonferroni or Sidak corrections (Benjamini and Hochberg 1995).

3.3 RESULTS

3.3.1 Surface Characterisation

3.3.3.1 Surface Topography

SEM of the electrochemically deposited coatings showed the presence of a combination of needle shaped, plate shaped and globular microcrystals on HA and HAAg surfaces. HAAg100 coatings appeared to have a greater proportion of larger plate shaped crystals and a more disorganised morphology than HAAg50 and HAAg10 coatings. The presence of a protein film was visible on surfaces that had been preconditioned. As it was necessary to dry the samples prior to performing SEM, cracks were visible within the protein film. Few needle shaped and plate shaped crystals were visible on preconditioned surfaces and the crystals appeared to be predominantly aggregated together as globules beneath the film (Figure 3.2).

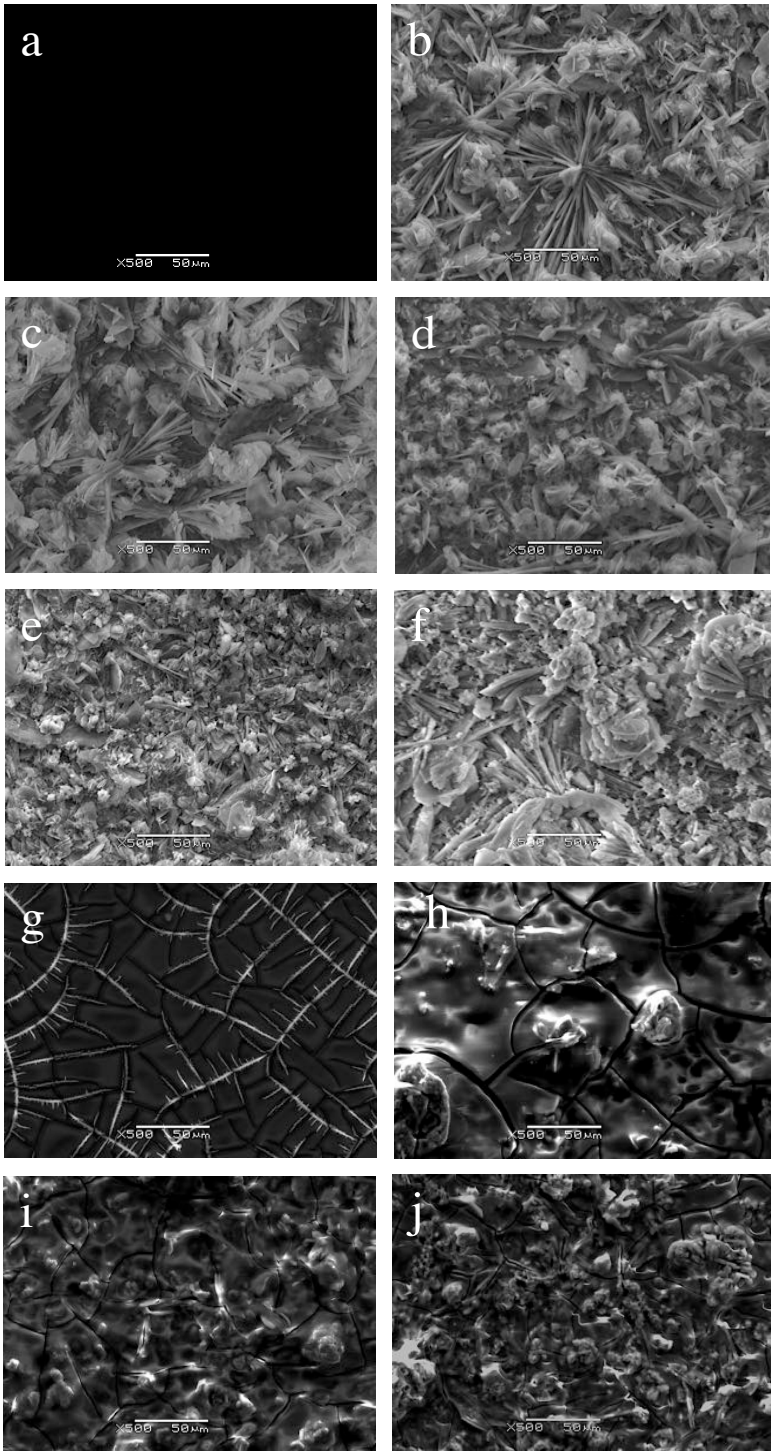

Figure 3.2 Scanning electron micrographs showing the surface topography of (a) Pol (b) HA (c) HAFn (d) HAAg10 (e) HAAg50 (f) HAAg100 (g) Pol (P24) (h) HA (P24) (i) HAAg50 (P24) (j) HAAg100 (P24).

3.3.3.2 EDX Analysis

EDX analysis detected the presence of silver in all HAAg coatings and confirmed the absence of silver in the control coatings. The silver-containing coatings were from different population distributions (p=0.000) with HAAg100 coatings having the highest percentage silver content (median atomic silver percentage 0.665 and weight percentage 2.985) and HAAg10 having the lowest percentage silver content (median atomic percentage 0.205 and weight percentage 0.885) (Table 3.1). The addition of fibronectin and preconditioning resulted in the appearance of other elements not detected in HA and HAAg coatings such as Cl, K, Mg and N (Figure 3.3). In some cases HAAg surfaces that had been preconditioned had a lower silver content than non-preconditioned HAAg surfaces (Table 3.1). However, these reductions were not statistically significant (p>0.05. Exact p values for individual comparisons are shown in Appendix 3.1.1).

Surface	**Ag Atomic %**	**Weight % Ag**
Pol (P0/P24)	0.000	0.000
HA (P0/P24)	0.000	0.000
HAFn (P0/P24)	0.000	0.000
HAAg10	0.205 (0.190 to 0.230)	0.885 (0.840 to 0.990)
HAAgFn10	0.145 (0.090 to 0.240)	0.635 (0.390 to 1.030)
HAAg50	0.280 (0.270 to 0.330)	1.220 (1.200 to 1.430)
HAAgFn50	0.290 (0.230 to 0.370)	1.195 (1.010 to 1.560)
HAAg100	0.665 (0.440 to 0.820)	2.985 (1.980 to 3.620)
HAAgFn100	0.595 (0.440 to 0.760)	2.350 (1.960 to 3.240)
HAAg10 (P24)	0.200 (0.150 to 0.230)	1.040 (0.760 to 1.130)
HAAgFn10 (P24)	0.150 (0.130 to 0.180)	0.860 (0.710 to 0.980)
HAAg50 (P24)	0.270 (0.230 to 0.390)	1.165 (1.020 to 1.380)
HAAgFn50 (P24)	0.290 (0.200 to 0.400)	1.145 (0.880 to 1.610)
HAAg100 (P24)	0.460 (0.310 to 0.620)	2.340 (1.580 to 3.160)
HAAgFn100 (P24)	0.535 (0.440 to 0.690)	2.620 (2.150 to 3.460)

Table 3.1 Atomic and weight percentage of silver for each surface presented as median values and (95% confidence intervals).

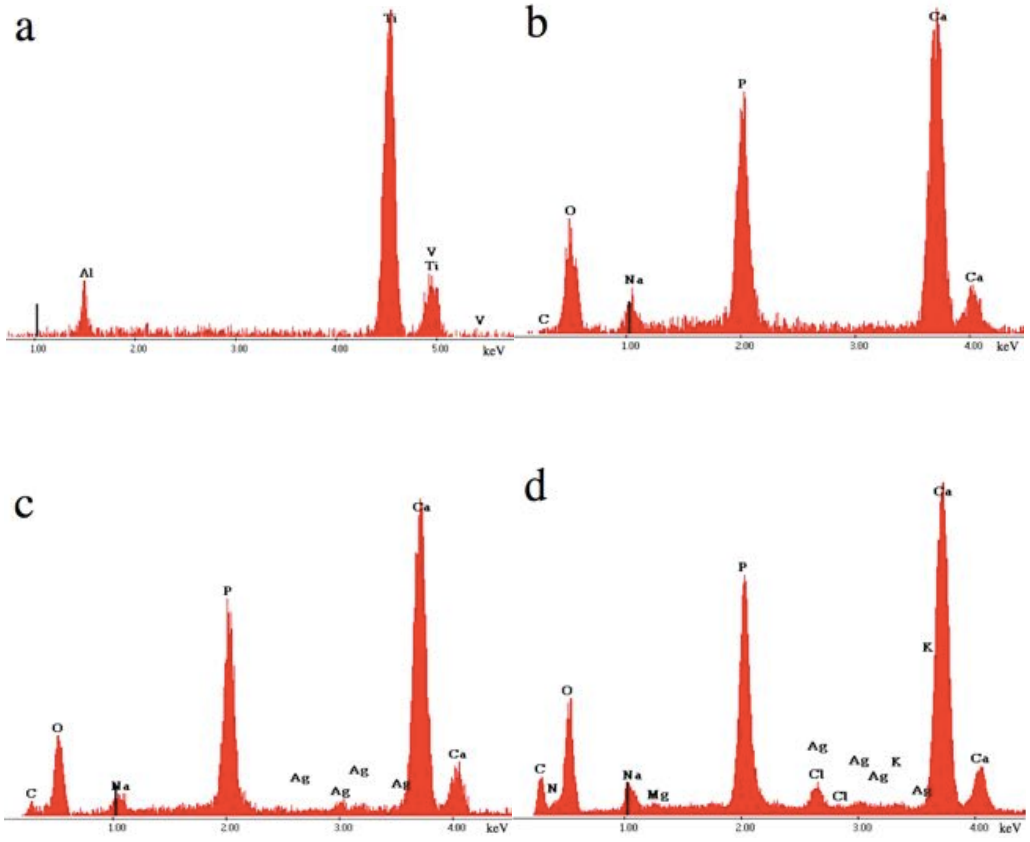

Figure 3.3 EDX spectra (a) Pol (b) HA (c) HAAg100 (d) HAAgFn100 (P24).

3.3.3.3 Surface Roughness

Profilometry showed that Pol was smoother than HA (p=0.000). There was no difference in the roughness (R_a) of HA, HAAg10 and 50 surfaces (p=0.302). However, HAAg100 and HAAgFn100 surfaces were significantly rougher than all other surfaces (p<0.05. Exact p values for individual comparisons are shown in Appendix 3.2.1). Preconditioning of HA and HAAg surfaces resulted in reduced R_a values. This reduction was statistically significant for HAFn, HAAgFn10, HAAg50 and HAAgFn100 (p=0.000, 0.000, 0.002 and 0.019 respectively) but was insignificant for all other surfaces. The adsorption of fibronectin onto surfaces did not affect the R_a values of any surfaces (p>0.05. Exact p values for individual comparisons are shown in Appendix 3.2.1) (Table 3.2).

Surface	**Ra (μm)**
Pol	0.031 (0.028 to 0.033)
HA	2.952 (2.828 to 3.451)
HAFn	3.317 (2.802 to 3.444)
HAAg10	2.804 (2.345 to 3.504)
HAAgFn10	3.261 (2.602 to 3.683)
HAAg50	3.022 (2.735 to 3.678)
HAAgFn50	3.301 (2.411 to 3.635)
HAAg100	4.774 (4.663 to 5.327)
HAAgFn100	4.550 (4.302 to 4.715)
Pol (P24)	0.030 (0.025 to 0.041)
HA (P24)	2.800 (2.488 to 3.482)
HAFn (P24)	2.394 (2.086 to 2.696)
HAAg10 (P24)	2.597 (2.334 to 3.802)
HAAgFn10 (P24)	2.255 (2.087 to 2.605)
HAAg50 (P24)	2.333 (2.250 to 3.028)
HAAgFn50 (P24)	2.540 (1.947 to 4.059)
HAAg100 (P24)	4.358 (3.296 to 5.579)
HAAgFn100 (P24)	4.184 (3.477 to 4.638)

Table 3.2 Surface roughness results presented as median values and (95% confidence intervals).

3.3.2 Fibroblast Viability

Non-preconditioned HAAg10 surfaces were cytotoxic to fibroblasts compared with HA, HAFn and Pol controls. HAAg50 had a greater cytotoxic effect than HAAg10 ($p=0.000$). HAAg100 exhibited the greatest cytotoxicity and there was a further reduction in the percentage of live cells on this surface compared with HAAg50 ($p=0.002$). Preconditioning of HAAg surfaces significantly reduced the cytotoxic effects. After 24 hours preconditioning all surfaces were cytocompatible with more than 90% cell viability. There was no reduction in viability on HAAg (P24) surfaces compared with Pol, HA and HAFn controls ($p>0.05$. Exact p values for individual comparisons are shown in Appendix 3.3.2). On HAAg10 and 50 surfaces, which were preconditioned for 4, 8 and 24 hours, it was observed that increasing the length of the time period of preconditioning increased the percentage of live cells on these surfaces. Increasing the time period of preconditioning from 24 hours to 48 hours (for HAAg100+/-Fn) did not significantly further increase the cytocompatibility. Preconditioning did not affect the cytocompatibility of the control surfaces. Adsorption of fibronectin onto surfaces did not significantly improve the cytocompatibility of surfaces (Figures 3.4 and 3.5).

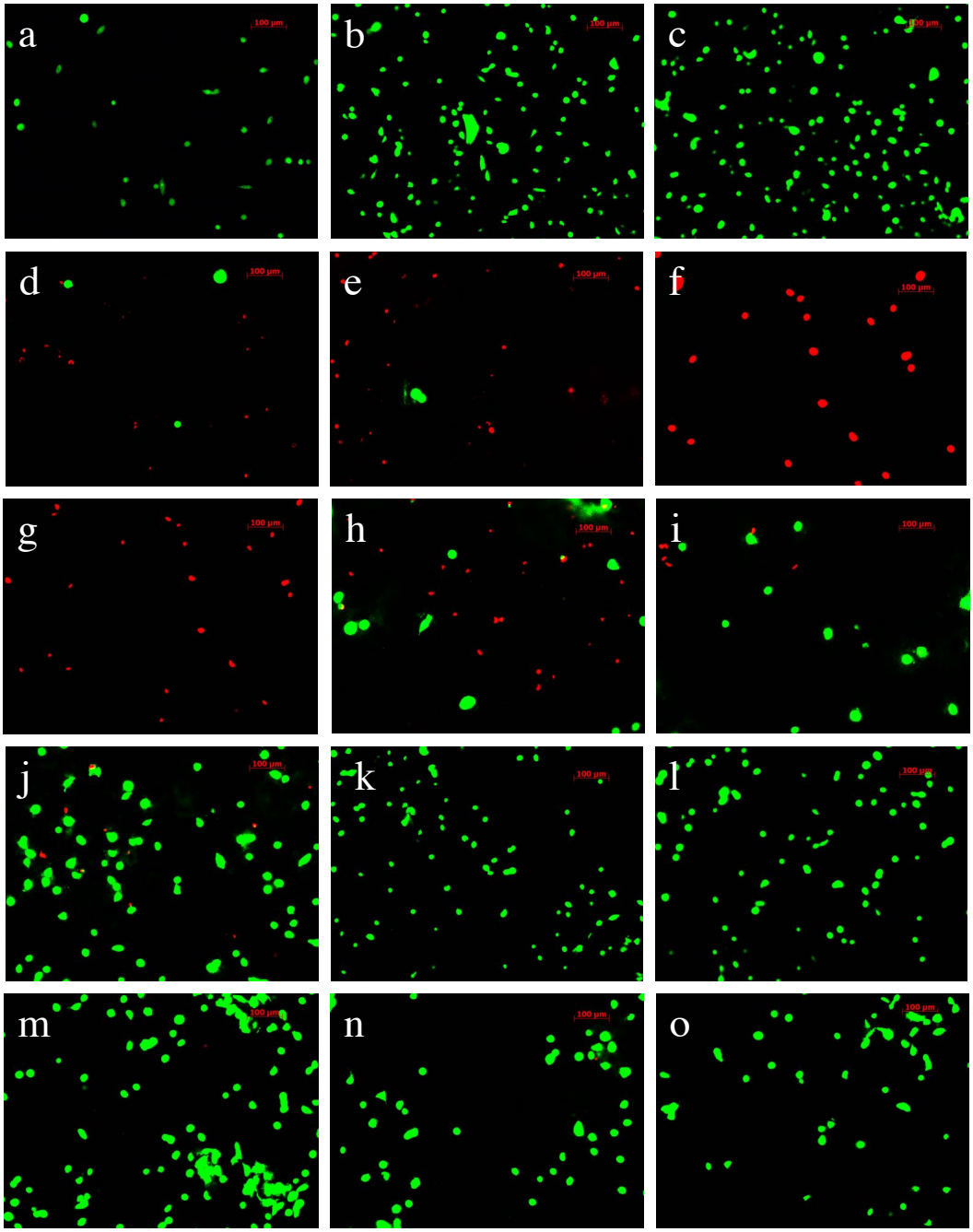

Figure 3.4 Live (green): dead (red) staining images of fibroblasts (a) Pol (b) HA (c) HAFn (d) HAAg10 (e) HAAg50 (f) HAAg100 (g) HAAgFn100 (h) HAAg50 (P4) (i) HAAg10 (P8) (j) HAAgFn50 (P8) (k) HAAg10 (P24) (l) HAAg50 (P24) (m) HAAg100 (P24) (n) HAAg100 (P48) (o) HAAgFn100 (P48).

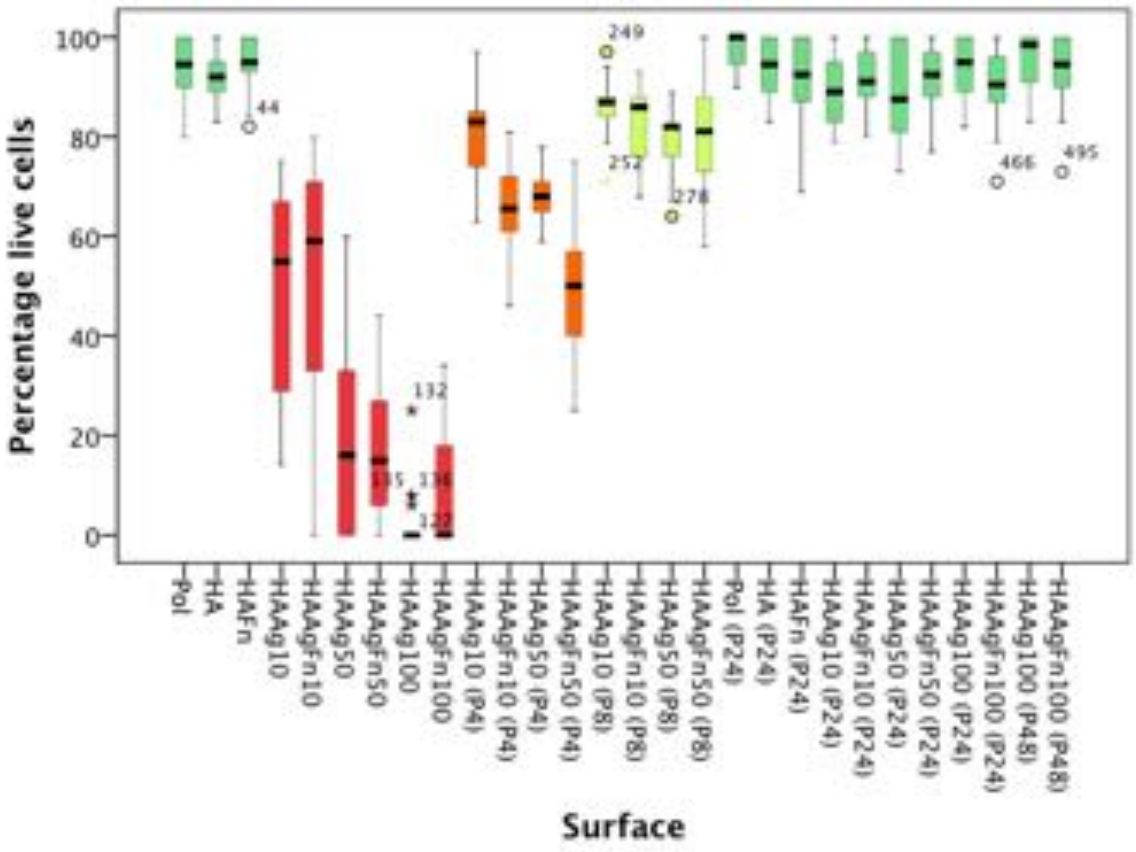

Figure 3.5 Box-and-whisker plot showing the percentage of live fibroblasts on each surface.

3.3.3 Fibroblast Metabolism

The greatest cell metabolism was observed on HAFn controls, which was significantly greater than Pol ($p=0.008$) but was not significantly different when compared with HA ($p=0.143$). There was less cell metabolism on non-preconditioned HAAg surfaces compared with controls ($p=0.000$). Increasing the silver content of coatings was associated with a reduction in cell metabolism. Decreased cell metabolism was observed on HAAg100 surfaces compared with HAAg50 and HAAg10 surfaces ($p=0.000$). The cell metabolism on HAAg surfaces increased after preconditioning, compared with HAAg surfaces that had not been preconditioned. Increasing the time period for preconditioning up to 24 hours resulted in increased cell metabolism (HAAg10 and 50 groups). Increasing the length of the time period from 24 hours to 48 hours did not result in any further increase in cell metabolism (HAAg100 groups). There was no difference in cell metabolism between HAAg10, HAAg50 and HAAg100 surfaces after 24 hours preconditioning ($p=0.574$) and no difference between these surfaces and Pol and HA controls ($p>0.05$. Exact p values for individual comparisons are shown in Appendix 3.4.2). However, greater cell metabolism was observed on HAFn controls than on HAAg (P24) surfaces ($p<0.05$). Adsorption of fibronectin onto HAAg10 and HAAg100 did not significantly increase cell metabolism ($p=0.799$ and $p=0.977$ respectively). However, adsorption of fibronectin onto HAAg50 resulted in an increase in cell metabolism ($p=0.003$). Increased cell metabolism was observed on HAAgFn50 (P4) compared with HAAg50 (P4) ($p=0.000$). Fibronectin did not have any other statistically significant effects on HAAg surfaces that had been preconditioned ($p=000$) (Figure 3.6).

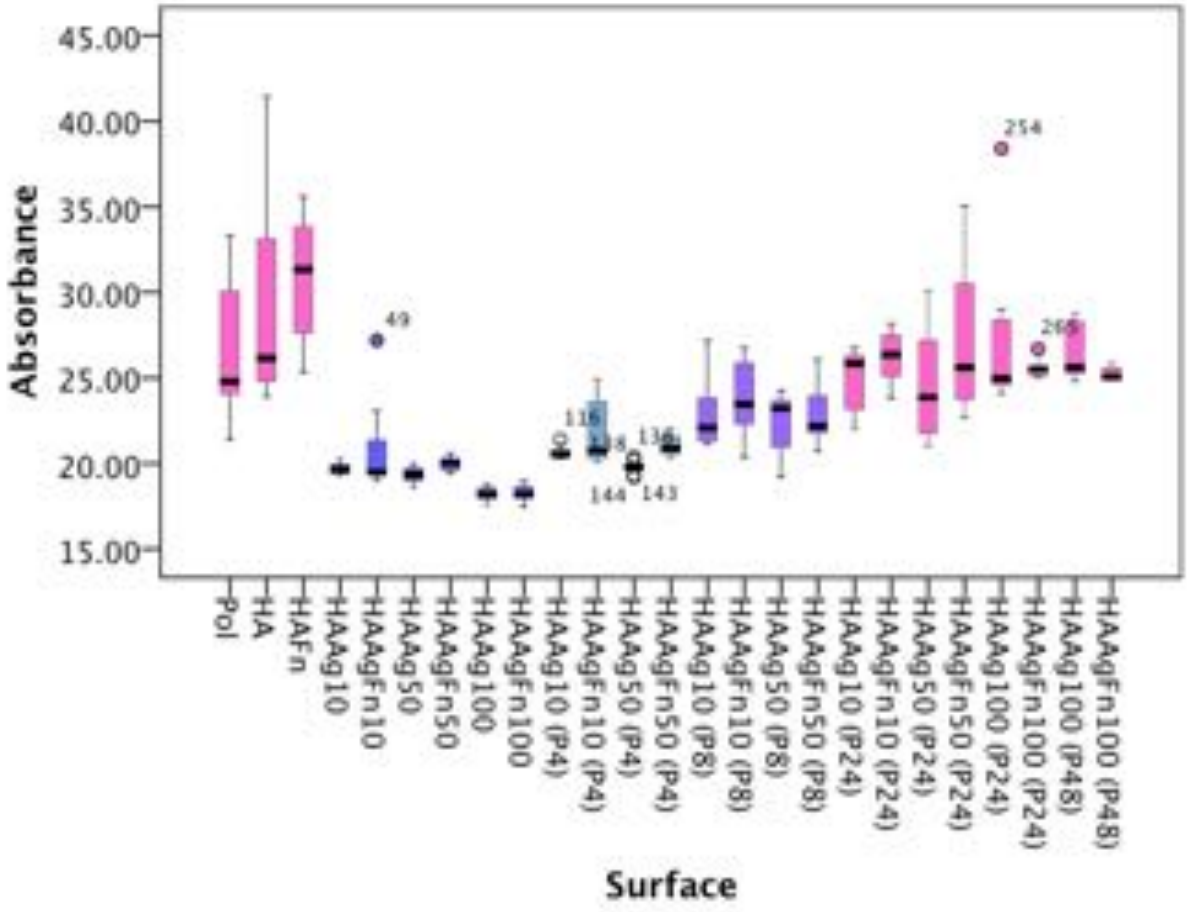

Figure 3.6 Box-and-whisker plot showing the Alamar blue absorbance results for each surface.

3.3.4 Fibroblast Morphology

Fibroblasts cultured on HA surfaces appeared larger and flatter than fibroblasts on Pol surfaces, which were smaller and rounder. Greater cell spreading was observed on HAFn surfaces than HA surfaces. Cells were seen to grow on HAAg10 and 50 surfaces that had not been preconditioned but the morphology was poor with minimal cell spreading and pseudopodia. Few cells were seen on HAAg100 and HAAgFn100. Predominantly cell remnants were seen on these surfaces. Preconditioning of HAAg surfaces resulted in greater cell spreading and improved cell morphology for all silver content coatings. The presence of pseudopodia was often obscured by the HA crystals; however, some pseudopodia were visible on HA and HAFn controls and HAAg and HAAgFn surfaces that had been preconditioned. In most cases, pseudopodia were not visible on non-preconditioned HAAg surfaces (Figures 3.7 and 3.8).

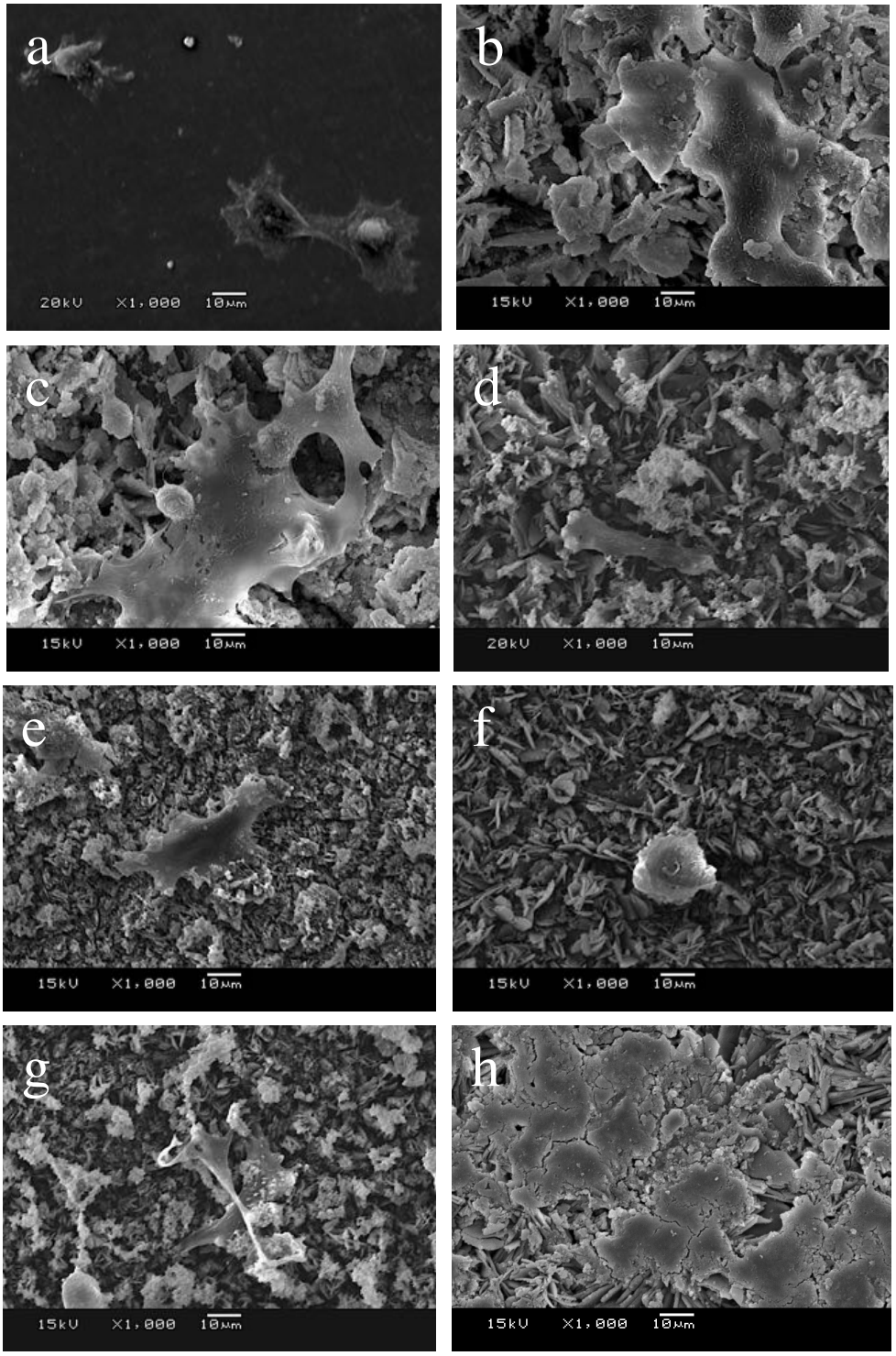

Figure 3.7 Scanning electron micrographs of fibroblasts on non-preconditioned surfaces (a) Pol (b) HA (c) HAFn (d) HAAg10 (e) HAAgFn10 (f) HAAg50 (g) HAAgFn50 and (h) HAAg100.

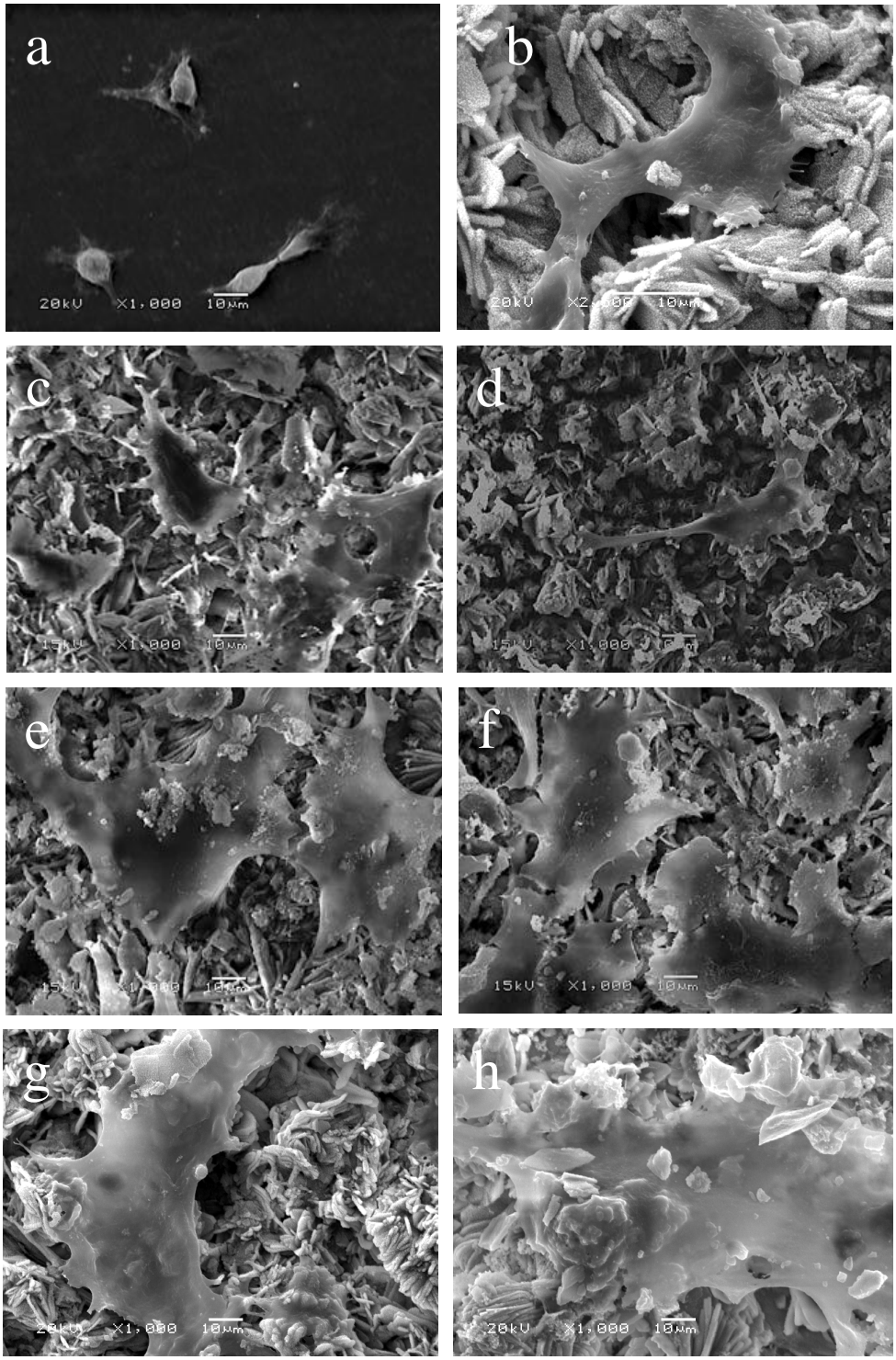

Figure 3.8 Scanning electron micrographs of fibroblasts on preconditioned surfaces (a) Pol (P24) (b) HA (P24) (c) HAAg10 (P4) (d) HAAg50 (P4) (e) HAAg10 (P24) (f) HAAgFn50 (P24) (g) HAAg100 (P24) and (h) HAAg100 (P48).

3.4 DISCUSSION

This study has shown that incorporation of silver into hydroxyapatite (with and without fibronectin) produces a coating that is cytotoxic. The cytotoxic effects of the coating are reversed after serum preconditioning for 24 hours. Cell metabolism is also increased after preconditioning, which may be due to increased cell proliferation.

Reasons for Increased Cytocompatibility after Preconditioning

Previous studies using inductively coupled plasma mass spectrometry (ICP MS) by Ghani et al (2012) have demonstrated a sustained release of silver from HAAg produced using this method of electrochemical deposition over a period of 22 days (Ghani et al 2012). They quantified silver release from HAAg coatings into phosphate buffer solution. The phosphate buffer solution was changed daily to mimic continuous replenishment of body fluids *in vivo* and therefore non-cumulative levels were measured. The amount of silver in the elution fluids was measured on days 10, 15 and 22. Silver was found to be released at each of the three time points with the highest amount of silver measured at 10 days and the lowest amount at 22 days (Ghani et al 2012). Ghani et al (2012) did not measure silver release over the first 24 hours, however, the results of their study indicate that silver release from HAAg reduces over time. As a result, it is hypothesised that after preconditioning surfaces, the release of silver would be slower, hence accounting for the improved cytocompatibility. (Release of silver from HAAg coatings into fetal calf serum over a wider range of time points (including 24 hours) will be presented in Chapter Five). Surprisingly, EDX analysis results showed that the reductions in the percentage of silver observed after preconditioning were not significant. This may be due to loss of other elements in addition to silver. It could also be due to the number of silver ions initially released being a very small proportion of the total number of silver ions. Further studies to determine the overall amount of silver within the coatings using atomic absorption spectroscopy or ICP MS (rather than a percentage as measured by EDX) may be of value. Extraction of silver into nitric acid could be used to quantify the amount of silver within the coating after preconditioning. It has already been

shown by Sandrucci et al that preconditioning removes silver ions from silver-containing surfaces, which indicates that overall silver levels (but not necessarily the percentage) within the substrate would be reduced (Sandrucci et al 2005). This is an explanation for the improved cytocompatibility associated with preconditioning.

An alternative explanation for the lack of significant reductions in the percentage content after preconditioning that should be considered is that silver content reduction may not be the only reason for the increased cytocompatibility associated with preconditioning. As the percentage of silver was not reduced on preconditioned surfaces, it is possible that the effect of preconditioning could be associated with other factors such as the deposition of proteins. One observation that supports this theory is that the percentage of live cells on HAAg (P24) surfaces was equal to that of controls that did not contain silver. Furthermore, there were no differences in the cell viability between HAAg10, 50 and 100 (P24) surfaces. Furno et al (2004) concluded that silver ions were able to penetrate protein-conditioning films and maintain their bactericidal activity (Furno et al 2004). Similarly in our study, a substantial amount of the silver may have resided in the preconditioning film resulting in the reductions in silver content detected by EDX being insignificant. The finding of improved viability on preconditioned surfaces may be partly due to less of the silver being in a biologically active ionised form due to binding to serum proteins such as albumin (Schierholtz et al 1998). The number of ions involved in this process would be very difficult to measure. However, it should be noted that the study by Furno et al suggested that not all silver bound to proteins is inactivated as their conditioned substrates did not exhibit any loss of antibacterial activity (Furno et al 2004). The following chapter of this thesis will present the effect of preconditioning on the antibacterial activity of HAAg and HAAgFn surfaces.

Another EDX analysis finding was that after preconditioning, additional elements such as Cl, K, N and Mg were incorporated into the coatings. Other studies have concluded that immersion in simulated body fluids affects the composition and consequently may influence the biological behaviour of HA coatings (Zhang et al 2003; Garcia-Gareta et al 2013). It has also been noted by other studies that

preconditioning may affect the crystallinity of ceramics and result in different apatite phases, which may contribute towards the increased cytocompatibility (Foppiano et al 2007). Additionally, as silver is part of the crystalline structure of HAAg, the release of silver from HAAg coatings would imply that HA resorption occurs. Future studies of the crystallographic structure of HAAg using X-ray diffraction analysis would be able to assess this.

Surface Topography

The increased time period and higher current density used for electrochemical deposition may have contributed to the increased roughness of HAAg100 compared with HAAg50 and HAAg10. Higher current densities are associated with more vigorous hydrogen evolution and the overall process is less efficient as a larger proportion of brushite crystals are unable to survive the turbulent environment of a high current density and are thus lost (Redepenning et al 1996). Redepenning et al (1996) reported that the crystals that do survive this environment would be expected to adhere better resulting in coatings with an overall greater integrity (Redepenning et al 1996). The same current density and time was used to produce HA coatings, which were not as rough as HAAg100 indicating that the silver content affects the topography of these surfaces. Previous X-ray diffraction analysis of HAAg showed peaks that were sharper than those observed for HA suggesting that the Ag^{+} ion incorporation may increase the crystallinity (Ghani et al 2012). The reduction in R_a observed on preconditioned surfaces was not statistically significant for all surfaces. Nevertheless, it was evident from the scanning electron micrographs that the crystal morphology was markedly different after preconditioning. This may be due to the fact that when a hydroxyapatite surface is immersed into a simulated body fluid, resorption of hydroxyapatite and the deposition of an apatite layer on the surface as described by Kokubo et al, may occur (Kokubo et al 1990; Kokubo 1998). Fibroblasts are known to be sensitive to surface topography and previous studies have shown that reductions in roughness even on a nanometric scale are associated with improved fibroblast attachment, proliferation or viability (Wang et al 2009; Ranella et al 2010; Pennisi et al 2011; Wang et al 2011; Teng et al 2012; Zhou et al 2012). However, many factors such as wettability and surface chemistry influence

fibroblast responses, which change the way fibroblasts to respond to surfaces. This may enable these cells to grow on rougher surfaces despite the fact that they usually respond better to smoother surfaces. (Lydon and Clay 1985; Ranella et al 2010; Lopez-Santos et al 2013).

Potential Implications of Preconditioning Resulting in Increased Cytocompatibility

The finding that preconditioning is necessary before HAAg surfaces become cytocompatible, suggests that in clinical practice HAAg may be cytotoxic initially; and a short time period (up to 24 hours) may be required for cells to attach to these surfaces. The clinical implications of this delay are not known. In clinical practice, preconditioning prior to implantation with autologous serum in order to promote earlier soft tissue attachment would be an option, but would be logistically less convenient.

Effects of Hydroxyapatite and Fibronectin

Cells attaching to HA demonstrated greater cell spreading than cells cultured on Pol; but HA was not associated with significantly greater cell metabolism than Pol. HAFn was the only surface to increase cell metabolism compared with Pol. HA and HAFn did not improve the percentage of live cells compared with Pol as cell viability was already more than 90% on Pol controls. HAFn was the only surface to significantly increase cell metabolism compared with Pol. This is in keeping with the findings of Sawyer et al (2005) who found that HA alone was not a good substrate for cell attachment, but that RGD functionalisation was necessary to promote full cell spreading (Sawyer et al 2005). Additionally, Pendegrass et al (2010) showed that cell areas and attachment were not greater on HA than on Pol *in vitro*; but HAFn was greater than both Pol and HA (Pendegrass et al 2010a). However, the same study found that *in vivo*, HA resulted in significantly better soft tissue attachment than uncoated surfaces in addition to HAFn resulting in better soft tissue attachment than HA (Pendegrass et al 2010a). This raises the possibility that *in vivo* the differences between HA and HAFn as well as the differences between HA and Pol could be

more marked than the differences seen *in vitro*. This could potentially be due to the longer duration of *in vivo* experiments.

In the presence of silver, fibronectin did not have a consistent beneficial effect on cell metabolism. Fibronectin did not improve cell viability. There was a trend that HAAgFn increased cell metabolism compared with HAAg; but this was only statistically significant for HAAg50. This suggests that silver counteracts some of the effects of fibronectin on cell metabolism.

It is known from previous studies that some fibronectin adsorbed onto hydroxyapatite coatings is lost after immersion into fetal calf serum. Pendegrass et al (2012) showed that only one fifth of the initial fibronectin coating remained on substrates after 24 hours in fetal calf serum, but that this remaining fibronectin resulted in a sevenfold fold increase in fibroblast attachment (Pendegrass et al 2012b). It is possible that increasing the fibronectin concentration may have resulted in more marked effects on cell viability, metabolism and morphology. However, increasing the fibronectin concentration may also increase the bacterial colonisation. Therefore, it was decided to determine the effect of the concentration of fibronectin used in this experiment on bacterial colonisation before consideration of increasing the amount the fibronectin used.

Limitations of This Study

It is important to determine the effect of HAAg/HAAgFn coatings on cell viability as this chapter has done. However, it would have also been useful to directly assess *in vitro* cell attachment. SEM showed that cells present on control surfaces and preconditioned HAAg/HAAgFn surfaces. The cell viability assay also showed that viable cells were present surfaces. Non-adherent cells had been removed from the surface by rinsing with phosphate buffered saline prior to visualisation. However, the strength of cell attachment was not measured. The method of using a flow apparatus where shear stress is applied to detach cells from surfaces could not be used for this study. This is because the roughness of the surfaces would result in turbulent flow

rather than laminar flow (Pendegrass et al 2010b). Immunolocalisation of cell vinculin markers has been previously shown to correlate with measures of biophysical strength. This technique was attempted but was not successful due to autofluorescence resulting in uninterpretable images. An alternative approach would be to use sintered hydroxyapatite for vinculin bioassay experiments as this has been shown not to produce autofluorescence. However, the results of this may not be applicable to electrochemically deposited coatings due to differences in topography. Soft tissue dermal contact will be assessed *in vivo*.

Future Directions

It would be useful to assess the effect of HAAg and HAAgFn surfaces on other cell types to widen the potential clinical applicability of this coating. In contrast to fibroblasts, osteoblasts are known to respond better to rougher surfaces. Osteoblasts have been reported to respond well to surfaces with similar R_a microroughness levels to the surfaces investigated in this study (Kunzler et al 2007; Teng et al 2012; Zink et al 2012). It is well known that hydroxyapatite increases osteoblast adhesion. Studies have also shown that the addition of fibronectin improves osteoblast responses further (Deligianni et al 2006; Schönmeyr et al 2008; Fernández et al 2012)). If osteoblasts were found to respond well to HAAg and HAAgFn, this technique could be useful for the intraosseous portion of osseointegrated transcutaneous implants as well as more widely for other orthopaedic implants such as arthroplasty prostheses. This would be advantageous because hip and knee arthroplasties are associated with an infection rate of approximately 1%, which is associated with significant morbidity and substantial economic costs.

Ghani et al (2012) have shown that HAAg100 has antibacterial activity (Ghani et al 2012). However, the antibacterial activity of HAAg50 and HAAg10 as well as the effect of adsorption of fibronectin and preconditioning has not been studied. The next chapter of this thesis explores this before proceeding onto *in vivo* experiments.

3.5 CONCLUSION

In conclusion, incorporation of silver into HA and HAFn coatings results in cytotoxicity. After serum-preconditioning HAAg and HAAgFn coatings become cytocompatible. This suggests that in clinical practice, after a period of contact with serum following implantation, these coatings would be expected to support viable fibroblast growth. Before conducting *in vivo* studies, it is necessary to assess the antibacterial activity of these coatings. This will be presented in the next chapter of this thesis.

CHAPTER FOUR

In Vitro Assessment of Bacterial Colonisation on Hydroxyapatite, Silver and Fibronectin Coatings

4.1 INTRODUCTION

The infection rate of osseointegrated transcutaneous implants has been reported to vary between approximately 18% and 55% (Tillander et al 2010; Brånemark 2014). The majority of infections have been superficial soft tissue infections (Brånemark 2014). *Staphylococcus aureus (S aureus)* is known to be the commonest infecting organism (Tillander et al 2010). A range of other organisms have been found to cause infection e.g. *Coagulase negative Staphylococcus*; *Streptococcus Groups A*, *B* and *G*, *Enterococci* and *Pseudomonas aeruginosa (P aeruginosa)* (Tillander et al 2010). In clinical cases of the ITAP model, infections have been caused by *S aureus* and *P aeruginosa* (Chimutengwende-Gordon 2010, unpublished). As discussed in Chapter One, for soft tissue to win the 'race for the surface' against bacteria, it is necessary to prevent bacterial adhesion and hence biofilm formation on the surface of the implant. It is also important to prevent bacterial colonisation within the surrounding tissues. Early infection of surgical implants (i.e. within three months postoperatively) is believed to develop due to the introduction of bacteria into the tissues at the time of surgical implantation (Moran et al 2010). The introduction of very small numbers of bacteria intraoperatively may cause infection (Gosden et al 1998). Late infections may also result from intraoperative bacterial contamination with low virulence organisms or when bacteria become dormant for extended time periods (Trampuz and Widmer 2006; Ribeiro et al 2012). However, later infections are often more likely to occur as a result of haematogenous spread of bacteria from other tissues (Moran et al 2010; Ribeiro et al 2012). Silver released from an implant surface would be expected to reduce bacterial colonisation and the risk of infection associated with surgery; but it is important that this is not at the expense of tissue integration (Agarwal et al 2010). For this reason I have utilised a coating that combines hydroxyapatite and fibronectin with silver. The rationale is to manage the 'race for the surface' where tissue integration is promoted over bacterial colonisation and biofilm formation.

Chapter Three has shown that HAAg and HAAgFn surfaces are cytocompatible after preconditioning. Depending on the method of coating and the surface characteristics, HA coatings may be associated with increased bacterial colonisation and could

potentially increase the risk of infection (Smith et al 2006; Laure et al 2008). It is however encouraging that electrodeposited HA coatings have been shown to promote bacterial colonisation to a lesser degree than plasma-sprayed coatings due to increased surface roughness and wettability (Mathew et al 2014). Fibronectin has also been shown to increase the colonisation of some bacterial species such as *S aureus*, which contains fibronectin-binding proteins (Henderson et al 2010). Delmi et al (1994) demonstrated that *S aureus* and *S epidermidis* adhesion was significantly greater on coverslips of stainless steel, pure titanium and titanium-aluminium-nobium alloy coated with fibronectin compared with albumin-coated controls. The presence of anti-fibronectin immunoglobulin G (IgG) antibodies, but not of preimmune IgG, reduced the extent of *Staphylococcal* adhesion by 70-90% (Delmi et al 1994).

Some studies have suggested that adsorption of blood proteins inactivates silver due to binding of silver ions (Schierholz et al 1998). It is possible that preconditioning surfaces with serum may result in less silver being in a biologically active ionised form due to binding with proteins. This would be expected to result in reduced antibacterial activity. However, it has been shown that coating surfaces with serum or albumin (a hydrophilic component of serum) provides a barrier to bacterial adhesion and so may counteract the effects of binding silver (Pascual et al 1986; Kinnari et al 2005). Furno et al found that preconditioning silver surfaces with plasma does not inhibit antibacterial activity (Furno et al 2004).

Although, Ghani et al have demonstrated that HAAg100 has antibacterial activity against *S aureus*, it is necessary to determine if this activity is affected by fibronectin and serum-preconditioning. As the lower silver content surfaces tested in Chapter Three (i.e. HAAg50 and HAAg10) were less cytotoxic to fibroblasts (before preconditioning) they may have a benefit over HAAg100 and so it would also be valuable to test the antibacterial activity of these surfaces.

The aim of this chapter is to assess the antibacterial activity of the HAAg and HAAgFn surfaces tested in Chapter Three against *S aureus* and *P aeruginosa*. The effect of these coatings on both biofilm formation and bacteria in surrounding planktonic suspensions will be described. This chapter also aims to determine if the antibacterial activity of these surfaces is maintained after serum-preconditioning.

It was hypothesised that:

1. The HAAg and HAAgFn surfaces would reduce *S aureus* and *P aeruginosa* colonisation compared with HA, HAFn and Pol controls.

2. The higher content silver coatings would have greater antibacterial activity.

3. HAFn would increase bacterial colonisation, but the addition of silver (HAAgFn) would counteract the effects of HAFn on promoting bacterial colonisation.

4. HAAg and HAAgFn surfaces would maintain their antibacterial activity after serum-preconditioning.

4.2 MATERIALS AND METHODS

4.2.1 Bacterial Challenges

10 mm x 3 mm titanium alloy (Ti6Al4V) discs were prepared using the methods described in Section 3.2.1. 10^6 colony forming units (cfu) of *S aureus* ATCC 29213 was used to challenge Pol, HA, HAFn, HAAg10, HAAgFn10, HAAg50, HAAgFn50, HAAg100, HAAgFn100 surfaces at P0 and P24. Pol, HA, HAFn, HAAg100, HAAgFn100 surfaces at P0 and P24 were also challenged with a clinical isolate of *P aeruginosa* F1896 (10^6 cfu as well as a smaller challenge of 5 x 10^4 cfu). Each disc was placed into a 1 mL planktonic suspension of the bacteria in nutrient broth (Oxoid Ltd, Basingstoke, UK). The samples were then incubated for 24 hours at 37°C on a shaking tray at 50 revolutions per minute (rpm).

4.2.2 Biofilm Direct Colony Counts

The samples were rinsed with phosphate buffered saline in order to remove poorly adhered bacteria. The attached biofilms that had formed on the surfaces were removed by ultrasonication in phosphate buffered saline for two minutes. The resultant bacterial suspension was vortexed for 10 seconds to separate the bacterial aggregates and serially diluted in phosphate buffered saline over a 6-log range. Three discs per group were used and 10 μL of each dilution was plated onto agar (Oxoid Ltd, Basingstoke, UK) in triplicate. Columbia horse blood agar plates were used for surfaces challenged with *S aureus*. MacKonkey agar plates were used for surfaces that had been challenged with *P aeruginosa*. The plates were incubated at 37°C. After 24 hours, the colonies were counted. The number of colony forming units per mL (cfu/mL) was calculated.

4.2.3 Planktonic Direct Colony Counts

The planktonic bacterial suspensions that discs had been immersed in were also serially diluted and plated. Direct colony counts were performed using the same method as for the biofilm direct colony counts described above in Section 4.2.2.

4.2.4 Scanning Electron Microscopy

The bacterial colonisation and the presence of glycocalyx/biofilm formation on two discs per group was visualised using SEM. The method for SEM preparation described in Section 3.2.6 (Appendix 1.2) was used.

4.2.5 Statistical Analysis

The data were analysed using SPSS, version 21.0 for Windows (Chicago, US). Non-parametric tests were performed as the data did not fit the assumptions for parametric testing. The Kruskall Wallis test was used to determine whether the groups were from the same population distribution. Pair-wise Mann-Whitney U tests were used to perform comparisons between individual groups. Due to the large range of cfu/mL, colony count data was logarithmically transformed for presentation in box-and-whisker plots. A post-hoc Benjamini-Hochberg analysis was carried out for the data from the *S aureus* bacterial challenge experiments as more than 20 comparisons were made. Median values and 95% confidence intervals are presented in Appendix 4.

4.3 RESULTS

4.3.1 Direct Colony Counts for *S aureus*

4.3.1.2 Biofilm Direct Colony Counts

Greater numbers of bacteria were present within biofilms that formed on HA compared with Pol (p=0.008). There was a further increase in the numbers of bacteria within biofilms formed on HAFn compared with HA (p=0.001). Non-preconditioned HAAg surfaces reduced bacterial colonisation compared with Pol, HA and HAFn controls ($p<0.05$. Exact individual p values for each comparison are shown in Appendix 4.1.2). Increasing the silver content, increased the degree of antibacterial activity. HAAg100 and HAAgFn100 showed the greatest antibacterial activity and there was complete suppression of bacterial colonisation on these surfaces. After preconditioning, some bacterial colonisation occurred on HAAg100 surfaces. However, the numbers of bacteria colonising HAAg100 (P24) surfaces remained significantly lower than the control surfaces (HAAg100 (P24) compared with Pol (P24) p=0.005). There was a reduction of 1.997×10^6 cfu/mL on HAAg100 (P24) compared with HA (P24), which is equivalent to a 99.85% reduction in bacterial colonisation. There was a reduction of 1.983×10^6 cfu/mL on HAAgFn100 (P24) compared with HAFn (P24) (99.15% reduction). After preconditioning, HAAg10 and HAAg50 lost their antibacterial activity compared with Pol, but fewer bacteria colonised these surfaces than HA (p=0.04 and 0.02 respectively). It was noted that reduced numbers of bacteria colonised Pol, HA and HAFn control surfaces after they were preconditioned (p=0.001, 0.088 and 0.000 respectively). In contrast increased numbers of bacteria colonised HAAg and HAAgFn surfaces after they were preconditioned (HAAg10 p=0.002; HAAgFn10 p=0.000; HAAg50 p=0.001; HAAgFn50 p=0.020; HAAg100 p=0.000; HAAgFn100 p=0.000). HAAg100 was the only surface that maintained an antibacterial effect after preconditioning compared with Pol (P24) surfaces (p=0.005). Fibronectin resulted in an increase in bacterial colonisation on HAAg100 (P24) but did not affect the bacterial colonisation on other HAAg (P24) surfaces (Figure 4.1).

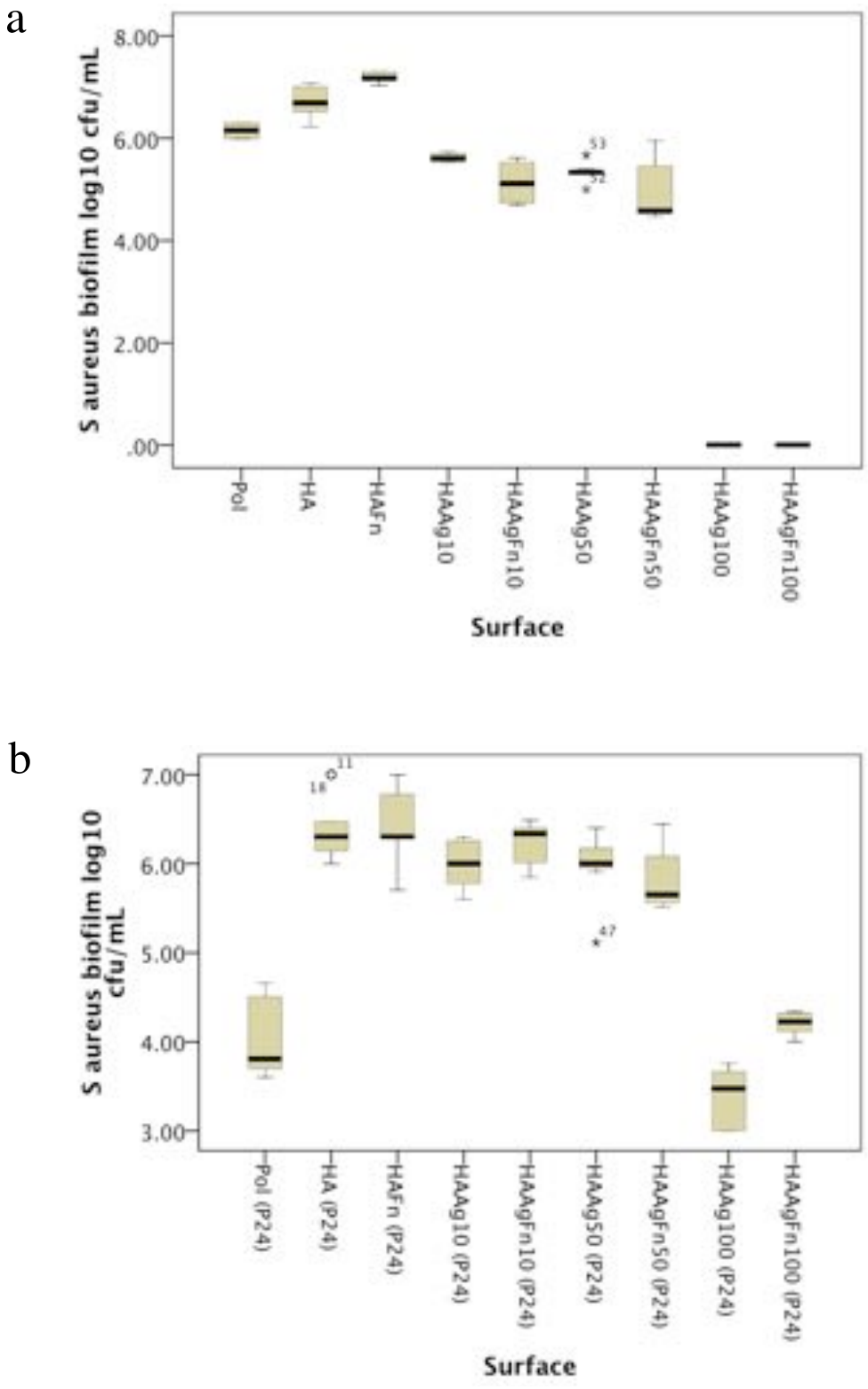

Figure 4.1 Results for number of *S aureus* colony forming units per mL within biofilms presented as $\log_{10}$ transformed numbers: (a) non-preconditioned surfaces and (b) preconditioned surfaces.

4.3.1.2 Planktonic Direct Colony Counts

HAAg100 and HAAgFn100 had the greatest antibacterial activity and were the only surfaces to reduce bacterial colonisation compared with all three control surfaces before and after serum-preconditioning ($p<0.05$. Exact individual p values for each comparison are shown in Appendix 4.1.5). HAAg100 (P24) was associated with a 2.493×10^7 cfu/mL reduction in planktonic colonisation compared with HA (P24) (99.72% reduction). HAAgFn100 (P24) reduced planktonic colonisation by 1.994×10^7 cfu/mL compared with HAFn (P24) (99.68% reduction). Fibronectin increased bacterial colonisation when adsorbed onto HAAg50 (P24) ($p=0.000$). This effect was not observed on other surfaces (Figure 4.2).

a

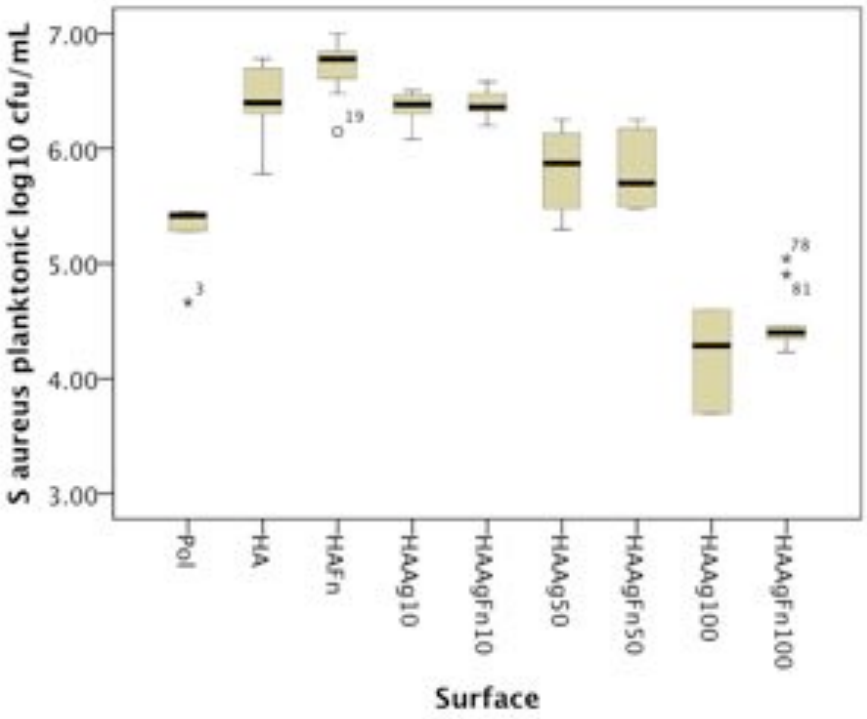

b

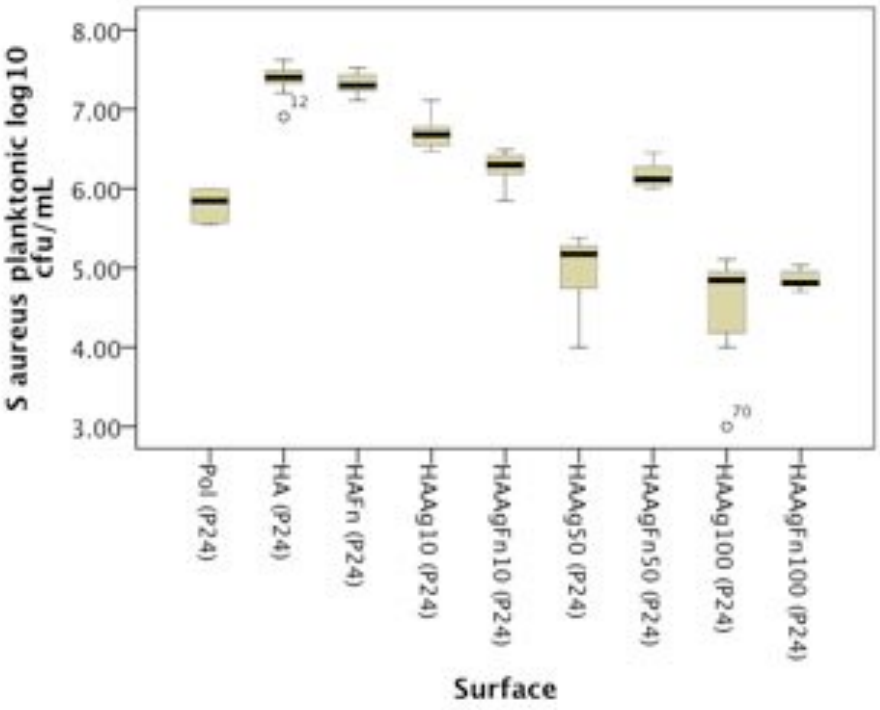

Figure 4.2 Results for number of *S aureus* colony forming units per mL within planktonic suspensions presented as $\log_{10}$ transformed numbers: (a) non-preconditioned surfaces and (b) preconditioned surfaces.

4.3.2 Direct Colony Counts for *P aeruginosa*

4.3.2.1 Biofilm Direct Colony Counts (10^6 cfu challenge)

HAAg100 (P0) reduced *P aeruginosa* colonisation within biofilms significantly compared with HA (p=0.001). Although the numbers of bacteria within *P aeruginosa* biofilms were fewer on HAAg100 than on Pol, there was no statistically significant difference (p=0.059). There was no difference between HAAg100 and HAAgFn100 (p=0.963). However, HAAgFn100 was the only surface to reduce bacterial colonisation compared with Pol (p=0.040). After preconditioning HAAg100 +/- Fn no longer had any antibacterial activity against *P aeruginosa* compared with Pol, HA and HAFn controls ($p<0.05$. Exact individual p values for each comparison are shown in Appendix 4.2.2) (Figure 4.3).

a

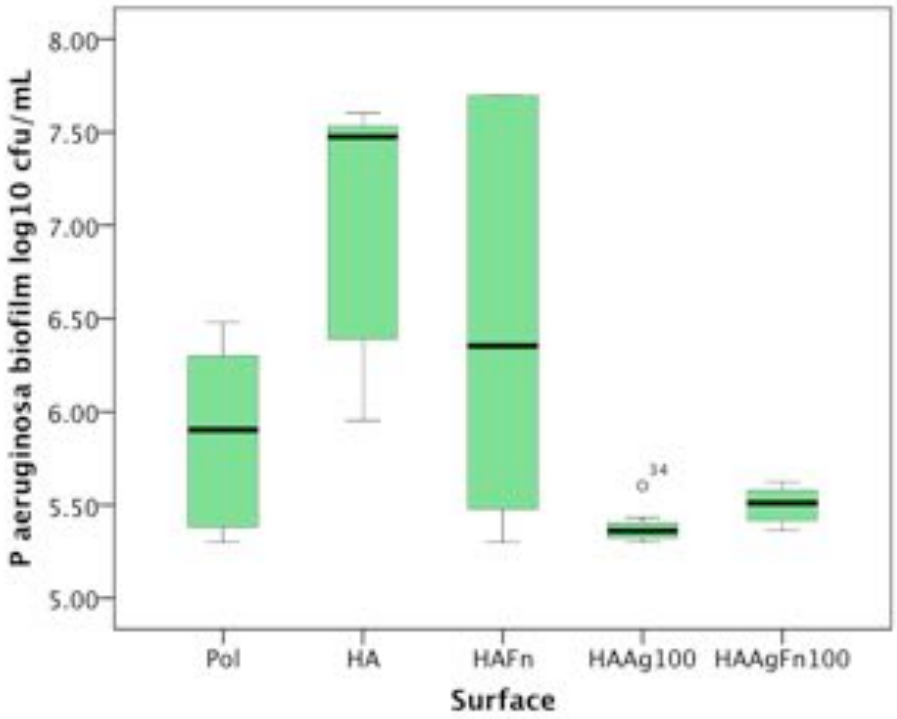

b

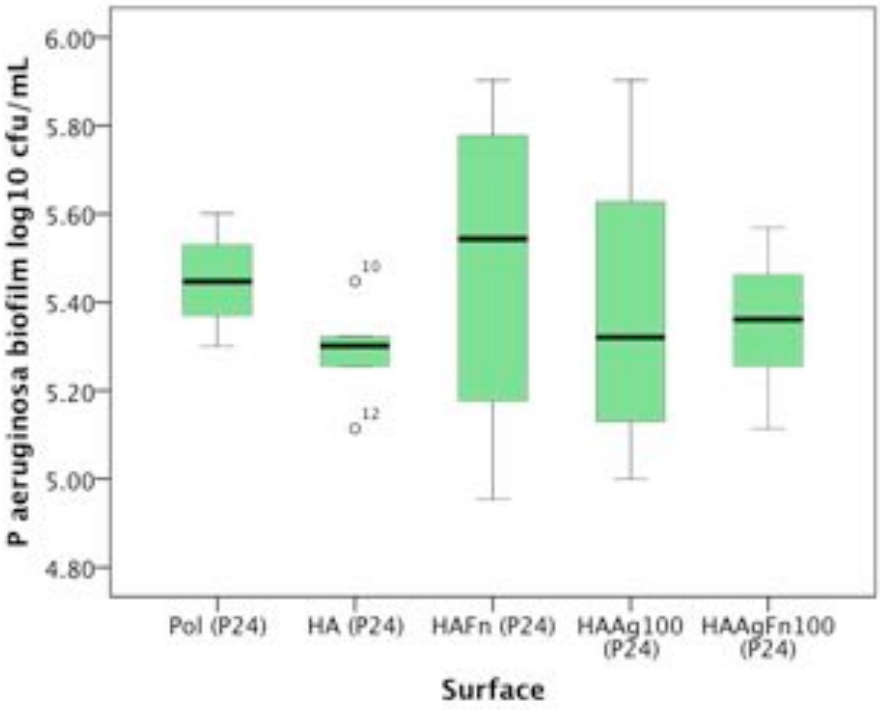

Figure 4.3 Results for number of *P aeruginosa* colony forming units per mL within biofilms presented as $\log_{10}$ transformed numbers: (a) non-preconditioned surfaces and (b) preconditioned surfaces.

4.3.2.2 Planktonic Direct Colony Counts (10^6 cfu challenge)

There were no differences in planktonic bacterial colonisation between the groups. HAAg100 +/- Fn (before and after preconditioning) did not have an antibacterial effect compared with controls (p=0.114) (Figure 4.4).

a

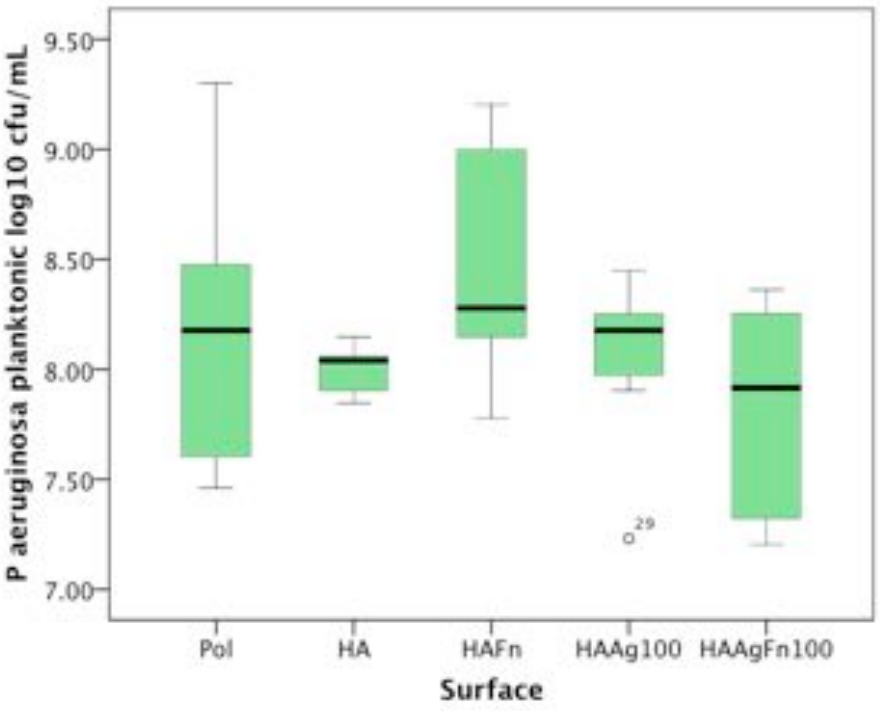

b

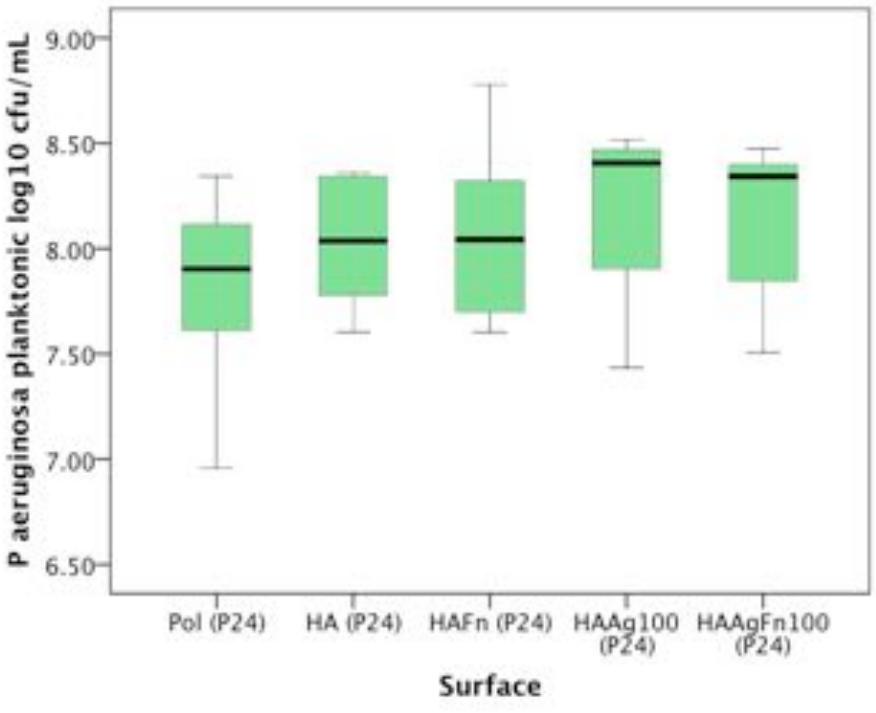

Figure 4.4 Results for number of *P aeruginosa* colony forming units per mL within planktonic suspensions presented as $\log_{10}$ transformed numbers: (a) non-preconditioned surfaces and (b) preconditioned surfaces.

4.3.2.3 Biofilm Direct Colony Counts (5 x 10^4 cfu challenge)

HAAg100 +/- Fn decreased bacterial numbers within biofilms compared with controls whether preconditioned or not ($p<0.05$. Exact individual p values for each comparison are shown in Appendix 4.1) (Figure 4.2.5). HAAgFn100 reduced bacterial colonisation compared with HAAg100 ($p=0.000$), however, after preconditioning there was no difference in bacterial colonisation between HAAg100 and HAAgFn100 ($p=0.055$). There was a reduction of 2.5 x 10^6 cfu/mL on HAAg100 (P24) compared with HA (P24), which is equivalent to a 62.5% reduction in bacterial colonisation. There was a reduction of 4.3 x 10^6 cfu/mL on HAAgFn100 (P24) compared with HAFn (P24) (71.66% reduction).

a

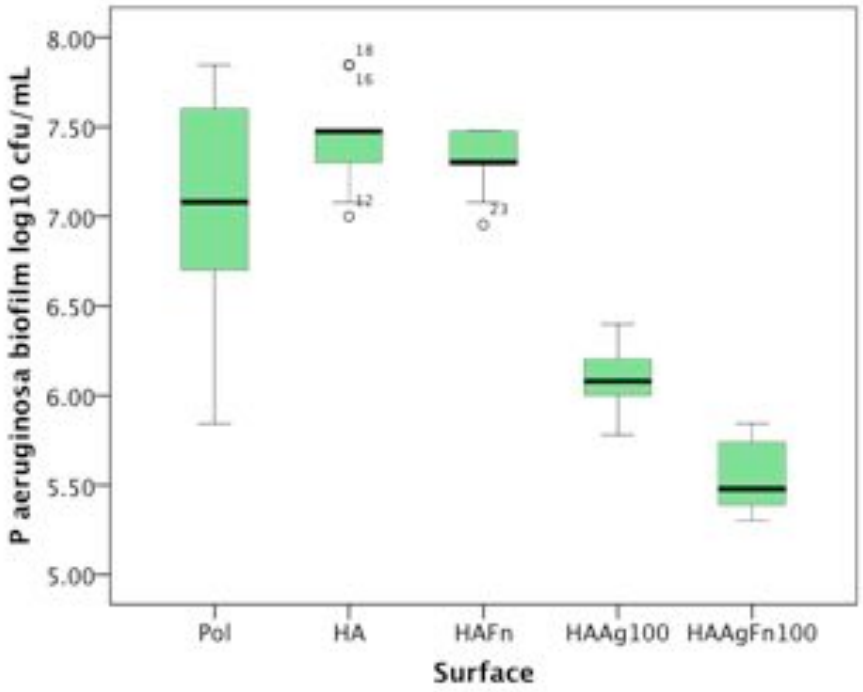

b

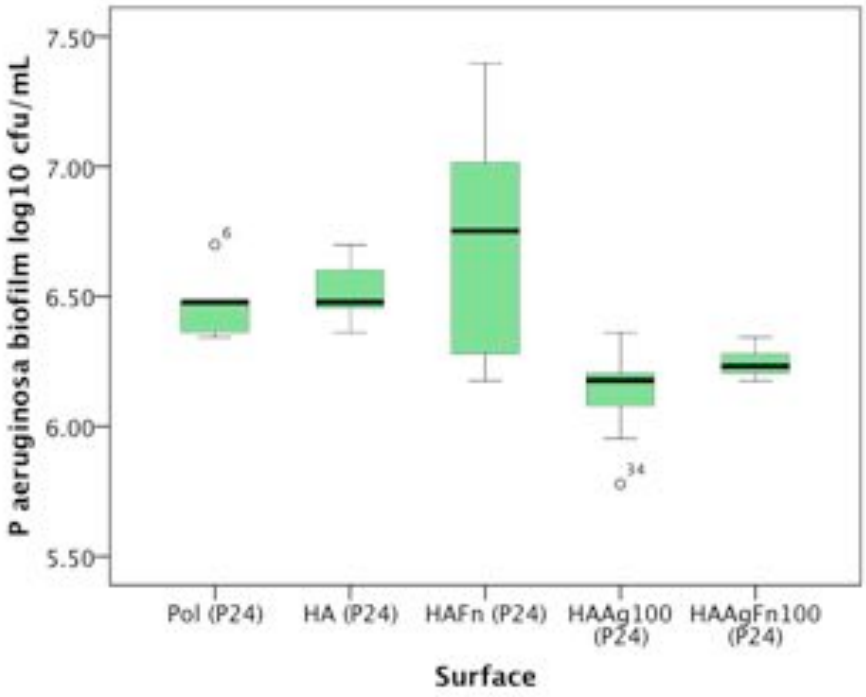

Figure 4.5 Results for number of *P aeruginosa* colony forming units per mL within planktonic suspensions presented as $\log_{10}$ transformed numbers: (a) non-preconditioned surfaces and (b) preconditioned surfaces.

4.3.2.4 Planktonic Direct Colony Counts (5 x 10^4 cfu challenge)

Similarly to the results presented above for biofilm colony counts, HAAg100 +/-Fn, whether preconditioned or not, reduced bacterial numbers within the planktonic suspensions significantly compared with the controls (p=0.000) (Figure 4.6). HAAgFn100 reduced bacterial colonisation compared with HAAg100 before and after preconditioning (p=0.000 and p=0.014 respectively). There was a reduction of 3.87 x 10^9 cfu/mL on HAAg100 (P24) compared with HA (P24), which is equivalent to a 92.14% reduction in bacterial colonisation. There was a reduction of 6.65 x 10^9 cfu/mL on HAAgFn100 (P24) compared with HAFn (P24) (97.08% reduction).

a

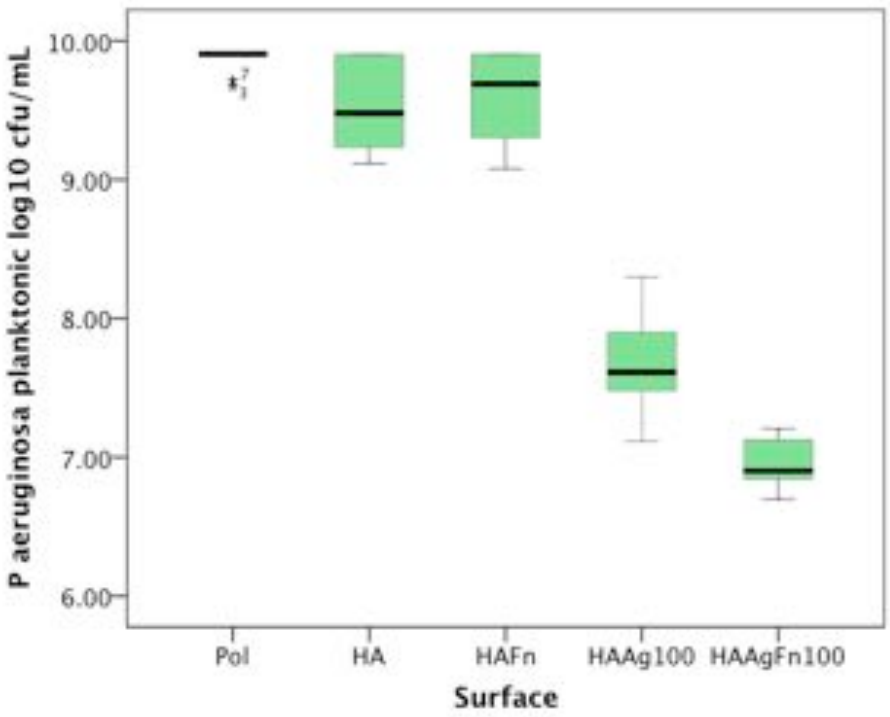

b

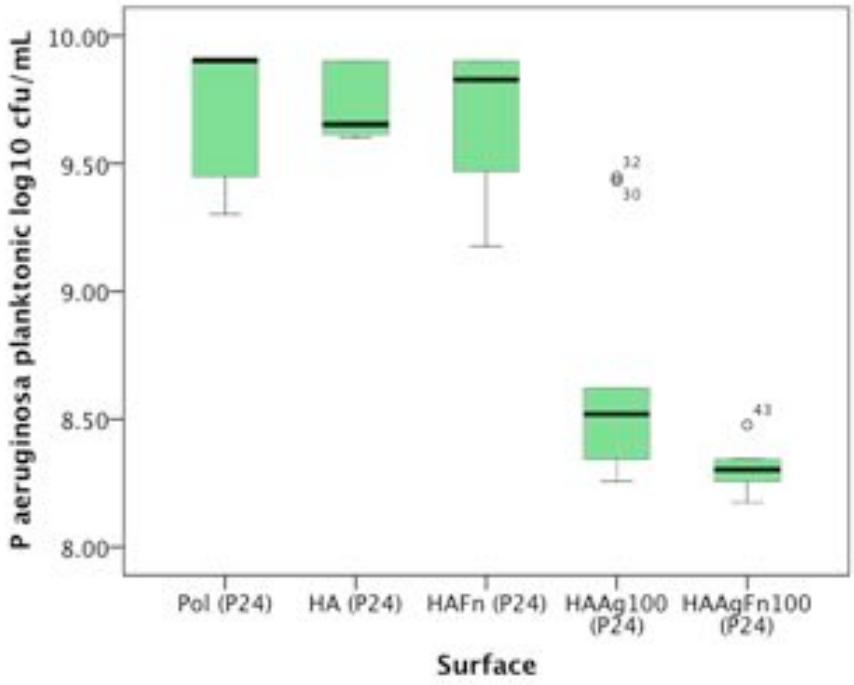

Figure 4.6 Results for number of *P aeruginosa* colony forming units per mL within planktonic suspensions presented as $\log_{10}$ transformed numbers: (a) non-preconditioned surfaces and (b) preconditioned surfaces.

4.3.3 Scanning Electron Microscopy *S aureus*

SEM findings were in keeping with the direct colony count results. The least bacterial colonisation was seen HAAg100 (before and after preconditioning). Extensive glycocalyx formation was observed on HA and HAFn and to a lesser extent on HAAg10 and 50 surfaces. Increased glycocalyx formation occurred on surfaces coated with fibronectin. After preconditioning, reduced bacterial growth was seen on Pol surfaces. This effect was not clearly observed on HA and HAFn. Preconditioning appeared to increase bacterial numbers on HAAg10 and 50 (+/- Fn). Differences in bacterial colonisation on HAAg100 and HAAgFn100 after preconditioning were not clear. Scanning electron micrographs showing *S aureus* colonisation on preconditioned are presented in Fig 4.7 (i) and (ii).

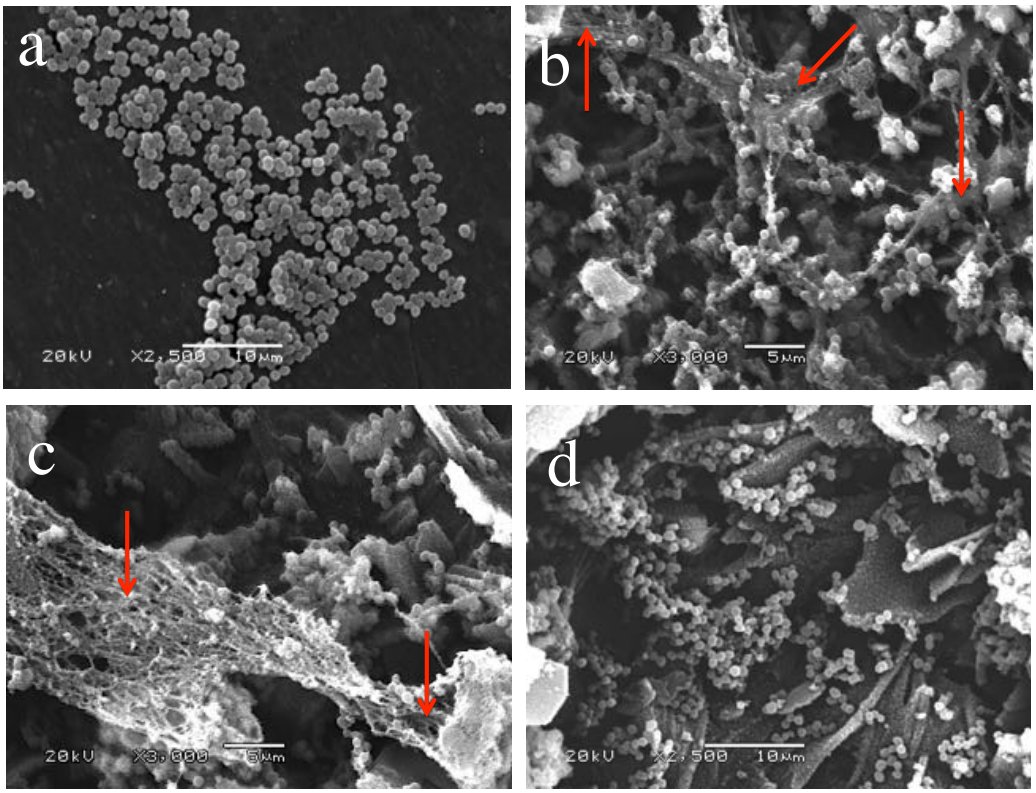

Figure 4.7 (i) Scanning electron micrographs showing *S aureus* colonisation on (a) Pol (P24) (b) HA (P24) (c) HAFn (P24) (d) HAAg10 (P24). The red arrows indicate glycocalyx formation.

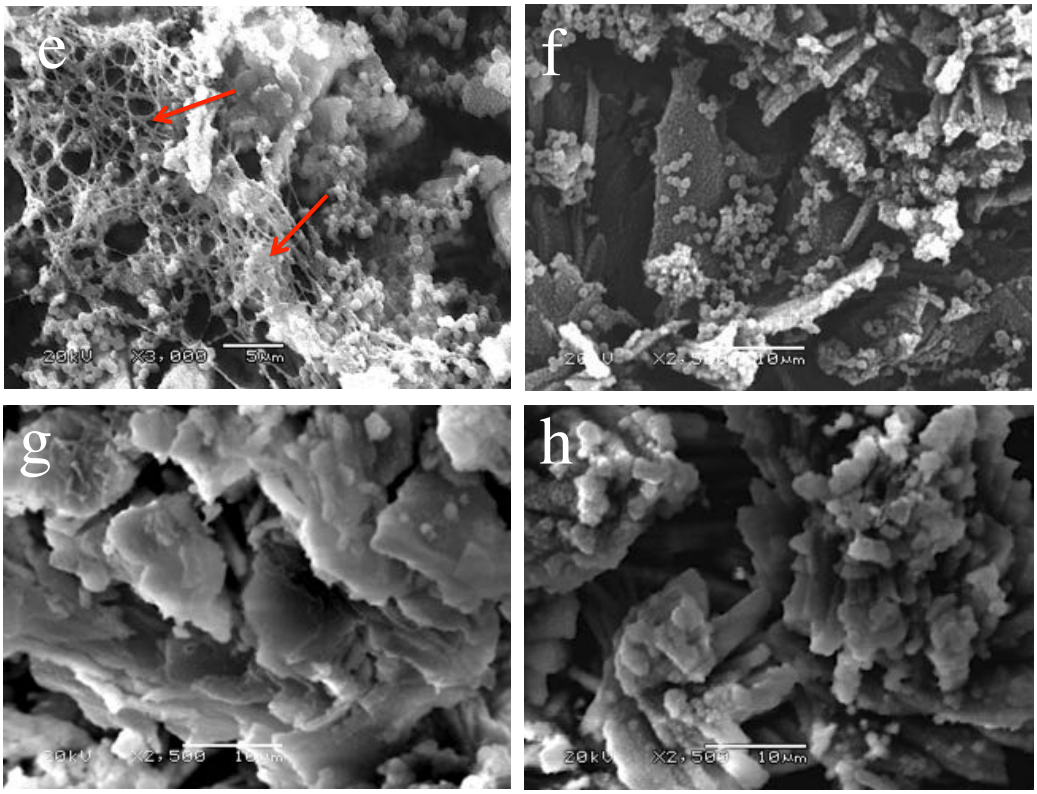

Figure 4.7 (ii) Scanning electron micrographs showing *S aureus* colonisation on (e) HAAgFn10 (P24) (f) HAAg50 (P24) (g) HAAg100 (P24) (h) HAAgFn100 (P24). The red arrows indicate glycocalyx formation.

4.3.4 Scanning Electron Microscopy *P aeruginosa*

The least bacterial colonisation was seen HAAg100 and HAAgFn100 (before and after preconditioning). There was no clear difference in bacterial colonisation associated with the presence of fibronectin. Heavy bacterial growth was present on control surfaces, with the presence of glycocalyx formation on HA and HAFn surfaces. Clear differences in numbers of bacteria on HAAg100 and HAAgFn100 surfaces after preconditioning were not observed. Scanning electron micrographs showing *P aeruginosa* colonisation on preconditioned surfaces are presented in Figure 4.8.

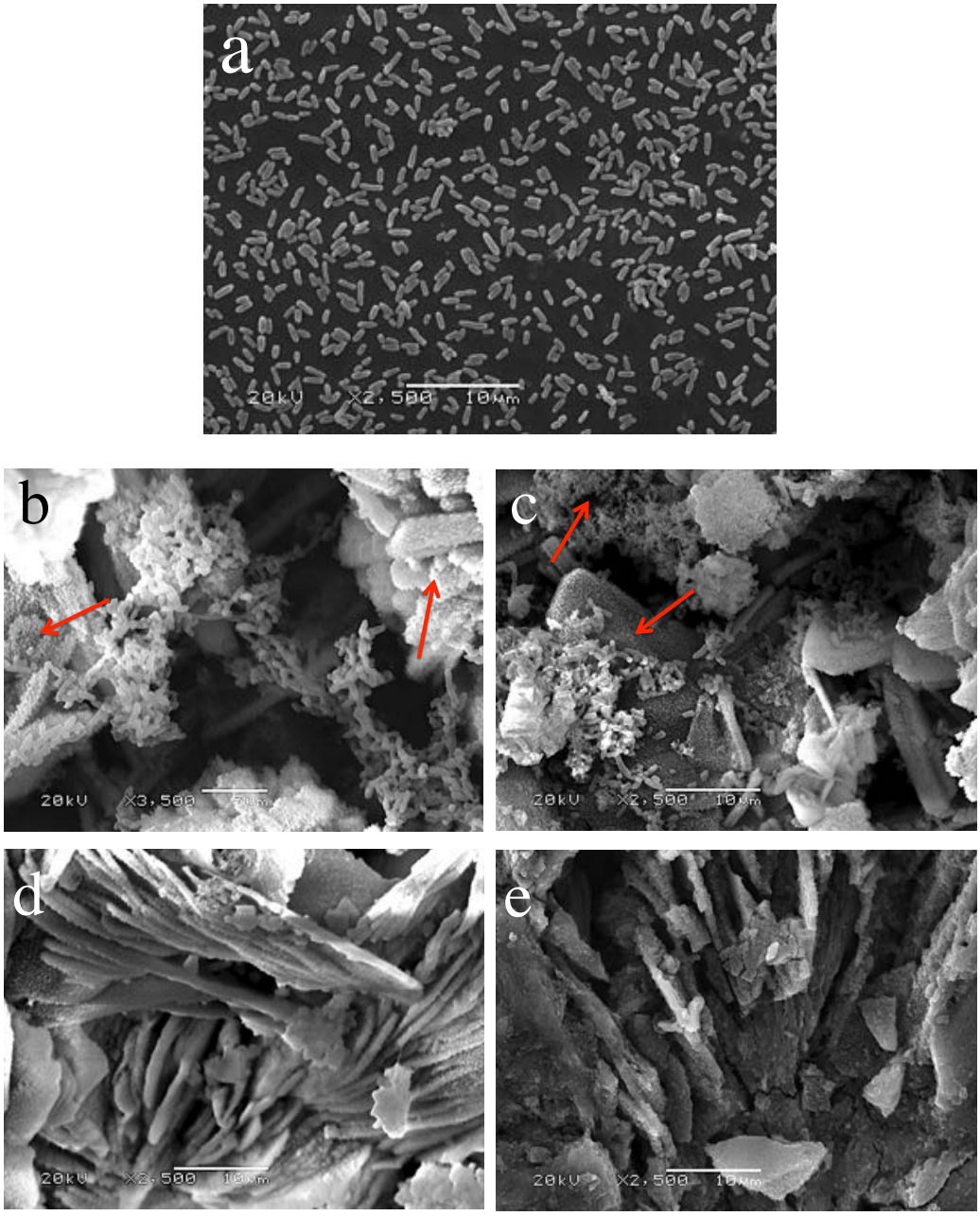

Figure 4.8 Scanning electron micrographs showing *P aeruginosa* colonisation (5 x 10^4 cfu challenge) on (a) Pol (P24) (b) HA (P24) (c) HAFn (P24) (d) HAAg100 (P24) (e) HAAgFn100 (P24). The red arrows indicate glycocalyx formation.

4.4 DISCUSSION

This chapter has shown that electrochemically deposited HAAg100 suppresses *S aureus* colonisation before and after preconditioning in fetal calf serum. *P aeruginosa* colonisation was also suppressed by HAAg100 before and after preconditioning when a smaller bacterial challenge was used.

Effect of Preconditioning on Antibacterial activity

Although HAAg100 and HAAgFn100 exerted an antibacterial effect compared with controls after preconditioning, some antibacterial activity was lost. This may be due to the same reasons that preconditioning increased the cytocompatibility of surfaces i.e. the slower release of silver after preconditioning. The observation that HAAg surfaces reduced planktonic bacterial numbers also indicates that silver is released from HAAg surfaces into the surrounding fluid. Studies of release kinetics of HAAg would be of value and will be conducted from porous ITAP flanges in Chapter Five in preparation for the *in vivo* study.

Interestingly, the effect of preconditioning on *S aureus* colonisation was different on controls and HAAg surfaces. Less bacterial colonisation was observed on Pol discs after they were preconditioned. Similar findings have been previously reported by other studies where adhesion of bacteria was significantly inhibited on surfaces treated with serum or proteins due to the formation of a barrier to bacterial adhesion (Pascual et al 1986; Paulsson et al 1993; Wassall et al 1997; Kinnari et al 2005). Hydrophilic proteins within serum such as albumin are believed to be responsible for this phenomenon as bacteria adhere better to hydrophobic surfaces (Pascual et al 1986; Kinnari et al 2005; Harris and Richards 2006). Conversely, Antoci et al (2007) ound an abundance of live adherent bacteria on titanium rods coated with serum (Antoci et al 2007b). The reason for this conflicting finding is unclear, but differences in the initial surface characteristics of the underlying substrate may be relevant. Further research on the wettability of these surfaces may be of value and will be conducted in Chapter Five. Reductions in *S aureus* colonisation were also seen on HA and HAFn but were less marked than those seen on Pol. Indeed, large

numbers of bacteria in the range of more than 10^6 colonies remained present on HA and HAFn surfaces after preconditioning meaning this reduction is unlikely to be clinically useful. The reduction in *S aureus* colonisation on Pol is also not likely to be exploited clinically as Pol would be unsuitable as a surface for osseointegrated transcutaneous implants due to inadequate soft tissue attachment *in vivo* (Pendegrass et al 2006a). Preconditioning HAAg surfaces had the opposite effect to preconditioning controls and there was an increase in *S aureus* colonisation. If silver from preconditioned HAAg coatings had become bound to proteins and some silver had been inactivated as discussed earlier, it is expected that the effect of this postulated increase in wettability would have been counteracted.

The effects of preconditioning on *P aeruginosa* colonisation were less marked and less consistent than those observed with *S aureus*. *P aeruginosa* biofilm formation was significantly reduced on controls when the lower bacterial challenge was administered; but there was no difference when a higher bacterial challenge was used and there was no difference in planktonic colonisation. Planktonic *P aeruginosa* colonisation associated with HAAg and HAAgFn increased after preconditioning when the lower bacterial challenge was used. No other significant differences were associated with preconditioning. *P aeruginosa* is a 'notorious' producer of glycocalyx (Neut et al 2005). This may be responsible for the finding that preconditioning had less of an effect on reducing *P aeruginosa* biofilm formation on controls compared with *S aureus*. Increased glycocalyx formation may also be a potential reason for the less marked effect of preconditioning on *P aeruginosa* colonisation on HAAg surfaces. This is because it may cause *P aeruginosa* to be less sensitive to the antibacterial effects of HAAg meaning that any inactivation of silver by the proteins from the preconditioning film would have a reduced effect. As discussed in Chapter One, it has been suggested that the encasement of bacteria by glycocalyx prevents penetration of antimicrobial agents through biofilms and physically prevents access to the bacterial cell (Foley and Brown 1999; Donlan and Costerton 2002). However, as glycocalyx is composed predominantly of water, it may be considered that this is unlikely and that the effect of glycocalyx is mainly due to modification of the microenvironment leading to nutrient limitation, reduced

bacterial growth rates and consequently protection of the bacteria from antimicrobial agents (Prosser et al 1987; Stewart and Costerton 2001). This is an explanation for the reduced susceptibility of *P aeruginosa* to silver due to its increased glycocalyx formation.

Effect of Silver Content of Coatings on Antibacterial Activity

In terms of *S aureus* colonisation, HAAg50 and 10 did not perform as well as HAAg100 in terms of antibacterial activity. The only potential advantage of these lower silver content coatings is that before preconditioning they were less cytotoxic than HAAg100 as shown in Chapter Three. This raises the possibility that they may be able to promote earlier attachment of viable fibroblasts but this is not conclusive. After preconditioning there was no difference in HAAg50 and 10 groups in terms of cytotoxicity compared with HAAg100. Therefore, only HAAg100 surfaces were challenged with *P aeruginosa* as HAAg10 and HAAg50 would thus be less clinically useful due to this.

Differences in Colonisation between *P aeruginosa* and *S aureus*

P aeruginosa was less susceptible to HAAg100 than *S aureus,* which may be due to increased glycocalyx formation as discussed above. In particular, *P aeruginosa* biofilm bacteria were much more resistant to the antibacterial effects of HAAg than *S aureus* biofilm bacteria as indicated by the considerably lower percentage reductions of *P aeruginosa* biofilm cfu/mL compared with *S aureus*. When the 10^6 cfu bacterial challenge was used, HAAg100 (before preconditioning) suppressed *S aureus* colonisation completely but only reduced *P aeruginosa* biofilm bacterial numbers compared with HA and HAFn and not compared with Pol. After preconditioning HAAg100 had no significant antibacterial effect on *P aeruginosa* even compared with HA. When the bacterial challenge was reduced by a factor of 50 to 5 x 10^4 cfu/mL, HAAg100 still did not suppress *P aeruginosa* colonisation completely but reduced colonisation compared with all controls before and after preconditioning. It is possible that the administration of bacterial challenges of 10^6 and 5 x 10^4 cfu *P aeruginosa* colony forming units for a 10 mm x 3 mm disc (surface

area of 251 mm^2) could be considered excessively large quantities of bacteria which should rarely be encountered clinically in the early post-operative period before a soft tissue seal forms. Therefore, the fact that these surfaces were only antibacterial to *P aeruginosa* with the smaller bacterial challenge may still make these surfaces clinically useful. It is possible that with a smaller bacterial challenge HAAg10 and HAAg50 may have been able to demonstrate a greater antibacterial effect on *S aureus*. If HAAg surfaces are exposed to just a few bacteria it would be more likely to be able to suppress *P aeruginosa* as well *S aureus* colonisation completely. This is relevant as infection of surgical implants may start with small numbers of bacteria colonising the surface (Gosden et al 1998).

As *S aureus* is the most common organism causing infection of osseointegrated transcutaneous implants (Tillander et al 2010), the effect of HAAg against *S aureus* is particularly important. It was encouraging to ascertain that HAAg100 was able to withstand such a large bacterial challenge of 10^6 cfu of *S aureus*. Further challenges with other bacterial strains would be of interest for future research. For example, challenges with *Acinetobacter Baumannii,* a multi-drug resistant bacterium that has become a significant cause of war-related traumatic soft tissue infections may be relevant to ITAP (Guerrero et al 2010). Challenges with bacteria isolated from clinical infections of ITAP or other transcutaneous implants would be of particular value.

It is likely that increasing the silver content in the electrolyte solution would have produced a greater antibacterial effect. However, a higher silver content is likely to increase the cytotoxicity. This approach would have required further assessment of the effects on fibroblasts. If higher silver contents were found to be cytocompatible after preconditioning, there would still be an increased risk of adverse local tissue effects *in vivo* as well as higher circulating blood levels and potentially an increased risk of systemic toxicity.

Although this study found that *P aeruginosa* was less susceptible to HAAg than *S aureus* other researchers have found the opposite and have concluded that gram-negative bacteria are more susceptible to silver ions than gram-positive bacteria (Feng et al 2000; Kawahara et al 2000). It has been proposed that the increased thickness of the peptidoglycan in the cell walls of gram-positive bacteria protect the cell from penetration of silver ions into the cytoplasm (Feng et al 2000). Kawahara et al tested the susceptibility of a range of gram-negative and gram-positive oral bacteria and concluded that gram-positive bacteria were less susceptible due to the fact that peptidoglycans are negatively charged resulting in the thicker peptidoglycan wall of gram-positive bacteria allowing less positively charged silver ions to reach the plasma membrane (Kawahara et al 2000). A reason for this conflicting finding is that the gram-negative bacteria tested in these studies were not *P aeruginosa* specifically. On the other hand, Niakan et al (2013) found a slight decrease in the antimicrobial activity of silver against *P aeruginosa* compared with *S aureus*, which is in keeping with this study (Niakan et al 2013). Additionally, it has been shown that silver has varying inhibitory effects on different strains of *P aeruginosa* (Palanisamy et al 2014). It is likely that the degree of glycocalyx production varies between different strains of *P aeruginosa,* which would result in differences in the susceptibility to silver and other antimicrobials.

Effects of Fibronectin on Bacterial Colonisation

The adsorption of fibronectin onto preconditioned HAAg100 surfaces significantly increased *S aureus* colonisation to the extent that HAAgFn100 (P24) was not antibacterial compared with Pol; (although it was still antibacterial compared with HA and HAFn (P24)). In addition to the possibility of some inactivation of silver associated with fibronectin, fibronectin contains *Staphylococcal* binding sites (Bozzini et al 1992). The results of this study indicate that silver does not counteract the effect of these binding sites. It has been shown that functionalisation of biomaterials with the RGD sequence of fibronectin, which is responsible for cell binding, does not increase adhesion of *S aureus*, *S epidermidis, Streptococcus mutans* and *P aeruginosa* (Maddikeri et al 2008; Shi et al 2008). Therefore, RGD

coatings may be less likely to increase bacterial colonisation than fibronectin and would ultimately be more commercially acceptable.

The significant increase in *S aureus* colonisation associated with fibronectin was not observed with *P aeruginosa*. This is likely to be due to differences in fibronectin binding sites. Decreased hydrophobicity caused by adsorption of fibronectin may also contribute to the reduced adhesion of bacteria (Dexter et al 2001). Similarly to this study, previous research has shown that *P aeruginosa* has a lower affinity for fibronectin than *S aureus*. For example, Plotkowski et al (1993) exposed coverslips coated with plasma or cellular fibronectin to radiolabelled bacteria. They showed that adhesion of *S aureus* to coverslips coated with fibronectin was significantly greater than adhesion to control coverslips coated with bovine serum albumin. There was no difference in *P aeruginosa* adhesion to fibronectin coated or control coverslips (Plotkowski et al 1993). It is also noted that when the lower bacterial challenge was used in this chapter, fibronectin was associated with a reduction in *P aeruginosa* colonisation on HAAg100 surfaces (before preconditioning). This is in keeping with the findings of studies on the colonisation of the upper respiratory tract and adherence of gram-negative bacilli to epithelial cells. An inverse relationship between cell-surface fibronectin and the adherence of gram-negative bacteria to these cells has been described (Woods et al 1980; Woods et al 1981; Abraham et al 1983; Simpson et al 1985; Woods 1987). Woods et al trypsinised buccal epithelial cells and reduced the amount of fibronectin on the cell surface. The loss of fibronectin increased the adherence of *P aeruginosa* (Woods et al 1981). It has been postulated that gram-negative bacterial adhesion to fibronectin-coated surfaces could be enhanced by proteolytic enzymes produced by the bacteria that are able to degrade fibronectin (Abraham et al 1983; Woods 1987). The clinical implications of this are that proteases produced by *P aeruginosa in vivo* that degrade fibronectin could result in any inhibitory effects of fibronectin coatings on *P aeruginosa* adhesion being lost. It may also mean that fibroblasts are less likely to win the 'race for the surface' against *P aeruginosa*. This is because if these coatings are colonised with *P aeruginosa*, the effect of fibronectin on soft tissue attachment could be reduced due to degradation of fibronectin.

It is possible that other strains of *P aeruginosa* may behave differently and colonise fibronectin-coated surfaces to a greater extent as contrary to the research discussed above, some studies have found that *P aeruginosa* binds to fibronectin and that fibronectin enhances *P aeruginosa* adherence (Mohammad et al 1988; Baleriola-Lucas and Wilcox et al 1998). Fibronectin-binding is known to be strain specific with different strains of the same species having different affinities for fibronectin. Studies on a range of *S epidermidis* strains have illustrated this point and shown that the adhesion of some strains may be increased by fibronectin coatings while the adhesion of other strains of the same species is decreased (Herrmann et al 1988; Dunne and Burd 1993; Dexter et al 2001).

Limitations of This Study

Fetal calf serum was chosen over simulated body fluid for preconditioning as it contains serum proteins such as albumin and globulins and so was more representative of the *in vivo* environment than simulated body fluids. Nonetheless, it could be argued that a limitation of this study is that plasma would have been more representative as it contains clotting factors such as fibrinogen in addition to serum proteins. This may be relevant as *S aureus* contains fibrinogen-binding proteins.

Another potential limitation of the i*n vitro* work presented in this chapter and Chapter Three is that the coatings were applied to solid surfaces but will be applied to a porous titanium alloy for the *in vivo* studies. Bacterial colonisation and cell viability are likely to be different on a porous surface and this may result in the effect of the coatings being different when applied to a porous surface. This may render the findings of these *in vitro* studies less representative of what will occur *in vivo*. It would not have been feasible to apply these coatings to the porous structure that will be used *in vivo* as the bacteria and cells would have fallen though the pores due to the larger size of the pores that will be used (based on the results of Chapter Two).

4.5 CONCLUSION

This study has shown that electrochemically deposited HAAg surfaces have antibacterial activity against both *S aureus* and *P aeruginosa in vitro*. Before preconditioning, complete suppression of *S aureus* biofilm formation was observed on HAAg100 and HAAgFn100 when challenged with 10^6 cfu/mL. After serum-preconditioning more than 99% of the antibacterial activity of HAAg100 and HAAgFn100 against *S aureus* compared with HA and HAFn controls was maintained for both biofilm and planktonic colonisation. *P aeruginosa* was less susceptible to the antibacterial effects of HAAg100 and HAAgFn100 than *S aureus*. HAAg100 and HAAgFn100 resulted in smaller reductions in *P aeruginosa* colonisation and only demonstrated significant antibacterial activity after preconditioning when a smaller bacterial challenge of 5 x 10^4 cfu/mL was used. When considering the results of this chapter in conjunction with those from Chapter Three, the findings indicate that fibroblasts would win the 'race for the surface' against bacteria on HAAg100 and HAAgFn100 after serum-preconditioning depending on the strain and the quantity of the bacteria they are exposed to. It is important that the antibacterial effects of the HAAg coatings persist for a sufficient period of time for cell attachment to occur. This may mean that antibacterial activity is required until a soft tissue seal has formed, which may be between two and four weeks. The duration of the release of silver from the HAAg coating (when applied to porous titanium implants) will be studied in Chapter Five. The *in vivo* performance of these coatings applied to porous titanium will be presented in Chapters Six and Seven of this thesis.

CHAPTER FIVE

Preparation of Transcutaneous Pins with Hydroxyapatite, Silver and Fibronectin-Coated Porous Titanium Alloy Flanges

5.1 INTRODUCTION

A transcutaneous pin *in vivo* ovine model will be used in Chapters Six and Seven to study the effects of porous titanium alloy flanges coated with HAAgFn on soft tissue integration and bacterial colonisation. The HAAg100 and HAAgFn100 coatings that were shown in Chapters Three and Four to have antibacterial activity and to promote viable fibroblast growth after serum-preconditioning will be used to coat the flanges. The flanges will have a pore size of 700 μm and a strut size of 300 μm, as this was found to support soft tissue ingrowth and revascularisation in Chapter Two. This chapter presents the transcutaneous pin design and the characterisation of the coatings produced on the flanges. It is important to determine that the coatings produced on the porous titanium alloy flanges have a similar composition and topography to the coatings selected from the *in vitro* studies as the aim is to produce a similar effect on fibroblasts and bacteria *in vivo*. The coatings should be present throughout the porous structure without occluding the pores.

It is also important to determine the release of silver from the coatings. The *in vivo* studies will be conducted over a four-week period in order to allow adequate time for a soft tissue seal to form. Ideally, silver should continue to be released until cells have been able to attach and it may be of value to have continued silver release for two to four weeks until the soft tissue seal has formed. Electrochemically deposited HAAg coatings have previously been shown to provide a controlled and sustained release of low levels of silver ions over 22 days. Ghani et al (2012) demonstrated median silver release levels of 444 ppb (4.116 μmol/L) at 10 days, 376.5 ppb (3.490 μmol/L) at 15 days and 170 ppb (1.576 μmol/L) at 22 days. These levels were found to have bactericidal activity *in vitro* (Ghani et al 2012). The amount of silver released and the amount of silver passing into the blood circulation must be below toxic levels to avoid local and systemic toxicity. The results of the *in vitro* sections of this thesis indicate that cells may not attach initially due to local toxicity but that following exposure to serum for up to 24 hours the local toxic effects will be reversed. The *in vitro* bacterial colonisation studies presented in this thesis have indicated that the level of release (even when eukaryotic cells are able to attach) would be bactericidal. In other words there is a 'window of opportunity' when

surfaces allow cell growth but at the same time prevent viable bacterial attachment. *In vivo*, the porous implants used will have a larger surface area than those tested *in vitro*. This means that although the composition of coatings used *in vivo* will be similar to those tested *in vitro*, the absolute silver content will be greater. If the overall silver content of the coatings and the amounts released into the tissues are not sufficiently low, local cellular toxicity may persist for longer than 24 hours and may have a detrimental effect on wound healing. Systemic toxic effects such as argyria and argyrosis may also occur. Argyria and argyrosis occur due to the deposition of silver in the dermis and cornea and/or conjunctivae resulting in irreversible discolouration of the tissues (Drake and Hazelwood 2005; Lansdown 2010). Total body silver concentrations ranging from 3.8 to 6 g have been found to produce argyria and argyrosis (Gosheger et al 2004; Lansdown 2010). Other systemic toxic effects of silver that have been described include leucopenia, liver and renal toxicity (Choban and Marshall 1987; Gamelli et al 1993; Chaby et al 2005; Trop et al 2006).

Chapter Three has shown that the topography of HA and HAAg coatings is altered by preconditioning. Differences in topography influence wettability of surfaces (Wenzel 1936). Wettability is known to affect cell spreading and attachment. Studies have demonstrated improved cell attachment to hydrophilic surfaces (Teare et al 2000; Shen and Horbett 2001). Other studies have found that increased wettability improves cell attachment up to a point and that moderate wettability produces the most favourable cellular responses (van Wachem et al 1987; Tamada and Ikada 1993; Lee et al 1998; Kim et al 2007). It would be of interest to determine if the wettability of surfaces is affected by preconditioning. Additionally, the effect of serum-preconditioning on the crystallinity of HAAg coatings has not been studied. Foppiano et al (2006) showed that the crystallinity of ceramics is altered by preconditioning and they postulated that changes in crystallinity may contribute to improved cytocompatibility of preconditioned surfaces (Foppiano et al 2006; Foppiano et al 2007). XRD analysis of bioactive glass coatings showed that the intensity of peaks corresponding to crystalline phases is reduced after immersion in simulated body fluids (Foppiano et al 2006).

The aim of this chapter was to produce HAAgFn coatings on porous titanium alloy and to determine the topography and composition of the coatings as well as the release of silver from the coatings. Additionally, this chapter aimed to assess the crystallinity and wettability of the coatings and the effect of serum-preconditioning on the coatings.

It was hypothesised that HAAgFn coatings with a similar topography and composition to the coatings tested *in vitro* could be applied throughout porous titanium alloy structures. It was also hypothesised that serum-preconditioning would reduce the crystallinity and increase the wettability of coatings. Finally, it was hypothesised that the release of silver would be sustained over a four-week period and that the release rate would reduce over time.

5.2.1 Transcutaneous Pin Designs and Coatings

Transcutaneous pins with a laser sintered porous titanium alloy flange (pore size 700 μm and strut size 300 μm) (Eurocoatings, Trentino, Italy) were used. A dome-shaped flange was designed in an attempt to further increase soft tissue integration. Laser sintering was used instead of the electron beam manufacturing technique reported in Chapter Two because it was able to produce structures with a finer surface finish (Koike et al 2011a). Figure 5.1 is a photograph of the basic pin design. The flanges were either uncoated (PT) or coated with HA (PT-HA), HAFn (PT-HAFn), HAAg100 (PT-HAAg) or HAAgFn100 (PT-HAAgFn).

Figure 5.1 Photograph of the transcutaneous pin design.

5.2.2 Surface Preparation

5.2.2.1 Cleaning of Implants

The pins were ultrasonicated in 10% Decon 90 for 20 minutes. An air gun was used to fire debris out from within the pores of the implants before and after ultrasonication in 10% Decon 90. This was followed by ultrasonication in Industrial Methylated Spirits for 20 minutes.

5.2.2.2 Electrochemical Deposition

As described previously, a 0.13 M calcium phosphate monobasic solution was used with 100 mg of $AgNO_3$ added per litre of solution to produce HAAg coatings (in view of the findings from Chapter Three and Four that HAAg100 had the most antibacterial activity whilst being cytocompatible after preconditioning). The current density and time period used to produce HA and HAAg100 coatings in the *in vitro* chapter did not produce a uniform coating throughout the porous structures. As a result the current density and time period were modified. Electrochemically deposited coatings were produced using a current density of 58 mA/cm^2 for 270 seconds because this was the highest current density and longest time period that produced uniform coatings of both HA and HAAg.

5.2.2.3 Sterilisation

Implants were sterilised with dry heat at 160°C for one hour.

5.2.2.4 Adsorption of Fibronectin

Fibronectin was adsorbed onto the porous flanges by immersing implants (with the intraosseous and transcutaneous pin portions masked) into a solution containing 2745 ng of fibronectin for 1.5 hours. This was in order to coat the flanges with 6.37 ng/mm^2 of fibronectin (equivalent to the amount of fibronectin used for the *in vitro* experiments). This technique has been described previously (Pendegrass et al 2010a).

5.2.3 Surface Characterisation

Separate flanges without the transcutaneous pins were manufactured specifically for surface characterisation.

5.2.3.1 Surface Topography, Coating Morphology and Thickness

SEM was performed to visualise the surface topography and morphology of all coatings on the outer surface of the implants (n=3, N=6). Additionally, SEM was used to measure the thickness of HA and HAAg coatings on the outer surface of the implant and within the central pores after embedding samples in LR White Resin (n=2, N=4). The embedded samples were cut longitudinally through the centre with the Exakt diamond edge saw and polished (using the polishing technique described in Section 3.2.1). A ruler was used to measure the coating thickness. The measurements in millimetres were transformed to micrometres by taking into account the magnification bar of the scanning electron micrographs.

5.2.3.2 Elemental Composition and Percentage of Silver

EDX analysis was performed to determine the Ca/P ratio of HA coatings and to measure the atomic and weight percentage of Ag within coatings (n=3, N=6).

5.2.3.3 Silver Release

The amount of silver released into fetal calf serum from PT-HAAg was measured over a four-week period (n=3). PT-HA was used as a control. The flanges were placed in 5 mL of fetal calf serum at room temperature. Flanges were removed on days 0 (at 4 hours and 8 hours), 1 (at 24 hours), 2, 3, 4, 5, 8, 11, 14, 18 and 28. Flanges were placed into a fresh fetal calf serum solution at each time point. Inductively Coupled Plasma Mass Spectrometry (ICP-MS) (Dr Barry Sampson, Trace Element Laboratory, Imperial College London, UK) was used to quantify the silver content in elution fluids. This allowed the silver release between time points to be determined.

5.2.3.4 Absolute Silver Content of Coatings

Coatings were removed from PT-HA and PT-HAAg flanges by immersion in 2 N nitric acid (HNO_3) for 30 minutes. SEM and EDX analysis was performed to confirm that the coatings had been removed from these samples. ICP-MS (Dr Barry Sampson, Trace Element Laboratory, Imperial College London, UK) was performed to measure the silver content of coatings extracted into the HNO_3 solution.

5.2.3.5 X-ray diffraction analysis

X-ray diffraction analysis (XRD) (Dr George Georgiou, Department of Biomaterials and Tissue Engineering, Eastman Dental Unit, University College London, UK) was performed on solid discs - Pol, HA, HAFn, HAAg, HAAgFn, HAAg after serum-preconditioning for 24 hours (P24) and HAAgFn P24 (n=3). The preconditioned surfaces were tested in order to observe the effect of contact with serum on crystallinity. The same electrochemical deposition method used for porous flanges described in section 5.2.2 was used. Adsorption of fibronectin onto disc surfaces was performed by addition of a 20 μL droplet containing 500 ng of fibronectin. XRD analysis was performed using a Brüker D8 Advance Diffractometer (Brüker, UK) operated with Ni-filtered Cu Kα radiation. Data were collected from 2θ 10° to 100° with a count time of 0.1 seconds per point with a Brüker Lynx Eye detector. Due to the detection of background noise, further data collection was carried out for HA, HAAg and HAAgP24 with a longer count time of 1 second per point. Peaks in the resultant diffraction patterns were identified by comparison with pure Ti, HA and Ag diffraction patterns from the Inorganic Crystal Structure Database (ICSD).

5.2.3.6 Wettability

Fresh samples of the same surfaces (on solid discs) that underwent XRD analysis were assessed. The KSV CAM 200 goniometer (KSV Instruments, Finland) was used for contact angle measurement. A precision syringe was used to allow precise control over the volume of a droplet of ultrapure water that was placed on each disc surface. Images were collected each second for 10 seconds. The CAM 200 computer software was used to measure the contact angle between the droplet and the surface

(on both the left and the right side of the droplet). Figure 5.2 shows the angles measured for contact angle measurement.

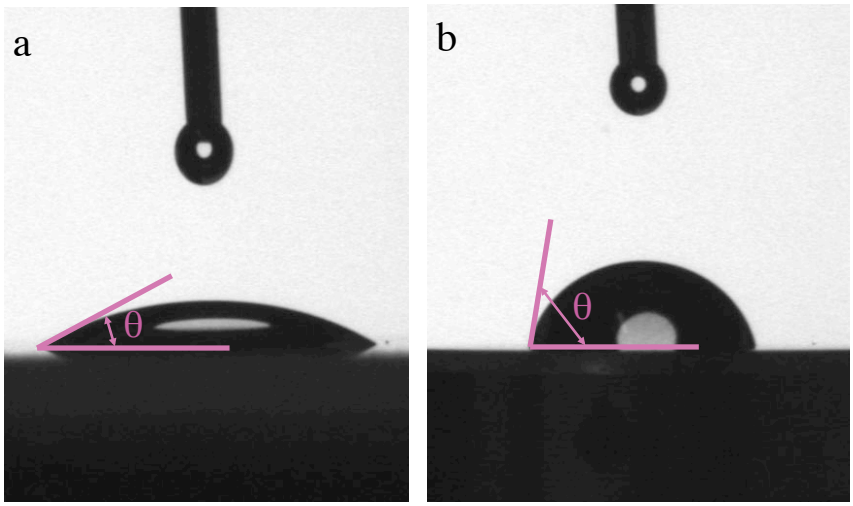

Figure 5.2 Contact angle measurement. A lower contact angle (θ) indicates increased hydrophilicity (i.e. wettability): (a) a hydrophilic surface and (b) a hydrophobic surface.

5.2.4 Statistical Analysis

Data were analysed using SPSS, version 21.0 for Windows (Chicago, US). As described in the previous chapters of this thesis, non-parametric tests were performed as the data did not fit assumptions for parametric testing. The Kruskall Wallis test was used to determine if differences existed between the groups. Mann-Whitney tests were used to perform pair-wise comparisons.

5.3 RESULTS

5.3.1 SEM and EDX Analysis

The electrochemically deposited coatings on the porous titanium alloy flanges contained a combination of plate-like, needle-shaped and globular crystals similar to that observed on solid discs for the *in vitro* experiments from Chapter Three. The coatings on the porous flanges were more uniform in their appearance than those seen on the solid discs. EDX analysis showed that there was no significant difference in the percentage silver content between PT-HAAg +/- Fn and the HAAg100 +/- Fn coatings used for the *in vitro* experiments (Kruskall Wallis Test: weight percentage p=0.357, atomic percentage p=0.611). (Table 5.1). The median calcium:phosphate atomic percentage ratio for electrochemically deposited HA coatings was 1.74 (95% confidence interval 1.62 to 1.86). The median calcium:phosphate weight percentage ratio was 2.25 (95% confidence interval 2.09 to 2.41). This indicated that these HA coatings were close in composition to pure stoichiometric HA. SEM images are shown in Figure 5.3. There were no statistically significant differences between the thickness of the coatings (p=0.336). However, there was a non-significant trend that PT-HAAg coatings were thicker than PT-HA coatings (p=0.645 outer surface p=0.161 inner surface) and coatings on the outer surface of implants were thicker than coatings on the inner pores (p=0.161 PT-HA, p=0.798 PT-HAAg). Table 5.2 summarises the thickness of the coatings. SEM images of resin-embedded implants with coatings are shown in Figure 5.4.

Surface	**Ag Atomic %** median value and (95% confidence interval)	**Ag Weight %** median value and (95% confidence interval)
HAAg100 (*in vitro* disc)	0.665 (0.527 to 0.723)	2.985 (2.416 to 3.286)
HAAgFn100 (*in vitro* disc)	0.595 (0.500 to 0.7111)	2.630 (2.160 to 3.098)
PT-HAAg (*in vivo* flange)	0.700 (0.582 to 0.757)	3.175 (2.672 to 3.405)
PT-HAAgFn (*in vivo* flange)	0.610 (0.591 to 0.652)	2.950 (2.854 to 3.119)

Table 5.1 Silver percentages within HAAg coatings measured by EDX analysis.

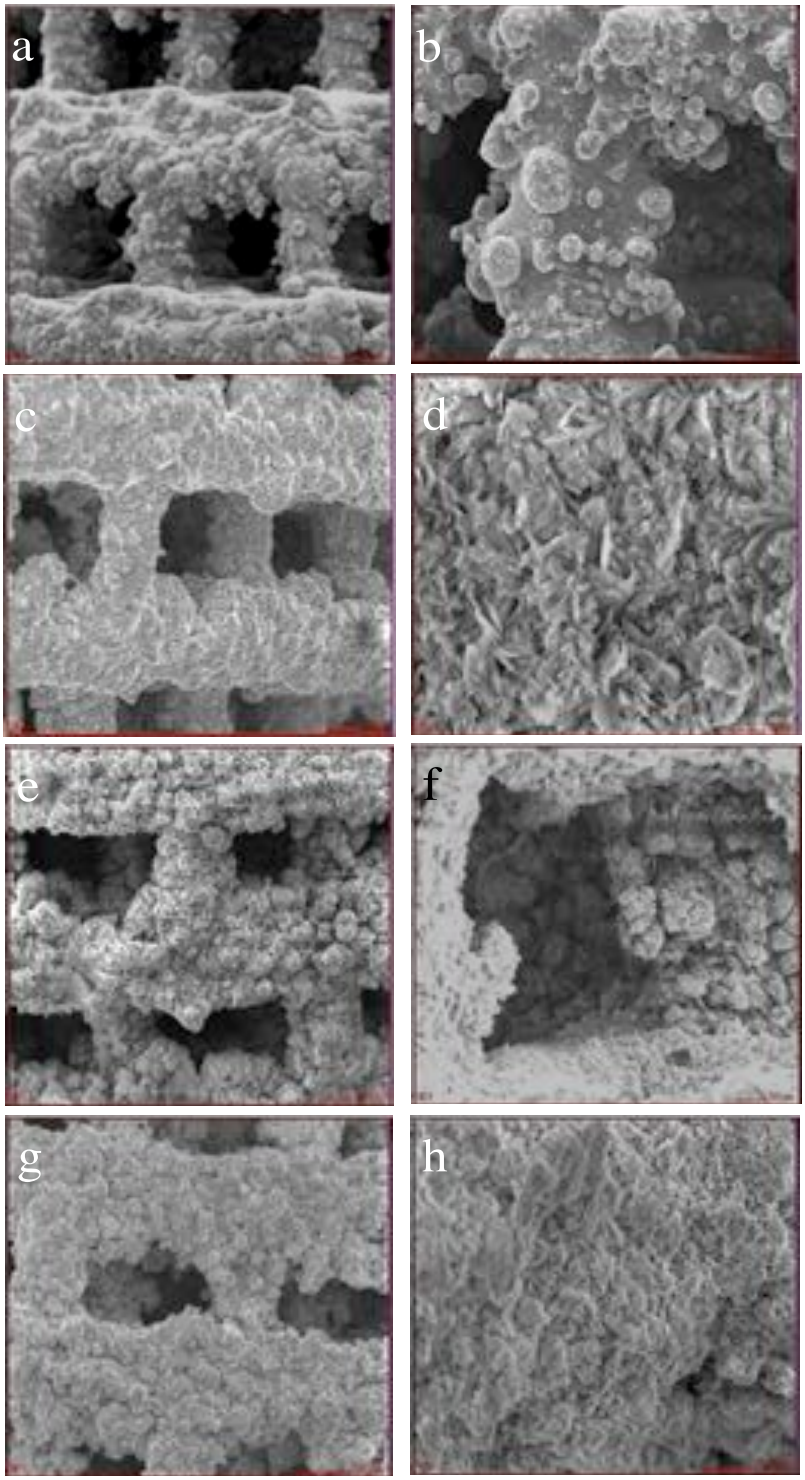

Figure 5.3 Scanning electron micrographs of flanges (a and b) Uncoated PT (c and d) PT-HA (e and f) PT-HAAg (g and H) PT-HAAgFn.

Surface	Coating Thickness (μm) median value and (95% confidence interval)
PT-HA (outer surface)	47 (30 to 76)
PT-HA (inner pores)	36 (12 to 55)
PT-HAAg (outer surface)	56 (24 to 101)
PT-HAAg (inner pores)	46 (31 to 82)

Table 5.2 Thickness of coatings.

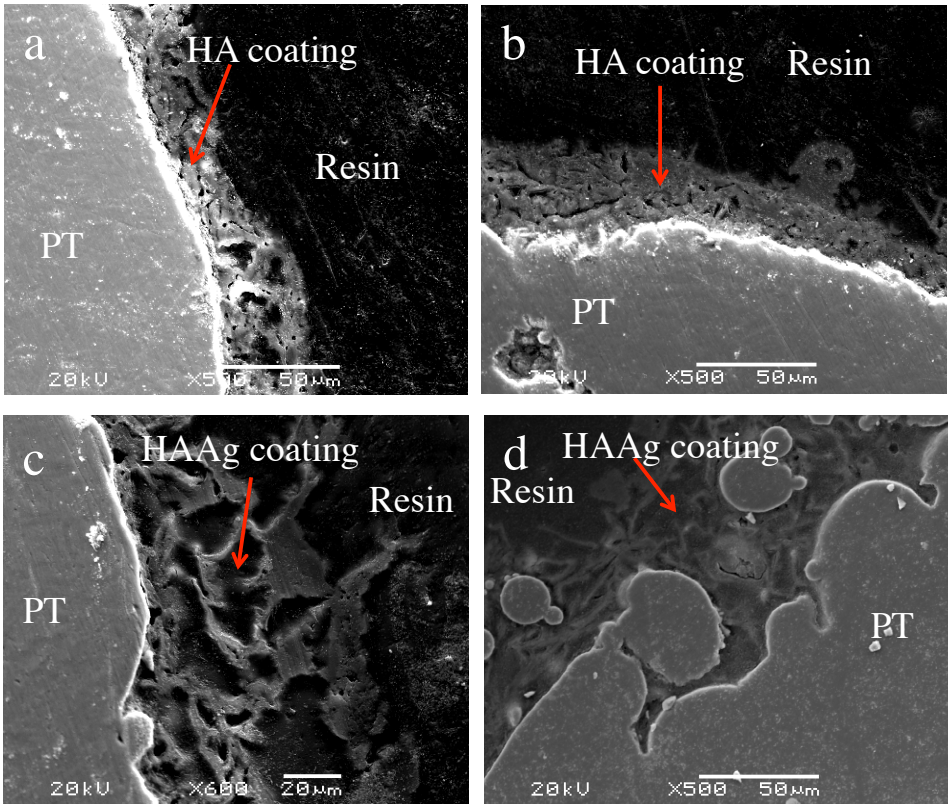

Figure 5.4 SEM images of resin-embedded implants with coatings. (a) PT-HA (outer surface of implant). (b) PT-HA (inner pores). (c) PT-HAAg (outer surface of implant). (d) PT-HAAg (inner pores).

5.3.2 Silver Release

The silver release was greatest over the first 24 hours and then gradually reduced over time. The release rate was slowest between days 11 and day 28. Silver continued to be released from PT-HAAg throughout the whole 28-day test period. The release of silver from PT-HAAg over the 28 days is presented in Figure 5.5. Negligible amounts of silver were released from the HA-coated control implant (0.025 μmol/L at 48 hours).

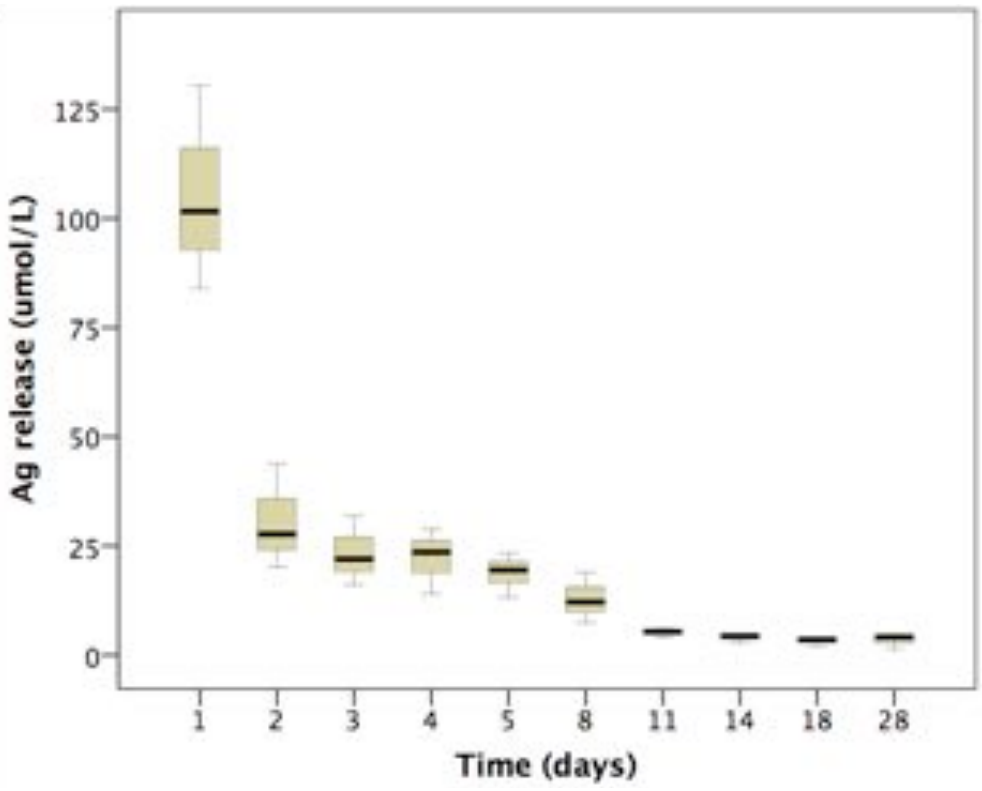

Figure 5.5 Box-and-whisker plot showing the release of silver from PT-HAAg over 28 days.

5.3.3 Absolute Silver Content of Coatings

The HA control contained negligible amounts of silver (11.19 μmol/L), whereas the median silver content of HAAg and HAAg P24 was 362.67 μmol/L and 240.76 μmol/L respectively. Due to the low n number, the differences between these coatings were not statistically significant (p=0.276).

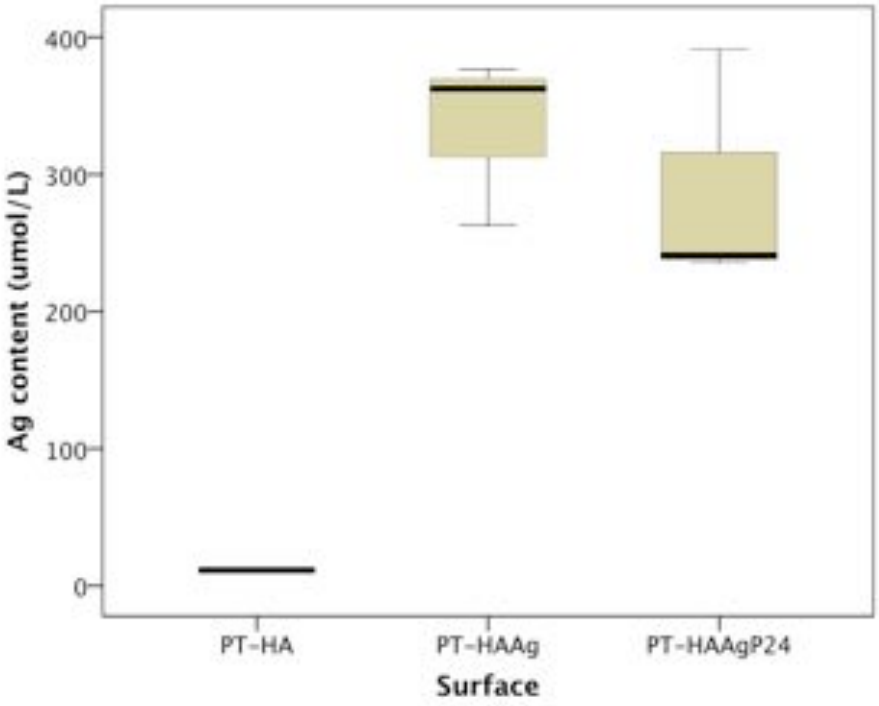

Figure 5.6 Box-and-whisker plot showing the silver content of coatings.

5.3.4 X-ray diffraction analysis

XRD analysis of HA and HAAg coatings showed peaks at 31.8°, 32.3° and 33° corresponding to the presence of hydroxyapatite. The addition of fibronectin did not result in any differences to XRD patterns. Results from HAAg coatings showed peaks at 38.1°, 38.3° and 44.5° corresponding to the presence of silver. The HA peak intensity relative to titanium peaks was greater for HAAg coatings than for HA coatings which indicated that HAAg coatings were thicker. Preconditioning did not affect the crystallinity of these coatings. Figure 5.7 shows XRD patterns.

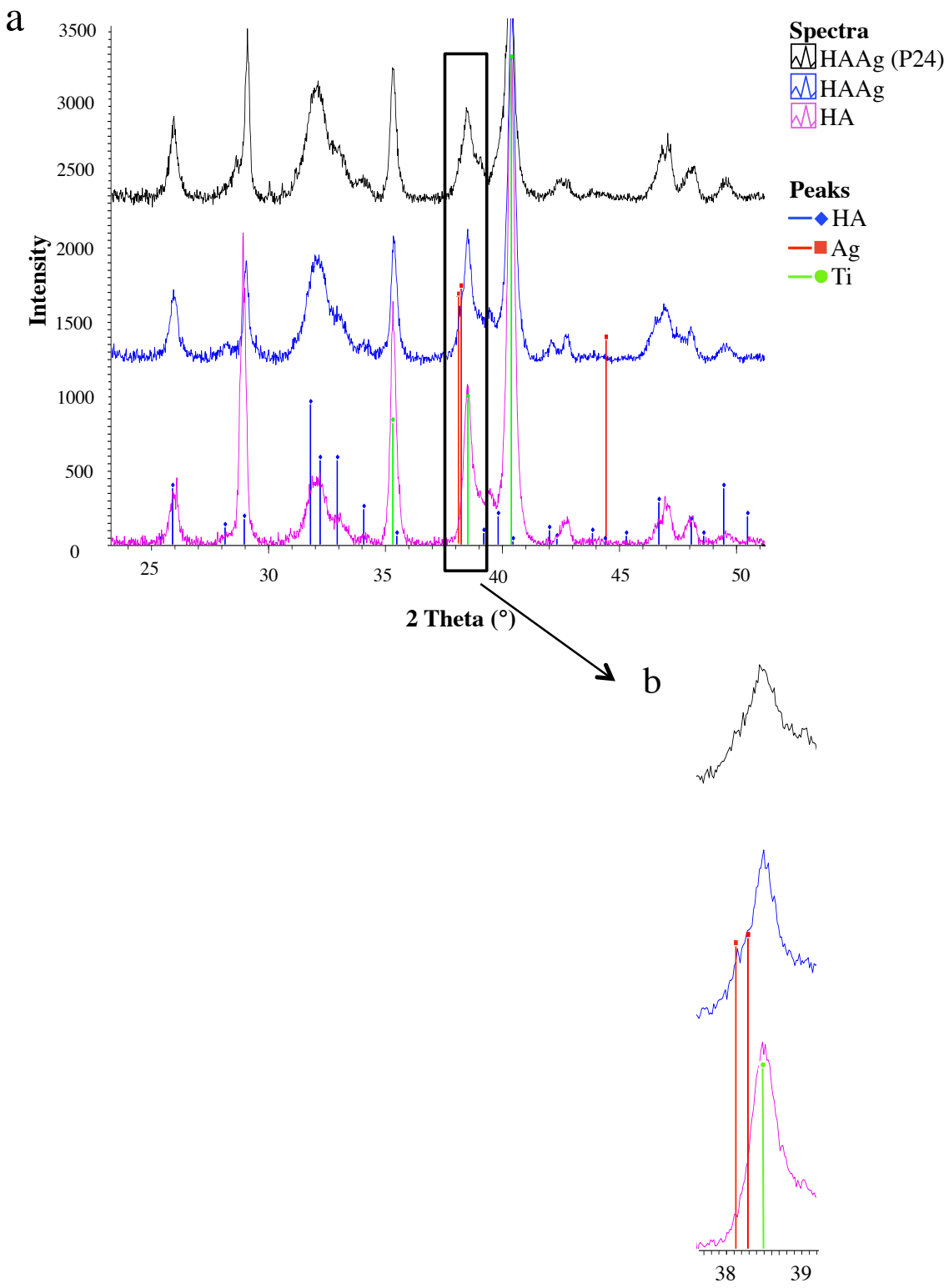

Figure 5.7 XRD patterns for (a) HA, HAAg and HAAg (P24) (b) Zoomed-in image to highlight silver peaks.

5.3.5 Wettability

The uncoated Pol surfaces were significantly more hydrophobic than HA+/-Ag+/-Fn ($p<0.05$. Exact individual p values are shown in Appendix 5). HA+/-Ag+/-Fn surfaces were very hydrophilic with low contact angles. Preconditioning did not significantly affect the wettability of HAAg or HAAgFn ($p=0.310$ and $p=0.171$ respectively). Overall, there were no significant differences in wettability between HA+/-Ag+/-Fn surfaces (Table 5.3 and Figure 5.8).

Surface	**Contact Angle (°)** median value and (95% confidence interval)
Pol	74.86 (70.36 to 79.35)
HA	10.91 (1.38 to 15.34)
HAFn	8.69 (-5.98 to 46.64)
HAAg	10.11 (2.44 to 13.55)
HAAgFn	9.45 (1.30 to 13.98)
HAAg (P24)	17.09 (0.35 to 37.30)
HAAgFn (P24)	12.79 (11.18 to 14.23)

Table 5.3 Contact angles for each surface.

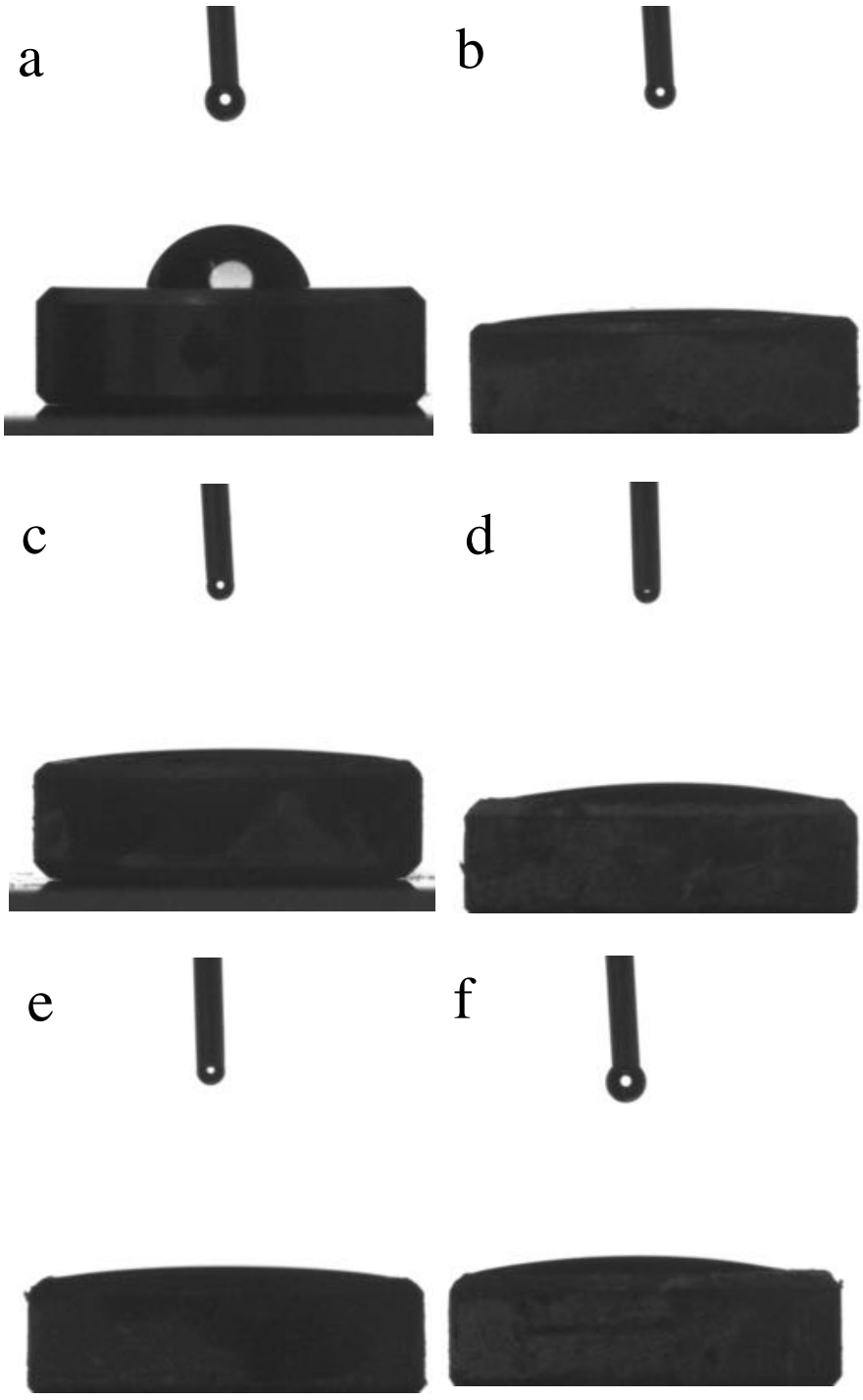

Figure 5.8 Images of contact angles taken with the CAM 200, KSV Instruments (a) Pol (b) HA (c) HAFn (d) HAAg (e) HAAgFn (f) HAAgFn (P24).

5.4 DISCUSSION

SEM and EDX Analysis

This study has shown that electrochemical deposition is able to produce HA and HAAg coatings throughout the porous titanium alloy structures with a similar morphology and composition to the coatings produced on the solid discs used in the *in vitro* chapters of this thesis. The HAAg produced in the *in vitro* section of this thesis supported viable fibroblast growth after serum-preconditioning and had bactericidal activity. The electrochemical deposition technique produced coatings with median thicknesses of less than 50 μm throughout the porous structures. It is possible that altering the thickness of coatings may influence the effects of the coatings on promoting tissue attachment. Svehla et al (2002) found that increasing the thickness of HA coatings from 50 to 100 μm increased bone fixation and ongrowth and resulted in less resorption of the coating (Svehla et al 2002). It is not known whether increasing the HA and/or HAAg coating thickness would have a similar affect on soft tissue integration. It is also unclear how bacterial colonisation would be affected by increasing the thickness of these coatings. It was decided not to attempt to achieve a thicker coating as increasing the thickness further would reduce the space within the pores for soft tissue infiltration which could potentially counteract the effect of the selected pore size of 700 μm on soft tissue integration. Furthermore, it has been shown that bonding strength between micro-scale HA coatings and metal substrates decreases with increasing coating thickness (Aksakal et al 2010; Sonmez et al 2014).

Silver Release and Silver Content

ICP-MS showed that the greatest amount of silver release occurred within the first 24 hours. The release rate reduces over time, explaining why preconditioning reverses the cytotoxic effect of coatings. The release was sustained over the 28 days at a slow rate indicating that the coating persists for 28 days. The levels of silver released at 28 days were low (median 4.14 μmol/L) but remained greater than levels shown to have bactericidal activity *in vitro* (Ghani et al 2012).

The levels of silver released indicate that the HAAg coatings are unlikely to cause systemic toxicity. Normal silver whole blood or serum levels may range up to 10 μg/L (Parelli and Piolatto 1992). The overall cumulative release of silver at 28 days was 229 μmol/L (i.e. 0.0247 μg/L). The release was measured into 5 mL of fetal calf serum, which is a very small volume in comparison to the average 70 kg adult human blood volume of approximately 5 litres (Pocock and Richards 2004). As a result, the amount of silver released from these implants into the blood circulation will be diluted by a factor of approximately 1000-fold. Additionally, the proportion of the silver released into tissues surrounding the implants (represented by the fetal calf serum) that will be absorbed, enter the circulation and be retained is unknown (Lansdown 2010). The blood volume is continually replenished *in vivo* and 90% of absorbed silver will be eliminated in faeces through biliary excretion and a smaller variable amount of will be excreted in urine (Perrelli and Piolatto 1992; Lansdown 2010; Ghani et al 2012). The size of the implant will be scaled up for human use but not to the extent that will overcome the aforementioned factors. Silver blood levels will be measured *in vivo* in Chapter Six to test this theory.

The median absolute silver content of HAAg-coated flanges was 362.669 μmol/L (i.e. a total of 1.813 μmol in the 5 mL). This is equivalent to 0.196 mg, which would be a safe overall implant silver load even after scaling the implant up several times for use in humans. This implant silver load is well below the No Observable Adverse Effect Level (NOAEL) of 10 g silver (World Health Organization, 2003). It is also well below the levels previously shown to produce argyria and argyrosis (Gosheger et al 2004; Lansdown 2010). The reduction of absolute silver content within HAAg coatings was not statistically significant. The small n number (n=3, N=1) would account for the fact that these differences were not detected as statistically significant. Due to availability of implants, costs and clinical relevance, the experiment was not repeated with a larger n number. The information from the release study, which showed that silver is released, answered the question as to whether silver is lost from the coating.

X-ray diffraction analysis

The HA and HAAg coatings were semi-crystalline with some HA peaks displaying intermediate broadness. The X-ray diffraction pattern was not affected by serum-preconditioning. A more highly crystalline coating would be expected to be less resorbable and persist for a longer time period (Overgaard et al 1999; Xue et al 2004). A further area of study that was not assessed in this chapter is the composition of the coatings and the thickness of the coatings after the 28-day period in fetal calf serum. The release study has shown that some silver is released for 28 days indicating that some coating is present; but the components of the coating remaining after 28 days are unknown. It is possible that after 28 days very little coating remains and/or that a greater proportion of HA is lost than silver. It could be argued that developing a more highly crystalline coating in order to increase the longevity of the coating would be beneficial. However, this argument is not necessarily true as that the coating only needs to be present for short period. Strictly speaking, the 'race for the surface' only requires the coating to be present to repel bacteria while promoting cells attachment and during the formation of initial cell monolayer. It may not be necessary for the HA component of coating to be present for weeks in order for a robust soft tissue seal to occur. *In vitro* (Chapters Three and Four), cell attachment and bacterial inhibition is seen to occur within the first 24 hours.

There is conflicting evidence in the literature on the effect of crystallinity on tissue ingrowth. A number of studies have shown that decreased crystallinity is associated with enhanced bone ingrowth (De Bruijn et al 1994; Overgaard et al 1999). Xue et al (2004) showed that increased crystallinity is beneficial for bone tissue integration (Xue et al 2004). Chou et al (1999) found that increased crystallinity of HA was associated with reduced *in vitro* fibroblast attachment but lower crystallinity surfaces resulted in elevated medium pH, which was associated with reduced fibroblast proliferation rates (Chou et al 1999). The variation in results may be due to differences in experimental conditions such as coating manufacturing technique, purity, thickness and topography.

Wettability

HA and HAAg surfaces were hydrophilic. This was expected due to the surface chemistry of HA and further enhancement of the wettability due to roughness (Wenzel 1936). Serum-preconditioning did not result in further increases in wettability. This suggests that changes in wettability do not contribute to the increased cytocompatibility of coatings after preconditioning. Hydrophilicity is associated with increased cell adhesion and decreased bacterial adhesion and is therefore a desirable characteristic for ITAP flange coatings (Wilson et al 2005; Murakami et al 2012; Wu et al 2013).

5.5 CONCLUSION

This chapter has established that the inner pores of porous titanium alloy flanged transcutaneous pins can be coated using electrochemical deposition. The current density and time period for the electrochemical deposition process was modified to obtain coatings with a morphology and composition that was similar to that achieved in the *in vitro* experiments. Release of non-toxic levels of silver reduced over time but continued for 28 days. The coatings were semi-crystalline and hydrophilic. The coating method used in this chapter will be used to coat implants for *in vivo* investigation.

CHAPTER SIX

The Effect of Porous Titanium Alloy Transcutaneous Pins Coated with Hydroxyapatite, Silver and Fibronectin on Soft Tissue Integration: An *In Vivo* Ovine Model

6.1 INTRODUCTION

The key finding from Chapter Two was that a fully porous titanium alloy structure with a pore size of 700 μm and strut size of 300 μm (P700 S300) promotes soft tissue ingrowth, cellularity and vascularisation. This suggests that soft tissue could potentially win the 'race for the surface' against bacteria on P700 S300 porous titanium alloy structures despite the potential of porous materials to increase bacterial adhesion (Shin and Akao 1997; Braem et al 2013). However, in a transcutaneous pin model there will be greater exposure to bacteria, which may affect the outcome of the 'race for the surface.' As a result application of antibacterial coatings to porous titanium alloy may be beneficial and could have the potential to influence soft tissue integration indirectly. *In vivo* studies are necessary to evaluate the effect of porous titanium alloy flanged transcutaneous pins with and without HAAgFn coatings before use in humans. Both soft tissue integration and bacterial colonisation must be assessed in order the determine the effect on the 'race for the surface.' This chapter presents an assessment of *in vivo* soft tissue integration.

A large animal model was used as it was considered to be more representative of human clinical conditions than a small animal model. For example, it allowed investigation of an ITAP device with a flange consisting of the potential pore sizes that would be used clinically. A well-established ovine model was used with ITAP pins being inserted through both the near and far cortex of the tibia (Pendegrass et al 2006a). An amputation model was not used for ethical reasons. Sheep were selected as their tibiae are of sufficient length to allow implantation of up to four implants along the length of the bone, which is useful when testing multiple coatings and allows a reduction in the numbers of animals used. Additionally, sheep have been used by a number of research groups for histological studies of soft tissue integration as their skin possesses soft tissue characteristics, such as thickness and mobility, which are similar to human skin (Larsson et al 2012). A pig model would be an alternative as pig skin anato resembles human skin more closely than sheep. In particular, pig skin has a sparse hair follicle pattern and the vascular organisation, collagen and elastin content is very similar to that of humans (Winter 1974; Avon et al 2005; Sullivan et al 2001; Swindle et al 2012). However, their shorter legs would

be a significant disadvantage. Comparisons between soft tissue integration into porous coated osseointegrated transcutaneous implants in both pig and sheep have shown similar cutaneous responses indicating that wound healing mechanisms in sheep are similar to pigs (Jeyapalina et al 2012; Holt et al 2013).

Other animal models of soft tissue integration of osseointegrated transcutaneous implants studies have found that a porous titanium alloy subdermal barrier reduces epithelial downgrowth but that marsupialisation is not eliminated (Jeyapalina et al 2012; Isackson et al 2011). However, these studies did not assess the effect of fully porous titanium alloy and used porous titanium alloy surface coatings with smaller pore sizes. Additionally, these studies have compared porous titanium alloy with solid implants only and have not made comparisons with drilled holes or studied the effect of bioactive or antibacterial coatings (Isackson et al 2011; Jeyapalina et al 2012).

This chapter aimed to determine whether osseointegrated transcutaneous pins with a fully porous titanium alloy flange (P700 S300) reduce epithelial downgrowth and increase epithelial attachment, dermal attachment, soft tissue ingrowth and vascularisation compared with the standard ITAP drilled flange design. The study also aimed to determine if the combination of hydroxyapatite, silver and fibronectin coatings would enhance the soft tissue attachment. The *in vitro* studies presented in Chapters Three and Four have shown that HA and HAFn coatings promote increased fibroblast spreading compared with uncoated titanium alloy. HAFn resulted in the greatest fibroblast metabolism. HAAg and HAAgFn coatings are antibacterial and support viable fibroblast growth after preconditioning in serum for 24 hours. HAAgFn was not associated with improved fibroblast viability compared with HAAg suggesting that silver may counteract some of the effects of fibronectin. However, the effect on *in vivo* soft tissue attachment cannot be predicted from this *in vitro* data. The *in vitro* studies also showed that addition of fibronectin resulted in increased *S aureus* colonisation but decreased *P aeruginosa* colonisation. As a result of these findings as well as the finding from Chapter Two that P700 S300 porous titanium alloy structures enhance soft tissue integration, it was hypothesised that:

1. Transcutaneous pins with a porous titanium alloy flange (P700 S300) would reduce epithelial downgrowth, increase epithelial and dermal attachment and improve soft tissue ingrowth and vascularisation of tissue within pores compared with the standard ITAP drilled-hole flange model and a straight non-flanged pin.

2. HA coatings would further enhance the effects of PT on soft tissue integration and HAFn, HAAg and HAAgFn would improve soft tissue integration compared with HA.

3. HAAgFn would not increase the soft tissue integration compared with HAAg. This was hypothesised in view of the finding from Chapter Three that HAAgFn was not associated with increased fibroblast viability compared with HAAg.

6.2.1 Transcutaneous Pin Designs and Coatings

The transcutaneous pin design and coatings described in Chapter Five were used. In addition, the current standard ITAP pin (DF) was used as a control. This consists of a flat flange with 24 drilled holes (with a diameter of 700 μm) and a tapered intraosseous stem. The flange and the stem are coated with plasma sprayed HA (Plasma Biotal Ltd, Derbyshire, UK). A straight pin (SP) without a flange was included as a control for DF (in order to mirror the surfaces that will be studied in the bacterial colonisation study that will be presented in Chapter Seven). Table 6.1 summarises the implant designs and coatings used. Photographs of the control pin designs are shown in Figure 6.1. The surface preparation method described in Section 5.2.2 was employed.

Implant and Coating	Abbreviation
Straight pin	SP
Standard ITAP pin (drilled-hole flange)	DF
Porous Ti6Al4V flange	PT
Porous Ti6Al4V flange with HA	PT-HA
Porous Ti6Al4V flange with HAFn	PT-HAFn
Porous Ti6Al4V flange with HAAg	PT-HAAg
Porous Ti6Al4V flange with HAAgFn	PT-HAAgFn

Table 6.1 Summary of transcutaneous pins and coatings.

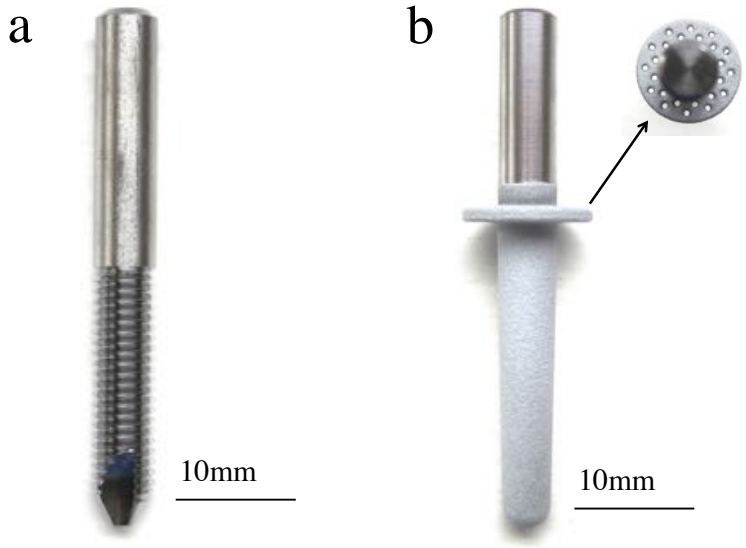

Figure 6.1 Photographs of the control pins (a) SP and (b) DF.

6.2.2 Ovine Model to Assess *In Vivo* Soft Tissue Attachment

Skeletally mature female sheep (Mules) n=6 weighing between 66 and 88 kg were used. The same premedication and anaesthesia detailed in Section 2.2.2 was used. Perioperative analgesia was maintained with fentanyl transdermal patches (75 μm/hour) (Duragesic®, Janssen Pharmaceuticals, NJ, USA).

6.2.2.1 Surgical Procedure

Both hindlegs were shaved and prepared with povidone iodine scrub and solution. Implants were inserted along the length of the tibiae under aseptic conditions. A separate 15 mm longitudinal skin incision over the medial aspect of the tibia was made. A periosteal elevator was used to expose the bone. A 4.2 mm hole was drilled through both cortices. A conical reamer was used prior to insertion of DF pins. The pins were inserted using a T-handle. Flanged implants were positioned with the flange placed subdermally. The intraosseous portion of the pins was a self-tapping threaded screw with the exception of DF, which was a tapered press-fit implant. The skin and subcutaneous tissues were closed with interrupted 2-0 vicryl sutures. Opsite spray dressing, mepitel, gauze and a crepe bandage were used to dress the wounds. The order of implantation of pins was alternated for each animal in order to account

for the usual reduction in soft-tissue thickness from the proximal to the distal end of the tibia. Intraoperative photographs showing the insertion of pins are shown in Figure 6.2.

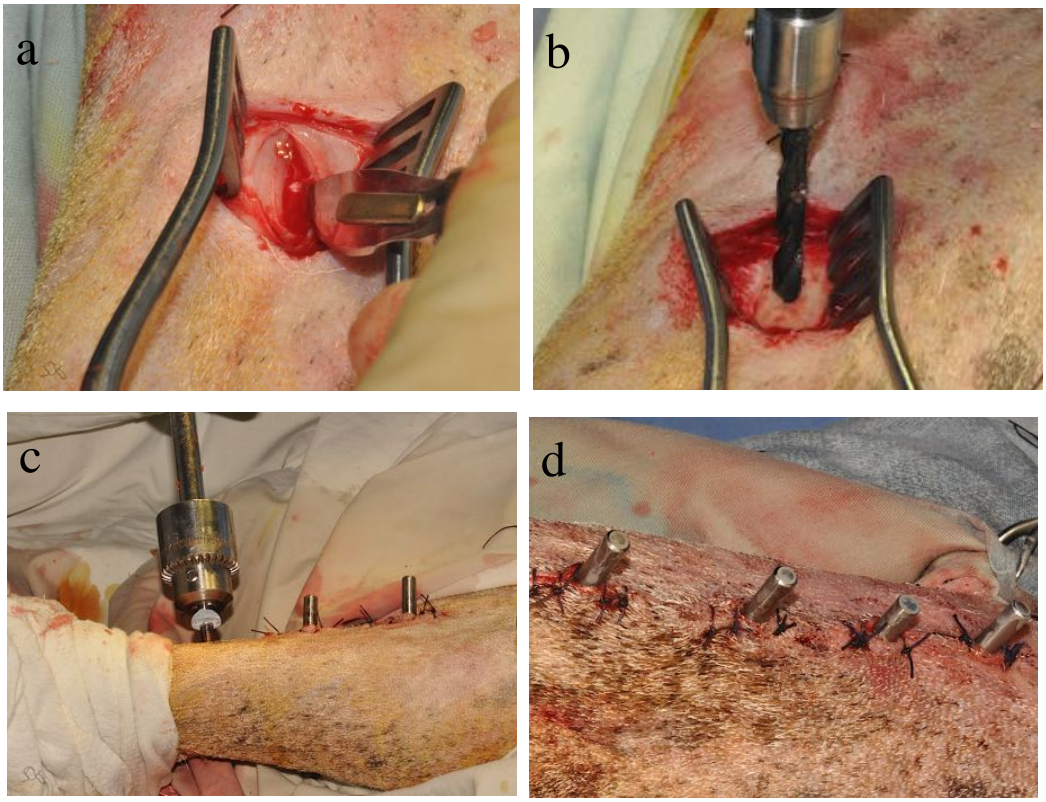

Figure 6.2 Intraoperative photographs showing (a) incision of the skin and subcutaneous tissue. (b) Drilling of a 4.2 mm drill-hole into the bone. (c) Insertion of a PT-HA pin. (d) Four pins that have been inserted into one tibia.

6.2.2.2 Postoperative course

Cefalexin was administered for three days postoperatively. The fentanyl patch was replaced two days after surgery. The wounds were reviewed weekly to assess for clinical evidence of infection. The wounds were re-dressed after each wound review. Four weeks postoperatively, the hindlegs were amputated following euthanasia with approximately 0.7 mL/kg of intravenous pentobarbitone sodium. A four-week time period was chosen in order to allow sufficient time for a soft tissue seal to form. The implants were removed *en bloc* with the overlying soft tissues and the underlying

periosteum and tibia using a hack saw. Care was taken not to disrupt the interface between the soft tissue and the implant.

6.2.3 Hard Grade Resin Histology

6.2.3.1 Histological Processing

The protocol used in Section 2.2.4 (Appendix 1.1) was used.

6.2.3.2 Histological Sectioning

The method for histological sectioning described in Section 2.2.4 was used. However, instead of a transverse section, a longitudinal section was taken through the centre of each specimen. Additionally, the slides were mounted with coverslips using Pertex® xylene-based mounting medium (CellPath plc, Hemel Hempstead, UK) prior to visualisation with the Zeiss microscope.

6.2.4 Histological Analysis

Two sections were analysed for each implant. The following outcomes were measured:

(a) Epithelial downgrowth (mm)
(b) Percentage epithelial attachment
(c) Percentage subepithelial (i.e. dermal) attachment

A line intercept method was used to measure epithelial downgrowth, epithelial attachment and subepithelial attachment as described by Pendegrass et al (2006) (Figure 6.3). The thickness of the epithelial and subepithelial tissue layers was measured and the percentage of these layers in contact with the implant surface was calculated.

(d) Percentage soft tissue fill within the inner pores. The semi-quantitative assessment described in Section 2.2.4 was used.

(e) Number of cell nuclei/mm^2 within the inner pores - Fibroblast nuclei were counted within a defined area and the number of nuclei per mm^2 was calculated.

(f) Number of blood vessels/mm^2 within the inner pores - The blood vessels were counted within a defined area and the number of blood vessels per mm^2 was calculated.

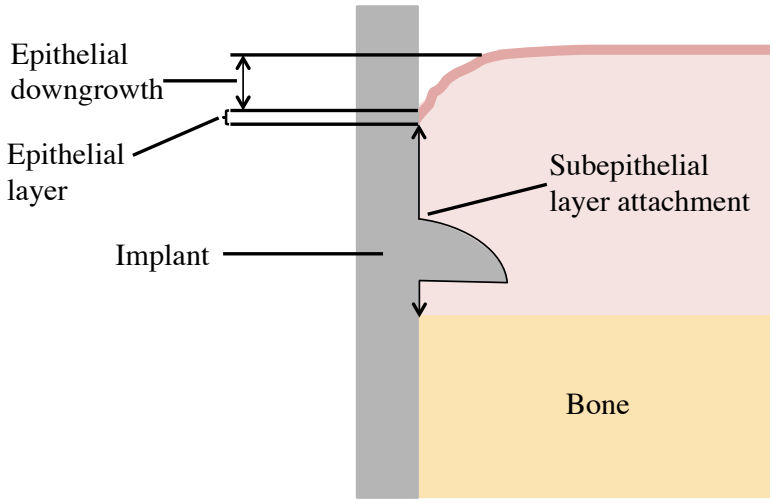

Figure 6.3 Schematic diagram showing the measurements for epithelial downgrowth, epithelial and subepithelial attachment for a flanged implant (Adapted from Pendegrass et al 2006).

6.2.5 Measurement of Silver Blood levels

Whole blood samples were collected for measurement of silver levels pre-induction (day 0) and then daily for three days post-operatively (days 1, 2 and 3). This was followed by weekly blood sampling for three weeks (days 10, 17 and 24). A final sample was taken prior to euthanasia on day 28. The blood samples were stored in a standard trace element tube with EDTA and frozen at -20°C until dispatch for analysis. Silver blood levels were measured by ICP-MS (Dr Barry Sampson, Trace Element Laboratory, Imperial College London, UK).

6.2.6 Statistical Analysis

Non-parametric testing as described in Section 2.2.5 of this thesis were used.

6.3 RESULTS

6.3.1 Postoperative Clinical Outcomes

All sheep remained clinically well throughout the study period. However, one pin site in one sheep (a PT implant) was complicated by intraoperative haemorrhage. Haemostasis was achieved prior to wound closure following application of pressure. There was continued bleeding from the wound during the first five postoperative days and a haematoma formed. At three weeks postoperatively, clinical evidence of soft tissue infection (i.e. erythema, warmth and a purulent discharge) was observed at this pin site. No systemic signs of sepsis were observed, however, the sheep displayed signs of pain and intermittently would not bear weight fully on the affected limb. A five-day course of intravenous cephalexin was started at this point and the signs of infection resolved. There was no clinical evidence of infection or any other complications affecting the other sheep or any of the other pins in this sheep. All pins were included in the analysis. However, data for epithelial downgrowth for the pin that had been complicated by infection was removed by SPSS as an extreme outlier. Figure 6.3 shows some examples of the appearance of pin sites from the postoperative period.

Figure 6.4 Postoperative photographs of pin sites at (a) two weeks, (b) three weeks and (c) four weeks. (d) The pin that was complicated by infection at three weeks.

6.3.2 Epithelial Downgrowth

SP resulted in the greatest degree of epidermal downgrowth. Epithelium was seen to migrate from the incised edges vertically down along the entire transcutaneous portion of SP implants down to the intraosseous portion. This resulted in a tract being present from the exterior down to the bone. DF reduced epithelial downgrowth compared with SP (p=0.000). PT resulted in a further reduction in epithelial downgrowth compared with DF (p=0.027). The addition of coatings to PT did not result in any further reduction in epidermal downgrowth. Similarly to PT, PT-HAFn, PT-HAAg and PT-HAAgFn reduced epidermal downgrowth compared with DF (p=0.003, p=0.017 and p=0.001 respectively). However, PT-HA did not significantly reduce epidermal downgrowth compared with DF (p=0.052).

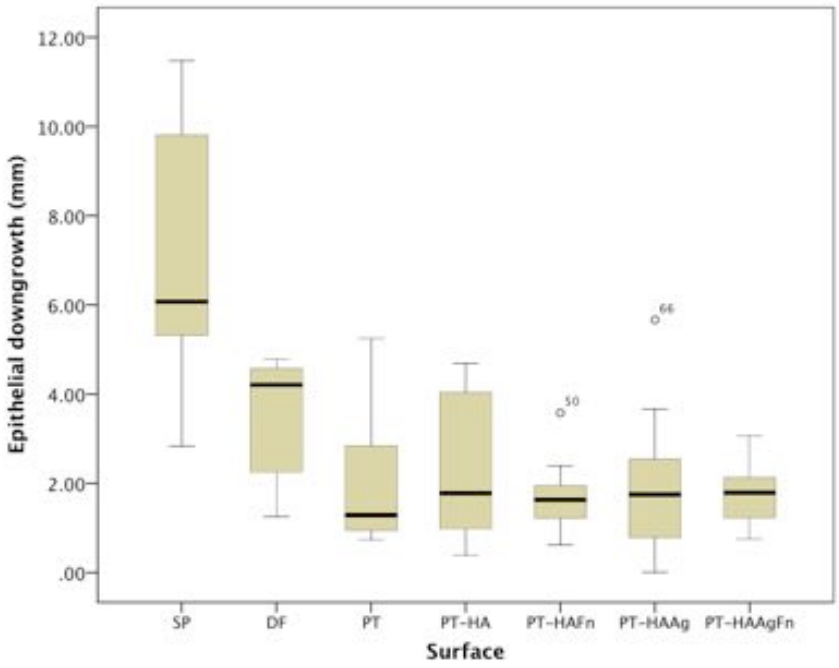

Figure 6.5 Box-and-whisker plot showing the degree of epithelial downgrowth associated with each implant.

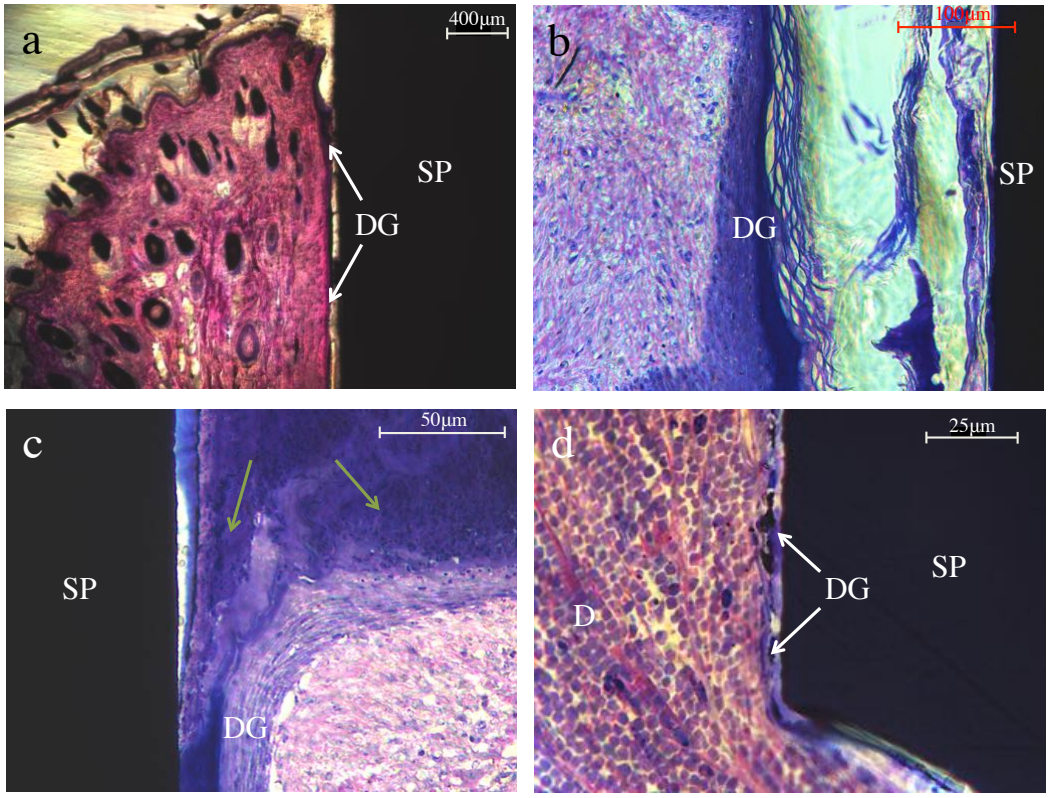

Figure 6.6 (i) Histological sections demonstrating the degree of epithelial downgrowth (DG) associated with SP implants. (a) Low magnification image (x2.5) showing epithelium separate from side of implant and migrating vertically downwards along length of transcutaneous portion. (b) Higher magnification image (x20) showing epithelial downgrowth. (c) Epithelium migrating beneath a blood clot and fibrinous exudate rich in polymorphonuclear cells (green arrows). (d) The epithelium has migrated along the entire length of the transcutaneous portion of the implant. The adjacent dermal tissue (D) contains a high-density inflammatory infiltrate of lymphocytes, neutrophils, macrophages and foreign body giant cells.

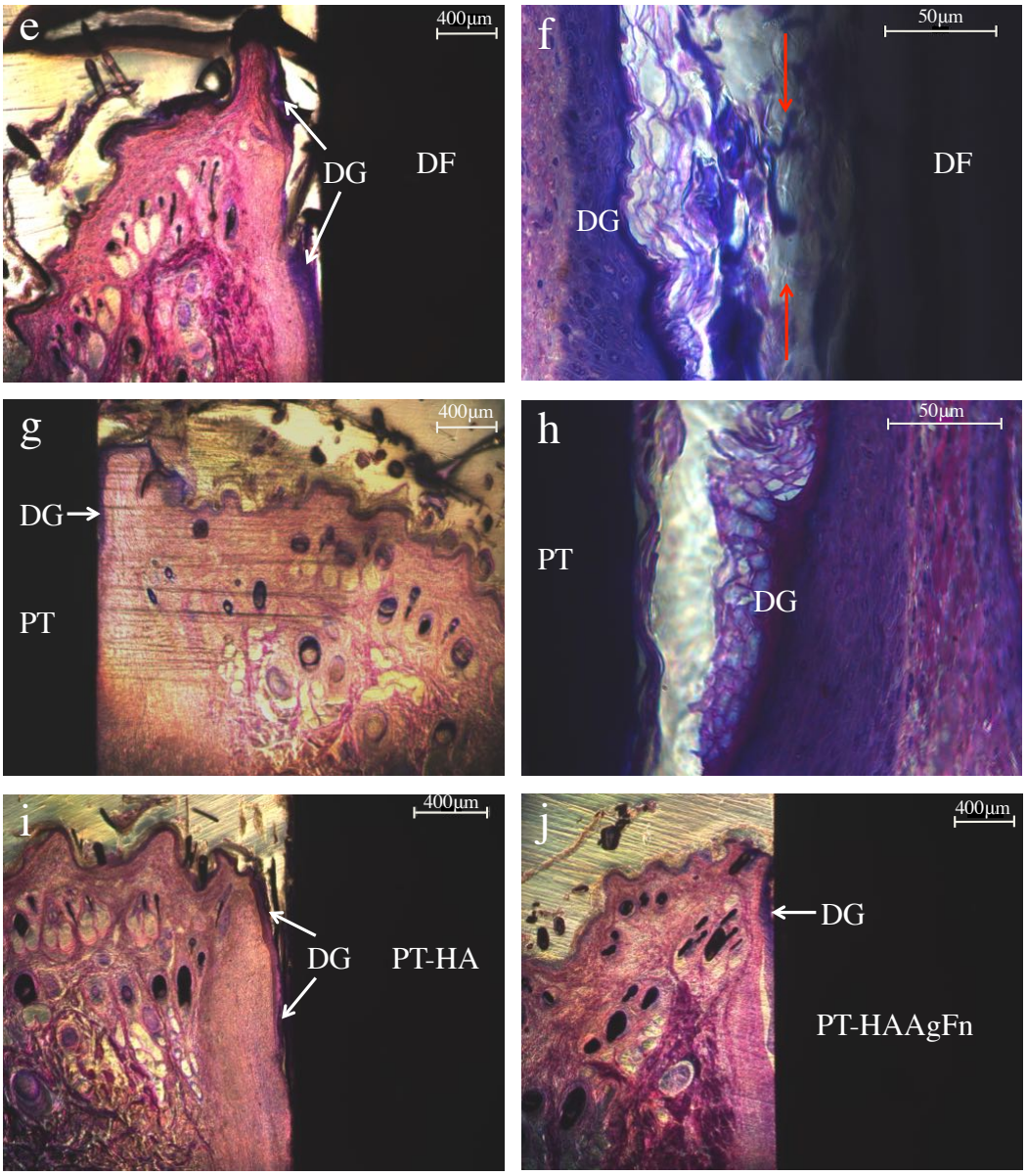

Figure 6.6 (ii) Histological sections demonstrating the degree of epithelial downgrowth associated with implants. (e) DF at x2.5 magnification. (f) DF at x40 magnification. The red arrows indicate the presence of blood and exudate within the gap between the epithelium and the implant (g and h). There is reduced epithelial downgrowth around PT implants and a reduced amount of blood and exudate in the gap between the epithelium and the implant. (i) PT-HA. (j) PT-HAAgFn.

6.3.3 Percentage Epithelial Attachment

SP was associated with the lowest percentage epithelial attachment. DF increased epithelial attachment compared with DP (p=0.045). However, there was no difference between DF and PT implants irrespective of coating (p=0.859). A very wide variation in percentage epithelial attachment between implants from the same group was observed for all implant types, ranging from 0 to 100%.

Implant	**% Epithelial Attachment** median value and (95% confidence interval)
SP	0.000 (-10.008 to 26.675)
DF	63.430 (21.261 to 83.215)
PT	100.000 (40.339 to 98.679)
PT-HA	79.055 (29.939 to 89.306)
PT-HAFn	85.700 (35.580 to 91.102)
PT-HAAg	100.000 (25.616 to 91.050)
PT-HAAgFn	40.600 (16.124 to 80.743)

Table 6.2 Percentage epithelial attachment.

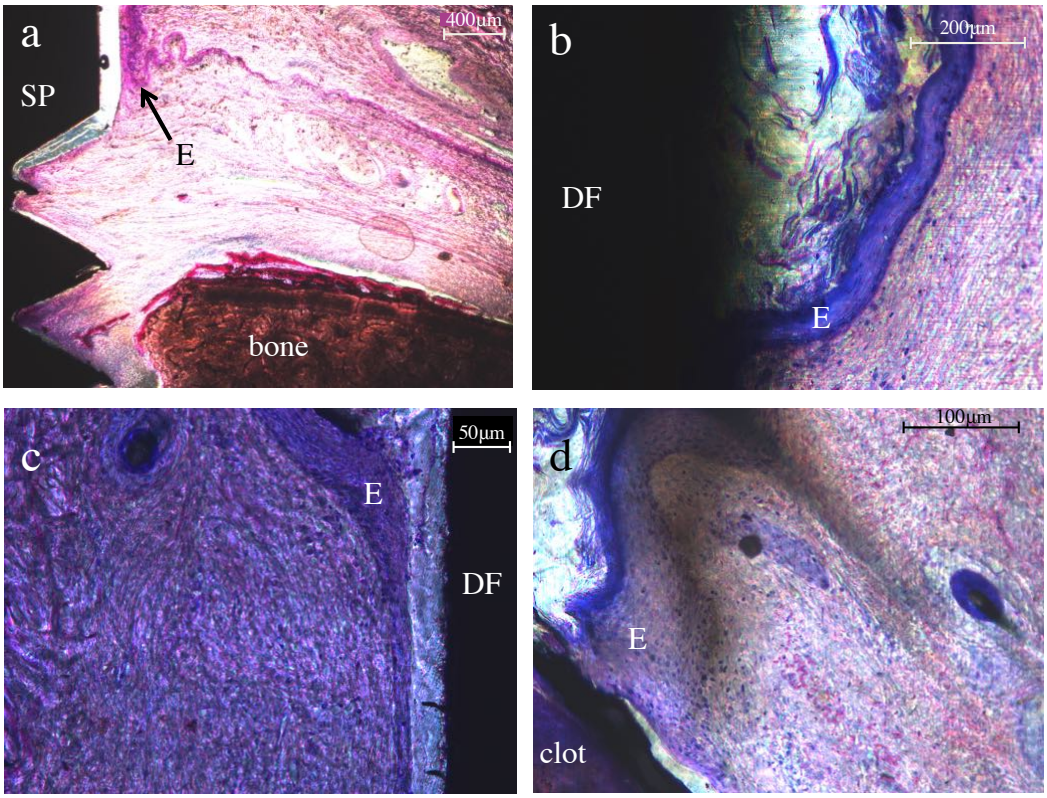

Figure 6.7 (i) Histological sections showing epithelial attachment to implants. (a) Lack of epithelial attachment to SP. The epithelial layer (E) terminates within the dermis and there is a gap between the implant and the soft tissues. (b) Epithelium attaching to the side of a DF implant. (c) Lack of epithelial attachment to a DF implant. (d) Failure of the epithelium to attach to a PT implant. The epithelium is partly in contact with a clot.

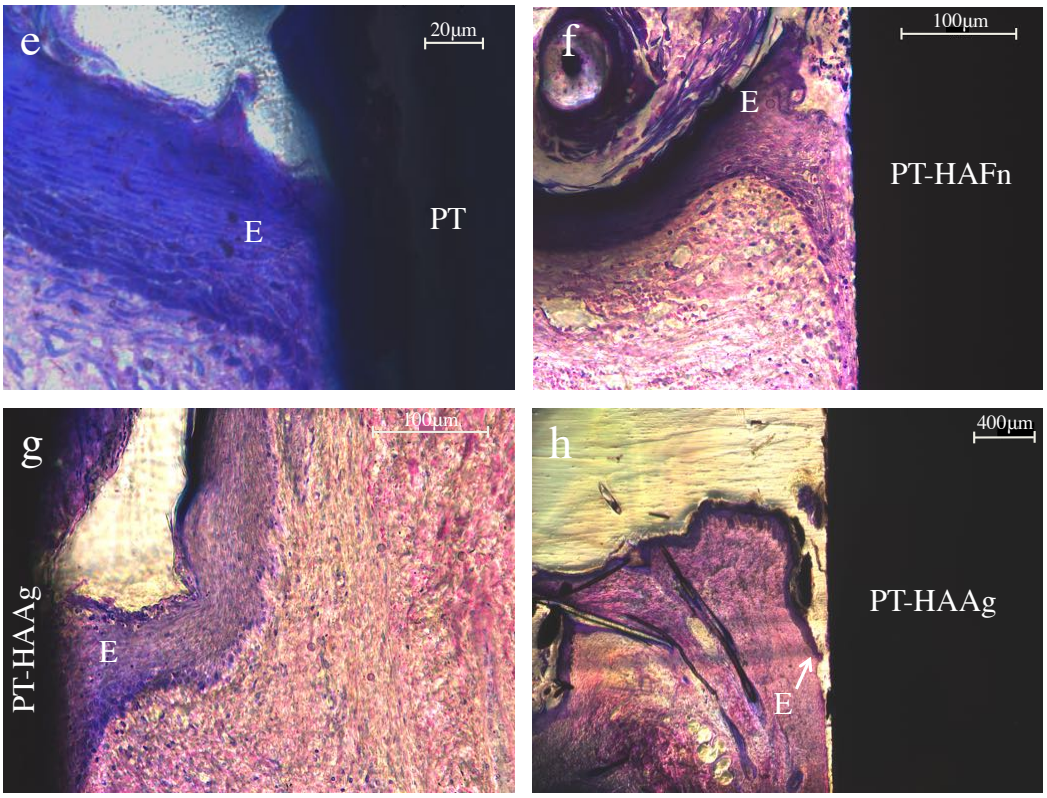

Figure 6.7 (ii) Histological sections showing epithelial attachment to implants. (e) Epithelial layer completely in contact with a PT implant. (f) Partial contact between the epithelium and a PT-HAFn implant. (g) Epithelium attaching to a PT-HAAg implant. (h) Lack of epithelial attachment to a PT-HAAg implant.

6.3.4 Percentage Subepithelial/Dermal Attachment

PT-HAFn had the highest median value for percentage dermal attachment (87.6%). SP was associated with the lowest median percentage dermal attachment (0%). DF was associated with greater dermal attachment than SP (p=0.017). PT was associated with greater dermal attachment than DF (p=0.020). The addition of coatings to PT did not result in any further statistically significant improvements in dermal attachment (HA p=0.590, HAFn p=0.091, HAAg p=0.410, HAAgFn p=0.443). There was greater dermal attachment to PT-HA, PT-HAFn, PT-HAAgFn than to DF (p=0.014, p=0.002 and p=0.004 respectively), but there was no significant difference between PT-HAAg and DF (p=0.089). PT-HAFn improved dermal attachment compared with PT-HA (p=0.023). PT-HAAgFn improved dermal attachment compared with PT-HAAg (p=0.039). There was no difference between PT-HA and PT-HAAg (p=0.977).

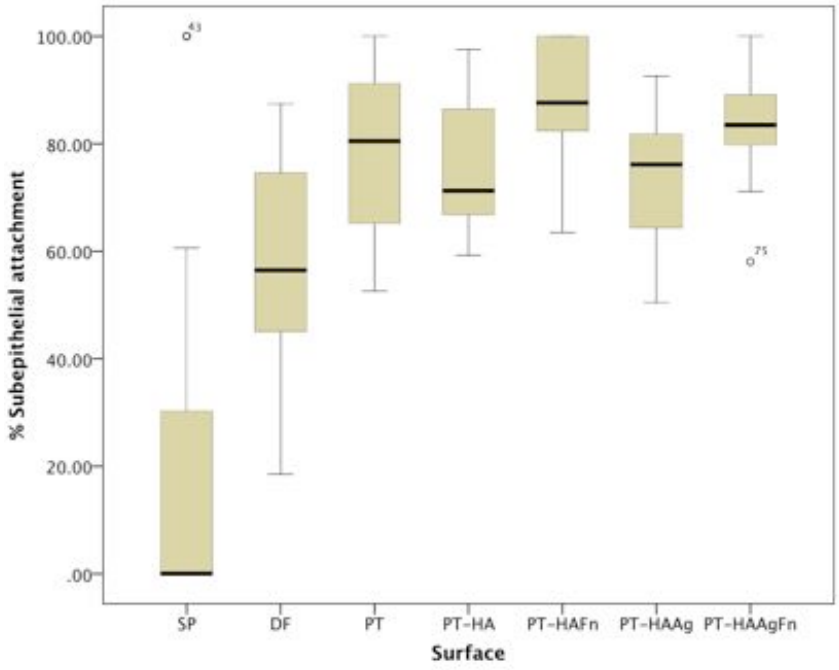

Figure 6.8 Box-and-whisker plot showing dermal attachment to implants.

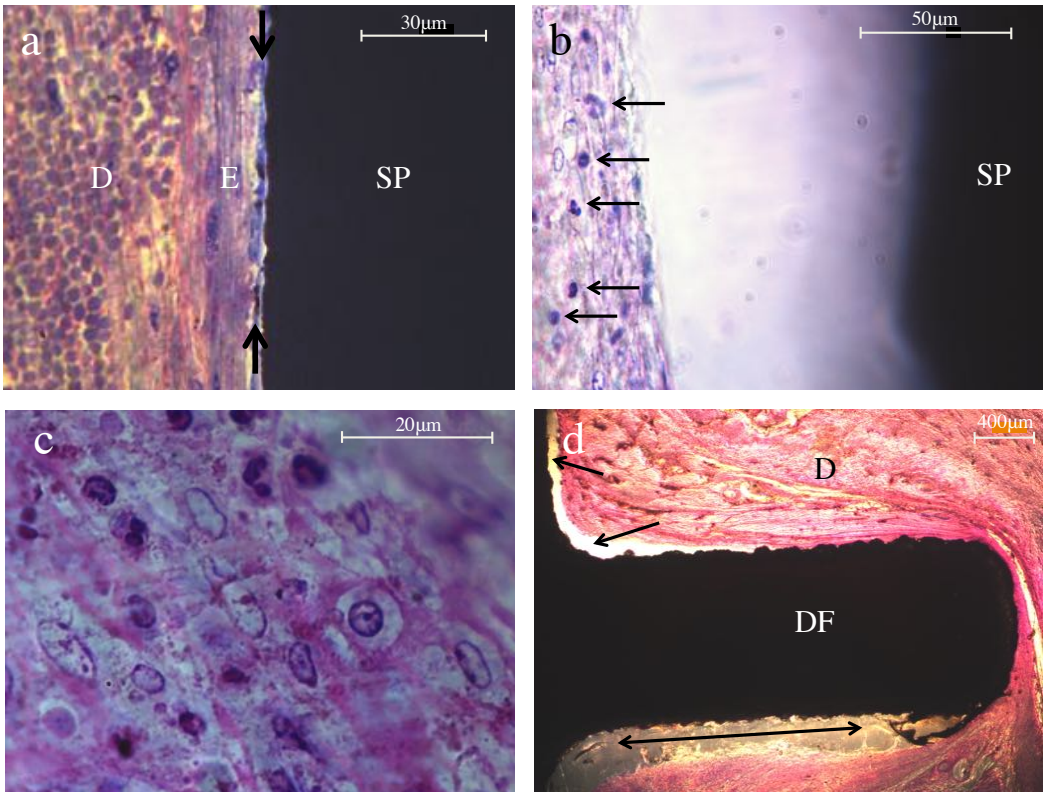

Figure 6.9 (i) Histological sections showing dermal attachment to implants. (a) Absence of dermal attachment to SP. There is a layer of exudate (arrows) along the side of the implant. The migrating epithelium (E) separates the dermis (D) from the exudate layer. The dermis contains a heavy infiltration of inflammatory cells. (b) Gap between the soft tissues and SP. The arrows indicate polymorphonucelar cells, macrophages and lymphocytes within the soft tissues. (c) x100 magnification image of inflammatory cells in tissue adjacent to SP. (d) Areas of lack of the dermal attachment to the flange of a DF implant (arrows).

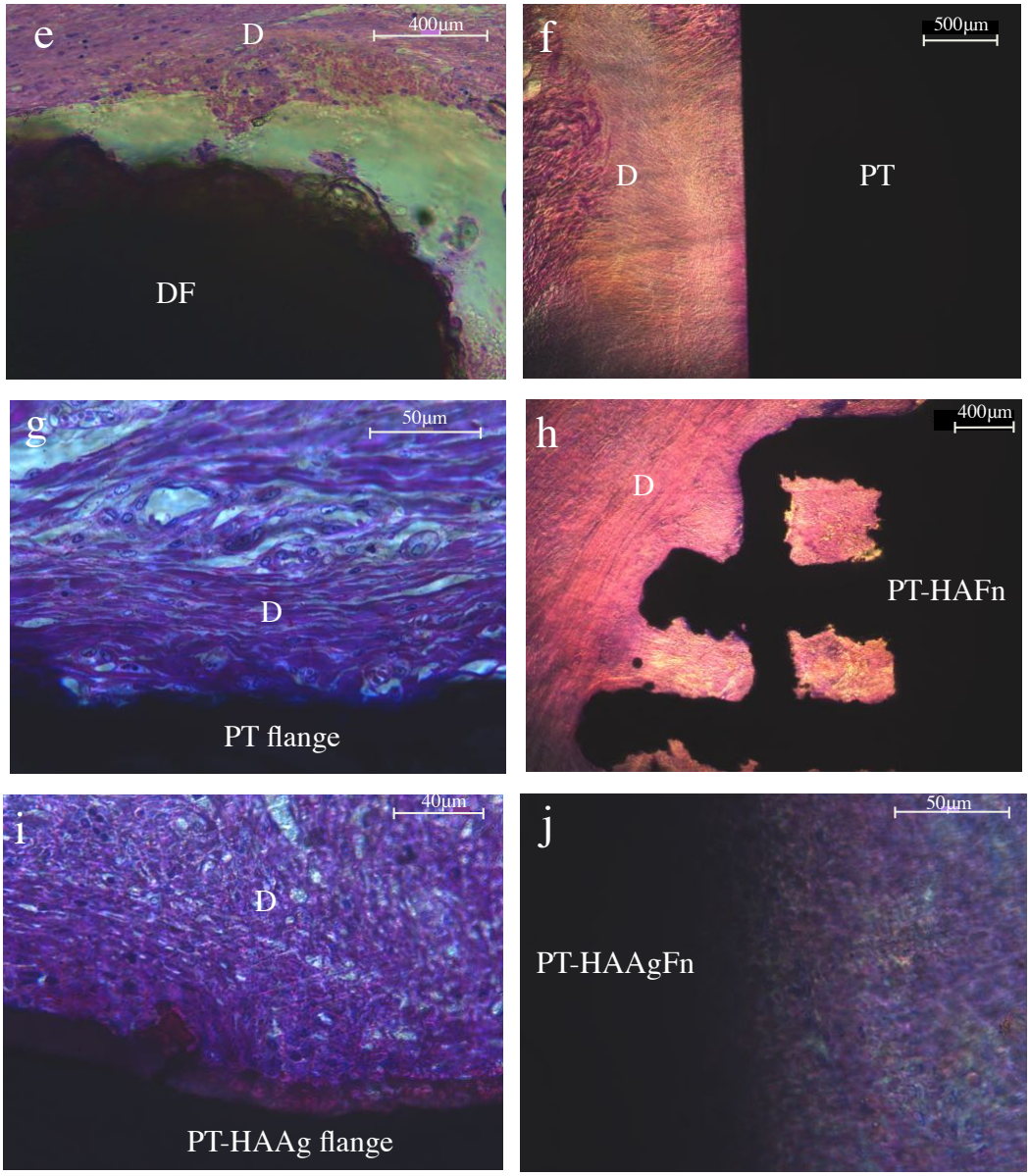

Figure 6.9 (ii) Histological sections showing dermal attachment to implants. (e) Dermal tissue has failed to attach to DF. Fewer inflammatory cells are seen within the tissue adjacent to DF than within the tissue adjacent to SP. (f) Dermal tissue attaching to the transcutaneous portion of PT. (g) Few inflammatory cells are seen within the dermal tissue attaching to PT. (h) Dermis attaching to PT-HAFn flange. (i) Few inflammatory cells are present within the dermal tissue attaching to a PT-HAAg flange. (j) Dermal tissue attachment to the transcutaneous portion of PT-HAAgFn.

6.3.5 Percentage Soft Tissue Fill within the Inner Pores

The percentage soft tissue fill within the inner pores of PT was significantly greater than that of DF (p=0.000). The addition of coatings to PT did not result in any further increases in percentage soft tissue fill. There was a trend that PT-HAFn was associated with a greater median percentage soft tissue fill than PT-HA (90% and 82.5% respectively) and PT-HAAgFn was associated with a greater median percentage soft tissue fill than PT-HAAg (90% and 80% respectively), but these differences were not statistically significantly different (p=0.068 and p=0.143). The only statistically significant difference between the coatings was that PT-HAFn was associated with greater soft tissue fill within the pores than PT-HAAg (p=0.002).

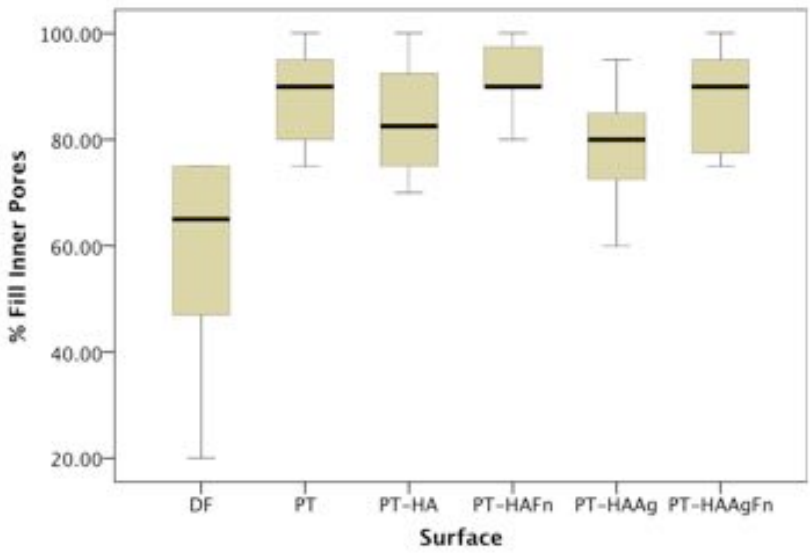

Figure 6.10 Box-and-whisker plot showing the percentage soft tissue fill within the inner pores of each implant.

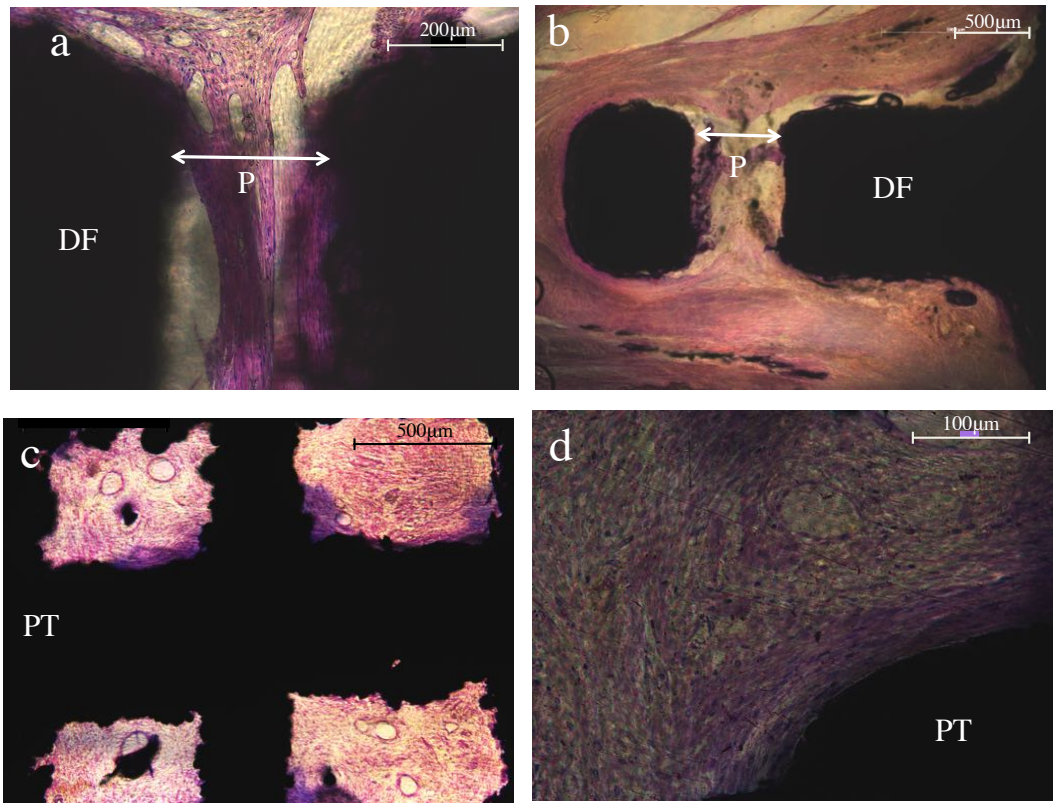

Figure 6.11 (i) Histological sections demonstrating the percentage soft tissue fill within the inner pores of implants. (a and b) Incomplete soft tissue fill within a DF pore (P). (c and d) Intimate contact between PT pore edges and soft tissue PT. Increased collagen deposition is seen at the pore periphery.

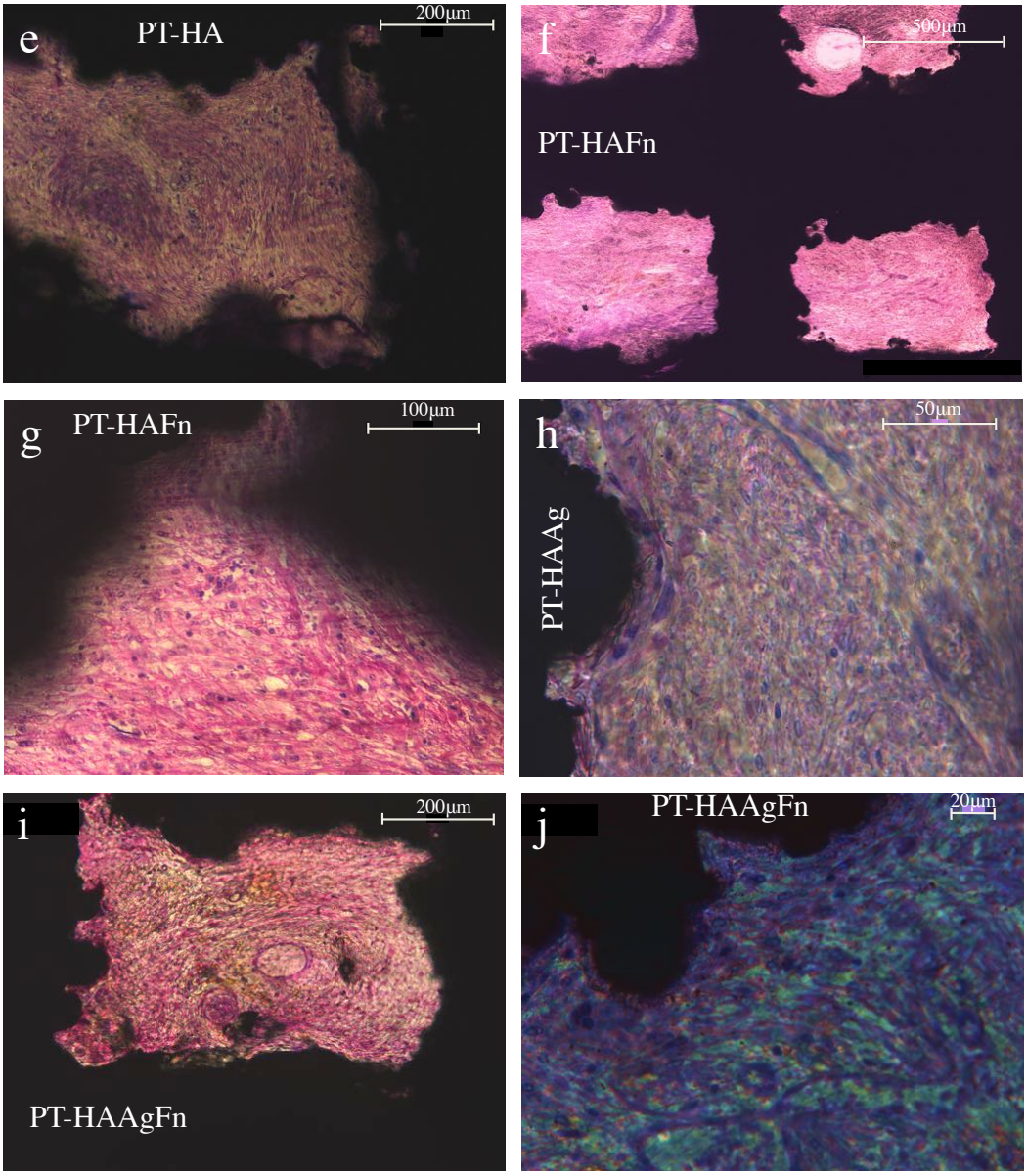

Figure 6.11 (ii) Histological sections demonstrating the percentage soft tissue fill within the inner pores of implants. Soft tissue fills the pores of all PT implants irrespective of the coating. There is intimate contact between the pore edges and the soft tissue. (e) PT-HA (f and g) PT-HAFn (h) PT-HAAg (i and j) PT-HAAgFn.

6.3.6 Number of Cell Nuclei/mm^2 within the Inner Pores

There was a greater cell nuclei density within the inner pores of PT than DF (p=0.018). There were no differences between PT, PT-HA, PT-HAFn, PT-HAAg and PT-HAAgFn (p=0.889).

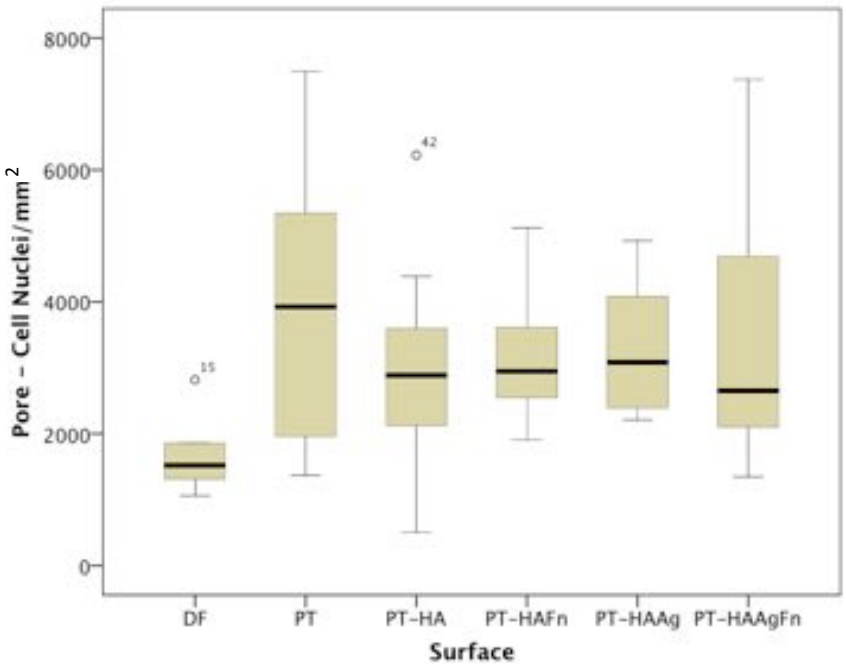

Figure 6.12 Box-and-whisker plot showing the number of nuclei/mm^2 within the inner pores.

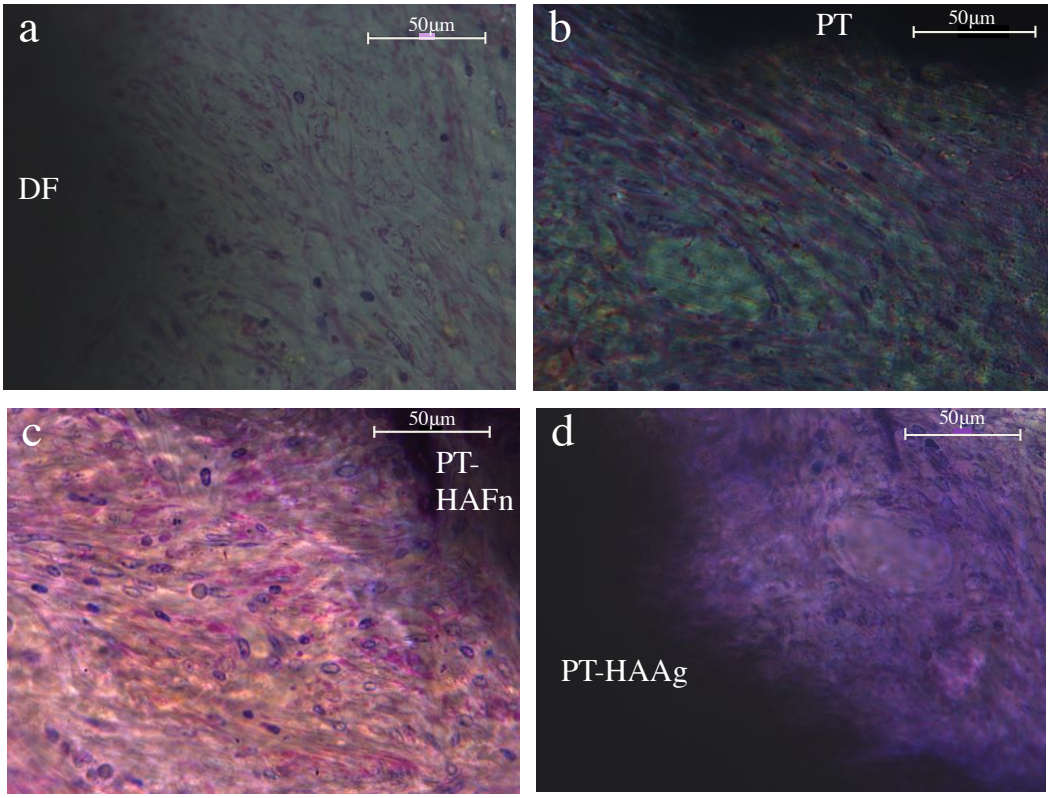

Figure 6.13 Histological sections demonstrating the cell nuclei density within the inner pores of implants. (a) DF has the lowest cell nuclei density. (b) PT (c) PT-HAFn (d) PT-HAAg.

6.3.7 Number of Blood Vessels/mm^2 within the Inner Pores

There was a greater blood vessel density within the inner pores of PT than DF (p=0.002). The addition of coatings to PT did not result in further increases in blood vessel ingrowth (p>0.05. Appendix 6.6.2). Similarly to PT, PT-HAFn, PT-HAAg and PT-HAAgFn were associated with a greater blood vessel density within the inner pores than DF (p=0.001, p=0.005 and p=0.005 respectively); but there was no significant difference between PT-HA and DF (p=0.102). PT-HAAg was associated with a greater blood vessel density within the inner pores than PT-HA (p=0.024).

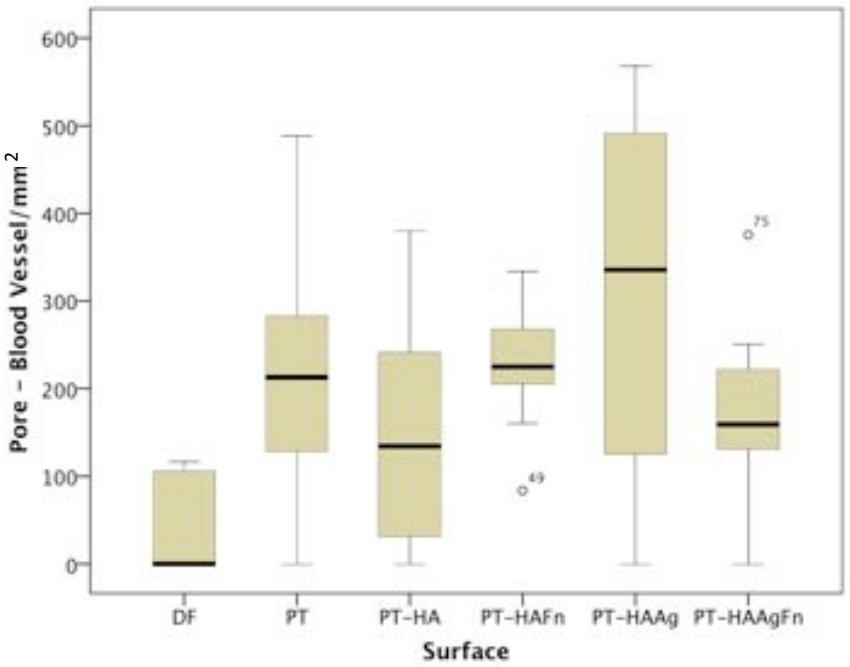

Figure 6.14 Box-and-whisker plot showing the number of blood vessels/mm^2 within the inner pores of each implant.

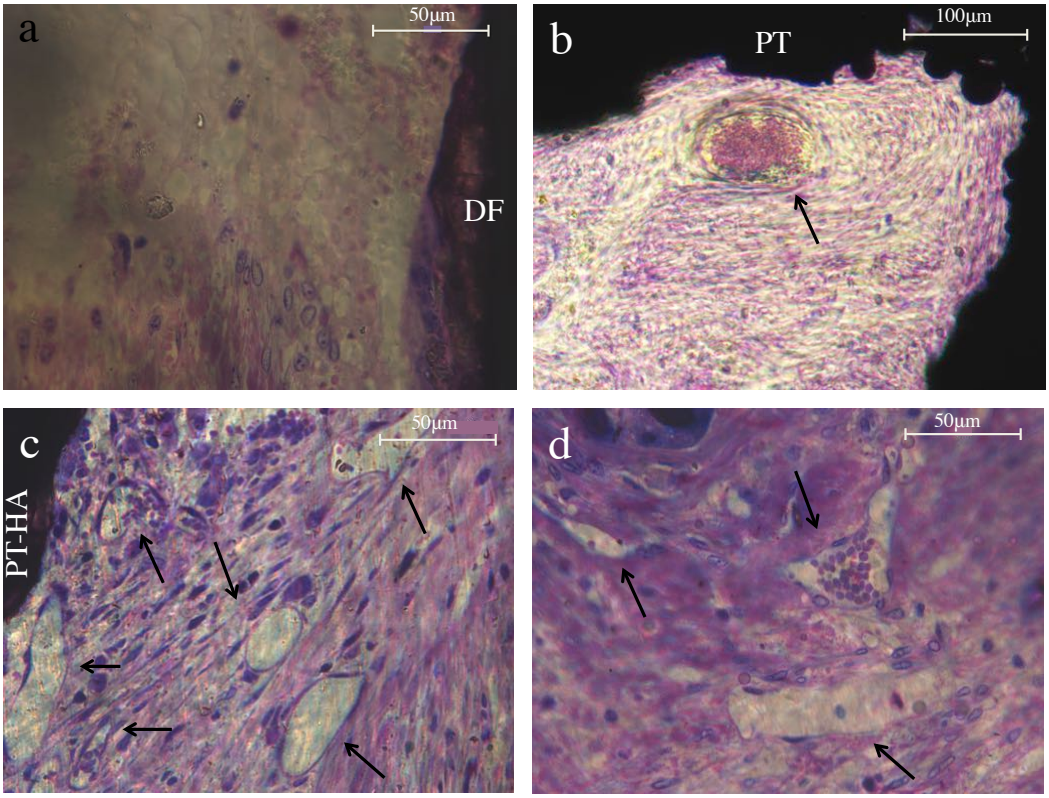

Figure 6.15 (i) Histological sections demonstrating the density of blood vessels (arrows) within the inner pores of implants. (a) DF has the lowest blood vessel density. (b) PT (c) PT-HA (d) PT-HAFn.

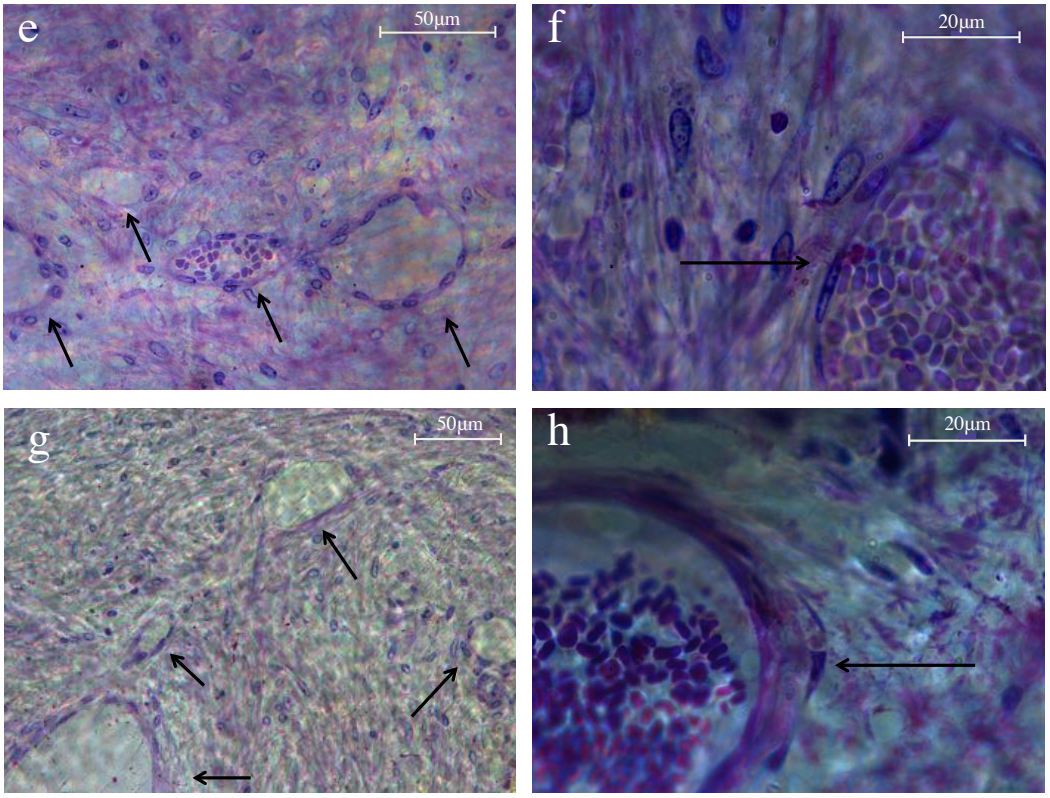

Figure 6.15 (ii) Histological sections demonstrating the density of blood vessels (arrows) within the inner pores of implants. (e and f) PT-HAAg (g and h) PT-HAAgFn.

6.3.8 Silver Blood Levels

Trace levels of silver (less than 10 nmol/L) were detected in all blood samples throughout the 28-day experimental period. There was no increase in silver blood levels postoperatively and there were no statistically significant differences in silver blood levels between time periods (p=0.067).

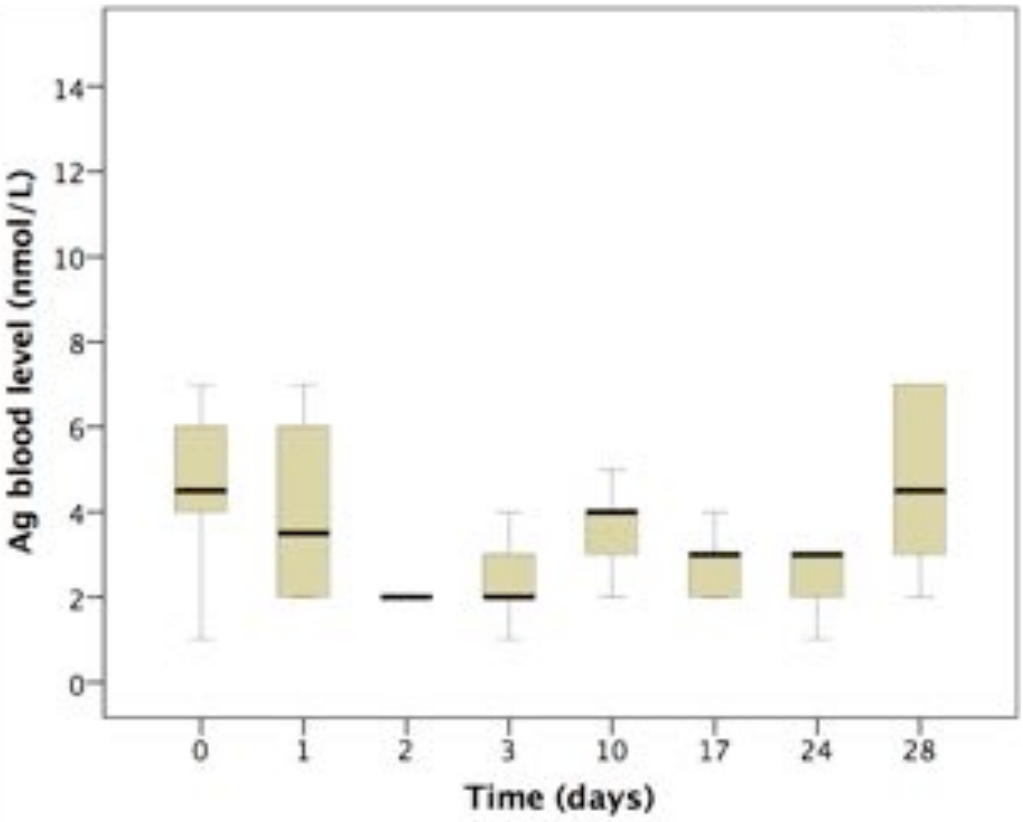

Figure 6.16 Box-and-whisker plot showing the silver whole blood levels over four weeks.

6.3.9 Correlation Analysis

The Spearman's rho analysis identified associations between variables. There was a negative correlation between dermal attachment and epithelial downgrowth. This was significant at the 0.01 level (p=0.000, Correlation Coefficient=-0.439). A positive correlation, which was significant at the 0.01 level, was observed between dermal attachment and epithelial attachment (p=0.000, Correlation Coefficient=0.412). Positive correlations were observed between percentage soft tissue fill, cell nuclei density and blood vessel density within the inner pores (Appendix 6.7). A weak positive correlation existed between dermal attachment and percentage soft tissue fill of the inner pores. This was significant at the 0.05 level (p=0.048, Correlation Coefficient=0.246). There was no significant association between dermal attachment and cell nuclei density or blood vessel density within the inner pores (Appendix 6.7).

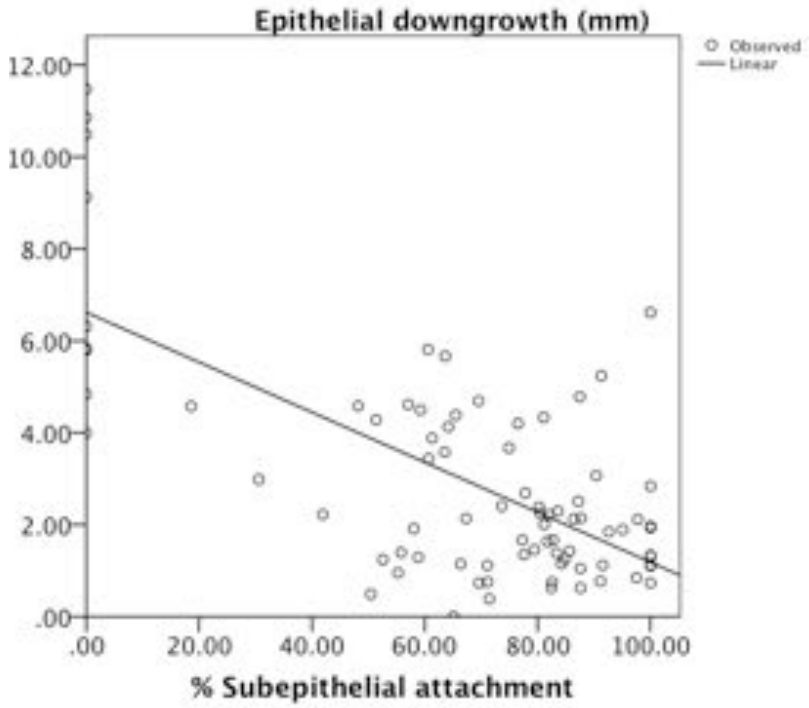

Figure 6.17 Correlation between dermal attachment and epithelial downgrowth.

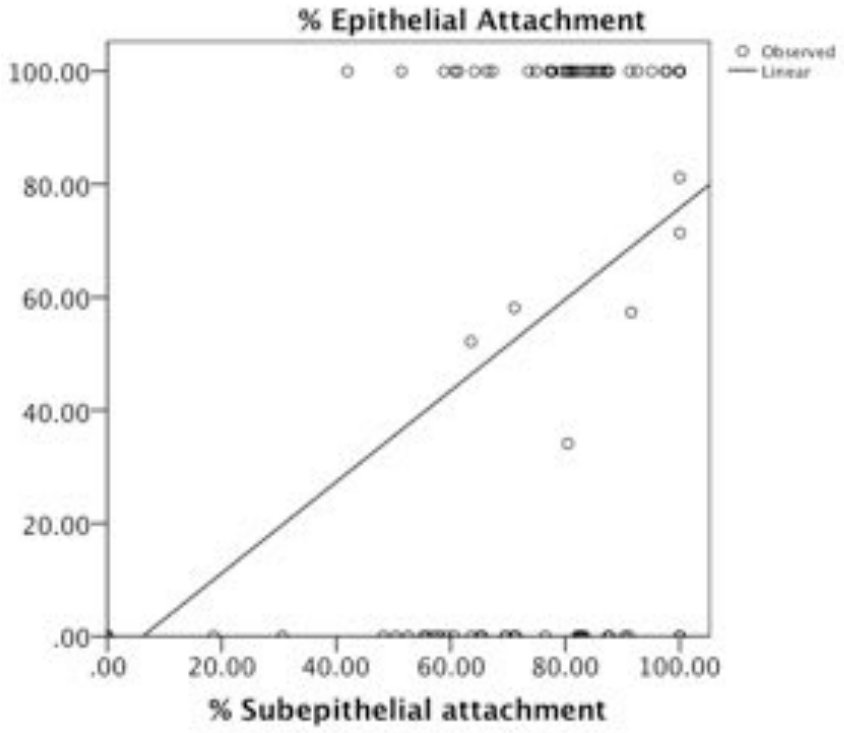

Figure 6.18 Correlation between dermal attachment and epithelial attachment.

6.4 DISCUSSION

Effect of a Porous Titanium Alloy Flange on Soft Tissue Integration

This study has shown that using a fully porous titanium alloy flange reduces epithelial downgrowth and increases dermal attachment as well as ingrowth of vascularised soft tissue into pores compared with the standard drilled-hole ITAP flange. This has not been previously shown. The only other study of the effect of the ITAP model using a fully porous titanium alloy flange was conducted by Dowling et al (2014). In contrast to the findings of this chapter, Dowling et al did not find that use of a porous titanium alloy flange significantly decreased epithelial downgrowth. However, they did find that the porous titanium alloy flange improved soft tissue infiltration, vascularisation and cellularity within pores compared with the standard drilled-hole ITAP flange (Dowling et al 2014). They used a P700 S300 structure as used in this chapter but the implant consisted of two layers of pores in contrast to the dome-shaped flange with four layers of pores used in this study. It is postulated that this difference in the shape of the flange was a key factor in the increased success of the model used in this thesis. A flange with rounded, smooth edges rather than a flange with sharper edges was designed for this study so that the metalwork would be less prominent at the edges. Ideally subcutaneous orthopaedic implants should be low profile with rounded edges to avoid soft tissue irritation and abrasion, which would be detrimental to soft tissue healing (Mudgal and Jupiter 2006; Day and Franko 2007; Jupiter et al 2009). The results of this study indicate that this is a particularly important consideration for ITAP.

Comparison with Other Porous Titanium Alloy Transcutaneous Pin Models

The results of the previous studies in the literature on the effect of porous titanium alloy transcutaneous pins on soft tissue integration are variable. A lapine model of transcutaneous pins with a subcutaneous disc found that a porous titanium alloy surface coating with average pore sizes of approximately 400 μm was associated with a seven-fold reduction in infection risk compared with uncoated smooth implants (Isackson et al 2011). The implants were inserted into the dorsal subcutaneous tissues of the rabbits. This study included a bacterial challenge and animals were euthanised between five and 14 weeks post-op. Histological

assessment demonstrated improved tissue ingrowth into porous coated implants. Organised fibrotic capsules that were separate from the implant surface were seen to be present around uncoated smooth implants. They did not find any statistically significant differences in epithelial downgrowth or soft tissue attachment between porous coated and smooth implants. The dermal attachment to the transcutaneous portion of the pins was very low for both groups (approximately 5 to 6%) (Isackson et al 2011). These poor results may have been due to the infection that was induced. The fact that the pins were not bone anchored would be expected to lead to increased interfacial motion, which would also affect the results. A study of porous titanium rods (pore sizes ranging from 40 to 160 μm) inserted into the backs of rats found approximately 30% soft tissue ingrowth after three weeks and 50% at four to six weeks (Farrell et al 2014). The results with the larger pore sizes and the flanged design used in this chapter were considerably better. However, the lack of bone-anchoring and differences between species may also contribute to the discrepancy in results.

Jeyapalina et al (2012) used a bone-anchored transcutaneous pin model in sheep. They found that a porous titanium alloy surface coating eliminated infection of transcutaneous pins with a subdermal disc implanted into sheep metacarpals compared with a 25% infection rate of their solid pins. However, they found that marsupialisation was present around all implants. They found that epithelial downgrowth was reduced around porous-coated implants, but did not report whether the reduction was statistically significant. Photographs of the implants showed the lack of a seal with visible migration of the solid control implants and also the porous-coated implants to a lesser degree. They did not report data on epithelial and dermal attachment (Jeyapalina et al 2012). On clinical assessment of the pin sites from this chapter, the epithelial migration was not visible, (this was only visible microscropically). This could be interpreted to suggest that the fully porous design and the larger pore sizes used in this chapter were advantageous. However, the fact that Jeyapalina et al used a load-bearing amputation model that continued for nine months is likely to have affected the results and therefore, it is difficult to make direct comparisons.

Effect of Hydroxyapatite, Silver and Fibronectin Coatings on Soft Tissue Integration

The coatings studied in this chapter did not have any statistically significant advantages over PT. The median dermal attachment of PT was 80% and the median soft tissue fill of inner pores was 90%. The median epithelial downgrowth was 1.2 mm. It may be difficult to achieve significant improvements or 100% soft tissue attachment with the model used in this chapter. In this animal model, the sheep mobilised fully weight-bearing from the first postoperative day. Although this is not an amputation model, weight-bearing that occurred would create some movement at the skin-implant interface before the soft tissue-implant seal had been able to form. In humans there would be a rest period where the implant is not loaded during the early wound-healing period. For this reason, it may be unrealistic to achieve better results with this model. There is also more exposure to bacteria than there would be in humans as inevitably dressings become soiled during the immediate postoperative period in sheep, whereas in humans care is taken to avoid this. Additionally, cleaning of pins sites was not included in this model. In human clinical practice, regular cleaning of pins sites is a strategy that may prevent infection and hence enhance the soft tissue seal (Ferreira and Marais 2012).

Hydroxyapatite

Although there were no statistically significant differences when coatings were added to PT, PT-HA lost some of the beneficial effects associated with PT. The reduction in epithelial downgrowth associated with PT-HA compared with DF was not statistically significant. PT and all other coatings reduced epithelial downgrowth significantly. Additionally, PT-HA was the only PT implant that was not associated with significantly improved blood vessel ingrowth compared with DF. Previous studies have found that HA has a favourable effect on soft tissue integration (Oddy et al 2005; Pendegrass et al 2006a; Smith et al 2006; Larsson et al 2012). Moroni et al (2001) showed that HA coated external fixator pins reduce the rate of pin tract infection (Moroni et al 2001). They did not measure soft tissue attachment but showed that improved strength of fixation at the bone-pin interface corresponded with reduced infection. It can be speculated that the reduced infection may be due to

an improvement in the soft tissue-implant seal due to less motion at the interface due to the improved osseointegration. Smith et al (2006) found that fully HA coated transcutaneous pins increased dermal attachment despite also increasing bacterial colonisation (Smith et al 2006).

The negative effect of HA may be due to increased bacterial colonisation. It is postulated that the combination of HA with PT that are both known to promote bacterial colonisation resulted in a sufficient increase in bacterial colonisation to allow bacteria to win the 'race for the surface.' This is investigated in Chapter Seven. It was considered that the rough surface topography of the electrochemically deposited HA may have contributed to the less favourable soft tissue attachment observed as fibroblast attachment has been shown to be impaired on rougher surfaces (Ranella et al 2010; Chimutengwende-Gordon et al 2011; Teng et al 2012). However, it is unclear how this would contribute to reduced soft tissue integration as the surface chemistry and wettability of the HA would be expected to overcome the effects of the roughness. Several *in vivo* studies have found that roughness does not reduce soft tissue attachment or reactions (Zitzmann et al 2002; Abrahamsson et al 2002; Kim et al 2006). Another alternative potential explanation for the effect of HA that was considered is that the HA coatings release debris, which over time leads to a foreign body reaction that is detrimental to soft tissue integration. However, a foreign body reaction was not observed around PT-HA implants in this study.

Fibronectin

PT-HAFn did not have a negative effect although, similarly to HA, HAFn would be expected to promote adhesion of some bacterial strains. The *in vitro* sections of this thesis have shown that fibronectin has a variable effect on different bacterial strains, increasing colonisation of gram-positive bacteria while decreasing gram-negative bacterial colonisation. The effect that the fibronectin has on bacterial colonisation thus depends on the bacteria in the vicinity of the implant. It is expected that the sheep would be exposed primarily to *Staphylococci* (Smith et al 2006). Therefore, a net overall increase in bacterial colonisation would be expected. It is possible that when fibronectin is added to HA, despite its potential to increase bacterial

colonisation, cells are able to win the 'race for the surface' due to earlier soft tissue adherence. This would lead to reduced bacterial colonisation and allow HAFn to overcome any loss of beneficial effects associated with HA.

HAFn and HAAgFn significantly improved dermal attachment compared with HA and HAAg respectively. This is interesting as it shows that fibronectin is not completely counteracted by silver as indicated by the *in vitro* study. The fact that fibronectin had an effect with HAAg *in vivo* but not *in vitro* may be associated with the longer duration of the *in vivo* study. A higher concentration of fibronectin may have a greater effect on soft tissue attachment but this may also risk further increases in bacterial colonisation.

Silver

HAAg coatings did not produce any adverse soft tissue reactions and silver blood levels were negligible. This indicates that the levels of silver used in this study are safe. PT-HAAg was associated with increased vascularisation within the inner pores compared with PT-HA. Additionally, PT-HAAg (and PT-HAAgFn) maintained the beneficial effects that PT had on epithelial downgrowth and vascularity over DF that PT-HA had lost. This indicates that silver had some effect. However, PT-HAAg did not result in greater percentage dermal attachment than DF. The effect of silver coatings without HA or increasing the concentration of silver may have a different effect. Alternative coating methods that could potentially be used to coat porous implants with silver while producing a sustained release similar to that observed with electrochemical deposition include covalently bonding silver to the implant surface using a silanisation technique (Antoci et al 2007a; Antoci et al 2007b; Juan et al 2010) sol-gel coating (Babapour et al 2011), anodisation (Wafa et al 2015) and silver nanoparticle coatings (Wang et al 2014).

It is possible that despite not having a beneficial effect on soft tissue attachment, silver could reduce bacterial colonisation, which could be of value in terms of preventing infection. If this were to be the case, the fact that this study has shown there is no adverse soft tissue reaction associated with silver would be useful.

Although the 'race for surface' theory is that soft tissue attachment is inversely proportional to bacterial colonisation, in practice the relationship between the two variables may be more complex and less predictable. The study by Smith et al (2006) illustrates this. Fully HA coated transcutaneous pin resulted in better dermal contact than uncoated, partly coated or diamond-like carbon (DLC) coated implants. The fully HA coated pins were covered in an exudate deposit and were associated with the greatest bacterial colonisation despite the effects on soft tissue attachment. The DLC coated pins were associated with the least bacterial colonisation but less soft tissue attachment than the HA coated pins (Smith et al 2006). It is expected that a more straightforward inversely proportional relationship between tissue integration and bacterial colonisation is only seen in the very early stages of soft tissue attachment. However, in the very early stages of soft tissue attachment, it is likely that a soft tissue seal would not have formed around any implants and differences in epithelial downgrowth, soft tissue attachment, cell nuclei and/or vascularisation may not be apparent. A study investigating the rate of soft tissue attachment by using a time course may be useful and would show the rate of formation of the soft tissue seal, which may affect long-term infection rates.

Correlation Between Variables

As expected, there was a negative correlation between epithelial downgrowth and dermal attachment. There was also a positive correlation between epithelial attachment and dermal attachment. This correlations were of moderate strength (rather than high strength) indicating that increasing dermal attachment alone is not necessarily sufficiently reliable to increase epithelial attachment. Adjunctive design features to specifically increase epithelial attachment may help to improve success rates e.g. coating the transcutaneous portion of the implant with proteins that enhance keratinocyte attachment (Gordon et al 2010; Pendegrass et al 2012a). It was noted that the results for epithelial attachment were extremely variable and ranged between 0 and 100% for all groups. Histology sections also showed that in some cases where there was minimal epithelial downgrowth and good dermal attachment, epithelium was separate from implant. It is possible that epithelium had attached to the implant in these cases, but due to the soft tissue-implant seal not being robust, the epithelial attachment was disrupted due to soft tissue movement at the interface.

The correlations between pore soft tissue fill, blood vessel and cell nuclei density were of moderate strength. Blood vessel and cell density was not significantly related to dermal attachment. This suggests that other factors influence soft tissue integration. Factors that may contribute include bacterial colonisation and differences in soft tissue thickness, movement of soft tissues at the skin-implant interface and differences in the speed of wound healing between individual sheep.

Limitations

The sheep with the pin complicated by infection was treated with intravenous antibiotics. It was deemed necessary to take this course of action in the sheep's best interest and to prevent suffering. It is possible that this may have had an effect on the results for all the pins implanted into that sheep. It may have also resulted in a reduction in the bacterial colonisation around the non-infected pins. An alternative course of action would have been to terminate the study at the point that the infection occurred (three weeks postoperatively) or to exclude the results of that sheep from the study. Terminating the study early potentially may have reduced the time available for a soft tissue seal to form. Excluding the sheep from the study would have reduced statistical power. Replacing the sheep is not ideal in the interest of reducing the numbers of animals sacrificed and did not seem necessary as on reviewing the data collected from the sheep treated with antibiotics, they were generally in keeping with the findings from the other sheep. In clinical practice, differences in the way individual patients respond in terms of wound healing and infections occur which require treatment with antibiotics. In a clinical trial, the data collected from patients treated for complications such as infection would often be included.

Another limitation of this study is that an assessment of mechanical strength of attachment was not made. This study measured soft tissue contact rather than attachment. An assessment of mechanical strength using peel tests would have necessitated a separate cohort of animals because the samples used for histological assessment had been embedded in resin and so could not be used for peel testing. As

epithelial downgrowth is known to be a key factor leading to infection and failure of ITAP, the detection of a reduction in epithelial downgrowth associated with PT implants is expected to be a reasonably good predictor for the likelihood of improved success of the ITAP. Therefore, in view of results of this chapter showing these advantages associated PT, sacrificing more animals in order to do peel tests is not necessarily essential.

6.5 CONCLUSION

This is the first study to demonstrate that a fully porous titanium alloy ITAP flange reduces epithelial downgrowth and increases dermal attachment, cell nuclei density and blood vessel ingrowth compared with the current standard ITAP model. This is a useful finding that has potential to be exploited for clinical application. The addition of coatings to PT did not significantly improve soft tissue integration. HA coatings resulted in a loss of the favourable effect of PT over DF on epithelial downgrowth and vascularisation. PT-HAFn had the highest median value for percentage dermal attachment and was statistically significantly better than PT-HA and PT-HAAg but was not statistically significantly better than PT. PT-HAAgFn improved dermal attachment compared with PT-HAAg demonstrating the potential for fibronectin to enhance soft tissue attachment. HAAg coatings did not improve soft tissue integration, but did not produce any adverse effects. The effect of these surfaces on bacterial colonisation will be presented in the next chapter and will be considered in conjunction with the findings from this chapter.

CHAPTER SEVEN

In Vivo Bacterial Colonisation on Porous Titanium Alloy Transcutaneous Pins Coated With Hydroxyapatite, Silver and Fibronectin

7.1 INTRODUCTION

A range of factors including surface energy, hydrophobicity, porosity and chemical composition of biomaterials affect bacterial adhesion and the susceptibility of different biomaterials to infection (Oga et al 1993). The finding from Chapter Six that a P700 S300 porous titanium alloy flanged transcutaneous pin improves *in vivo* soft tissue integration, indicates that this design feature has the potential to reduce infection rates for ITAP patients. Ideally, the porous titanium alloy flanges should also be associated with decreased bacterial colonisation, otherwise despite the soft tissue integration results, it would not be possible to conclude that infection susceptibility is reduced. If the bacterial colonisation were to be increased by porous titanium it is likely to affect long-term results adversely. It is particularly important to determine the effect on *in vivo* bacterial colonisation as previous studies have found that porous implants promote bacterial colonisation. Shin and Akao (1997) found that percutaneous devices composed of porous materials implanted through dorsal skin in a canine model increased infection. The pores produced new microbial foci as they created microgaps between the material and the tissue before the soft tissue grew into the pores. Bacteria were able to invade these microgaps (Shin and Akao 1997). *In vitro* assessment by Braem et al (2013) has demonstrated that porous titanium increases bacterial colonisation and that increasing pore size increases this effect. They studied porous titanium coatings with pore sizes ranging from 50 to 150 μm (Braem et al 2013). Cordero et al (1994) found that both porous titanium alloy and cobalt-chrome implants implanted into rabbit femora required smaller bacterial challenges than polished surfaces to induce infection. Cobalt-chrome implants were easier to infect, requiring 40 times fewer bacteria to induce infection than polished implants, whereas porous titanium alloy implants required 15 times fewer bacteria. The authors considered that this was due to the 'race for the surface' theory as cobalt-chrome is less biocompatible than titanium (Cordero et al 1994).

In theory, it is reasonable to expect that soft tissue would have a better chance of winning 'the race for the surface' on a porous titanium alloy flange than on a standard drilled-hole flange due to its effects on enhancing soft tissue integration. In practice, surfaces that increase soft tissue attachment may simultaneously increase

bacterial colonisation. For example, HA is well known to increase *in vivo* osseointegration but has been shown to also increase *in vivo* bacterial colonisation (Laure et al 2008). Wilke et al (1993) found that HA coatings increased bacterial colonisation while simultaneously resulting in good osseous ingrowth (Wilke et al 1993). Vogely et al (2000) found that HA-coated implants implanted in rabbit tibiae increased bacterial colonisation despite being biocompatible (Vogely et al 2000). Despite this, there has been some promising data on the use of porous titanium. As discussed in the previous chapters of this thesis, studies have shown that osseointegrated percutaneous pins with porous titanium alloy coated subdermal barriers decrease infection rates, although these studies have not quantified bacterial numbers (Jeyapalina et al 2012; Isackson et al 2011). Furthermore, these studies did not use fully porous implants and used smaller pore sizes than those in this thesis. Consequently, the effect on bacterial colonisation in this study may be different.

The soft tissue integration findings associated with the addition of hydroxyapatite, silver and fibronectin coatings to PT flanges may be explained by bacterial colonisation differences as discussed in Chapter Six. The studies described above have shown that hydroxyapatite is associated with increased bacterial colonisation (Wilke et al 1993; Vogely et al 2000; Laure et al 2008). This may account for the finding that HA coatings resulted in a loss of the favourable effect of PT over DF on epithelial downgrowth and blood vessel ingrowth. Conversely, other studies have demonstrated that hydroxyapatite and other calcium phosphate ceramics have an antimicrobial effect *in vitro* (Opalchenova et al 1996; Opalchenova et al 1996b; Arciola et al 1999). These findings suggest that variations in the surface properties or topography of different hydroxyapatite coatings may result in different effects on bacterial colonisation. In this study, there were no significant differences in soft tissue integration between PT-HAAg and PT, but this result does not necessarily indicate that bacterial colonisation will be similar on these two surfaces. As the 'race for the surface' relationship is not always entirely predictable, the silver-containing coatings may have an antibacterial effect despite the soft tissue integration results. Porous titanium with sol-gel silver containing coatings have been shown to have equivalent biocompatibility to hydroxyapatite while having an antibacterial effect

(Qu et al 2011). Moojen et al (2009) found that hydroxyapatite-tobramycin coatings had a significant antibacterial effect compared with hydroxyapatite in a lapine model. However, these coatings did not significantly improve bone contact compared with hydroxyapatite (Moojen et al 2009).

The aim of this chapter was to assess the bacterial colonisation on porous titanium alloy flanged transcutaneous pins coated with combinations of hydroxyapatite, silver and fibronectin coatings.

In view of the findings from Chapter Six, it was hypothesised that:

1. DF would decrease bacterial colonisation compared with SP and PT would decrease bacterial colonisation compared with DF.

2. PT-HA would not decrease bacterial colonisation compared with DF; but PT-HAFn, PT-HAAg and PT-HAAgFn would decrease bacterial colonisation compared with DF.

3. PT-HAAg and HAAgFn would decrease bacterial colonisation compared with PT due to the antibacterial action of the silver.

Fibronectin coatings were not expected to reduce bacterial colonisation significantly because apart from the improved dermal attachment no other significant differences in *in vivo* soft tissue integration were demonstrated in Chapter Six. However, due to the increased dermal attachment, it was hypothesised that there would potentially be a non-significant reduction in bacterial colonisation.

7.2 MATERIALS AND METHODS

7.2.1 Implants and Coatings

The same implant designs and coatings studied in Chapter Six were used for these experiments (Section 6.2.1).

7.2.2 Ovine Model to Assess Bacterial Colonisation

The ovine model (n=6) and the surgical procedure described in Section 6.2.2 was used with a separate cohort of sheep. The sheep weighed between 76 and 97 kg. The method was modified by omitting the administration of postoperative antibiotics. Dressings were removed at ten days postoperatively. A pilot study (n=1) was carried out before proceeding to the n=6 study in order to refine the methods.

7.2.3 Microbiological Sampling

At four weeks postoperatively, the animals were euthanised (as described in Section 6.2.2). Following this, soft tissue samples were taken for microbiological analysis. All samples were taken using an aseptic technique.

The following samples were taken:

7.2.3.1 Sample 1: Skin Surface Swab

A swab of the skin at the skin-implant interface was taken. Care was taken to ensure that the swabbing technique was as uniform as possible for each pin site. This sample was taken to give an indication as to whether or not each pin came into contact with (i.e. was challenged with) a similar number of bacteria from the environment.

7.2.3.2 Sample 2: Superficial Soft Tissue Biopsy

A biopsy of the superficial soft tissues (epidermis and minimal superficial dermis) was taken. The skin was incised with a No. 15 blade sterile scalpel and a sample of approximately 4 mm x 4 mm x 4 mm was taken and weighed.

7.2.3.3 Sample 3: Deep Soft Tissue Biopsy

A biopsy of the deep soft tissues was taken. The dermal tissue at the deepest part of the transcutaneous portion of the pin was incised with a fresh No. 15 blade sterile scalpel and a sample of approximately 4 mm x 4 mm x 4 mm was taken and weighed. For flanged implants this dermal tissue was overlying the flange. For the straight pin the dermal tissue was overlying the bone.

7.2.3.4 Sample 4: Deep Soft Tissue-Implant Interface Swab

Soft tissue overlying the flange was peeled back with forceps and a No.15 blade sterile scalpel. The flange was swabbed taking care to ensure that the swabbing technique was as uniform as possible for each pin site. For the straight pin, the deepest part of the transcutaneous pin was swabbed.

7.2.3.5 Sample 5: The Retrieved Implant

After the above samples were taken, the implant was retrieved.

7.2.4 Microbiological Analysis of Samples

7.2.4.1 Direct Colony Counts

Samples 1, 2, 3 and 4 were sonicated in phosphate buffered saline for four minutes. The tissue samples (2 and 3) were weighed prior to this. After sonication, the phosphate buffered saline samples were serially diluted over a 5-log range and plated onto Columbia horse blood agar. The undiluted sample was also plated. After incubation of the agar plates at 37°C for 24 hours, the colonies were counted. For samples 1 and 4, cfu/mL was calculated. For samples 2 and 3, cfu/mL per mg of tissue was calculated.

7.2.4.2 Bacterial Identification

Agar plates were inspected and each morphological type of colony was sampled and identified. The following assays were performed to identify bacterial strains: gram

staining, the catalase reaction, the oxidase test, the DNase test and methicillin sensitivity testing. Analytical Profile Indexing (API) identification kits (Biomérieux, France) were used for final identification of the bacterial strains. The protocols for conducting each of these tests are presented in Appendix 1.3.

7.2.4.3 Scanning Electron Microscopy

Sample 5, the retrieved implant, was prepared for SEM by fixation in formalin for 24 hours followed by the protocol described in Appendix 1.2. SEM was carried out to identify the presence of bacteria and to visualise any biofilms that had formed.

7.2.5 Statistical Analysis

The statistical analyses described in section 2.2.5 were performed. Correlation analysis between variables from this chapter and variables from Chapter Six was carried out. A post hoc Benjamini-Hochberg test was used to adjust for correlations (as more than 20 comparisons were made).

7.3 RESULTS

7.3.1 Direct Colony Counts

7.3.1.1 Skin Surface Swab

There were no statistically significant differences between numbers of bacteria on the surface of the skin at each pin site (p=0.255).

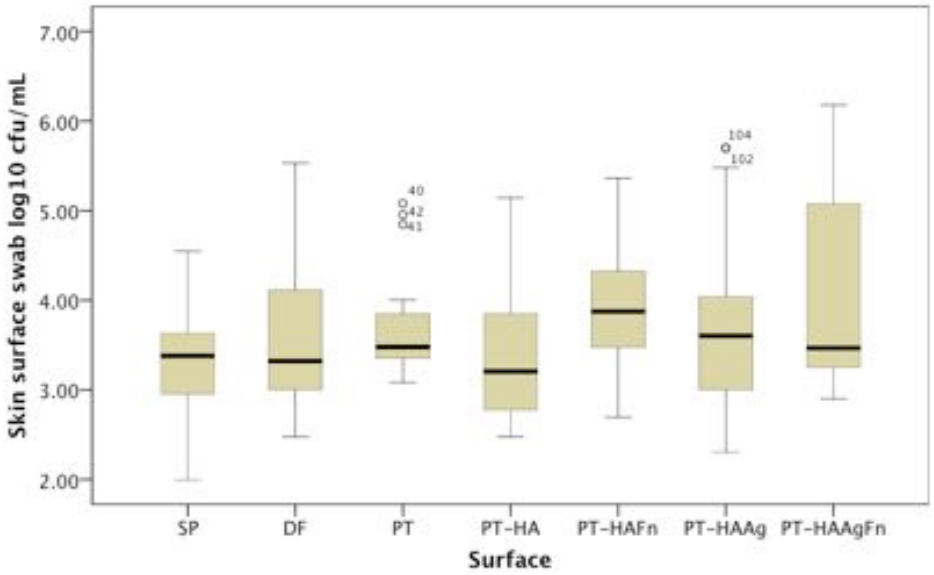

Figure 7.1 Results for colony forming units per mL for the skin surface swabs from each pin type.

7.3.1.2 Superficial Soft Tissue Biopsy

There was no statistically significant difference in the numbers of bacteria colonising the superficial soft tissues around SP and DF (p=0.355). PT was associated with significantly reduced superficial soft tissue bacterial colonisation compared with DF (p=0.000). PT-HAAg was also associated with significantly reduced superficial soft tissue bacterial colonisation compared with DF (p=0.000). PT-HA, PT-HAFn and PT-HAAgFn were not associated with a significant reduction in bacterial colonisation compared with DF (p=0.079, p=0.556 and p=0.171 respectively). There were greater numbers of bacteria colonising the superficial soft tissues around PT-HA and PT-HAFn than around PT (p=0.000 and p=0.019). There was no difference between either PT-HAAg or PT-HAAgFn and PT (p=0.602 and p=0.259). PT-HAAg reduced bacterial colonisation compared with PT-HA and PT-HAFn (p=0.011 and p=0.022). PT-HAAgFn did not have this beneficial effect over PT-HA and PT-HAFn (p= 0.673 and p=0.343).

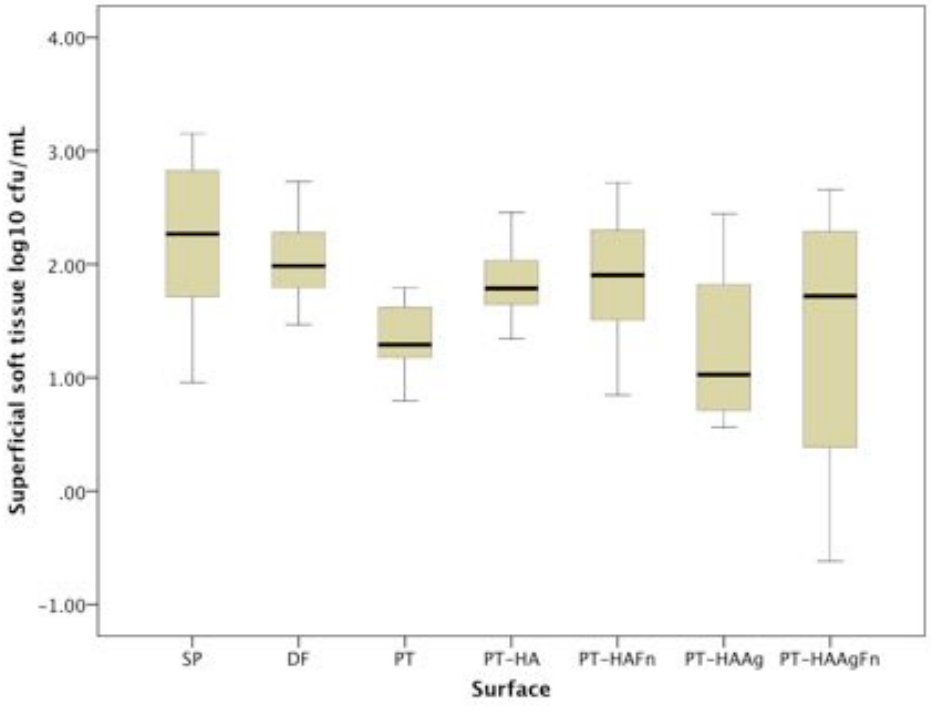

Figure 7.2 Results for colony forming units per mL (per mg of tissue) within the superficial soft tissues around each pin type.

7.3.1.3 Deep Soft Tissue Biopsy

There was no statistically significant difference between SP and DF (p=0.224). PT, PT-HAFn, PT-HAAg and PT-HAAgFn all reduced bacterial colonisation compared with DF (p=0.000). PT-HA did not reduce bacterial colonisation compared with DF (p=0.135) and was associated with increased bacterial colonisation compared with PT (p=0.008). However, there were no differences between PT and PT-HAFn, PT-HAAg or PT-HAAgFn (p=0.526, p=0.901 or p=0.766). PT-HAFn, PT-HAAg and PT-HAAgFn were all associated with less bacterial colonisation than PT-HA (p=0.007, p=0.009 and p=0.020). There was no difference between PT-HAFn and PT-HAAg (p=0.861); or between PT-HAFn and PT-HAAgFn (p=0.539) or between PT-HAAg and PT-HAAgFn (p=0.830).

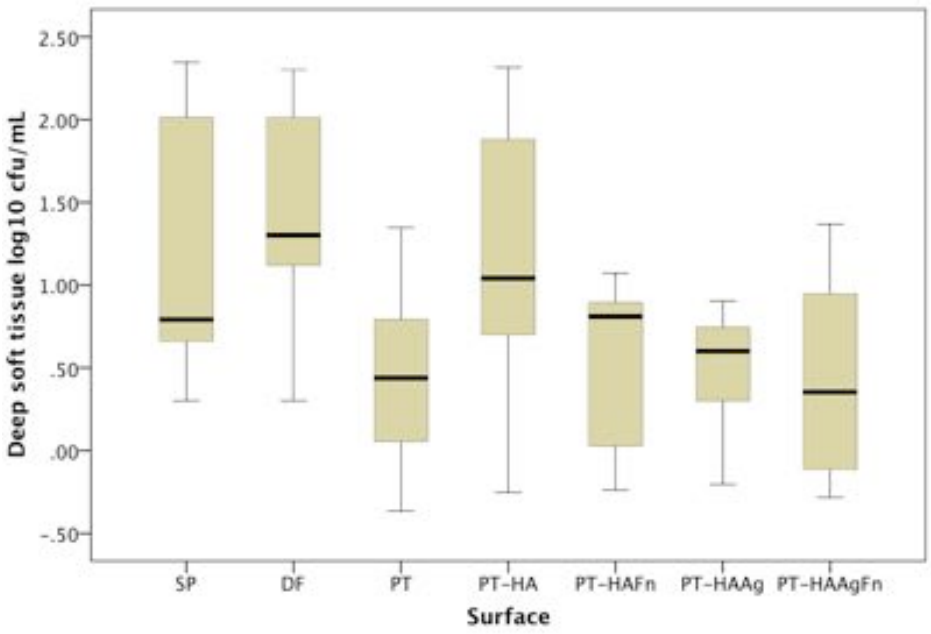

Figure 7.3 Results for colony forming units per mL (per mg of tissue) within the deep soft tissues around each pin type.

7.3.1.4 Deep Soft Tissue-Implant Interface Swab

DF did not reduce bacterial colonisation compared with SP (p=0.938). PT with and without all coatings was associated with reduced bacterial colonisation compared with DF (p=0.000). The addition of coatings to PT did not affect the bacterial colonisation (HA p=0.815, HAFn p=0.839, HAAg p=0.075, HAAgFn p=0.357). PT-HAAg reduced bacterial colonisation compared with PT-HA (p=0.012). There were no other differences between the coatings.

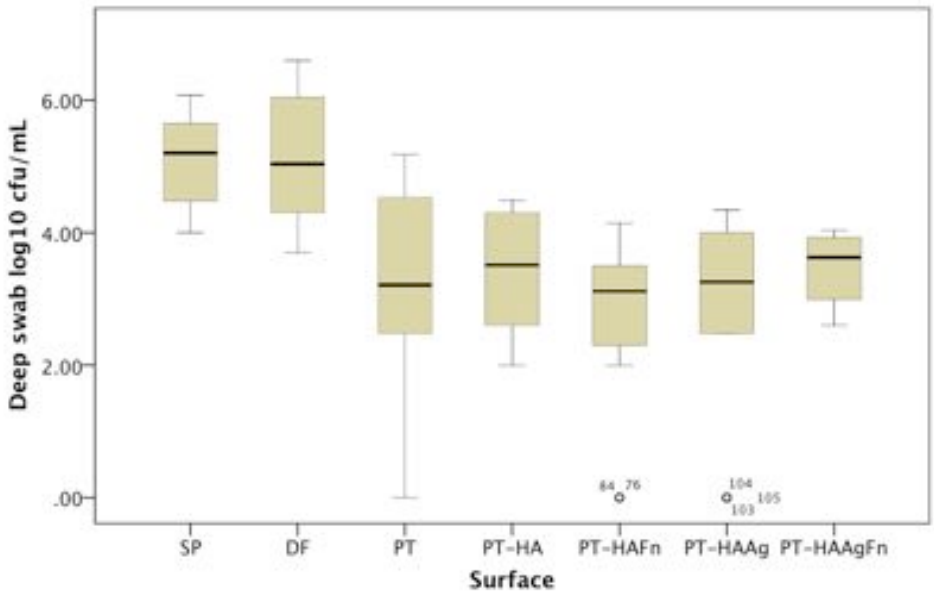

Figure 7.4 Results for colony forming units per mL for the deep skin-implant interface swabs for each pin type.

7.3.2 Bacterial Identification

A mixed growth of bacteria was identified. The bacteria present were predominantly *Staphylococci*. Four strains of *S xylosus* and one strain each of *S sciuri*, *Micrococcus spp*. and *S lentus* were cultured from samples from all six sheep. In addition *S hyicus* and *E coli* were present on samples from one sheep, a fifth strain of *S xylosus* was present on samples from another two sheep and a second strain of *S sciuri* was present on samples from another sheep (Table 7.1).

Sheep ID no.	Gram Stain	Catalase	Oxidase	DNase	Methicillin Sensitivity	API ID
6144/6164/6241/ 6222/6185/6135	Gram + cocci	+	-	-	S	*S xylosus* 6736552
6144/6164/6241/ 6222/6185/6135	Gram + cocci	+	-	-	S	*S xylosus* 6736542
6144/6164/6241/ 6222/6185/6135	Gram + cocci	+	-	-	S	*S sciuri* 6336510
6144/6164/6241/ 6222/6185/6135	Gram + cocci	-	weak +	-	S	*Micrococcus spp* 0006100
6144/6164/6241/ 6222/6185/6135	Gram + cocci	+	-	-	S	*S xylosus* 6734542
6144	Gram + cocci	+	-	-	S	*S xylosus* 6536672
6144	Gram + cocci	+	+	+	S	*S sciuri* 6136110
6241	Gram + cocci	+	-	-	S	S hyicus 6516051
6241	Gram - bacilli	+	-	-	R	*E coli* 5144572
6222/6185	Gram + cocci	weak +	-	-	S	*S xylosus* 6776552
6144/6164/6241/ 6222/6185/6135	Gram + cocci	+	-	-	R	*S lentus* 6777750

Table 7.1 Bacterial strains identified from sheep pin sites (+ = positive, - = negative, S = sensitive, R = resistant).

7.3.3 Correlation Analysis

The Spearman's rho test showed the following correlations between variables that were significant at the 0.01 level. There was a positive correlation between the numbers of bacteria within the superficial soft tissues and the deep soft tissue (p=0.000, Correlation Coefficient=0.470). There was a positive correlation between the numbers of bacteria within the deep soft tissues and the deep swab of the skin-implant interface (p=0.000, Correlation Coefficient=0.433). There was a positive correlation between the numbers of bacteria within the superficial soft tissues and the deep swab of the skin-implant interface (p=0.000, Correlation Coefficient=0.385). The numbers of bacteria isolated from the skin surface swab did not correlate significantly with the numbers of bacteria from the soft tissues or the deep skin-implant interface swab (p>0.05. Correlation Coefficients and p values are shown in Appendix 7.5).

The analysis of the results from this chapter in conjunction with those from Chapter Six showed that there was a positive correlation between the numbers of bacteria from the deep swab of the skin-implant interface and epithelial downgrowth (p=0.000, Correlation Coefficient=0.437). There was a negative correlation between the deep swab bacterial numbers and percentage dermal attachment (p=0.008, Correlation Coefficient=-0.297). Bacterial colonisation within the superficial soft tissues correlated negatively with cell nuclei density (p=0.012, Correlation Coefficient=-0.327) and with blood vessel density (p=0.001, Correlation Coefficient=-0.412). The relationships between bacterial colonisation within the superficial or deep soft tissues and percentage epithelial or dermal attachment were not statistically significant (Appendix 7.5).

7.3.4 Scanning Electron Microscopy

Bacteria were seen to be present on the surface of all implants. Heavy bacterial growth was observed on SP and DF implants and also less commonly on PT-HA implants. Sporadic smaller pockets of bacterial growth were observed on PT, PT-HAFn, PT-HAAg and PT-HAAgFn but there did not appear to be a clear difference between the amount of bacteria observed on these four implant types. At the time of extraction of the implants, it was noted that there was more resistance to removal of the soft tissues from PT flanges (irrespective of coating) than from SP or DF controls. Residual soft tissue adhesion was observed on PT flanges under SEM (with the exception of the area where the deep soft tissue biopsy had been taken). Minimal soft tissue adhesion was visible on SP and DF implants. Blood clots and inflammatory cells were seen on SP. Extracellular polymeric substance was not visualised on any surfaces.

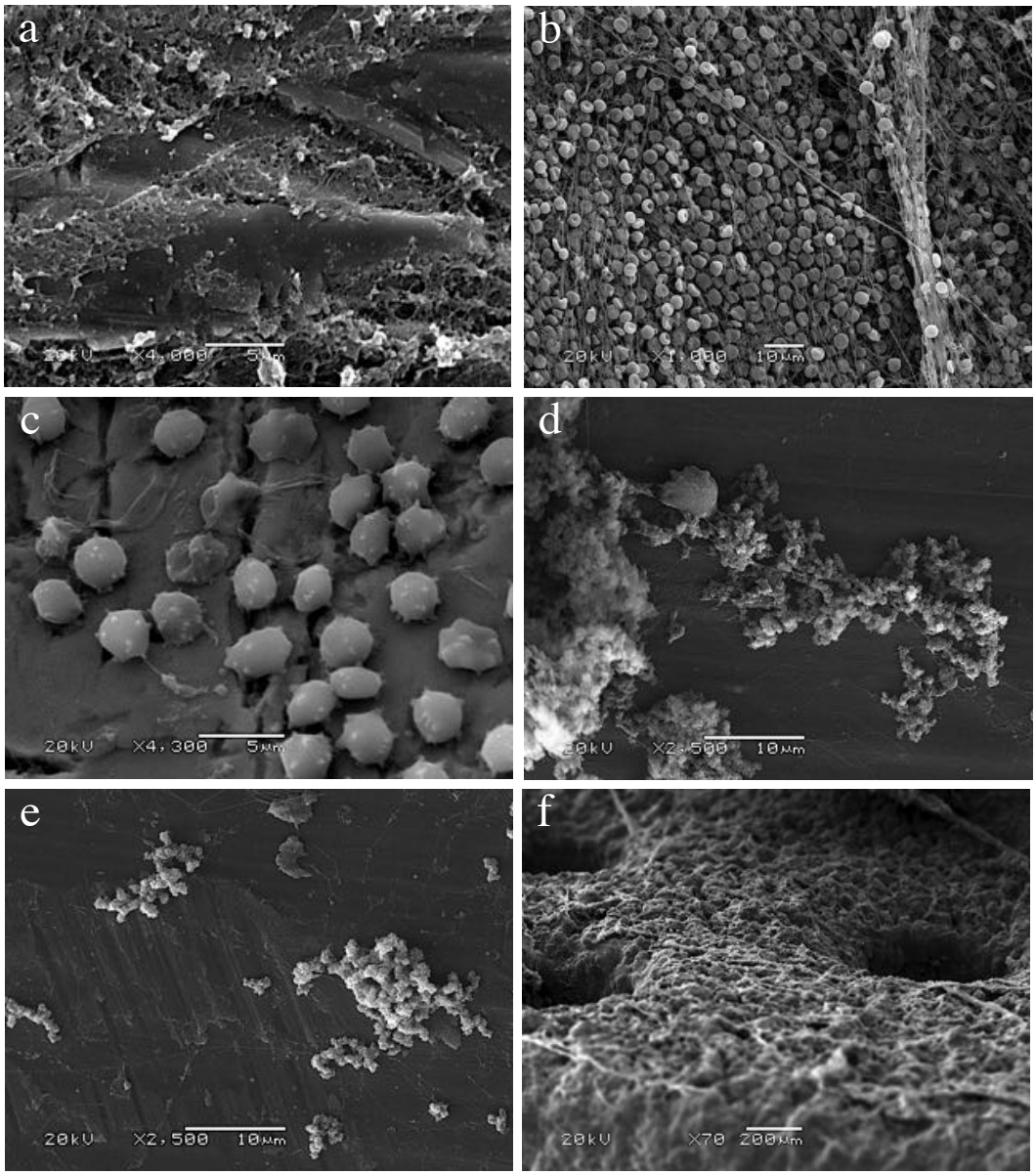

Figure 7.5 (i) Scanning electron micrographs of retrieved bacteria. (a) Bacterial colonisation within a fibrinous exudate on SP. (b) Blood clot covering the surface of SP. (c) Monocytes on the surface of SP. (d) Heavy bacterial growth on SP. (e) Clusters of bacteria colonising a DF pin. (f) DF flange at low magnification (x70) showing the absence of soft tissue adhesion.

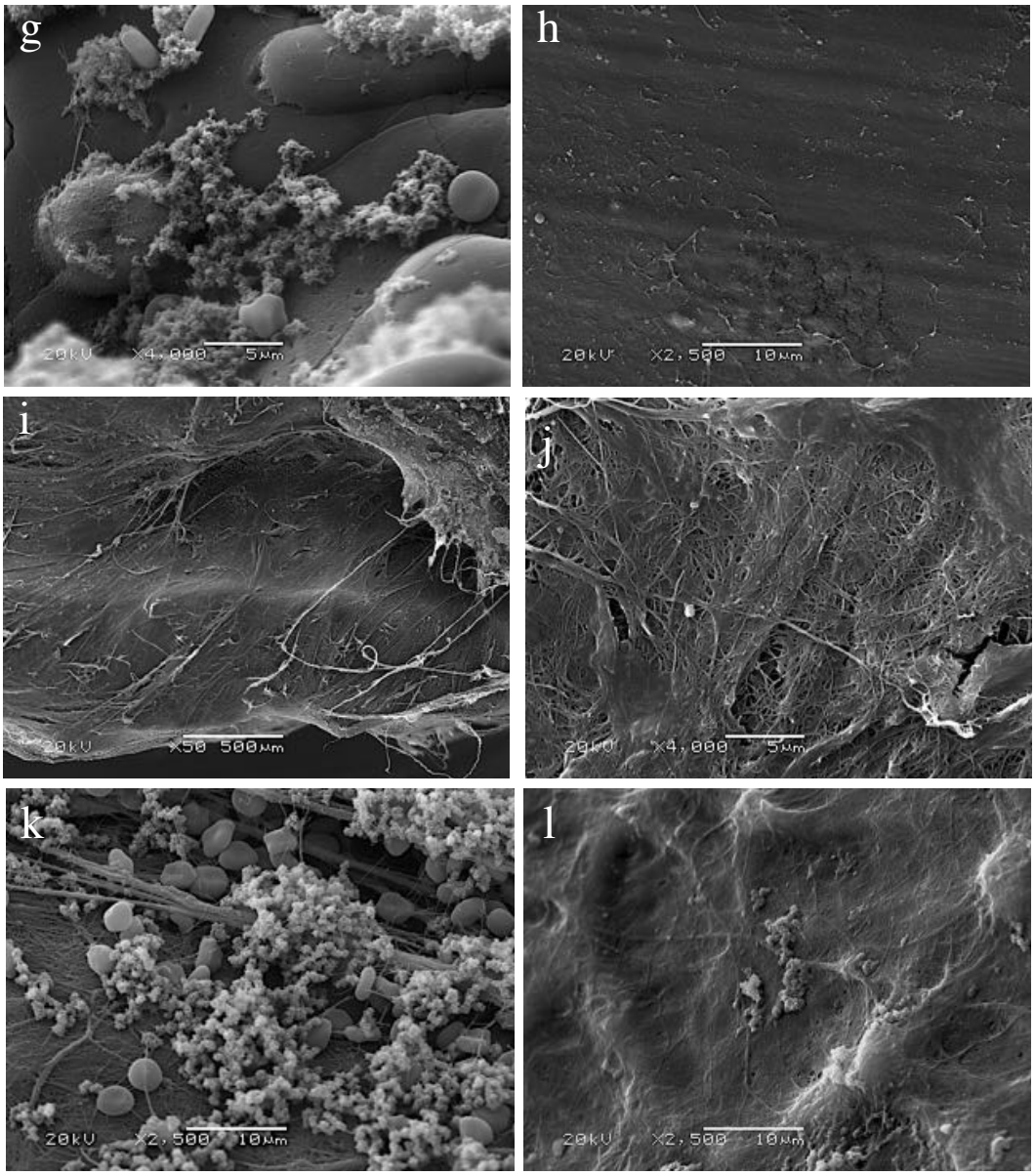

Figure 7.5 (ii) (g) DF flange at x4000 magnification showing the presence of bacteria and erythrocytes. (h) PT pin surface. (i) Soft tissue adhering to PT flange at x500 magnification. (j) Few bacteria are seen on a PT flange at x4000 magnification. (k) Heavy bacterial growth and erythrocytes on soft tissue covering the surface of a PT-HA flange. (j) Small pockets of bacteria are seen on the soft tissue covering a PT-HAAgFn flange.

7.4 DISCUSSION

The key finding of this chapter is that PT significantly reduces bacterial colonisation within the superficial and deep soft tissues and on the surface of the flange compared with DF. This suggests that modification of the current design of ITAP to include a PT flange may reduce the susceptibility to infection. There were some negative correlations between bacterial colonisation and soft tissue integration variables. However, the correlations between some of these variables were weak and/or not statistically significant. This may be due to the fact that some surfaces that promoted soft tissue integration were also still able to support bacterial colonisation. For example, although DF was shown in the previous chapter to improve soft tissue integration compared with SP, it did not reduce bacterial colonisation compared with SP. This demonstrates the complexity of the 'race for the surface' where in some cases the relationship between tissue integration and bacterial colonisation is not predictable as tissue and bacteria may attach simultaneously.

The addition of coatings to PT did not result in further significant reductions in bacterial colonisation. PT-HA was associated with greater bacterial colonisation than PT but did not increase soft tissue integration and resulted in a loss of the favourable effects of PT over DF on epithelial downgrowth and blood vessel ingrowth. Therefore, this method of HA-coating for PT is not recommended. Surface charge may be responsible for the increased bacterial colonisation observed on PT-HA. Hydroxyapatite is positively charged due to the presence of calcium and phosphate and as a result negatively charged bacteria are attracted to the surface (Clark et al 1978; Oga et al 1993). The porosity and surface area of hydroxyapatite coatings also promotes bacterial colonisation (Vogely et al 2000).

It could be argued that this study did not provide clear information about biofilm formation. SEM revealed the presence of bacteria but it was not possible to conclude that biofilm formation had occurred on any of the surfaces tested. Clusters of bacteria and areas of heavy bacterial growth were observed, but extracellular polymeric substance (as had been identified with SEM for the *in vitro* studies) was not seen. A

longer time period or a larger bacterial challenge may have been necessary for biofilm (or extracellular polymeric substance) formation to be observed. Furthermore, environmental SEM would be more sensitive in detecting the presence of extracellular polymeric substance, as the samples would not be dried prior to analysis.

Effects of Control Surfaces

An interesting finding was that DF did not significantly reduce bacterial colonisation compared with SP. This may partly explain the fact that despite improved soft tissue integration compared with SP, infection is still a high risk with the current ITAP design. A potential reason for this finding is that although DF improves soft tissue attachment, it does not improve it to a great enough degree to overcome the effects of the drilled holes on promoting bacterial colonisation. Furthermore, DF is coated with hydroxyapatite to increase soft tissue integration. As observed with PT-HA, the presence of hydroxyapatite may contribute to the bacterial colonisation on DF. The effect of an uncoated DF on bacterial colonisation has not been studied. It is possible that an uncoated DF could result in less bacterial colonisation but may be associated with poorer soft tissue integration.

Fibronectin and Silver

The effects of fibronectin varied in different ways and at different levels of the pin-tissue interface. Both PT-HA and PT-HAFn resulted in an increase in bacterial colonisation within the superficial tissues. Within the deeper tissues, PT-HA increased bacterial colonisation but PT-HAFn reduced it compared with PT-HA. This fits in with the data from Chapter Six, which showed PT-HAFn had its only significant beneficial effect on soft tissue integration at the subepithelial level. PT-HAFn did not have any advantage over PT. It would appear that PT-HAFn does not overcome the negative effect of PT-HA. This again points to the possibility of studying the use of PT with fibronectin bonded to it without hydroxyapatite. Dowling et al (2014) covalently bonded the RGD sequence of fibronectin to porous titanium using a silanisation technique (Dowling et al 2014). They did not study the

effect of RGD on bacterial colonisation but studied soft tissue integration. They did not find that RGD significantly increased soft tissue integration compared with uncoated surfaces but found that RGD coated porous titanium implants produced increased soft tissue infiltration, vascularisation and cell density compared with drilled hole implants coated with RGD. Porous titanium without RGD improved soft tissue infiltration compared with drilled-hole implants but did not have the advantageous effect on vascularisation and cell density (Dowling et al 2014). Several *in vitro* studies have shown that when antibacterial surfaces are functionalised with RGD, antibacterial activity is retained (Chua et al 2008; Maddikeri et al 2008; Shi et al 2008). It would be useful to determine if fewer bacteria colonise RGD coatings than fibronectin coatings and if increased concentrations of RGD on porous titanium to those used by Dowling et al may enhance soft tissue integration to a greater extent. If this were found to be the case, RGD may therefore become a viable alternative to fibronectin.

Similarly to PT-HAFn, PT-HAAg did not decrease bacterial colonisation compared with PT. However, PT-HAAg significantly reduced bacterial colonisation on the flange compared with PT-HA, thus corroborating the suggestion from the Chapter Six results that there may be some value in using silver without HA and/or increasing the concentration of silver used.

Bacterial Challenge

A 'natural' bacterial challenge from the environment was used rather than inoculating the pin sites with bacteria. In clinical practice, humans may be exposed to small numbers from bacteria intraoperatively and may also be exposed to bacteria from the environment. In this way, this model may be more representative of clinical practice in humans. However, it is not possible to ensure that all pins in all sheep are exposed to the same number and strains of bacteria. These bacteria would be present even if an 'artificial' challenge had been used and would affect the results. If an 'artificial' challenge had been used a strain of *S aureus* that has caused clinical infections of ITAPs would have been used to make the model more representative of

human conditions. On an agar plate, the *Staphylococci* found to be present on the sheep are visually indistinguishable from *S aureus*. It would not be logistically possible to type each individual colony as there were thousands of individual colonies. As a consequence of this, it would not be possible to know whether the bacteria being counted are those from the 'artificial' challenge or those from the 'natural' challenge. Additionally, license issues prevented the use of an 'artifical' challenge in any case. The risk of sepsis with an 'artificial' challenge would have been greater and it may have been necessary to use a shorter time period in view of this. As the time periods for this chapter and the previous chapter were the same in order to assess if the results mirrored each other, a shorter time period would have potentially meant it would have been too early to detect differences in soft tissue integration.

Limitations

The sheep were exposed to a range of bacteria from the environment in the immediate postoperative period. Although they were primarily exposed to *Staphylococci*, the strains were not those most commonly encountered by humans. *E coli* was identified and this has previously caused infection of osseointegrated transcutaneous implants (Tillander et al 2010; Brånemark et al 2014). However, this was only detected in samples from one sheep. This chapter assessed overall differences in numbers of bacteria, rather than differences in the numbers of specific strains. It would not have been possible to determine the differences in the numbers of individual strains accurately due to the fact that many strains were visually indistinguishable on agar plates as described above. As discussed above, there were thousands on individual colonies. Consequently, the individual colonies were not all typed and only a selection were typed that appeared visually different in order to get an idea of the strains present. It is therefore also possible that other strains were present that appeared the same visually to strains that had been typed were not identified. Therefore, this chapter is not a detailed microbiological characterisation of isolates, but rather a snapshot of the bacteria present on the pins. However, identification of a surface that reduces overall bacterial numbers is clinically useful.

The conditions in the barnyard were inevitably 'dirty' compared with the conditions humans would normally be exposed to after having an ITAP inserted. Perioperative antibiotics were not administered in order to avoid suppression of bacterial colonisation as a bacterial challenge was desired. However, a 'cleaner' model with less exposure to bacteria as well as prophylactic antibiotics may have been more representative of the conditions that humans encounter. With a smaller bacterial challenge it is possible that results may be different as the surfaces may be able to resist bacterial colonisation to a greater degree.

Another limitation is the potential effect of differences in the thickness of soft tissue between sheep. Differences in soft tissue thickness along the length of the tibiae, (which may affect the interfacial movement, the formation of the soft-tissue implant seal and consequently bacterial colonisation), were taken into account by rotating the position of implants in each sheep. However, overall differences in soft tissue thickness between sheep could not be accounted for. As a result the deep soft tissue biopsy may have been taken from different depths within the soft tissue for different animals. It is also likely that the deep soft tissue biopsy would have been taken from a deeper point within the tissues for SP implants than for flanged implants. This is because this sample was taken from the tissue overlying the flange of flanged implants, whereas for SP, (as there was no flange), it was taken from the tissue overlying the bone. This could potentially have affected the results for the deep samples taken from the SP-tissue interface.

7.5 CONCLUSION

The overall conclusion of this study is that incorporation of a fully porous titanium alloy flange into the current ITAP design has the potential to reduce the susceptibility of ITAP to infection. PT decreased bacterial colonisation compared with DF. In conjunction with the results from the previous chapter where soft tissue integration was investigated, these findings indicate that soft tissue is more likely to win the 'race for the surface' against bacteria on PT than on DF. DF did not reduce bacterial colonisation compared with SP providing a potential explanation for the

infection rate associated with clinical use of ITAP despite the ability of DF to increase soft tissue integration. PT-HA had a negative effect and PT-HAFn was associated with less bacterial colonisation within the deep soft tissues than PT-HA. PT-HAAg reduced bacterial colonisation on the flange surface compared with PT-HA. Further research into the use of silver and fibronectin/RGD coatings as an adjunct but without HA may have some potential to further enhance the effects of PT. However, in the clinical environment where there is less exposure to bacteria than in a barnyard animal model, it is a possibility that PT may be able to prevent bacterial colonisation to a greater degree and adjunctive coatings may not be required.

CHAPTER EIGHT

General Discussion and Conclusions

8.1 DISCUSSION

Key Findings and Contributions to Current Knowledge

The overall aim of this thesis was to develop a fully porous ITAP flange with appropriate coatings in order to enable soft tissue to win the 'race for the surface' against bacteria. **The key finding and original contribution to current knowledge from this thesis is that a fully porous titanium alloy flange with a pore size of 700 µm and a strut size of 300 µm increases dermal attachment and soft tissue ingrowth, cellularity and vascularisation of tissue within pores, whilst reducing epithelial downgrowth and bacterial colonisation compared with the drilled-hole ITAP flange which is currently used to treat amputees.** The *in vitro* studies found that electrochemically deposited HAAg coatings with and without adsorbed fibronectin had antibacterial activity and were cytocompatible while maintaining antibacterial activity after serum-preconditioning for 24 hours. The hypothesis that HAAg and/or HAAgFn coatings applied to the fully porous ITAP flange would further enhance soft tissue integration and decrease bacterial colonisation was not found to be true *in vivo*.

Chapter One of this thesis reviewed the background behind the development of osseointegrated transcutaneous amputation prostheses and explained the ITAP design, which is based on the deer antler. The problem of infection and how the success rate is dependent on soft tissue winning the 'race for the surface' against bacteria was considered. As a result of this review, potential strategies to enhance soft tissue integration and decrease bacterial colonisation associated with ITAP were selected for investigation in the subsequent chapters.

In order to improve dermal integration, which is the basis of the ITAP concept, Chapter Two presented a histological study of the effect of a range of porous titanium alloy structures on soft tissue integration. The aim of this chapter was to select an appropriate porous structure that could be taken forward in subsequent investigations. Porous titanium alloy cylinders with interconnected pores were implanted into the paraspinal muscles of sheep and left *in situ* for four weeks. It was

hypothesised that more open porous titanium alloy structures with larger pore sizes would improve soft tissue integration. The results proved this hypothesis demonstrating that three of the more open structures (P1000 S400, P1000 S200 and P700 S300) resulted in the greatest soft tissue ingrowth. P700 S300 supported revascularisation of tissues to the greatest degree and as a result this was the structure selected for the ITAP flange for use in a transcutaneous pin model in Chapters Six and Seven of this thesis.

In order to further promote soft tissue attachment and at the same time reduce bacterial adhesion appropriate coatings were investigated in Chapters Three and Four. The effect of incorporation of silver into HA and HAFn coatings on fibroblast viability and bacterial colonisation was studied *in vitro*. Silver was incorporated into these coatings using electrochemical deposition. Chapter Three hypothesised that HAAg and HAAgFn coatings with low silver concentrations would be cytocompatible. HAAg and HAAgFn coatings were found to be initially cytotoxic to fibroblasts, but after serum-preconditioning for 24 hours, these coatings were found to support viable fibroblast growth. This finding suggested that in a clinical setting, HAAg would be cytotoxic initially; and that a short time period of contact with the patient's serum after implantation (up to 24 hours) may be required to enable cells to attach to these surfaces. Chapter Four studied bacterial colonisation on HAAg and HAAgFn. It was hypothesised that HAAg and HAAgFn surfaces would reduce *S aureus* and *P aeruginosa* colonisation compared with HA, HAFn and Pol controls and that HAAg and HAAgFn surfaces would maintain their antibacterial activity after serum-preconditioning. The hypothesis was proven that these coatings had antibacterial activity against both *S aureus* and *P aeruginosa*. After serum-preconditioning more than 99% of the antibacterial activity of HAAg100 and HAAgFn100 against *S aureus* compared with HA and HAFn controls was maintained for both biofilm and planktonic colonisation. *P aeruginosa* was found to be less susceptible to the antibacterial effects of HAAg and HAAgFn than *S aureus* and these coatings were only able to maintain significant antibacterial activity after serum-preconditioning when a smaller challenge of *P aeruginosa* was administered (i.e. a challenge of 5×10^4 cfu/mL compared with 10^6 cfu/mL).

Bringing together the research findings from Chapters Two, Three and Four, a transcutaneous pin with a fully porous titanium alloy flange having a pore size of 700 μm and a strut thickness of 300 μm was investigated and reported in Chapter Five. Electrochemically deposited HA and HAAg coatings were produced throughout the porous structure. Fibronectin was adsorbed onto the surfaces by immersion of the implants in a solution of fibronectin. Surface characterisation showed that HA and HAAg coatings were semi-crystalline and hydrophilic. Silver release into fetal calf serum was sustained for 28 days but reduced over time. The silver levels released were levels previously shown to be bactericidal but below levels known to cause tissue or systemic toxicity. These transcutaneous pins were implanted along the length of the tibiae of twelve sheep and left in situ for four weeks. The current ITAP drilled-hole flange design and a straight pin were used as controls. A histological assessment of soft tissue integration was presented in Chapters Six. This chapter showed that the porous titanium alloy flange significantly reduced epithelial downgrowth and increased dermal attachment compared with the drilled-hole flange. The fully porous flange also increased soft tissue fill, cellularity and vascularisation within pores. Chapter Seven showed that the fully porous titanium alloy flange reduced bacterial colonisation within the superficial and deep soft tissues and on the surface of the flange compared with the drilled-hole flange. The addition of HA with or without silver and/or fibronectin coatings did not significantly increase soft tissue integration or decrease bacterial colonisation further compared with uncoated porous titanium alloy. HA coatings were associated with increased bacterial colonisation within the soft tissues and resulted in a loss of some of the favourable soft tissue integration effects of the porous flange compared with the drilled-hole flange.

Implications of the Effect of Using a Porous Flange for ITAP and Limitations

The results of the research presented in this thesis indicate that incorporating a fully porous flange into the ITAP design should reduce the susceptibility of ITAP to infection by increasing the ability of soft tissue to win the ‘race for the surface’ against bacteria. However, although the porous titanium alloy was found to improve soft tissue attachment and decrease bacterial colonisation, it did not eliminate epithelial downgrowth or bacterial colonisation and did not result in 100% soft tissue

attachment. This may be partly due to the postoperative conditions resulting in more exposure to bacteria than would be expected in a human model. Additionally, human skin has less hair, intraoperatively laminar flow systems are used, postoperatively dressings are changed and pin sites cleaned when necessary. In human clinical practice the interface is rested during the first few weeks until the soft tissues have healed sufficiently and the loading of the ITAP device is gradually increased over a period of several months (Kang et al 2010). Although an amputation model was not used in this thesis, the animals mobilised bearing full weight immediately postoperatively. This is expected to have resulted in more movement at the interface during the early postoperative period than would occur in clinical human practice and this may have affected the results. It could be argued that the main drawback of this research is that an animal model cannot be fully representative of the conditions in human clinical practice. Furthermore, although determining the effect on early soft tissue attachment and bacterial colonisation is important when studying the 'race for the surface' and should influence the long term outcomes, the long term effect is unknown and it may be necessary to assess this before proceeding onto clinical trials.

Coatings

The fact that the addition of silver and fibronectin overcame some of the negative effects of HA indicates that research on a range of concentrations of silver and fibronectin coatings without HA may be of value. It is also possible that the initial cytotoxicity associated with electrochemically deposited HAAg coatings (demonstrated in the *in vitro* studies of this thesis) may have contributed to the fact that HAAg coatings overall did not have a significant benefit. Preconditioning HAAg-coated flanges with simulated body fluids or autologous serum pre-implantation would be expected to overcome this cytotoxicity but at the same time would be expected to reduce the magnitude and duration of the antibacterial effect and may therefore be counterproductive. The coatings were kept deliberately thin (less than 100 μm) in order to avoid a significant reduction in the space within the pores for tissue ingrowth. However, the presence of the coatings would inevitably have some effect on the space within the pores. It is possible that this was another factor affecting the results of the coatings applied to the porous flanges. Increasing

the pore size to take into account the thickness of the coatings may be able to compensate for this effect.

General Clinical Applicability

Although, the main intended application of the findings from this research is for improving the success of ITAP, the findings could also be applied to other transcutaneous devices. For example, external fixator pin tract infection is a common problem, with reports of infection rates ranging between 3.9% and 100% (Parameswaran et al 2003; Coester et al 2006; Antoci et al 2008). Improving soft tissue integration at the skin-implant interface would also be beneficial for preventing infection of external fixator pins. Addition of a porous flange to external fixator pins may have the potential to reduce infection susceptibility. A potential disadvantage of flanged external fixator pins is that multiple pins are used in one limb and they are eventually removed. A more robust soft tissue seal is likely to make subsequent removal of the external fixator pins more difficult leading to soft tissue trauma and problems with wound healing at the site of pin removal. A flange with fewer layers of pores than the flange developed in this thesis (e.g. two layers) may reduce the risk of this problem while improving soft tissue integration, although to a lesser degree than with the ITAP flange.

The coatings developed in this thesis may be more likely to produce favourable *in vivo* results for osseointegration than for soft tissue integration due to the rough topography (Marinucci et al 2006; Osanthanon et al 2011; Teng et al 2012; Costa et al 2013). If HA has a more favourable effect on osseointegration, the susceptibility of HA to promote bacterial colonisation could be overcome. Further investigation of porous metals coated with electrochemically deposited HAAg (with and without fibronectin) to assess the effect on osseointegration would be useful to determine if these coatings could play a role in preventing loosening and bacterial colonisation of the intraosseous portion of ITAP or for uncemented arthroplasty surgery. This may be of particular value for revision surgery, where infection is an increased risk and particularly for revision surgery undertaken for infected arthroplasty (Suarez et al 2008; Mortazavi et al 2010). Additionally, this coating technique could be applied to endoprosthetic replacements with porous collars e.g. for tumour resection (Gupta et

al 2006; Myers et al 2007; Spiegelberg et al 2009; Coathup et al 2013; Batta et al 2014; Coathup et al 2015).

Future Work in Preparation for Clinical Translation

It is hoped that the advantages of the porous flange demonstrated in this thesis will be translated clinically. It may be useful to study the effect of a number of other strategies that could be used in conjunction with the porous-flanged implant and may increase the likelihood of success.

Suture Immobilisation of Skin to the Flange

Suturing of the soft tissues to the porous flange in order to immobilise the skin-implant interface during the healing process may enhance the soft tissue seal (Bobyn et al 1982; Kang et al 2010). The 700 μm pores used for the flange may be too small to allow a needle to pass through it and struts from adjacent layers would make suturing the tissues to the flange technically difficult. To overcome this, larger pores at the junction between the flange and the transcutaneous portion of the implant could be incorporated into the design to allow the tissues to be sutured to the implant. It would be important to use an absorbable suture and to avoid excessive suturing in order to reduce the amount of foreign material, which may cause a foreign body inflammatory response and delayed wound healing (Carr et al 2009; Sönmez et al 2009; Hansen and Gottrup 2014).

Epithelial Attachment

The porous flanges did not significantly increase epithelial attachment suggesting that design modifications to increase epithelial attachment specifically may be necessary. Laminin and E-cadherin have been shown to increase keratinocyte attachment and could be used to coat the transcutaneous portion of the implant (Gordon et al 2010; Pendegrass et al 2012a). Alternatively, coating the transcutaneous portion of the implant with layers of porous titanium alloy could potentially increase epithelial attachment. Studies to determine if the same porous structure as used for dermal tissue integration promotes epithelial tissue integration

would be necessary. However, if any of the porous titanium alloy coating were to be present on the portion of the pin that has penetrated the skin and is external to the tissues, there would be a risk of attracting bacteria onto the external pin surface. This risk could be reduced by either coating the porous titanium alloy coating with an antibacterial coating or using an antibacterial collar or sponge to cover the external pin and to protect the skin-implant interface from bacteria. The use of other coatings (including antibacterial coatings) and methods of external local delivery of antimicrobials (including the use of antibacterial collars or sponges) are discussed in the following sections.

Other Coatings

Although the effect of a porous titanium flange may be sufficient to prevent bacterial colonisation and reduce the risk of infection of ITAP, the use of other coatings that could be applied to the fully porous flange could be investigated with the aim of further reducing the risk of infection. Hydrophilic coatings such as poly(ethylene glycol) brush coatings with RGD (PEG-RGD) have been found to prevent adhesion of bacteria while allowing cell adhesion and spreading (Subbiahdoss et al 2010a; Muszanska et al 2014). RGD coatings may have the potential to be used as an alternative to fibronectin to increase soft tissue integration (Dowling et al 2012; Dowling et al 2014). Further investigation of the ability of RGD coatings to promote soft tissue integration and to determine whether bacterial colonisation is reduced on RGD coatings compared with fibronectin would be of value. Alternative methods of application of silver coatings have been discussed in Chapter Six (Section 6.4). The Agluna coating has been used for tumour endoprostheses and recently for coating the ITAP flange. This coating involves anodisation of titanium alloy followed by absorption of silver from an aqueous solution and has been found to reduce early periprosthetic infection rates (Wafa et al 2015). The use of sutures loaded with antimicrobials such as triclosan to close soft tissues has been associated with a reduced rate of surgical site infection and therefore may be an additional strategy that could help reduce infection rates of ITAP (Galal and El-Hindawi 2011; Sajid et al 2013; Okada et al 2014; Serrano et al 2015).

External Local Delivery of Antimicrobials to the Skin-Implant Interface

It may be useful to deliver antimicrobial agents to the interface to reduce the bacterial load. Antibiotic-impregnated collars are currently being investigated to prevent external fixator pin site infection (Arthritis Research UK 2010). A similar collar could be placed over the skin-implant interface of ITAP and would be changed regularly. An externally attached refillable device for automated release of antibiotics or antiseptics is an alternative option that may reduce the exposure of the soft tissues to bacteria (Bansal 2013). It would be important to ensure that the antimicrobial agent used is not cytotoxic and does not inhibit normal wound healing.

The Effect of Patient Factors

Research on ITAP has focused on modifying implant and/or surgical factors. However, patient factors are also relevant. ITAP patients are selected carefully and to date, patients with comorbidities such as peripheral vascular disease and diabetes have not been included in clinical trials. Other factors such as age, smoking, alcohol consumption, nutritional status, decreased host immunity and medications such as glucocorticoids and non-steroidal anti-inflammatory medications also affect wound healing (Guo and DiPietro 2010). General hygiene and likelihood of compliance with the rehabilitation programme must be considered. As outcomes vary between ITAP patients despite careful selection, there may be other differences between individual patients that affect wound healing. For example, differences in blood flow to the skin have not been studied for ITAP patients. Laser Doppler flowmetry could be used to evaluate blood flow to the skin (Zografos et al 1992). If differences were identified between patients, the cause would need to be considered. Further assessment of factors affecting wound healing in current ITAP patients may increase our understanding of why a successful skin-implant seal is formed in some patients but not others.

8.2 GENERAL CONCLUSIONS

The work presented in this thesis has shown that more open porous structures increase soft tissue integration more than less open structures with smaller pore sizes.

The overall hypothesis that the addition of a fully porous flange to the ITAP design increases soft tissue integration and decreases bacterial colonisation compared with the current drilled-hole ITAP flange was found to be true. *In vitro*, HAAg and HAAgFn coatings were found to have antibacterial activity while maintaining viable fibroblast growth after serum-preconditioning (mimicking the *in vivo* environment). However, *in vivo*, the hypothesis that the addition of HAAg and HAAgFn coatings would further enhance soft tissue integration and decrease bacterial colonisation was not confirmed. The porous flange did not completely eliminate epithelial downgrowth or bacterial colonisation, however, the significant improvements in soft tissue integration and reductions in bacterial colonisation represent a step forward for infection prevention of ITAP. There may be the potential to achieve more favourable results in a human model with improved perioperative hygiene conditions. Differences between individual coatings identified that HA resulted in a loss of some of the beneficial effects of the fully porous flange on soft integration (specifically epithelial downgrowth and vascularisation) compared with the drilled-hole flange. HA coatings were associated with increased bacterial colonisation within the soft tissues. Therefore, this method of HA-coating is not recommended for ITAP. Further modification of the technique used by altering the current density, the time period for electrochemical deposition and the amount of fibronectin and silver added to HA may have the potential to lead to more favourable results. Fibronectin improved dermal attachment when added to HA and HAAg coatings and the addition of silver to HA reduced bacterial colonisation. Further investigation of fibronectin and/or silver coatings without HA may be of value. Overall, the results indicate that a fully porous titanium alloy flange with a pore size of 700 μm and a strut size of 300 μm, without the addition of coatings, has the potential to increase the ability of soft tissue to win the ‘race for the surface’ against bacteria. It is therefore postulated that a fully porous flange should reduce the susceptibility of ITAP to infection compared with the current drilled-hole flange design. It is planned that a modified ITAP design with a fully porous flange will be translated into clinical practice.

APPENDIX

1 Laboratory Protocols

1.1 Histology Processing Protocol for implants retrieved from *in vivo* experiments

(Centre for Biomedical Engineering, University College London).

Fixation	
10% buffered formal saline	3 days
Serial Dehydration	
50% *IMS 50 % distilled water	3 days
75%IMS 25% distilled water	3 days
85% IMS 15% distilled water	3 days
95% IMS 5% distilled water	3 days
100% IMS (repeated twice)	3 days x 2
Defatting	
Choroform	3 days x 2
Clearing	3 days x 2
100% IMS	
Embedding in Resin	
50% IMS 50% LR White resin	3 days x 2
100% White resin	3 days x 2
(Under vacuum)	
Cast in LR White Resin	24 hours
1 drop of accelerator per 10 mL of resin.	(in fridge)

*IMS = Industrial Methylated Spirits

1.2 SEM preparation of biological samples

(Centre for Biomedical Engineering, University College London).

Wash Phosphate buffered saline	 5 minutes x 2
Fixation 2.5% Glutaraldehyde in 0.1 M sodium cacodylate buffer, pH 7.4	30 minutes
Wash 0.1 M sodium cacodylate buffer	 5 minutes x 2
Serial Dehydration IMS 20% IMS 30% IMS 40% IMS 50% IMS 60% IMS 70% IMS 80% IMS 90% Ethanol 90% Ethanol 96% Ethanol 100%	 5 minutes x 2 5 minutes x 2 5 minutes x 2 5 minutes x 2 5 minutes x 2 5 minutes x 2 5 minutes x 2 5 minutes x 2 5 minutes x 2 10 minutes x 2 15 minutes x 2
Transition Solvent Hexamethyldisalazane	 2 minutes x3
Dry in fume hood	24 hours

1.3 Bacterial identification protocols

(Based on Standard Operating Procedures from the Division of Orthopaedic and Accident Surgery, University of Nottingham).

1.3.1. Gram stain

1. Use a sterile inoculation loop to transfer a drop of bacterial suspension culture to a microscope slide.
2. Spread a culture to form an even film of approximately 1.5 cm in the centre of the slide.
3. Allow to air dry and then heat fix with a gentle flame.
4. Flood the slide with Crystal Violet staining reagent for 1 minute and then gently wash the slide with water.
5. Flood the slide with Gram's iodine stain and wait for 1 minute before washing with water.
6. Flood the slide with the decolourising agent (50:50 acetone:ethanol) and leave for 5 seconds before washing with water.
7. Flood the slide with Neutral Red counterstain.
8. Flood the slide with water and allow to dry.
9. Add a cover slip and mount with DPX mounting medium.
10. View the slide at x100 magnification under oil immersion.

1.3.2 Catalase Test

The catalase test is used to determine if bacteria possess the enzyme catalase. Catalase catalyses the breakdown of hydrogen peroxide to oxygen and water:

$$2H_2O_2 \rightarrow 2H_2O + O_2$$

Bacteria that possess catalase include *Staphylococci* and *Micrococci*. Catalase negative bacteria include *Streptococci* and *Enterococci*.

1. Use a Pasteur pipette to place a drop of hydrogen peroxide solution onto a microscope slide.
2. Use a sterile disposable inoculation loop to smear a colony of the bacteria to be tested onto a cover slip.
3. Lower the cover slip onto the hydrogen peroxide on the slide.
4. The appearance of gas bubbles (i.e. oxygen) indicates the presence of catalase.

Set up controls using *Staphylococcus epidermidis* (catalase positive) and *Enterococcus faecalis* (catalase negative).

1.3.3 Oxidase Test

The oxidase test is used to determine if bacteria possess cytochrome oxidase, an enzyme of the bacterial electron transport chain. Oxidase positive bacteria possess cytochrome oxidase or indophenol oxidase (an iron-containing haemoprotein) and can utilise oxygen for energy production with an electron transport chain. Examples of oxidase positive bacteria include *Pseudomonas aeruginosa* and *Neisseria gonorrhoea*. Examples of oxidase negative bacteria include *Staphylococcus aureus* and *Escherichia coli*.

1. Lay an oxidase test strip (Fluka-40560) in a petri dish that has been pre-moistened with a few drops of sterile distilled water.
2. Transfer a small amount of the bacterial culture to be tested to the strip using a sterile inoculation loop.
3. Gently spread the bacterial culture along the surface of the strip.
4. Observe the strip for 10 to 30 seconds. The appearance of a deep blue colour indicates that the bacteria are oxidase positive. The blue colour occurs as N,N-dimethyl-p-phenylenediamine and α-napthol within the test strips react to form the coloured compound indophenol blue in the presence of cytochrome oxidase.

Set up controls using *Pseudomonas aeruginosa* as a positive control and *Escherichia coli* as a negative control.

1.3.4 DNase test

The DNase test is used to identify *Staphylococci* that produce extracellular DNase (Deoxyribonuclease). DNase hydrolyses DNA in media containing DNA. The oligonucleotides liberated by the hydrolysis are soluble in acid. The addition of hydrochloric acid in the presence of a positive reaction results in a clear zone around the inoculum. Most strains of *Staphylococcus aureus* are DNase positive; however, some strains of MRSA are not. Some strains of coagulase negative *Staphylococci* e.g. *Staphylococcus epidermidis* may result in weak reactions to the test.

1. Inoculate a DNase agar plate with a heavy inoculum of the test bacteria into the centre of the plate. Use a spot of approximately 5 mm in diameter.
2. Incubate the plates at 37°C for 18 to 24 hours.
3. Flood each plate with 0.5 M hydrochloric acid to a depth of approximately 2 mm.
4. Observe the presence of a clear zone around the inoculum for DNase positive bacteria.

Set up controls using *Staphylococcus aureus Oxford* as a positive control and *Staphylococcus epidermidis* (F1228) as a negative control

1.3.5 Methicillin Sensitivity Test

The Methicillin sensitivity test is used to determine whether isolated strains of *Staphylococci* are methicillin sensitive resistant.

1. For each test organism prepare a suspension with an inoculum turbidity equivalent to a McFarland Standard of 0.5.
2. Inoculate Tryptone Soya agar plates with and without methicillin with the test organism.
3. Incubate plates at 37°C for 24 hours.

4. All isolates will grow on agar plates without methicillin. Methicillin resistant isolates will also grow on plates containing methicillin.

Use *MRSA F1228* as a methicillin resistant control and *Staphylococcus aureus Oxford* as a methicillin sensitive control.

1.3.6 Analytical Profile Indexing

The Analytical Profile Index (API) test kits (Biomérieux) are used to identify bacteria to the species level. Different test kits are used depending on the organism to be identified. For example, API Staph is used to identify *Staphylococci* and *Micrococci*. API 20 Strep is used to identify *Streptococci* or *Enterococci*. API 20E is used to identify *Enterobacteriacae* and other non-fastidious gram-negative bacteria. Each test kit contains test strips containing miniaturised biochemical tests within microtubes. The microtubes are inoculated with a suspension of the test organism. The reagents within the microtubes test for the presence of products of bacterial metabolism specific to certain bacterial species.

1. Subculture the test organism onto appropriate agar and incubate for 18 to 24 hours at 37°C.
2. Use API medium to prepare a homogenous bacterial suspension with a turbidity equivalent to 0.5 McFarland standard.
3. Use a sterile pastette to carefully fill each of the microtubes (but not the cupules) within the API test strip with the inoculum. Ensure anaerobiosis in the ADH and URE tests (See reagent list and reading table below) by filling the cupules with mineral oil to form a convex meniscus.
4. Close the inoculation box and incubate for 18 to 24 hours at 37°C.
5. Following the incubation period, follow the instructions in the booklet supplied with the API Biomérieux test kit. Some kits may require the addition of further reagents to develop the reactions.
6. Read the reactions by comparing the colour of each microtube within the test strip to the reading table in the API Biomérieux Instruction booklet. Write the results on the results sheet. The tests are separated into groups of three and a value of 1, 2 or 4 is assigned for each positive test. (An example of an API

Staph test strip with positive reactions, the reagent list/reading table and a results sheet are shown below).

7. Generate a seven-digit numerical profile by adding the values corresponding to positive reaction for each group.
8. Identify the bacterial species by looking up the seven-digit numerical profile in the Analytical Profile Index Manual or by entering the numerical profile into the apiweb^{TM} identification software.

An example API Staph test strip with positive reactions (*Staphylococcus xylosus*)

Reagent list/reading table

TESTS	ACTIVE INGREDIENTS	REACTIONS/ENZYMES	RESULT	
			NEGATIVE	POSITIVE
0	No substrate	Negative control	red	-
GLU	D-glucose	(Positive control) (D-GLUcose)	red	yellow
FRU	D-fructose	Acidification (D-FRUctose)		
MNE	D-mannose	Acidification (D-manNosE)		
MAL	D-maltose	Acidification (MALtose)		
LAC	D-lactose	Acidification (LACtose)		
TRE	D-trehalose	Acidification (D-TREhalose)		
MAN	D-mannitol	Acidification (D-MANnitol)		
XLT	xylitol	Acidification (XyLiTol)		
MEL	D-melibiose	Acidification (D-MELibiose)		
NIT	potassium nitrate	Reduction of NITrates to nitrites	NIT 1 + NIT 2 / 10 min	
			Colourless -light pink	red
PAL	β-naphthyl phosphate	Alkaline Phosphatase	ZYM A + ZYM B / 10 min	
			yellow	violet
VP	sodium pyruvate	Acetyl-methyl-carbinol production (Voges Proskauer)		
RAF	D-raffinose	Acidification (RAFfinose)	red	yellow
XYL	D-xylose	Acidification (XYLose)		
SAC	D-saccharose (sucrose)	Acidification (SACcharose)		
MDG	methyl-αD-glucopyranoside	Acidification (Methyl-αD-Glucopyranoside)		
NAG	N-acetyl-glucosamine	Acidification (N-Acetyl-Glucosamine)		
ADH	L-arginine	Arginine DiHydrolase	yellow	orange-red
URE	urea	UREase	yellow	red-violet

Results sheet

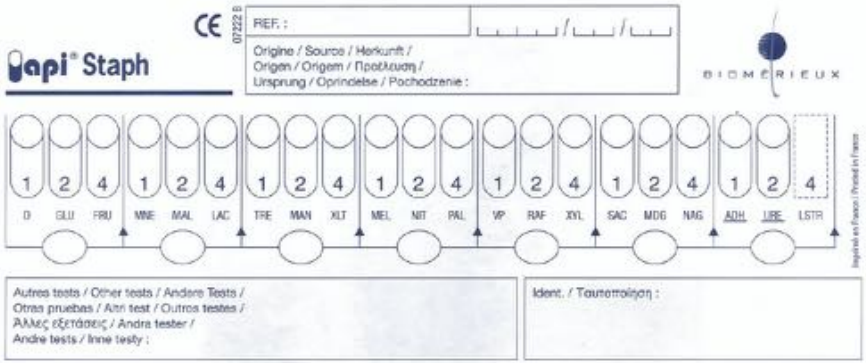

2. Chapter Two Statistics

2.1 Median Values and (95% confidence intervals)

Implant	Percentage soft tissue fill			Cell nuclei/mm^2			Blood vessel/mm^2		
	Zone 1	Zone 2	Zone 3	Zone 1	Zone 2	Zone 3	Zone 1	Zone 2	Zone 3
P1000 S400	100 (constant)	97 (94.28 to 100.52)	100 (84.89 to 107.11)	3074 (831.95 to 4662.05)	3733 (859.91 to 5017.69)	3618 (1130.85 to 5372.75)	4 (1.52 to 9.44)	3 (0.12 to 10.4)	3 (-2.32 to 12.96)
P1000 S200	100 (97.54 to 101.03)	100 (94.22 to 101.50)	100 (87.94 to 102.06)	5059 (3330.45 to 6312.70)	4527 (2402.37 to 5439.06)	5000 (3004.61 to 6293.96)	8 (4.28 to 10.29)	10 (4.52 to 12.05)	8 (2.83 to 11.74)
P700 S400	40 (11.84 to 78.66)	35 (18.61 to 53.89)	25 (7.27 to 37.73)	1190 (-409.57 to 2953.57)	700 (-392.4 to 2157.9)	584.5 (131.82 to 970.68)	4.5 (-1.03 to 9.03)	1 (-2.5 to 6.5)	2.5 (-1.29 to 6.29)
P700 S300	100 (92.45 to 103.55)	95 (30.19 to 125.81)	100 (92.43 to 103.55)	1389 (-390.62 to 7151.82)	1243 (172.19 to 3993.41)	1306 (266.55 to 4168.65)	15 (3.67 to 34.33)	6 (0.92 to 16.28)	11 (2.92 to 15.08)
P700 S200	88 (62.09 to 103.57)	87.5 (59.3 to 103.36)	90 (45.07 to 108.27)	815 (363.3 to 1315.36)	604 (420.53 to 749.47)	551.5 (-99.65 to 1662.32)	3 (0.48 to 8.52)	1.5 (-0.2 to 3.87)	0 (constant)
P500 S400	27.5 (-10.14 to 62.64)	22.5 (-8.31 to 53.31)	10 (-20.1 to 55.1)	250 (-317.35 to 985.35)	268.5 (-249.11 to 835.11)	251 (-316.48 to 984.48)	0 (-1.09 to 2.09)	0 (-0.55 to 1.05)	0 (-2.18 to 4.18)
P500 S300	60 (48.43 to 74.43)	45 (33.44 to 57.41)	40 (21.09 to 57.48)	1390 (110.59 to 5540.55)	1199 (478.45 to 1641.83)	821 (71.18 to 2351.40)	9 (3.25 to 17.89)	4 (0.33 to 5.39)	0 (-1.24 to 2.95)
P500 S200	60 (41.43 to 75.14)	63 (34.17 to 68.4)	60 (25.64 to 72.93)	890 (-187.08 to 3091.36)	645 (53.6 to 1850.68)	720 (122.22 to 2097.78)	8 (2.75 to 12.96)	4 (1.44 to 7.99)	4 (-0.42 to 11.56)

2.2 Chapter Two p values

Zone 1 - Percentage Fill

Kruskall Wallis p value=0.000

	P1000 S400	P1000 S200	P700 S400	P700 S300	P700 S200	P500 S400	P500 S300	P500 S200
P1000 S400		0.731	0.010			0.010		
P1000 S200					0.101			0.001
P700 S400				0.016	0.038	0.343		0.412
P700 S300					0.177		0.003	
P700 S200								0.035
P500 S400							0.024	0.073
P500 S300								0.710
P500 S200								

Zone 2 - Percentage Fill

Kruskall Wallis p value=0.000

	P1000 S400	P1000 S200	P700 S400	P700 S300	P700 S200	P500 S400	P500 S300	P500 S200
P1000 S400		0.731	0.010			0.010		
P1000 S200					0.138			0.001
P700 S400				0.190	0.010	0.343		
P700 S300					0.792		0.106	
P700 S200								0.051
P500 S400							0.073	0.073
P500 S300								0.383
P500 S200								

Zone 3 - Percentage Fill

Kruskall Wallis Test = 0.000

	P1000 S400	P1000 S200	P700 S400	P700 S300	P700 S200	P500 S400	P500 S300	P500 S200
P1000 S400		0.534	0.010			0.010		
P1000 S200					0.445			0.001
P700 S400				0.016	0.019	0.486		0.109
P700 S300					0.329		0.003	
P700 S200								0.101
P500 S400							0.164	0.073
P500 S300								0.535
P500 S200								

Zone 1 - Cell nuclei count/mm^2

Kruskall Wallis test p=0.002

	P1000 S400	P1000 S200	P700 S400	P700 S300	P700 S200	P500 S400	P500 S300	P500 S200
P1000 S400		0.051	0.114			0.019		
P1000 S200					0.001			0.007
P700 S400				0.413	0.762	0.343		
P700 S300					0.052		0.639	
P700 S200								0.836
P500 S400							0.024	0.073
P500 S300								0.259
P500 S200								

Zone 2 - Cell nuclei count/mm^2

Kruskall Wallis test p=0.001

	P1000 S400	P1000 S200	P700 S400	P700 S300	P700 S200	P500 S400	P500 S300	P500 S200
P1000 S400		0.138	0.114			0.038		
P1000 S200					0.001			0.002
P700 S400				0.286	1.000	0.343		
P700 S300					0.004		0.343	
P700 S200								1.000
P500 S400							0.042	0.164
P500 S300								0.535
P500 S200								

Zone 3 - Cell nuclei count/mm^2

Kruskall Wallis test p=0.000

	P1000 S400	P1000 S200	P700 S400	P700 S300	P700 S200	P500 S400	P500 S300	P500 S200
P1000 S400		0.073	0.067			0.038		
P1000 S200					0.002			0.001
P700 S400				0.016	0.914	0.686		
P700 S300					0.030		0.149	
P700 S200								0.101
P500 S400							0.109	0.109
P500 S300								0.902
P500 S200								

Zone 1 - Blood vessel count/mm^2

Kruskall Wallis Test = 0.010

	P1000 S400	P1000 S200	P700 S400	P700 S300	P700 S200	P500 S400	P500 S300	P500 S200
P1000 S400		0.343	0.556			0.016		
P1000 S200					0.234			0.902
P700 S400				0.016	0.914	0.114		
P700 S300					0.017		0.268	
P700 S200								0.234
P500 S400							0.024	0.024
P500 S300								0.535
P500 S200								

Zone 2 - Blood vessel count/mm^2

Kruskall Wallis test p=0.005

	P1000 S400	P1000 S200	P700 S400	P700 S300	P700 S200	P500 S400	P500 S300	P500 S200
P1000 S400		0.534	0.114			0.010		
P1000 S200					0.008			0.165
P700 S400				0.063	0.914	0.486		
P700 S300					0.009		0.048	
P700 S200								0.138
P500 S400							0.230	0.024
P500 S300								0.456
P500 S200								

Zone 3 - Blood vessel count/mm^2

Kruskall Wallis p=0.003

	P1000 S400	P1000 S200	P700 S400	P700 S300	P700 S200	P500 S400	P500 S300	P500 S200
P1000 S400		0.234	0.914			0.352		
P1000 S200					0.001			0.456
P700 S400				0.063	0.067	0.343		
P700 S300					0.004		0.005	
P700 S200								0.101
P500 S400							0.927	0.315
P500 S300								0.165
P500 S200								

2.3 Chapter Two Correlation

Spearman's rho			Percentage soft tissue fill			Cell nuclei/mm^2			Blood vessel/mm^2		
			Zone 1	Zone 2	Zone 3	Zone 1	Zone 2	Zone 3	Zone 1	Zone 2	Zone 3
Percentage soft tissue fill	Zone 1	Correlation Coefficient		0.877	0.941	0.620			0.323		
		Sig (2-tailed)		0.000	0.000	0.000			0.031		
	Zone 2	Correlation Coefficient			0.868		0.610			0.493	
		Sig (2-tailed)			0.000		0.000			0.001	
	Zone 3	Correlation Coefficient						0.621			0.432
		Sig (2-tailed)						0.000			0.003
Cell nuclei /mm^2	Zone 1	Correlation Coefficient					0.799	0.880	0.316		
		Sig (2-tailed)					0.000	0.000	0.035		
	Zone 2	Correlation Coefficient						0.765		0.635	
		Sig (2-tailed)						0.000		0.000	
	Zone 3	Correlation Coefficient									0.503
		Sig (2-tailed)									0.000
Blood vessel /mm^2	Zone 1	Correlation Coefficient								0.760	0.333
		Sig (2-tailed)								0.000	0.025
	Zone 2	Correlation Coefficient									0.629
		Sig (2-tailed)									0.000
	Zone 3	Correlation Coefficient									
		Sig (2-tailed)									

2.4 Intraclass Correlation Coefficient for Semi-quantitative Percentage Soft Tissue Fill Score

	Median value (and 95% Confidence Interval)	
	Observer 1	Observer 2
P1000 S400	100.00 (90.86 to 98.58)	100.00(96.06 to 100.83)
P1000 S200	90.00 (84.03 to 94.30)	100.00 (94.23 to 99.66)
P700 S400	75.00 (59.19 to 82.47)	30.00 (24.14 to 45.19)
P700 S300	100.00 (92.06 to 99.94)	100.00 (94.59 to 100.08)
P700 S200	85.00 (76.18 to 92.71)	87.50 (68.95 to 91.60)
P500 S400	35.00 (16.91 to 48.09)	35.00 (15.50 to 47.00)
P500 S300	50.00 (38.34 to 55.95)	50.00 (36.55 to 56.12)
P500 S200	60.00 (45.45 to 62.17)	60.00 (43.69 to 62.22)

Reliability Statistics

Cronbach's Alpha	N of Items
.932	2

Intraclass Correlation Coefficient

	Intraclass Correlation[b]	95% Confidence Interval		F Test with True Value 0			
		Lower Bound	Upper Bound	Value	df1	df2	Sig
Single Measures	.870[a]	.822	.906	14.673	134	134	.000
Average Measures	.931[c]	.902	.951	14.673	134	134	.000

Two-way mixed effects model where people effects are random and measures effects are fixed.

a. The estimator is the same, whether the interaction effect is present or not.

b. Type A intraclass correlation coefficients using an absolute agreement definition.

c. This estimate is computed assuming the interaction effect is absent, because it is not estimable otherwise.

3 Chapter Three Statistics

3.1 EDX Analysis

3.1.1 Percentage Silver Content - p values

(Pol, HA, HAFn = 0% Ag, therefore excluded from comparisons)

Kruskall Wallis
Atomic Percentage Silver p=0.000
Percentage Weight Silver p=0.000

	HA Ag 10	HA Ag Fn 10	HA Ag 50	HA Ag Fn 50	HA Ag 100	HA Ag Fn 100	HA Ag 10 (P24)	HA Ag Fn 10 (P24)	HA Ag 50 (P24)	HA Ag Fn 50 (P24)	HA Ag 100 (P24)	HA Ag Fn 100 (P24)
HAAg 10		0.037 0.034	0.000 0.000				0.293 0.203					
HAAg Fn10				0.001 0.001				0.732 0.134				
HAAg 50				0.786 0.483	0.000 0.000				0.660 0.143			
HAAg Fn50						0.000 0.000				0.832 0.988		
HAAg 100						0.851 0.372					0.111 0.424	
HAAg Fn100												0.551 0.521
HAAg 10 (P24)								0.029 0.153	0.000 0.034			
HAAg Fn10 (P24)										0.000 0.004		
HAAg 50 (P24)										0.815 0.988	0.001 0.000	
HAAg Fn50 (P24)												0.001 0.000
HAAg 100 (P24)												0.462 0.424
HAAg Fn100 (P24)												

3.1.2 Percentage Silver Content - Benjamini Hochberg Procedure

Threshold = (i/m)Q i = rank, m = total number of tests, Q = false discovery rate

Atomic Percentage Silver
Percentage Weight Silver

Rank	p value	Threshold (i/m)Q	Reject Null Hypothesis (Y/N)
1	0.000 0.000	0.0025	Y Y
2	0.000 0.000	0.005	Y Y
3	0.000 0.000	0.0075	Y Y
4	0.000 0.000	0.01	Y Y
5	0.000 0.000	0.0125	Y Y
6	0.000 0.001	0.015	Y Y
7	0.001 0.004	0.0175	Y Y
8	0.001 0.034	0.02	Y N
9	0.001 0.034	0.0225	Y N
10	0.029 0.134	0.025	N N
11	0.037 0.143	0.0275	N N
12	0.111 0.153	0.03	N N
13	0.293 0.203	0.0325	N N
14	0.462 0.372	0.035	N N
15	0.551 0.424	0.0375	N N
16	0.660 0.424	0.04	N N
17	0.732 0.483	0.0425	N N
18	0.786 0.521	0.045	N N
19	0.815 0.988	0.0475	N N
20	0.988 0.988	0.05	N N

3.2 Surface Roughness (R_a)

3.2.1 Surface Roughness (R_a) - p values

Kruskall Wallis p= 0.000

	Pol	HA	HA Fn	HA Ag 10	HA Ag Fn 10	HA Ag 50	HA Ag Fn 50	HA Ag 100	HA Ag Fn 100	Pol (P24)	HA (P24)	HA Fn (P24)	HA Ag 10 (P24)	HA Ag Fn 10 (P24)	HA Ag 50 (P24)	HA Ag Fn 50 (P24)	HA Ag 100 (P24)	HA Ag Fn 100 (P24)
Pol		0.000								0.742								
HA			0.389	0.203		0.791		0.000			0.297							
HAFn					0.988		0.815		0.001			0.000						
HAAg10					0.068	0.104		0.000					0.935					
HAAgFn10							0.673		0.001					0.000				
HAAg50							0.963	0.000							0.002			
HAAgFn50									0.002							0.212		
HAAg100									0.005								0.035	
HAAgFn100																		0.019
Pol (P24)											0.000							
HA (P24)												0.007	0.464		0.042		0.002	
HAFn (P24)														0.259		0.536		0.000
HAAg10 (P24)														0.006	0.114		0.002	
HAAgFn10 (P24)																0.252		0.000
HAAg50 (P24)																0.730	0.000	
HAAgFn50 (P24)																		0.011
HAAg100 (P24)																		0.606
HAAgFn100 (P24)																		

3.2.2 Surface Roughness (R_a) - Benjamini Hochberg Procedure

Rank	p value	Threshold (i/m)Q	Reject Null Hypothesis (Y/N)
1	0.000	0.00116279	Y
2	0.000	0.00232558	Y
3	0.000	0.00348837	Y
4	0.000	0.00465116	Y
5	0.000	0.00581395	Y
6	0.000	0.00697674	Y
7	0.000	0.00813953	Y
8	0.000	0.00930233	Y
9	0.000	0.01046512	Y
10	0.000	0.01162791	Y
11	0.001	0.0127907	Y
12	0.001	0.01395349	Y
13	0.002	0.01511628	Y
14	0.002	0.01627907	Y
15	0.002	0.01744186	Y
16	0.002	0.01860465	Y
17	0.005	0.01976744	Y
18	0.006	0.02093023	Y
19	0.007	0.02209302	Y
20	0.011	0.02325581	Y
21	0.019	0.0244186	Y
22	0.035	0.0255814	N
23	0.042	0.02674419	N
24	0.068	0.02790698	N
25	0.104	0.02906977	N
26	0.114	0.03023256	N
27	0.212	0.03139535	N
28	0.203	0.03255814	N
29	0.252	0.03372093	N
30	0.259	0.03488372	N
31	0.297	0.03604651	N
32	0.389	0.0372093	N
33	0.464	0.0387209	N
34	0.536	0.03953488	N
35	0.606	0.04069767	N
36	0.673	0.04186047	N
37	0.730	0.04302326	N
38	0.742	0.04418605	N
39	0.791	0.04534884	N
40	0.815	0.04651163	N
41	0.935	0.04767442	N
42	0.963	0.04883721	N
43	0.988	0.05	N

3.3 Fibroblast Viability

3.3.1 Percentage Live Cells - Median Values and (95% Confidence Intervals)

Surface	Median values and (95% confidence intervals)
Pol	94.5 (90.91 to 97.2)
HA	92.58 (89.98 to 94.96)
HAFn	95 (92.07 to 97.93)
HAAg10	55 (38.3 to 60.15)
HAAgFn10	59 (34.71 to 69.49)
HAAg50	16 (11.06 to 31.18)
HAAgFn50	15 (10.25 to 23.53)
HAAg100	0 (-0.50 to 5.72)
HAAgFn100	0 (3.83 to 16.17)
HAAg10 (P4)	83 (76.71 to 85.18)
HAAgFn10 (P4)	65.5 (62.09 to 70.47)
HAAg50 (P4)	68 (65.66 to 71.11)
HAAgFn50 (P4)	50 (42.30 to 56.4)
HAAg10 (P8)	87 (82.59 to 88.82)
HAAgFn10 (P8)	86 (79.24 to 87.20)
HAAg50 (P8)	82 (74.96 to 82.34)
HAAgFn50 (P8)	81 (74.27 to 86.08)

Surface	Median values and (95% confidence intervals)
Pol (P24)	100 (95 to 99.67)
HA (P24)	94.5 (90.58 to 96.86)
HAFn (P24)	92.5 (86.74 to 95.37)
HAAg10 (P24)	89 (85.93 to 93.07)
HAAgFn10 (P24)	91 (88.44 to 94.56)
HAAg50 (P24)	87.50 (83.86 to 93.47)
HAAgFn50 (P24)	92.50 (87.74 to 95.04)
HAAg100 (P24)	95 (90.47 to 96.86)
HAAgFn100 (P24)	90.5 (86.39 to 94.28)
HAAg100 (P48)	98.5 (92.63 to 98.48)
HAAgFn100 (P48)	94.5 (89.86 to 97.48)

3.3.2 Percentage Live Cells - p values

Kruskall Wallis p=0.000

	Pol	HA	HA Fn	HA Ag 10	HA Ag Fn10	HA Ag 50	HA Ag Fn50	HA Ag 100	HA Ag Fn100
Pol		0.335	0.597						
HA			0.081	0.000					
HAFn					0.000				
HAAg10					0.724	0.000			
HAAgFn10							0.000		
HAAg50							0.684	0.002	
HAAgFn50									0.111
HAAg100									0.134
HAAgFn100									

	HAAg 10 (P4)	HAAg Fn10 (P4)	HAAg 50 (P4)	HAAg Fn50 (P4)	HAAg 10 (P8)	HAAg Fn10 (P8)	HAAg 50 (P8)	HAAg Fn50 (P8)
Pol								
HA	0.000				0.001			
HAFn		0.000				0.000		
HAAg10	0.000				0.000			
HAAgFn10		0.133				0.000		
HAAg50			0.000					
HAAgFn50				0.000				0.000
HAAg100								
HAAgFn100								
HAAg10 (P4)		0.000	0.000		0.057			
HAAgFn10 (P4)				0.000		0.000		0.443
HAAg50 (P4)				0.000			0.000	
HAAgFn50 (P4)								0.000
HAAg10 (P8)						0.546	0.003	
HAAgFn10 (P8)								0.540
HAAg50 (P8)								
HAAgFn50 (P8)								

	Pol (P24)	HA (P24)	HAFn (P24)	HAAg 10 (P24)	HAAg Fn10 (P24)	HAAg 50 (P24)	HAAg Fn50 (P24)	HAAg 100 (P24)	HAAg Fn100 (P24)	HAAg 100 (P48)	HAAg Fn100 (P48)
Pol	0.185										
HA		0.424		0.219		0.219		0.424		0.067	
HAFn			0.144		0.059		0.109		0.059		0.772
HAAg10				0.000							
HAAgFn10					0.000						
HAAg50						0.000					
HAAgFn50							0.000				
HAAg100								0.000			
HAAgFn100											
HAAg10 (P4)											
HAAgFn10 (P4)											
HAAg50 (P4)											
HAAgFn50 (P4)											
HAAg10 (P8)				0.184							
HAAgFn10 (P8)					0.002						
HAAg50 (P8)						0.006					
HAAgFn50 (P8)							0.002				
Pol (P24)											
HA (P24)				0.079		0.118		0.963			
HAFn (P24)					0.719		0.988		0.628		
HAAg10 (P24)					0.406	0.791		0.091			
HAAgFn10 (P24)							0.913		0.791		
HAAg50 (P24)							0.501	0.161			
HAAgFn50 (P24)									0.673		
HAAg100 (P24)									0.203	0.323	
HAAgFn100 (P24)											0.152
HAAg100 (P48)											
HAAgFn100 (P48)											

3.3.3 Percentage Live Cells - Benjamini Hochberg Procedure

Rank	p value	Threshold (i/m)Q	Reject Null Hypothesis (Y/N)
1	0.000	0.00069444444444	Y
2	0.000	0.00138888888889	Y
3	0.000	0.00208333333333	Y
4	0.000	0.00277777777778	Y
5	0.000	0.00347222222222	Y
6	0.000	0.00416666666667	Y
7	0.000	0.00486111111111	Y
8	0.000	0.00555555555556	Y
9	0.000	0.00625	Y
10	0.000	0.00694444444444	Y
11	0.000	0.00763888888889	Y
12	0.000	0.00833333333333	Y
13	0.000	0.00902777777778	Y
14	0.000	0.00972222222222	Y
15	0.000	0.01041666666667	Y
16	0.000	0.01111111111111	Y
17	0.000	0.01180555555556	Y
18	0.000	0.0125	Y
19	0.000	0.01319444444444	Y
20	0.000	0.01388888888889	Y
21	0.000	0.01458333333333	Y
22	0.000	0.01527777777778	Y
23	0.000	0.01597222222222	Y
24	0.000	0.01666666666667	Y
25	0.000	0.01736111111111	Y
26	0.001	0.01805555555556	Y
27	0.002	0.01875	Y
28	0.002	0.01944444444444	Y
29	0.002	0.02013888888889	Y
30	0.003	0.02083333333333	Y
31	0.006	0.02152777777778	Y
32	0.057	0.02222222222222	Y
33	0.059	0.02291666666667	N
34	0.059	0.02361111111111	N
35	0.067	0.02430555555556	N
36	0.079	0.025	N
37	0.081	0.02569444444444	N
38	0.091	0.02638888888889	N
39	0.109	0.02708333333333	N
40	0.111	0.02777777777778	N
41	0.118	0.02847222222222	N
42	0.133	0.02916666666667	N
43	0.134	0.02986111111111	N
44	0.144	0.03055555555556	N

45	0.152	0.03125	N
46	0.161	0.03194444444444	N
47	0.184	0.03263888888889	N
48	0.185	0.03333333333333	N
49	0.203	0.03402777777778	N
50	0.219	0.03472222222222	N
51	0.219	0.03541666666667	N
52	0.323	0.03611111111111	N
53	0.335	0.03680555555556	N
54	0.406	0.0375	N
55	0.424	0.03819444444444	N
56	0.424	0.03888888888889	N
57	0.443	0.03958333333333	N
58	0.501	0.04027777777778	N
59	0.54	0.04097222222222	N
60	0.546	0.04166666666667	N
61	0.597	0.04236111111111	N
62	0.628	0.04305555555556	N
63	0.673	0.04375	N
64	0.684	0.04444444444444	N
65	0.719	0.04513888888889	N
66	0.724	0.04583333333333	N
67	0.772	0.04652777777778	N
68	0.791	0.04722222222222	N
69	0.791	0.04791666666667	N
70	0.913	0.04861111111111	N
71	0.963	0.04930555555556	N
72	0.988	0.05	N

3.4 Fibroblast Metabolism

3.4.1 Alamar Blue Absorbance - Median Values and (95% Confidence Intervals)

Surface	Median values and (95% confidence intervals)
Pol	24.8 (24.067 to 29.117)
HA	26.15 (25.22 to 33.297)
HAFn	31.35 (28.429 to 33.204)
HAAg10	19.65 (19.496 to 19.921)
HAAgFn10	19.5 (19.114 to 22.269)
HAAg50	19.350 (19.032 to 19.634)
HAAgFn50	20.05 (19.716 to 20.234)
HAAg100	18.2 (18.011 to 18.506)
HAAgFn100	18.2 (17.958 to 18.542)
HAAg10 (P4)	20.55 (20.46 to 20.874
HAAgFn10 (P4)	20.75 (20.519 to 22.931)
HAAg50 (P4)	19.8 (19.151 to 21.43)
HAAgFn50 (P4)	20.9 (20.732 to 21.468)
HAAg10 (P8)	22.1 (21.478 to 24.072)
HAAgFn10 (P8)	23.45 (22.251 to 24.999)
HAAg50 (P8)	23.2 (21.241 to 23.492)
HAAgFn50 (P8)	22.2 (21.86 to 23.857)

Surface	Median values and (95% confidence intervals)
HAAg10 (P24)	25.85 (23.792 to 26.191)
HAAgFn10 (P24)	26.35 (25.218 to 27.166)
HAAg50 (P24)	23.85 (22.451 to 26.749)
HAAgFn50 (P24)	25.6 (24.2 to 30.217)
HAAg100 (P24)	24.9 (24.505 to 27.004)
HAAgFn100 (P24)	25.55 (25.256 to 25.909)
HAAg100 (P48)	25.6 (25.397 to 27.403)
HAAgFn100 (P48)	25.05 (24.674 to 26.386)

3.4.2 Alamar Blue Absorbance - p values

Kruskall Wallis p= 0.000

	Pol	HA	HAFn	HAAg 10	HAAg Fn10	HAAg 50	HAAg Fn50	HAAg 100	HAAg Fn100	HAAg 10 (P4)	HAAg Fn10 (P4)	HAAg 50 (P4)	HAAg Fn50 (P4)
Pol		0.219	0.008										
HA			0.143	0.000		0.000				0.000			
HAFn					0.000		0.000				0.000		
HAAg10					0.799	0.060		0.000		0.000			
HAAgFn10							0.219		0.000		0.012		
HAAg50							0.003	0.000				0.043	
HAAgFn50									0.000				0.000
HAAg100									0.977				
HAAgFn100													
HAAg10 (P4)											0.671	0.000	
HAAgFn10 (P4)													0.799
HAAg50 (P4)													0.000
HAAgFn50 (P4)													

	HAAg 10 (P8)	HAAg Fn10 (P8)	HAAg 50 (P8)	HAAg Fn50 (P8)	HAAg 10 (P24)	HAAg Fn10 (P24)	HAAg 50 (P24)	HAAg Fn50 (P24)	HAAg 100 (P24)	HAAg Fn100 (P24)	HAAg 100 (P48)	HAAg Fn100 (P48)
Pol												
HA	0.001		0.000		0.198		0.045		0.291		0.977	
HAFn		0.000		0.000		0.002		0.068		0.001		0.000
HAAg10												
HAAgFn10												
HAAg50												
HAAgFn50												
HAAg100												
HAAgFn100												
HAAg10 (P4)	0.000											
HAAgFn10 (P4)		0.033										
HAAg50 (P4)			0.003									
HAAgFn50 (P4)				0.001								
HAAg10 (P8)		0.242	0.887		0.012							
HAAgFn10 (P8)				0.266		0.003						
HAAg50 (P8)							0.143					
HAAgFn50 (P8)								0.002				
HAAg10 (P24)						0.178	0.410					
HAAgFn10 (P24)												
HAAg50 (P24)									0.291			
HAAgFn50 (P24)												
HAAg100 (P24)											0.160	
HAAgFn100 (P24)												0.069
HAAg100 (P48)												
HAAgFn100 (P48)												

Kruskall Wallis Pol, HA (not HAFn) and HAAg+/-Fn groups after P24 and P48 p=0.548

3.4.3 Alamar Blue Absorbance - Benjamini Hochberg Procedure

Rank	p value	Threshold (i/m)Q	Reject Null Hypothesis (Y/N)
1	0.000	0.000909091	Y
2	0.000	0.001818182	Y
3	0.000	0.002727273	Y
4	0.000	0.003636364	Y
5	0.000	0.004545455	Y
6	0.000	0.005454545	Y
7	0.000	0.006363636	Y
8	0.000	0.007272727	Y
9	0.000	0.008181818	Y
10	0.000	0.009090909	Y
11	0.000	0.01	Y
12	0.000	0.010909091	Y
13	0.000	0.011818182	Y
14	0.000	0.012727273	Y
15	0.000	0.013636364	Y
16	0.000	0.014545455	Y
17	0.000	0.015454545	Y
18	0.000	0.016363636	Y
19	0.000	0.017272727	Y
20	0.000	0.018181818	Y
21	0.001	0.019090909	Y
22	0.001	0.02	Y
23	0.001	0.020909091	Y
24	0.002	0.021818182	Y
25	0.002	0.022727273	Y
26	0.003	0.023636364	Y
27	0.003	0.024545455	Y
28	0.003	0.025454545	Y
29	0.008	0.026363636	Y
30	0.012	0.027272727	Y
31	0.012	0.028181818	Y
32	0.033	0.029090909	N
33	0.043	0.03	N
34	0.045	0.030909091	N
35	0.060	0.031818182	N
36	0.068	0.032727273	N
37	0.069	0.033636364	N
38	0.143	0.034545455	N
39	0.143	0.035454545	N
40	0.16	0.036363636	N
41	0.178	0.037272727	N
42	0.198	0.038181818	N
43	0.219	0.039090909	N
44	0.219	0.04	N

45	0.242	0.040909091	N
46	0.266	0.041818182	N
47	0.291	0.042727273	N
48	0.291	0.043636364	N
49	0.410	0.044545455	N
50	0.671	0.045454545	N
51	0.799	0.046363636	N
52	0.799	0.047272727	N
53	0.887	0.048181818	N
54	0.977	0.049090909	N
55	0.977	0.05	N

4 Chapter Four Statistics

4.1 *S aureus* Direct Colony Counts

4.1.1 *S aureus*: Biofilm Direct Colony Counts

Median Values and (95% Confidence Intervals)

Surface	**Median values and (95% confidence intervals)**	
Pol	1500000	(925200.4274 to 2074799.5726)
HA	5000000	(1926808.1444 to 10406525.1889)
HAFn	15000000	(12969166.7744 to 19030833.2256)
HAAg10	410000	(353082.7610 to 496917.2390)
HAAgFn10	170000	(63412.2180 to 341587.7820)
HAAg50	215000	(149145.7784 to 323354.2216)
HAAgFn50	38000	(-143149.3237 to 586482.6570)
HAAg100	0	(constant)
HAAgFn100	0	(constant)
Pol (P24)	6500	(-2102.30 to 35435.63)
HA (P24)	2000000	(884450 to 6493327.78)
HAFn (P24)	2000000	(1453869.04 to 7257242.07)
HAAg10 (P24)	1000000	(688676.84 to 1711323.16)
HAAgFn10 (P24)	2000000	(910760.50 to 2533683.95)
HAAg50 (P24)	1000000	(795782.48 to 1718762.98)
HAAgFn50 (P24)	390000	(70593.01 to 1709406.99)
HAAg100 (P24)	3000	(1580.54 to 4619.46)
HAAgFn100 (P24)	17000	(11454.59 to 21878.75)

4.1.2 *S aureus*: Biofilm Direct Colony Counts - p values

Kruskall Wallis p= 0.000

	Pol	HA	HAFn	HAAg 10	HAAg Fn10	HAAg 50	HAAg Fn50	HAAg 100	HAAg Fn100	Pol P24	HA P24	HAFn P24	HAAg 10 P24	HAAg Fn10 P24	HAAg 50 P24	HAAg Fn50 P24	HAAg 100 P24	HAAg Fn100 P24
Pol		0.008		(0.000)						0.001								
HA			0.001	0.001							0.088							
HAFn					0.000							0.000						
HAAg10					0.010	0.002							0.002					
HAAgFn10							0.228		0.000					0.000				
HAAg50							0.272	0.000							0.001			
HAAgFn50									0.000							0.020		
HAAg100									1.000								0.000	
HAAgFn100																		0.000
Pol P24											0.000		0.000		0.000		0.005	0.394
HA P24												0.796	0.040		0.020			
HAFn P24														0.481		0.021		
HAAg10 P24														0.059	0.824			
HAAgFn10 P24																0.065		
HAAg50 P24																0.206	0.000	
HAAgFn50 P24																		0.001
HAAg100 P24																		0.000
HAAgFn100 P24																		

4.1.3 *S aureus*: Biofilm Direct Colony Counts - Benjamini Hochberg procedure

Rank	p value	Threshold (i/m)Q	Reject Null Hypothesis (Y/N)
1	0.000	0.001282051	Y
2	0.000	0.002564103	Y
3	0.000	0.003846154	Y
4	0.000	0.005128205	Y
5	0.000	0.006410256	Y
6	0.000	0.007692308	Y
7	0.000	0.008974359	Y
8	0.000	0.01025641	Y
9	0.000	0.011538462	Y
10	0.000	0.012820513	Y
11	0.000	0.014102564	Y
12	0.000	0.015384615	Y
13	0.000	0.016666667	Y
14	0.000	0.017948718	Y
15	0.001	0.019230769	Y
16	0.001	0.020512821	Y
17	0.001	0.021794872	Y
18	0.001	0.023076923	Y
19	0.001	0.024358974	Y
20	0.002	0.025641026	Y
21	0.002	0.026923077	Y
22	0.004	0.028205128	Y
23	0.008	0.029487179	Y
24	0.010	0.030769231	Y
25	0.020	0.032051282	Y
26	0.020	0.033333333	Y
27	0.021	0.034615385	Y
28	0.040	0.035897436	N
29	0.059	0.037179487	N
30	0.065	0.038461538	N
31	0.088	0.03974359	N
32	0.206	0.041025641	N
33	0.228	0.042307692	N
34	0.272	0.043589744	N
35	0.394	0.044871795	N
36	0.481	0.046153846	N
37	0.796	0.047435897	N
38	0.824	0.048717949	N
39	1.000	0.05	N

4.1.4 *S aureus*: Planktonic Direct Colony Counts - Median Values and (95% Confidence Intervals)

Surface	Median values and (95% confidence intervals)
Pol	260000 (123410.86 to 315255.81)
HA	3600000 (1687072.81 to 5979593.85)
HAFn	5000000 (3028182.06 to 7071817.94)
HAAg10	2550000 (1937358.96 to 3012641.04)
HAAgFn10	2200000 (1839358.97 to 3010641.03)
HAAg50	800000 (351153.67 to 1373846.33)
HAAgFn50	405000 (73492.98 to 1499840.36)
HAAg100	5000 (1275.73 to 29168.72)
HAAgFn100	25000 (14114.36 to 64330.08)
Pol (P24)	535000 (150225.74 to 989774.26)
HA (P24)	25000000 (17179959.51 to 32820040.49)
HAFn (P24)	20000000 (16980179.84 to 27686486.83)
HAAg10 (P24)	4800000 (3065903.63 to 7756318.59)
HAAgFn10 (P24)	2000000 (1502844.68 to 2652710.87)
HAAg50 (P24)	150000 (81829.76 to 193988.42)
HAAgFn50 (P24)	1300000 (1123431.05 to 2009902.28)
HAAg100 (P24)	70000 (24001.52 to 97331.81)
HAAgFn100 (P24)	65000 (49711.32 to 96955.35)

4.1.5 *S aureus*: Planktonic Direct Colony Counts - p values

Kruskall Wallis p= 0.000

	Pol	HA	HAFn	HAAg 10	HAAg Fn10	HAAg 50	HAAg Fn50	HAAg 100	HAAg Fn100	Pol P24	HA P24	HAFn P24	HAAg 10 P24	HAAg Fn10 P24	HAAg 50 P24	HAAg Fn50 P24	HAAg 100 P24	HAAg Fn100 P24
Pol		0.000		*(0.000)		*(0.008)		(0.002)	(0.002)	0.029								
HA			0.063	0.730		0.001					0.000							
HAFn					0.008							0.000						
HAAg10					0.863	0.001							0.000					
HAAgFn10							0.000							0.340				
HAAg50							0.743	0.001							0.000			
HAAgFn50									0.000							0.031		
HAAg100									0.529	0.000							0.181	
HAAgFn100																		0.031
Pol P24											0.000		*(0.000)		(0.000)		(0.000)	(0.000)
HA P24												0.489	0.000					
HAFn P24														0.000				
HAAg10 P24														0.000	0.000			
HAAgFn10 P24																0.113		0.000
HAAg50 P24																0.000	0.020	
HAAgFn50 P24																		0.000
HAAg100 P24																		0.931
HAAgFn100 P24																		

*HAAg10 and HAAg50 had greater bacterial numbers than Pol. HAAg100 and HAAgFn100 were the only surfaces that were antibacterial compared to Pol.

4.1.6 *S aureus*: Planktonic Direct Colony Counts - Benjamini Hochberg procedure

Rank	p value	Threshold (i/m)Q	Reject Null Hypothesis (Y/N)
1	0.000	0.001190476	Y
2	0.000	0.002380952	Y
3	0.000	0.003571429	Y
4	0.000	0.004761905	Y
5	0.000	0.005952381	Y
6	0.000	0.007142857	Y
7	0.000	0.008333333	Y
8	0.000	0.00952381	Y
9	0.000	0.010714286	Y
10	0.000	0.011904762	Y
11	0.000	0.013095238	Y
12	0.000	0.014285714	Y
13	0.000	0.01547619	Y
14	0.000	0.016666667	Y
15	0.000	0.017857143	Y
16	0.000	0.019047619	Y
17	0.000	0.020238095	Y
18	0.000	0.021428571	Y
19	0.000	0.022619048	Y
20	0.000	0.023809524	Y
21	0.000	0.025	Y
22	0.001	0.026190476	Y
23	0.001	0.027380952	Y
24	0.001	0.028571429	Y
25	0.002	0.029761905	Y
26	0.002	0.030952381	Y
27	0.008	0.032142857	Y
28	0.008	0.033333333	Y
29	0.020	0.03452381	Y
30	0.029	0.035714286	Y
31	0.031	0.036904762	Y
32	0.031	0.038095238	Y
33	0.063	0.039285714	N
34	0.113	0.04047619	N
35	0.181	0.041666667	N
36	0.340	0.042857143	N
37	0.489	0.044047619	N
38	0.529	0.045238095	N
39	0.730	0.046428571	N
40	0.743	0.047619048	N
41	0.863	0.048809524	N
42	0.931	0.05	N

4.2 *P aeruginosa* Direct Colony Counts

4.2.1 *P aeruginosa* Bacterial Challenge 10^6 cfu: Biofilm Direct Colony Counts - Median Values and 95% Confidence Intervals

Surface	Median values and (95% confidence intervals)
Pol	800000 (339224.83 to 1871886.29)
HA	30000000 (4158527.71 to 37241472.29)
HAFn	8650000 (-5971233.19 to 45237899.85)
HAAg100	235000 (-661844.75 to 2501844.75)
HAAgFn100	325000 (246885.23 to 399781.44)
Pol P24	280000 (221828.56 to 358171.44)
HA P24	200000 (149018.59 to 250981.41)
HAFn P24	350000 (166533.30 to 560133.37)
HAAg100 P24	210000 (99165.22 to 523334.78)
HAAgFn100 P24	230000 (180181.33 to 293152.00)

4.2.2 *P aeruginosa* Bacterial Challenge 10^6 cfu : Biofilm Direct Colony Counts - p values

Kruskall Wallis p= 0.001

	Pol	HA	HAFn	HAAg 100	HAAg Fn100	Pol P24	HA P24	HAFn P24	HAAg 100 P24	HAAg Fn100 P24
Pol		0.005		(0.190)	0.040	0.142				
HA			0.628	0.001			0.000			
HAFn					0.113			0.181		
HAAg100					0.730				0.321	
HAAgFn100										0.730
Pol P24							0.606		(0.397)	(0.210)
HA P24								0.931	0.673	
HAFn P24										0.605
HAAg100 P24										0.888
HAAgFn100 P24										

4.2.3 *P aeruginosa* Bacterial Challenge 10^6 cfu : Planktonic Direct Colony Counts - Median Values and 95% Confidence Intervals

Surface	Median values and (95% confidence intervals)
Pol	150000000 (95979413.48 to 1123312746.82)
HA	110000000 (77892763.50 to 124964379.36)
HAFn	190000000 (-128724657.15 to 1188724657.15)
HAAg100	150000000 (77593778.73 to 209156221.27)
HAAgFn100	105000000 (10434720.80 to 208565279.20)
Pol P24	80000000 (26951240.76 to 160763044.96)
HA P24	120000000 (42269367.90 to 221063965.44)
HAFn P24	110000000 (45480546.03 to 321852787.30)
HAAg100 P24	255000000 (108295104.27 to 305954895.73)
HAAgFn100 P24	220000000 (90341191.44 to 257214364.11)

4.2.4 *P aeruginosa* Bacterial challenge 10^6 cfu : Planktonic Direct Colony Counts - p values

Kruskall Wallis p=0.114

4.2.5 *P aeruginosa* Bacterial Challenge 5 x 10^4 cfu: Biofilm Direct Colony Counts - Median Values and 95% confidence intervals

Surface	Median values and (95% confidence intervals)
Pol	12000000 (5509240.65 to 44557426.02)
HA	30000000 (16561597.06 to 50549514.05)
HAFn	20000000 (16041514.22 to 28625152.45)
HAAg100	1200000 (878937.04 to 1743285.18)
HAAgFn100	300000 (215030.85 to 584969.15)
Pol P24	3000000 (2282230.21 to 3584436.46)
HA P24	4000000 (2173908.10 to 6714980.79)
HAFn P24	6000000 (1294653.75 to 14530346.25)
HAAg100 P24	1500000 (1033671.53 to 1788550.69)
HAAgFn100 P24	1700000 (856241.51 to 2014869.60)

4.2.6 *P aeruginosa* Bacterial Challenge 5 x 10^4 cfu: Biofilm Direct Colony Counts – p values

Kruskall Wallis p= 0.000

	Pol	HA	HAFn	HAAg 100	HAAg Fn100	Pol P24	HA P24	HAFn P24	HAAg 100 P24	HAAg Fn100 P24
Pol		0.387		(0.003)		0.024				
HA			0.340	0.000			0.000			
HAFn					0.000			0.002		
HAAg100					0.000				0.605	
HAAgFn100										0.071
Pol P24							0.094		(0.000)	(0.000)
HA P24								0.605	0.000	
HAFn P24										0.008
HAAg100 P24										0.436
HAAgFn100 P24										

4.2.7 *P aeruginosa* Bacterial Challenge 5 x 10^4 cfu: Planktonic Direct Colony Counts - Median Values and 95% Confidence Intervals

Surface	Median values and (95% confidence intervals)
Pol	8000000000 (6283966941.43 to 8360477503.01)
HA	3000000000 (1868167117.84 to 6442943993.27)
HAFn	4900000000 (2709823260.98 to 7401287850.13)
HAAg100	41000000 (20557925.99 to 111219851.79)
HAAgFn100	8000000 (6004209.68 to 13995790.32)
Pol P24	8000000000 (3999354029.46 to 8289534859.43)
HA P24	4200000000 (3108182336.52 to 6980706552.37)
HAFn P24	6850000000 (3316802337.87 to 7958197662.13)
HAAg100 P24	330000000 (336051.97 to 1672997281.36)
HAAgFn100 P24	200000000 (103335775.49 to 254442002.29)

4.2.8 *P aeruginosa* Bacterial Challenge 5 x 10^4 cfu: Planktonic Direct Colony Counts - p values

Kruskall Wallis p= 0.000

	Pol	HA	HAFn	HAAg 100	HAAg Fn100	Pol P24	HA P24	HAFn P24	HAAg 100 P24	HAAg Fn100 P24
Pol		0.031		(0.000)		0.546				
HA			0.730	0.000			0.297			
HAFn					0.000			0.673		
HAAg100					0.000				0.000	
HAAgFn100										0.000
Pol P24							0.546		(0.000)	
HA P24								0.815	0.000	
HAFn P24										0.000
HAAg100 P24										0.014
HAAgFn100 P24										

5 Chapter Five Statitstics

Wettability

Kruskall Wallis p=0.008

	Pol	HA	HAFn	HAAg	HAAgFn	HAAg (P24)	HAAgFn (P24)
Pol		0.002	0.002	0.002	0.002	0.002	0.010
HA			1.000	0.699			
HAFn					0.937		
HAAg					0.937	0.310	
HAAgFn							0.171
HAAg (P24)							0.476
HAAgFn (P24)							

Kruskall Wallis HA +/- Ag +/- Fn groups=0.671

N.B. The remainder of the statistics for Chapter Five are presented in the chapter.

6 Chapter Six Statistics

6.1 Epithelial Downgrowth

6.1.1 Median Values and 95% Confidence Intervals

Surface	Median value and (95% confidence interval)
SP	6.0753 (5.2082 to 8.7915)
DF	4.2043 (2.6040 to 4.3087)
PT	1.2900 (0.9936 to 3.1139)
PT-HA	1.7826 (1.2789 to 3.3195)
PT-HAFn	1.7655 (1.2074 to 2.3601)
PT-HAAg	1.7562 (0.9242 to 2.9181)
PT-HAAgFn	1.7888 (1.3366 to 2.1510)

6.1.2 Epithelial Downgrowth - p values

Kruskall Wallis p= 0.000

	SP	DF	PT	PT -HA	PT -HAFn	PT -HAAg	PT- HAAgFn
SP		0.000					
DF			0.027	0.052	0.003	0.017	0.001
PT				0.786	0.898	0.880	0.786
PT-HA					0.566	0.551	
PT-HAFn						0.976	0.695
PT-HAAg							0.799
PT-HAAgFn							

6.2 Epithelial Attachment - p values

Kruskall Wallis (all groups) p = 0.044
Kruskall Wallis (DF and PT +/- coatings) p=0.859

	SP	DF	PT	PT -HA	PT -HAFn	PT -HAAg	PT- HAAgFn
SP		0.045					
DF			0.347	0.713	0.590	0.713	0.843
PT				0.590	0.671	0.630	0.291
PT-HA					0.932	0.977	
PT-HAFn						0.932	0.514
PT-HAAg							0.590
PT-HAAgFn							

(Median values and 95% confidence intervals are shown in Chapter Six)

6.3 Subepithelial Attachment

6.3.1 Median Values and 95% Confidence Intervals

Surface	Median value and (95% confidence interval)
SP	0 (-3.9951 to 47.4251)
DF	56.4400 (43.8219 to 71.0281)
PT	80.4700 (67.5846 to 89.7167)
PT-HA	71.2850 (67.5673 to 83.2277)
PT-HAFn	91.3500 (80.4524 to 97.8596)
PT-HAAg	76.1200 (65.4293 to 81.5557)
PT-HAAgFn	83.5000 (76.2449 to 90.5268)

6.3.2 Subepithelial Attachment - p values

Kruskall Wallis p=0.000

	SP	DF	PT	PT -HA	PT -HAFn	PT -HAAg	PT-HAAgFn
SP		0.017					
DF			0.020	0.014	0.002	0.089	0.004
PT				0.590	0.091	0.410	0.443
PT-HA					0.023	0.977	
PT-HAFn						0.006	0.316
PT-HAAg							0.039
PT-HAAgFn							

6.4 Percentage Soft Tissue Fill within the Inner Pores

6.4.1 Median Values and 95% Confidence Intervals

Surface	Median value and (95% confidence interval)
SP	65 (35.3703 to 80.2963)
DF	90 (82.8587 to 93.8079)
PT	82.5 (77.2816 to 91.0517)
PT-HA	90 (87.6562 to 95.0711)
PT-HAFn	80 (71.5110 to 87.4890)
PT-HAAg	90 (81.9386 to 94.4251)
PT-HAAgFn	65 (35.3703 to 80.2963)

6.4.2 Percentage Soft Tissue Fill within the Inner Pores - p values

Kruskall Wallis p= 0.001

	DF	PT	PT -HA	PT -HAFn	PT -HAAg	PT-HAAgFn
DF		0.000	0.005	0.000	0.010	0.001
PT			0.319	0.266	0.060	0.755
PT-HA				0.068	0.443	
PT-HAFn					0.002	0.266
PT-HAAg						0.143
PT-HAAgFn						

6.5 Number of Cell Nuclei/mm^2 within the Inner Pores

6.5.1 Median Values and 95% Confidence Intervals

Surface	Median value and (95% confidence interval)
DF	1520.5050 (1028.8516 to 2332.6951)
PT	3922.6250 (2590.6413 to 5182.6021)
PT-HA	2883.8250 (2029.4570 to 3891.7696)
PT-HAFn	2945.8300 (2473.5655 to 3708.2709)
PT-HAAg	3086.2450 (2595.8449 to 4017.1911)
PT-HAAgFn	2606.3700 (1990.1559 to 4334.6132)

6.5.2 Number of Cell Nuclei/mm^2 within the Inner Pores - p values

Kruskall Wallis p = 0.084

	DF	PT	PT -HA	PT -HAFn	PT -HAAg	PT-HAAgFn
DF		0.018	0.041	0.002	0.003	0.024
PT			0.410	0.478	0.539	0.713
PT-HA				0.799	0.497	
PT-HAFn					0.674	0.799
PT-HAAg						0.674
PT-HAAgFn						

Kruskall Wallis PT +/- coatings p=0.889

6.6 Number of Blood Vessels/ mm^2 within the Inner Pores

6.6.1 Median Values and 95% Confidence Intervals

Surface	Median value and (95% confidence interval)
DF	0 (-23.2890 to 97.4090)
PT	213.2150 (133.9067 to 293.7583)
PT-HA	134.1550 (66.4745 to 224.9305)
PT-HAFn	224.7700 (182.1744 to 277.3820)
PT-HAAg	335.3450 (198.7168 to 431.9032)
PT-HAAgFn	159.1100 (108.2056 to 237.7671)

6.6.2 Number of Blood Vessels/ mm^2 within the Inner Pores - p values

Kruskall Wallis p = 0.005

	DF	PT	PT -HA	PT -HAFn	PT -HAAg	PT-HAAgFn
DF		0.002	0.102	0.001	0.005	0.005
PT			0.143	0.651	0.219	0.413
PT-HA				0.134	0.024	
PT-HAFn					0.316	0.101
PT-HAAg						0.104
PT-HAAgFn						

6.7 Chapter Six Correlation

Spearman's rho		Epithelial downgrowth (mm)	Percentage Epithelial Attachment	Percentage Subepithelial attachment	Percentage Fill Inner Pores	Pore - Cell Nuclei/mm^2	Pore - Blood Vessel/mm^2
Epithelial downgrowth (mm)	Correlation Coefficient		-0.214	-0.496	-0.149	-0.141	-0.145
	Sig (2-tailed)		0.053	0.000	0.240	0.732	0.322
Percentage Epithelial Attachment	Correlation Coefficient			0.412	0.027	-0.037	-0.103
	Sig (2-tailed)			0.000	0.831	0.774	0.420
Percentage Subepithelial attachment	Correlation Coefficient				0.246	0.074	0.094
	Sig (2-tailed)				0.048	0.566	0.462
Percentage Fill Inner Pores	Correlation Coefficient					0.360	0.373
	Sig (2-tailed)					0.004	0.002
Pore - Cell Nuclei/mm^2	Correlation Coefficient						0.439
	Sig (2-tailed)						0.000
Pore - Blood Vessel/mm^2	Correlation Coefficient						
	Sig (2-tailed)						

7 Chapter Seven Statistics

7.1 Skin Surface Swab Direct Colony Counts

7.1.1 Medians Values and 95% Confidence Intervals

Surface	Median value and (95% confidence interval)
SP	2050 (1060.29 to 13264.71)
DF	2200 (-4504.73 to 106592.23)
PT	2900 (-4136.42 to 36222.13)
PT-HA	1650 (-4348.12 to 27859.23)
PT-HAFn	5000 (-4120.76 to 104304.09)
PT-HAAg	4000 (-18993.45 to 259829.81)
PT-HAAgFn	90000 (-6853.25 to 807398.7)

7.1.2 Skin Surface Swab Direct Colony Counts - p values

Kruskall Wallis p=0.225

7.2 Superficial Soft Tissue Biopsy Direct Colony Counts

7.2.1 Medians Values and 95% Confidence Intervals

Surface	Median value and (95% confidence interval)
SP	83.965 (123.4488 to 566.2424)
DF	84.015 (61.9483 to 193.3567)
PT	19.755 (17.6234 to 40.958)
PT-HA	61.11 (49.866 to 121.084)
PT-HAFn	142.5 (67.5629 to 277.0088)
PT-HAAg	43.64 (19.0178 to 74.284)
PT-HAAgFn	51.16 (36.4087 to 256.5949)

7.2.2 Superficial Soft Tissue Biopsy Direct Colony Counts - p values

Kruskall Wallis p=0.000

	SP	DF	PT	PT -HA	PT -HAFn	PT -HAAg	PT- HAAgFn
SP		0.355					
DF			0.000	0.079	0.556	0.000	0.171
PT				0.000	0.019	0.602	0.259
PT-HA					0.656	0.011	0.673
PT-HAFn						0.022	0.343
PT-HAAg							0.503
PT-HAAgFn							

7.3 Deep soft tissue biopsy

7.3.1 Medians values and 95% confidence intervals

Surface	Median value and (95% confidence interval)
SP	6.2 (11.1668 to 88.1857)
DF	25.625 (19.8165 to 154.9747)
PT	1.485 (0.7332 to 4.4425)
PT-HA	10.5 (13.6632 to 78.1946)
PT-HAFn	0.8250 (0.1559 to 5.1608)
PT-HAAg	4 (2.6592 to 6.0553)
PT-HAAgFn	6.25 (2.0437 to 11.7599)

7.3.2 Deep soft tissue biopsy - p values

Kruskall Wallis p= 0.000

	SP	DF	PT	PT -HA	PT -HAFn	PT -HAAg	PT- HAAgFn
SP		0.224					
DF			0.000	0.135	0.000	0.000	0.000
PT				0.008	0.526	0.901	0.766
PT-HA					0.007	0.009	0.020
PT-HAFn						0.861	0.539
PT-HAAg							0.830
PT-HAAgFn							

7.4 Deep Soft Tissue-Implant Interface Swab

7.4.1 Medians Values and 95% Confidence Intervals

Surface	Median value and (95% confidence interval)
SP	160000 (99137.85 to 439112.15)
DF	60000 (-22380.62 to 1570380.62)
PT	850 (1008.13 to 55420.44)
PT-HA	3250 (3671.48 to 15517.41)
PT-HAFn	1900 (1017.78 to 9698.89)
PT-HAAg	300 (1.81 to 4998.19)
PT-HAAgFn	400 (289.42 to 6583.31)

7.4.2 Deep Soft Tissue-Implant Interface Swab - p values

Kruskall Wallis p=0.000

	SP	DF	PT	PT -HA	PT -HAFn	PT -HAAg	PT- HAAgFn
SP		0.938					
DF			0.000	0.000	0.000	0.000	0.000
PT				0.815	0.839	0.075	0.357
PT-HA					0.214	0.012	0.220
PT-HAFn						0.106	0.808
PT-HAAg							0.259
PT-HAAgFn							

7.5 Correlation (Chapter Seven results combined Chapter Six)

Spearman's rho		Skin surface swab cfu/mL	Superficial soft tissue cfu/mL	Deep soft tissue cfu/mL	Deep swab cfu/mL	Epithelial downgrowth (mm)	Percentage epithelial attachment	Percentage sub-epithelial attachment	Percentage fill inner pores	Pore - cell nuclei /mm^2	Pore - blood vessels /mm^2
Skin surface swab cfu/mL	Correlation Coefficient		-0.174	-0.022	-0.154	-0.349	-0.116	0.000	0.133	0.170	0.051
	Sig (2-tailed)		0.059	0.816	0.098	0.001	0.294	1.000	0.287	0.178	0.688
Superficial soft tissue cfu/mL	Correlation Coefficient			0.470	0.385	0.165	-0.115	-0.221	-0.103	-0.327	-0.412
	Sig (2-tailed)			0.000	0.000	0.155	0.315	0.052	0.435	0.012	0.001
Deep soft tissue cfu/mL	Correlation Coefficient				0.433	-0.080	-0.105	-0.239	-0.053	0.066	-0.258
	Sig (2-tailed)				0.000	0.485	0.355	0.034	0.683	0.615	0.048
Deep swab cfu/mL	Correlation Coefficient					0.437	-0.203	-0.297	-0.021	-0.318	-0.190
	Sig (2-tailed)					0.000	0.073	0.008	0.872	0.014	0.150

7.6 Chapter Seven Correlation - Benjamini Hochberg procedure

Rank	p value	Threshold (i/m)Q	Reject Null Hypothesis (Y/N)
1	0	0.001666667	Y
2	0	0.003333333	Y
3	0	0.005	Y
4	0	0.006666667	Y
5	0.001	0.008333333	Y
6	0.001	0.01	Y
7	0.008	0.011666667	Y
8	0.012	0.013333333	Y
9	0.014	0.015	N
10	0.034	0.016666667	N
11	0.048	0.018333333	N
12	0.052	0.02	N
13	0.059	0.021666667	N
14	0.073	0.023333333	N
15	0.098	0.025	N
16	0.15	0.026666667	N
17	0.155	0.028333333	N
18	0.178	0.03	N
19	0.287	0.031666667	N
20	0.294	0.033333333	N
21	0.315	0.035	N
22	0.355	0.036666667	N
23	0.435	0.038333333	N
24	0.485	0.04	N
25	0.615	0.041666667	N
26	0.683	0.043333333	N
27	0.688	0.045	N
28	0.816	0.046666667	N
29	0.872	0.048333333	N
30	1	0.05	N

BIBLIOGRAPHY

Abarca, M., Van Steenberghe, D., Malevez, C., and Jacobs, R. (2006). The neurophysiology of osseointegrated oral implants. A clinically underestimated aspect. *J Oral Rehabil* 33, 161-9.

Abraham, S. N., Beachey, E. H., and Simpson, W. A. (1983). Adherence of streptococcus pyogenes, Escherichia coli, and Pseudomonas aeruginosa to fibronectin-coated and uncoated epithelial cells. *Infect Immun* 41, 1261-8.

Abrahamsson, I., Zitzmann, N. U., Berglundh, T., Linder, E., Wennerberg, A., and Lindhe, J. (2002). The mucosal attachment to titanium implants with different surface characteristics: an experimental study in dogs. *J Clin Periodontol* 29, 448-55.

Adell, R., Lekholm, U., Rockler, B., and Brånemark, P. I. (1981). A 15-year study of osseointegrated implants in the treatment of the edentulous jaw. *Int J Oral Surg* 10, 387-416.

Agarwal, A., Weis, T. L., Schurr, M. J., Faith, N. G., Czuprynski, C. J., McAnulty, J. F., Murphy, C. J., and Abbott, N. L. (2010). Surfaces modified with nanometer-thick silver-impregnated polymeric films that kill bacteria but support growth of mammalian cells. *Biomaterials* 31, 680-90.

Agins, H.J., Alcock, N.W., Bansal, M., Salvati, E.A. Wilson, P.D. Jr., Pellicci, P.M., and Bullough, P.G. (1988). Metallic wear in failed titanium-alloy total hip replacements. A histological and quantitative analysis. *J Bone Joint Surg Am* 70 (3):347-56

Ahl, T., Dalén, N., Jörbeck, H., and Hoborn, J. (1995) Air contamination during hip and knee arthroplasties: Horizontal laminar flow randomized vs. conventional ventilation. *Acta Orthop Scand* 66, 17-20.

Akhundov, K., Pietramaggiori, G., Waselle, L., Darwiche, S., Guerid, S., Scaletta, C., Hirt-Burri, N., Applegate, L. A., and Raffoul, W. V. (2012). Development of a cost-effective method for platelet-rich plasma (PRP) preparation for topical wound healing. *Ann Burns Fire Disasters* 25, 207-13.

Akiyama, T., Miyamoto, H., Yonekura, Y., Tsukamoto, M., Ando, Y., Noda, I., Sonohata, M., and Mawatari, M. (2013). Silver oxide-containing hydroxyapatite coating has in vivo antibacterial activity in the rat tibia. *J Orthop Res* 31, 1195-200.

Aksakal, B., Gavgali, M., and Dikici, B. (2010). The Effect of Coating Thickness on Corrosion Resistance of Hydroxyapatite Coated Ti6Al4V and 316L SS Implants. *J Mat Eng Perform* 19, 894-899.

Alberts, B., Johnson, A., Lewis, J., Raff, M., Roberts, K., and Walter, P. (2002). Integrins. In: Molecular Biology of the Cell. 4th Edition. Garland Science, New York.

Albrektsson, T., and Johansson, C. (2001). Osteoinduction, osteoconduction and osseointegration. *Eur Spine J* 10 Suppl 2, S96-101.

Alt, V., Bechert, T., Steinrucke, P., Wagener, M., Seidel, P., Dingeldein, E., Domann, E., and Schnettler, R. (2004). An in vitro assessment of the antibacterial properties and cytotoxicity of nanoparticulate silver bone cement. *Biomaterials* 25, 4383-91.

Alt, V., Bitschnau, A., Bohner, F., Heerich, K. E., Magesin, E., Sewing, A., Pavlidis, T., Szalay, G., Heiss, C., Thormann, U., Hartmann, S., Pabst, W., Wenisch, S., and Schnettler, R. (2011). Effects of gentamicin and gentamicin-RGD coatings on bone ingrowth and biocompatibility of cementless joint prostheses: an experimental study in rabbits. *Acta Biomater* 7, 1274-80.

The Amputee Statistical Database for the United Kingdom 2006/7, Information Services Division NHS Scotland on behalf of National Amputee Statistical Database (NASDAB).

Antoci, V.Jr., Adams, C.S., Hickok, N.J., Shapiro, I.M., and Parvizi, J. (2007a). Antibiotics for Local Delivery Systems Cause Skeletal Cell Toxicity In Vitro. *Clin Orthop Relat Res* 462, 200-206.

Antoci, V., Jr., King, S. B., Jose, B., Parvizi, J., Zeiger, A. R., Wickstrom, E., Freeman, T. A., Composto, R. J., Ducheyne, P., Shapiro, I. M., Hickok, N. J., and Adams, C. S. (2007b). Vancomycin covalently bonded to titanium alloy prevents bacterial colonization. *J Orthop Res* 25, 858-66.

Antoci, V., Jr., Adams, C. S., Hickok, N. J., Shapiro, I. M., and Parvizi, J. (2007c). Vancomycin bound to Ti rods reduces periprosthetic infection: preliminary study. *Clin Orthop Relat Res* 461, 88-95.

Antoci, V., Ono, C. M., Antoci, V., Jr., and Raney, E. M. (2008). Pin-tract infection during limb lengthening using external fixation. *Am J Orthop (Belle Mead NJ)* 37, E150-4.

Arciola, C. R., Montanaro, L., Moroni, A., Giordano, M., Pizzoferrato, A., and Donati, M. E. (1999). Hydroxyapatite-coated orthopaedic screws as infection resistant materials: in vitro study. *Biomaterials* 20, 323-7.

Aschoff, H. H., Clausen, A., Tsoumpris, K., and Hoffmeister, T. (2011). [Implantation of the endo-exo femur prosthesis to improve the mobility of amputees]. *Oper Orthop Traumatol* 23, 462-72.

Aschoff, H. H., and Juhnke, D. L. (2012). [Evaluation of 10 years experience with endo-exo femur prostheses - background, data and results]. *Z Orthop Unfall* 150, 607-14.

Aschoff, H. H., Kennon, R. E., Keggi, J. M., and Rubin, L. E. (2010). Transcutaneous, Distal Femoral, Intramedullary Attachment for Above-the-Knee Prostheses: An Endo-Exo Device. *J Bone Joint Surg Am* 92 Suppl, 180-6.

Avon, S. L., and Wood, R. E. (2005). Porcine skin as an in-vivo model for ageing of human bite marks. *J Forensic Odontostomatol* 23, 30-9.

Aydin, C., Karakoca, S., and Yilmaz, H. (2007). Implant-retained digital prostheses with custom-designed attachments: a clinical report. *J Prosthet Dent* 97, 191-5.

Aydin, C., Karakoca, S., Yilmaz, H., Yilmaz, C., and Yamalik, K. (2008). The use of dental implants to retain thumb prostheses: a short-term evaluation of 2 cases. *Int J Prosthodont* 21, 138-40.

Babapour, A., Yang, B., Bahang, S., and Cao, W. (2011). Low-temperature sol-gel-derived nanosilver-embedded silane coating as biofilm inhibitor. *Nanotechnology* 22, 155602.

Bai, X., Sandukas, S., Appleford, M., Ong, J. L., and Rabiei, A. (2012). Antibacterial effect and cytotoxicity of Ag-doped functionally graded hydroxyapatite coatings. *J Biomed Mater Res B Appl Biomater* 100, 553-61.

Baleriola-Lucas, C., and Wilcox, M. D. P. (1998). The ability of ocular bacteria to bind to fibronectin. *Clin Exp Optom* 81, 81-87.

Bansal, K. (2013). IV Prev: Preventing Infections. A technology to save lives. Medicen Devise/Gabriel http://www.gabriel-is.com/wp-content/uploads/.../IV-Prev_Gabriel_Final.pptx.

Batta, V., Coathup, M. J., Parratt, M. T., Pollock, R. C., Aston, W. J., Cannon, S. R., Skinner, J. A., Briggs, T. W., and Blunn, G. W. (2014). Uncemented,

custom-made, hydroxyapatite-coated collared distal femoral endoprostheses: up to 18 years' follow-up. *Bone Joint J* 96-B, 263-9.

Beaudoin, T., Zhang, L., Hinz, A. J., Parr, C. J., and Mah, T. F. (2012). The biofilm-specific antibiotic resistance gene ndvB is important for expression of ethanol oxidation genes in Pseudomonas aeruginosa biofilms. *J Bacteriol* 194, 3128-36.

Benjamini, Y., and Hochberg, Y. (1995). Controlling the False Discovery Rate: a Practical and Powerful Approach to Multiple Testing. *J R Statist Soc B* 57, 289-300.

Berlin, O., Brånemark, R., Hagberg, K., Rydevik, B., Bergh, P., and Gunterberg, B. (2012). Osseointegrated Prosthesis for the Rehabilitation of Amputees: Two-year results of the prospective OPRA study. *In* "4th International Conference: ADVANCES IN ORTHOPAEDIC OSSEOINTEGRATION". Orthopaedic Surgical Osseointegration Society, Mission Bay Conference Center at UCSF.

Bobyn, J. D., Wilson, G. J., MacGregor, D. C., Pilliar, R. M., and Weatherly, G. C. (1982). Effect of pore size on the peel strength of attachment of fibrous tissue to porous-surfaced implants. *J Biomed Mater Res* 16, 571-84.

Bonewald, L. F., and Johnson, M. L. (2008). Osteocytes, mechanosensing and Wnt signaling. *Bone* 42, 606-15.

Bosetti, M., Masse, A., Tobin, E., and Cannas, M. (2002). Silver coated materials for external fixation devices: in vitro biocompatibility and genotoxicity. *Biomaterials* 23, 887-92.

Bozzini, S., Visai, L., Pignatti, P., Petersen, T. E., and Speziale, P. (1992). Multiple binding sites in fibronectin and the staphylococcal fibronectin receptor. *Eur J Biochem* 207, 327-33.

Braem, A., Van Mellaert, L., Hofmans, D., De Waelheyns, E., Anne, J., Schrooten, J., and Vleugels, J. (2013). Bacterial colonisation of porous titanium coatings for orthopaedic implant applications - effect of surface roughness and porosity. *Powder Mettalurgy* 56, 267-271.

Braem, A., Van Mellaert, L., Mattheys, T., Hofmans, D., De Waelheyns, E., Geris, L., Anne, J., Schrooten, J., and Vleugels, J. (2014). Staphylococcal biofilm growth on smooth and porous titanium coatings for biomedical applications. *J Biomed Mater Res A* 102, 215-24.

Brånemark, R., Berlin, O., Hagberg, K., Bergh, P., Gunterberg, B., and Rydevik, B. (2014). A novel osseointegrated percutaneous prosthetic system for the treatment of patients with transfemoral amputation: A prospective study of 51 patients. *Bone Joint J* 96-B, 106-13.

Brånemark, R., Brånemark, P.-I., Rydevik, B., and Myers, R. R. (2001). Osseointegration in skeletal reconstruction and rehabilitation. *J Rehabil Res Dev* 38, 1-8.

Broughton, G., 2nd, Janis, J. E., and Attinger, C. E. (2006). The basic science of wound healing. *Plast Reconstr Surg* 117, 12S-34S.

Buck, D. W., 2nd, and Dumanian, G. A. (2012). Bone biology and physiology: Part I. The fundamentals. *Plast Reconstr Surg* 129, 1314-20.

Buckwalter, J. A., M.J., G., Cooper, R. R., and Recker, R. (1995). Bone Biology. *J Bone Joint Surg Am* 77, 1256-1275.

Burkitt, H. G., Young, B., and Heath, J. W. (1993). "Wheater's Functional Histology- a Text and Colour Atlas 3rd Edition. ," Churchill Livingstone.

Busscher, H. J., van der Mei, H. C., Subbiahdoss, G., Jutte, P. C., van den Dungen, J. J., Zaat, S. A., Schultz, M. J., and Grainger, D. W. (2012). Biomaterial-associated infection: locating the finish line in the race for the surface. *Sci Transl Med* 4, 153rv10.

Calori, G. M., Mazza, E., Colombo, M., and Ripamonti, C. (2011). The use of bone-graft substitutes in large bone defects: any specific needs? *Injury* 42 Suppl 2, S56-63.

Campbell, A. A., Song, L., Li, X. S., Nelson, B. J., Bottoni, C., Brooks, D. E., and DeJong, E. S. (2000). Development, characterization, and anti-microbial efficacy of hydroxyapatite-chlorhexidine coatings produced by surface-induced mineralization. *J Biomed Mater Res* 53, 400-7.

Canavan, R. J., Unwin, N. C., Kelly, W. F., and Connolly, V. M. (2008). Diabetes- and nondiabetes-related lower extremity amputation incidence before and after the introduction of better organized diabetes foot care: continuous longitudinal monitoring using a standard method. *Diabetes Care* 31, 459-63.

Cannas, M., Denicolai, F., Webb, L. X., and Gristina, A. G. (1988). Bioimplant surfaces: binding of fibronectin and fibroblast adhesion. *J Orthop Res* 6, 58-62.

Cao, W., and Hench, L. (1996). Bioactive Materials. *Ceramics International* 22, 493-507.

Carr, B. J., Ochoa, L., Rankin, D., and Owens, B. D. (2009). Biologic response to orthopedic sutures: a histologic study in a rabbit model. *Orthopedics* 32, 828.

Ceri, H., Olson, M. E., Stremick, C., Read, R. R., Morck, D., and Buret, A. (1999). The Calgary Biofilm Device: new technology for rapid determination of antibiotic susceptibilities of bacterial biofilms. *J Clin Microbiol* 37, 1771-6.

Chaby, G., Viseux, V., Poulain, J. F., De Cagny, B., Denoeux, J. P., and Lok, C. (2005). [Topical silver sulfadiazine-induced acute renal failure]. *Ann Dermatol Venereol* 132, 891-3.

Chen, W., Liu, Y., Courtney, H. S., Bettenga, M., Agrawal, C. M., Bumgardner, J. D., and Ong, J. L. (2006). In vitro anti-bacterial and biological properties of magnetron co-sputtered silver-containing hydroxyapatite coating. *Biomaterials* 27, 5512-7.

Chen, Y., Zheng, X., Xie, Y., Ding, C., Ruan, H., and Fan, C. (2008). Anti-bacterial and cytotoxic properties of plasma sprayed silver-containing HA coatings. *J Mater Sci Mater Med* 19, 3603-9.

Chimutengwende-Gordon, M. (2010). "Microbiological review of the RNOH transfemoral ITAP trial," (unpublished).

Chimutengwende-Gordon, M., Pendegrass, C., and Blunn, G. (2011). Enhancing the soft tissue seal around intraosseous transcutaneous amputation prostheses using silanized fibronectin titanium alloy. *Biomed Mater* 6, 025008.

Choban, P. S., and Marshall, W. J. (1987). Leukopenia secondary to silver sulfadiazine: frequency, characteristics and clinical consequences. *Am Surg* 53, 515-7.

Chou, L., Marek, B., and Wagner, W. R. (1999). Effects of hydroxylapatite coating crystallinity on biosolubility, cell attachment efficiency and proliferation in vitro. *Biomaterials* 20, 977-85.

Chua, P. H., Neoh, K. G., Kang, E. T., and Wang, W. (2008). Surface functionalization of titanium with hyaluronic acid/chitosan polyelectrolyte multilayers and RGD for promoting osteoblast functions and inhibiting bacterial adhesion. *Biomaterials* 29, 1412-21.

Clark, W. B., Bammann, L. L., and Gibbons, R. J. (1978). Comparative estimates of bacterial affinities and adsorption sites on hydroxyapatite surfaces. *Infect Immun* 19, 846-53.

Clement, J. L., and Jarrett, P. S. (1994). Antibacterial silver. *Met Based Drugs* 1, 467-82.

Coathup, M. J., Batta, V., Pollock, R. C., Aston, W. J., Cannon, S. R., Skinner, J. A., Briggs, T. W., Unwin, P. S., and Blunn, G. W. (2013). Long-term survival of cemented distal femoral endoprostheses with a hydroxyapatite-coated collar: a histological study and a radiographic follow-up. *J Bone Joint Surg Am* 95, 1569-75.

Coathup, M. J., Sanghrajka, A., Aston, W. J., Gikas, P. D., Pollock, R. C., Cannon, S. R., Skinner, J. A., Briggs, T. W., and Blunn, G. W. (2015). Hydroxyapatite-coated collars reduce radiolucent line progression in cemented distal femoral bone tumor implants. *Clin Orthop Relat Res* 473, 1505-14.

Coathup, M. J., Shawcross, J., Scarsbrook, C., Korda, M., Hanoun, A., Pickford, M., Agg, P., and Blunn, G. W. (2012). Osseointegration of silver treated titanium alloy. *J Bone Joint Surg Br* 94-B no. SUPP XXXVI 100.

Coester, L. M., Nepola, J. V., Allen, J., and Marsh, J. L. (2006). The effects of silver coated external fixation pins. *Iowa Orthop J* 26, 48-53.

Collinge, C. A., Goll, G., Seligson, D., and Easley, K. J. (1994). Pin tract infections: silver vs uncoated pins. *Orthopedics* 17, 445-8.

Cooper, G. M. (2000). The Origin and Evolution of Cells. In: The Cell: A Molecular Approach. Sunderland (MA): Sinauer Associates. NCBI Bookshelf. A service of the National Library of Medicine, National Institutes of Health. http://www.ncbi.nlm.nih.gov/books/NBK9841/.

Cordero, J., Munuera, L., and Folgueira, M. D. (1994). Influence of metal implants on infection. An experimental study in rabbits. *J Bone Joint Surg Br* 76, 717-20.

Costa, D. O., Prowse, P. D., Chrones, T., Sims, S. M., Hamilton, D. W., Rizkalla, A. S., and Dixon, S. J. (2013). The differential regulation of osteoblast and osteoclast activity by surface topography of hydroxyapatite coatings. *Biomaterials* 34, 7215-26.

Costerton, J. W., Stewart, P. S., and Greenberg, E. P. (1999). Bacterial biofilms: a common cause of persistent infections. *Science* 284, 1318-22.

Cunha, A., Renz, R. P., Blando, E., de Oliveira, R. B., and Hubler, R. (2014). Osseointegration of atmospheric plasma-sprayed titanium implants: Influence of the native oxide layer. *J Biomed Mater Res A* 102, 30-6.

Curtis, A.S. and Tsimbouri, P.M. (2014). Epigenesis: roles of nanotopography, nanoforces and nanovibration. *Expert Rev Med Devices* 11, 417-423.

D'Antonio, J. A., Capello, W. N., Manley, M. T., and Geesink, R. (2001). Hydroxyapatite femoral stems for total hip arthroplasty: 10- to 13-year followup. *Clin Orthop Relat Res*, 101-11.

Darouiche, R. O. (1999). Anti-infective efficacy of silver-coated medical prostheses. *Clin Infect Dis* 29, 1371-7; quiz 1378.

Darouiche, R. O., Green, G., and Mansouri, M. D. (1998). Antimicrobial activity of antiseptic-coated orthopaedic devices. *Int J Antimicrob Agents* 10, 83-6.

Darouiche, R. O., Mansouri, M. D., Zakarevicz, D., Alsharif, A., and Landon, G. C. (2007). In vivo efficacy of antimicrobial-coated devices. *J Bone Joint Surg Am* 89, 792-7.

Davies, D. (2003). Understanding biofilm resistance to antibacterial agents. *Nat Rev Drug Discov* 2, 114-22.

Day, C. S., and Franko, O. I. (2007). Low-profile dorsal plating for dorsally angulated distal radius fractures. *Tech Hand Up Extrem Surg* 11, 142-8.

de Bruijn, J. D., Bovell, Y. P., and van Blitterswijk, C. A. (1993). Structural arrangements at the interface between plasma sprayed calcium phosphate and bone. *Biomaterials* 15, 543-550.

De Giglio, E., Cometa, S., Ricci, M. A., Cafagna, D., Savino, A. M., Sabbatini, L., Orciani, M., Ceci, E., Novello, L., Tantillo, G. M., and Mattioli-Belmonte, M. (2011). Ciprofloxacin-modified electrosynthesized hydrogel coatings to prevent titanium-implant-associated infections. *Acta Biomater* 7, 882-91.

de Oliviera, P.T., and Nanci, A. (2004). Nanotexturing of titanium-based surfaces upregulates expression of bone sialoprotein and osteopontin by cultured osteogenic cells. *Biomaterials* 25, 403-413.

de Oliveira, P.T., Zalzal, S.F., Beloti, M.M., Rosa, A.L., and Nanci, A. (2007). Enhancement of in vitro osteogenesis on titanium by chemically produced nanotopography. *J Biomed Mater Res* 80A, 554-564.

Dean, J. W., 3rd, Culbertson, K. C., and D'Angelo, A. M. (1995). Fibronectin and laminin enhance gingival cell attachment to dental implant surfaces in vitro. *Int J Oral Maxillofac Implants* 10, 721-8.

Deligianni, D., Korovessis, P., Porte-Derrieu, M. C., Amedee, J., and Repantis, T. (2006). Experimental usage of hydroxyapatite preadsorption with fibronectin to increase permanent stability and longevity of spinal implants. *Stud Health Technol Inform* 123, 289-98.

Delmi, M., Vaudaux, P., Lew, D. P., and Vasey, H. (1994). Role of fibronectin in staphylococcal adhesion to metallic surfaces used as models of orthopaedic devices. *J Orthop Res* 12, 432-8.

Demet, K., Martinet, N., Guillemin, F., Paysant, J., and André, J. M. (2003). Health related quality of life and related factors in 539 persons with amputation of upper and lower limb. *Disabil Rehabil* 25, 480-486.

Dexter, S. J., Pearson, R. G., Davies, M. C., Camara, M., and Shakesheff, K. M. (2001). A comparison of the adhesion of mammalian cells and Staphylococcus epidermidis on fibronectin-modified polymer surfaces. *J Biomed Mater Res* 56, 222-7.

Dolatshahi-Pirouz, A., Jensen, T. H., Kolind, K., Bunger, C., Kassem, M., Foss, M., and Besenbacher, F. (2011). Cell shape and spreading of stromal (mesenchymal) stem cells cultured on fibronectin coated gold and hydroxyapatite surfaces. *Colloids Surf B Biointerfaces* 84, 18-25.

Dong, X., Wang, Q., Wu, T., and Pan, H. (2007). Understanding adsorption-desorption dynamics of BMP-2 on hydroxyapatite (001) surface. *Biophys J* 93, 750-9.

Donlan, R. M., and Costerton, J. W. (2002). Biofilms: survival mechanisms of clinically relevant microorganisms. *Clin Microbiol Rev* 15, 167-93.

Doppen, P., Solomons, M., and Kritzinger, S. (2009). Osseointegrated finger prostheses. *J Hand Surg Eur Vol* 34, 29-34.

Dowling, R., Pendegrass, C., Thomas, B., and Blunn, G. (2014). In vivo assessment of porous implants functionalused with RGD peptides in enhancing osseointegrated amputation prostheses. *Bone Joint J* 96-B.

Dowling, R. P., Pendegrass, C. J., and Blunn, G. W. (2012). A Comparison of Fibronectin and RGD Peptide Coatings for Improving Dermal Fibroblast Attachment to Intraosseous Transcutaneous Amputation Prostheses In Vitro. *In* "Orthopaedic Research Society Annual Meeting". Poster 0638.

Downey, P. A., and Siegel, M. I. (2006). Bone biology and the clinical implications for osteoporosis. *Phys Ther* 86, 77-91.

Drake, P. L., and Hazelwood, K. J. (2005). Exposure-related health effects of silver and silver compounds: a review. *Ann Occup Hyg* 49, 575-85.

Drinias, V., Granstrom, G., and Tjellstrom, A. (2007). High age at the time of implant installation is correlated with increased loss of osseointegrated implants in the temporal bone. *Clin Implant Dent Relat Res* 9, 94-9.

Ducheyne, P., and Qiu, Q. (1999). Bioactive ceramics: the effect of surface reactivity on bone formation and bone cell function. *Biomaterials* 20, 2287-303.

Dudek, N. L., Marks, M. B., Marshall, S. C., and Chardon, J. P. (2005). Dermatologic conditions associated with use of a lower-extremity prosthesis. *Arch Phys Med Rehabil* 86, 659-63.

Duguid, I. G., Evans, E., Brown, M. R., and Gilbert, P. (1992). Growth-rate-independent killing by ciprofloxacin of biofilm-derived Staphylococcus epidermidis; evidence for cell-cycle dependency. *J Antimicrob Chemother* 30, 791-802.

Dunne, W. M., and Burd, E. M. (1993). Fibronectin and proteolytic fragments of fibronectin interfere with the adhesion of Staphylococcus epidermidis to plastic. *J Appl Bacteriol* 74, 411-6.

Ekelund, J. A., Lindquist, L. W., Carlsson, G. E., and Jemt, T. (2003). Implant treatment in the edentulous mandible: a prospective study on Brånemark system implants over more than 20 years. *Int J Prosthodont* 16, 602-8.

Evans, D. J., Allison, D. G., Brown, M. R., and Gilbert, P. (1990). Effect of growth-rate on resistance of gram-negative biofilms to cetrimide. *J Antimicrob Chemother* 26, 473-8.

Ewald, A., Gluckermann, S. K., Thull, R., and Gbureck, U. (2006). Antimicrobial titanium/silver PVD coatings on titanium. *Biomed Eng Online* 5, 22.

Farrell, B. J., Prilutsky, B. I., Ritter, J. M., Kelley, S., Popat, K., and Pitkin, M. (2014). Effects of pore size, implantation time, and nano-surface properties on rat skin ingrowth into percutaneous porous titanium implants. *J Biomed Mater Res A* 102, 1305-15.

Feller, L., Jadwat, Y., Khammissa, R.A., Meyerov, R., Schechter, I., and Lemmer, J. (2015). Cellular Responses Evoked by Different Surface Characteristics of Intraosseous Titanium Implants. *BioMed Res Int* 2015, 171945.

Feng, B., Jinkang, Z., Zhen, W., Jianxi, L., Jiang, C., Jian, L., Guolin, M., and Xin, D. (2011). The effect of pore size on tissue ingrowth and neovascularization in porous bioceramics of controlled architecture in vivo. *Biomed Mater* 6, 015007.

Feng, Q. L., Cui, F. Z., Kim, T. N., and Kim, J. W. (1999). Ag-substituted hydroxyapatite coatings with both antimicrobial effects and biocompatibility. *J Mater Sci Lett* 18, 559-561.

Feng, Q. L., Wu, J., Chen, G. Q., Cui, F. Z., Kim, T. N., and Kim, J. O. (2000). A mechanistic study of the antibacterial effect of silver ions on Escherichia coli and Staphylococcus aureus. *J Biomed Mater Res* 52, 662-8.

Fernandez, M. S., Arias, J. I., Martinez, M. J., Saenz, L., Neira-Carrillo, A., Yazdani-Pedram, M., and Arias, J. L. (2012). Evaluation of a multilayered chitosan-hydroxy-apatite porous composite enriched with fibronectin or an in vitro-generated bone-like extracellular matrix on proliferation and diferentiation of osteoblasts. *J Tissue Eng Regen Med* 6, 497-504.

Ferreira, N., and Marais, L. C. (2012). Prevention and management of external fixator pin track sepsis. *Strategies Trauma Limb Reconstr* 7, 67-72.

Ferreira, M.B., Myiagi, S., Nogales, C.G., Campos, M.S., and Lage-Marques, J.L. (2010). Time- and concentration-dependent cytotoxicity of antibiotics used in endodontic therapy. *J Appl Oral Sci* 18, 259-63.

Fitzgerald, R. H., Jr. (1979). Microbiologic environment of the conventional operating room. *Arch Surg* 114, 772-5.

Fitzpatrick, N., Smith, T. J., Pendegrass, C. J., Yeadon, R., Ring, M., Goodship, A. E., and Blunn, G. W. (2011). Intraosseous transcutaneous amputation prosthesis (ITAP) for limb salvage in 4 dogs. *Vet Surg* 40, 909-25.

Foley, I., and Brown, M. R. W. (1999). Activity of Antibiotics Against Adherent/Slow-growing Bacteria Reflecting the Situation in vivo. *In* "Handbook of Animal Models of Infection" (O. Zak and M. A. Sande, eds.). Academic Press, Bath, Avon, UK.

Foppiano, S., Marshall, S. J., Marshall, G. W., Saiz, E., and Tomsia, A. P. (2007). Bioactive glass coatings affect the behavior of osteoblast-like cells. *Acta Biomater* 3, 765-71.

Foppiano, S., Marshall, S. J., Saiz, E., Tomsia, A. P., and Marshall, G. W. (2006). Functionally graded bioactive coatings: reproducibility and stability of the coating under cell culture conditions. *Acta Biomater* 2, 133-42.

Freemont, A. J. (1993). Basic bone cell biology. *Int J Exp Path* 74, 411-416.

Fuchs, T., Stange, R., Schmidmaier, G., and Raschke, M. J. (2011). The use of gentamicin-coated nails in the tibia: preliminary results of a prospective study. *Arch Orthop Trauma Surg* 131, 1419-25.

Furno, F., Morley, K. S., Wong, B., Sharp, B. L., Arnold, P. L., Howdle, S. M., Bayston, R., Brown, P. D., Winship, P. D., and Reid, H. J. (2004). Silver nanoparticles and polymeric medical devices: a new approach to prevention of infection? *J Antimicrob Chemother* 54, 1019-24.

Galal, I., and El-Hindawy, K. (2011). Impact of using triclosan-antibacterial sutures on incidence of surgical site infection. *Am J Surg* 202, 133-8.

Gamelli, R. L., Paxton, T. P., and O'Reilly, M. (1993). Bone marrow toxicity by silver sulfadiazine. *Surg Gynecol Obstet* 177, 115-20.

Garcia-Gareta, E., Hua, J., Knowles, J. C., and Blunn, G. W. (2013). Comparison of mesenchymal stem cell proliferation and differentiation between biomimetic and electrochemical coatings on different topographic surfaces. *J Mater Sci Mater Med* 24, 199-210.

Garcia-Gareta, E., Hua, J., Rayan, F., and Blunn, G. W. (2014). Stem cell engineered bone with calcium-phosphate coated porous titanium scaffold or silicon hydroxyapatite granules for revision total joint arthroplasty. *J Mater Sci Mater Med* 25, 1553-62.

Geetha, M., Singh, A.K., Asokamani, R., and Gogia, A.K. (2009). Ti based biomaterials, the ultimate choice for orthopaedic implants - A review. *Prog Mat Sci* 54, 397-425.

Gendaszewska-Darmach, E., and Kucharska, M. (2011). Nucleotide receptors as targets in the pharmacological enhancement of dermal wound healing. *Purinergic Signal* 7, 193-206.

Ghani, Y., Coathup, M. J., Hing, K. A., and Blunn, G. W. (2012). Development of a hydroxyapatite coating containing silver for the prevention of peri-prosthetic infection. *J Orthop Res* 30, 356-63.

The Global Lower Extremity Amputation Study Group. (2000). Epidemiology of lower extremity amputation in centres in Europe, North America and East Asia. . *Br J Surg* 87, 328-337.

Gong, X., Anderson, T., and Chou, K. (2014). Review on powder-based electron beam additive manufacturing technology. *Manufacturing Rev* 1, 1-12.

Gordon, D. J., Bhagawati, D. D., Pendegrass, C. J., Middleton, C. A., and Blunn, G. W. (2010). Modification of titanium alloy surfaces for percutaneous implants by covalently attaching laminin. *J Biomed Mater Res A* 94, 586-93.

Gori, F., Hofbauer, L. C., Dunstan, C. R., Spelsberg, T. C., Khosla, S., and Riggs, B. L. (2000). The expression of osteoprotegerin and RANK ligand and the support of osteoclast formation by stromal-osteoblast lineage cells is developmentally regulated. *Endocrinology* 141, 4768-76.

Gosain, A., and DiPietro, L. A. (2004). Aging and wound healing. *World J Surg* 28, 321-6.

Gosden, P. E., MacGowan, A. P., and Bannister, G. C. (1998). Importance of air quality and related factors in the prevention of infection in orthopaedic implant surgery. *J Hosp Infect* 39, 173-80.

Gosheger, G., Hardes, J., Ahrens, H., Streitburger, A., Buerger, H., Erren, M., Gunsel, A., Kemper, F. H., Winkelmann, W., and Von Eiff, C. (2004). Silver-coated megaendoprostheses in a rabbit model--an analysis of the infection rate and toxicological side effects. *Biomaterials* 25, 5547-56.

Granstrom, G. (2007). Craniofacial osseointegration. *Oral Dis* 13, 261-9.

Grinnell, F. (1984). Fibronectin and wound healing. *J Cell Biochem* 26, 107-16.

Gristina, A. G. (1987). Biomaterial-centered infection: microbial adhesion versus tissue integration. *Science* 237, 1588-95.

Gristina, A. G., Naylor, P., and Myrvik, Q. (1988). Infections from biomaterials and implants: a race for the surface. *Med Prog Technol* 14, 205-24.

Gron, B., Stoltze, K., Andersson, A., and Dabelsteen, E. (2002). Oral fibroblasts produce more HGF and KGF than skin fibroblasts in response to co-culture with keratinocytes. *APMIS* 110, 892-8.

Guerrero, D. M., Perez, F., Conger, N. G., Solomkin, J. S., Adams, M. D., Rather, P. N., and Bonomo, R. A. (2010). Acinetobacter baumannii-associated skin and soft tissue infections: recognizing a broadening spectrum of disease. *Surg Infect (Larchmt)* 11, 49-57.

Guggenbichler, J.-P., Boswald, S., Lagauer, S., and Krall, T. (1999). A New Technology of Microdispersed Silver in Polyurethane Induces Antimicrobial Activity in Central Venous Catheters. *Infection* 27, S16-S23.

Guo, C. Y., Matinlinna, J. P., and Tang, A. T. (2012). Effects of surface charges on dental implants: past, present, and future. *Int J Biomater* 2012, 381535.

Guo, S., and Dipietro, L. A. (2010). Factors affecting wound healing. *J Dent Res* 89, 219-29.

Gupta, A., Pollock, R., Cannon, S. R., Briggs, T. W., Skinner, J., and Blunn, G. (2006). A knee-sparing distal femoral endoprosthesis using hydroxyapatite-coated extracortical plates. Preliminary results. *J Bone Joint Surg Br* 88, 1367-72.

Gutacker, N., Neumann, A., Santosa, F., Moysidis, T., and Kroger, K. (2010). Amputations in PAD patients: data from the German Federal Statistical Office. *Vasc Med* 15, 9-14.

Hacking, S. A., Bobyn, J. D., Toh, K., Tanzer, M., and Krygier, J. J. (2000). Fibrous tissue ingrowth and attachment to porous tantalum. *J Biomed Mater Res* 52, 631-8.

Hagberg, K., and Brånemark, R. (2001). Consequences of non-vascular trans-femoral amputation: a survey of quality of life, prosthetic use and problems. *Prosthet Orthot Int* 25, 186-94.

Hagberg, K., and Brånemark, R. (2009). One hundred patients treated with osseointegrated transfemoral amputation prostheses--rehabilitation perspective. *J Rehabil Res Dev* 46, 331-44.

Hagr, A. (2007). BAHA: Bone-Anchored Hearing Aid. *Int J Health Sci (Qassim)* 1, 265-76.

Hall-Stoodley, L., Costerton, J.W. and Stoodley, P. (2004). Bacterial biofilms: From the natural environment to infectious diseases. *Nature Reviews: Microbiology* 2:95-108.

Hansen, K. B., and Gottrup, F. (2014). Chronic Ulceration and Sinus Formation due to Foreign Body: An Often-Forgotten Problem. *Int J Low Extrem Wounds*.

Hardes, J., von Eiff, C., Streitbuerger, A., Balke, M., Budny, T., Henrichs, M. P., Hauschild, G., and Ahrens, H. (2010). Reduction of periprosthetic infection with silver-coated megaprostheses in patients with bone sarcoma. *J Surg Oncol* 101, 389-95.

Harker, J. (2006). Wound healing complications associated with lower limb amputation. *World Wide Wounds*. www.worldwidewounds.com/september/Harker/wound-healing-complications-limb-amputations.html

Harris, L. G., and Richards, R. G. (2006). Staphylococci and implant surfaces: a review. *Injury* 37 Suppl 2, S3-14.

Henderson, B., Nair, S., Pallas, J., and Williams, M. A. (2011). Fibronectin: a multidomain host adhesin targeted by bacterial fibronectin-binding proteins. *FEMS Microbiol Rev* 35, 147-200.

Herrmann, M., Vaudaux, P. E., Pittet, D., Auckenthaler, R., Lew, P. D., Schumacher-Perdreau, F., Peters, G., and Waldvogel, F. A. (1988). Fibronectin, fibrinogen, and laminin act as mediators of adherence of clinical staphylococcal isolates to foreign material. *J Infect Dis* 158, 693-701.

Hickok, N. J., and Shapiro, I. M. (2012). Immobilized antibiotics to prevent orthopaedic implant infections. *Adv Drug Deliv Rev* 64, 1165-76.

Hidalgo, E., and Dominguez, C. (1998). Study of cytotoxicity mechanisms of silver nitrate in human dermal fibroblasts. *Toxicol Lett* 98, 169-79.

Holman, N., Young, R. J., and Jeffcoate, W. J. (2012). Variation in the recorded incidence of amputation of the lower limb in England. *Diabetologia* 55, 1919-25.

Holt, B. M., Betz, D. H., Ford, T. A., Beck, J. P., Bloebaum, R. D., and Jeyapalina, S. (2013). Pig dorsum model for examining impaired wound healing at the skin-implant interface of percutaneous devices. *J Mater Sci Mater Med* 24, 2181-93.

Hotchin, N. A., and Hall, A. (1995). The assembly of integrin adhesion complexes requires both extracellular matrix and intracellular rho/rac GTPases. *J Cell Biol* 131, 1857-65.

Hu, Y., and Miao, X. (2004). Comparison of hydroxyapatite ceramics and hydroxyapatite/borosilicate glass composites prepared by slip casting. *Ceramics International* 30, 1787-1791.

Hulbert, S. F., Young, F. A., Mathews, R. S., Klawitter, J. J., Talbert, C. D., and Stelling, F. H. (1970). Potential of ceramic materials as permanently implantable skeletal prostheses. *J Biomed Mater Res* 4, 433-56.

Isackson, D., McGill, L. D., and Bachus, K. N. (2011). Percutaneous implants with porous titanium dermal barriers: an in vivo evaluation of infection risk. *Med Eng Phys* 33, 418-26.

Isefuku, S., Joyner, C.J., and Simpson, A.H. (2001). Toxic effect of rifampicin on human osteoblast-like cells. *J Orthop Res* 19, 950-954.

Isefuku, S., Joyner, C.J., Simpson, A.H. (2003). Gentamicin May Have an Adverse Effect on Osteogenesis. *J Orthop Trauma* 17, 212-216.

Jadalannagari, S., Deshmukh, K., Ramanan, S. R., and Kowshik, M. (2014). Antimicrobial activity of hemocompatible silver doped hydroxyapatite nanoparticles synthesized by modified sol-gel technique. *Appl Nanosci* 4, 133-141.

Jain, R. K., Au, P., Tam, J., Duda, D. G., and Fukumura, D. (2005). Engineering vascularized tissue. *Nat Biotechnol* 23, 821-3.

Jaiswal, S., McHale, P., and Duffy, B. (2012). Preparation and rapid analysis of antibacterial silver, copper and zinc doped sol-gel surfaces. *Colloids Surf B Biointerfaces* 94, 170-6.

Jeyapalina, S., Beck, J. P., Bachus, K. N., Williams, D. L., and Bloebaum, R. D. (2012). Efficacy of a porous-structured titanium subdermal barrier for preventing infection in percutaneous osseointegrated prostheses. *J Orthop Res* 30, 1304-11.

Johansson, S., Svineng, G., Wennerberg, K., Armulik, A., and Lohikangas, L. (1997). Fibronectin-integrin interactions. *Front Biosci* 2, d126-46.

Juan, L., Zhimin, Z., Anchun, M., Lei, L., and Jingchao, Z. (2010). Deposition of silver nanoparticles on titanium surface for antibacterial effect. *Int J Nanomedicine* 5, 261-7.

Jupiter, J. B., Marent-Huber, M., and Group, L. C. P. S. (2009). Operative management of distal radial fractures with 2.4-millimeter locking plates. A multicenter prospective case series. *J Bone Joint Surg Am* 91, 55-65.

Kalfas, I. H. (2001). Principles of bone healing. *Neurosurg Focus* 10, E1.

Kalicke, T., Schierholz, J., Schlegel, U., Frangen, T. M., Koller, M., Printzen, G., Seybold, D., Klockner, S., Muhr, G., and Arens, S. (2006). Effect on infection resistance of a local antiseptic and antibiotic coating on osteosynthesis implants: an in vitro and in vivo study. *J Orthop Res* 24, 1622-40.

Kang, N. V., Pendegrass, C., Marks, L., and Blunn, G. (2010). Osseocutaneous integration of an intraosseous transcutaneous amputation prosthesis implant used for reconstruction of a transhumeral amputee: case report. *J Hand Surg Am* 35, 1130-4.

Kanitakis, J. (2002). Anatomy, histology and immunohistochemistry of normal human skin. *Eur J Dermatol* 12, 390-401.

Karageorgiou, V., and Kaplan, D. (2005). Porosity of 3D biomaterial scaffolds and osteogenesis. *Biomaterials* 26, 5474-91.

Kawahara, K., Tsuruda, K., Morishita, M., and Uchida, M. (2000). Antibacterial effect of silver-zeolite on oral bacteria under anaerobic conditions. *Dent Mater* 16, 452-5.

Kay, M. I., Young, R. A., and Posner, A. S. (1964). Crystal Structure of Hydroxyapatite. *Nature* 204, 1050-2.

Kim, H., Murakami, H., Chehroudi, B., Textor, M., and Brunette, D. M. (2006). Effects of surface topography on the connective tissue attachment to subcutaneous implants. *Int J Oral Maxillofac Implants* 21, 354-65.

Kim, P.S., Ko, J., O'Shaughnessy, K.O., Kuiken, T.A., Dumanian, G.A. (2010). Novel model for end-neuroma formation in the amputated rabbit forelimb. *J Brachial Plex Peripher Nerve Inj* 5:6.

Kim, S. H., Ha, H. J., Ko, Y. K., Yoon, S. J., Rhee, J. M., Kim, M. S., Lee, H. B., and Khang, G. (2007). Correlation of proliferation, morphology and biological responses of fibroblasts on LDPE with different surface wettability. *J Biomater Sci Polym Ed* 18, 609-22.

Kinnari, T. J., Peltonen, L. I., Kuusela, P., Kivilahti, J., Kononen, M., and Jero, J. (2005). Bacterial adherence to titanium surface coated with human serum albumin. *Otol Neurotol* 26, 380-4.

Kitsugi, T., Yamamuro, T., Nakamura, T., Kotani, S., Kokubo, T., and Takeuchi, H. (1993). Four calcium phosphate ceramics as bone substitutes for non-weight-bearing. *Biomaterials* 14, 216-24.

Koc, E., Tunca, M., Akar, A., Erbil, A. H., Demiralp, B., and Arca, E. (2008). Skin problems in amputees: a descriptive study. *Int J Dermatol* 47, 463-6.

Koike, M., Greer, P., Owen, K., Guo, L., Murr, L. E., Gaytan, S. M., Martinez, E., and Okabe, T. (2011a). Evaluation of Titanium Alloys Fabricated Using Rapid Prototyping Technologies—Electron Beam Melting and Laser Beam Melting. *Materials* 4, 1776-1792.

Koike, M., Martinez, K., Guo, L., Chahine, G., Kovacevic, R., and Okabe, T. (2011b). Evaluation of titanium alloy fabricated using electron beam melting system for dental applications. *Journal of Materials Processing Technology* 211, 1400-1408.

Kokubo, T. (1998). Apatite formation on surfaces of ceramics, metals and polymers in body environment. *Acta Mater* 46, 2519-2527.

Kokubo, T., Kushitani, H., Sakka, S., Kitsugi, T., and Yamamuro, T. (1990). Solutions able to reproduce in vivo surface-structure changes in bioactive glass-ceramic A-W. *J Biomed Mater Res* 24, 721-34.

Krishnan, S., Nash, F., Baker, N., Fowler, D., and Rayman, G. (2008). Reduction in diabetic amputations over 11 years in a defined U.K. population: benefits of multidisciplinary team work and continuous prospective audit. *Diabetes Care* 31, 99-101.

Krueger, C. A., Wenke, J. C., and Ficke, J. R. (2012). Ten years at war: comprehensive analysis of amputation trends. *J Trauma Acute Care Surg* 73, S438-44.

Kuboki, Y., Takita, H., Kobayashi, D., Tsuruga, E., Inoue, M., Murata, M., Nagai, N., Dohi, Y., and Ohgushi, H. (1998). BMP-induced osteogenesis on the surface of hydroxyapatite with geometrically feasible and nonfeasible structures: topology of osteogenesis. *J Biomed Mater Res* 39, 190-9.

Kunzler, T. P., Drobek, T., Schuler, M., and Spencer, N. D. (2007). Systematic study of osteoblast and fibroblast response to roughness by means of surface-morphology gradients. *Biomaterials* 28, 2175-82.

LaBerge, M., Bobyn, J. D., Rivard, C. H., Drouin, G., and Duval, P. (1990). Study of soft tissue ingrowth into canine porous coated femoral implants designed for osteosarcomas management. *J Biomed Mater Res* 24, 959-71.

Lansdown, A. B. (2010). A pharmacological and toxicological profile of silver as an antimicrobial agent in medical devices. *Adv Pharmacol Sci* 2010, 910686.

Larsson, A., Wigren, S., Andersson, M., Ekeroth, G., Flynn, M., and Nannmark, U. (2012). Histologic evaluation of soft tissue integration of experimental abutments for bone anchored hearing implants using surgery without soft tissue reduction. *Otol Neurotol* 33, 1445-51.

Larsson, J., Eneroth, M., Apelqvist, J., and Stenstrom, A. (2008). Sustained reduction in major amputations in diabetic patients: 628 amputations in 461 patients in a defined population over a 20-year period. *Acta Orthop* 79, 665-73.

Laure, B., Besnier, J. M., Bergemer-Fouquet, A. M., Marquet-Van Der Mee, N., Damie, F., Quentin, R., Favard, L., and Rosset, P. (2008). Effect of hydroxyapatite coating and polymethylmethacrylate on stainless steel implant-site infection with Staphylococcus epidermidis in a sheep model. *J Biomed Mater Res A* 84, 92-8.

Lee, J. H., Khang, G., Lee, J. W., and Lee, H. B. (1998). Interaction of Different Types of Cells on Polymer Surfaces with Wettability Gradient. *J Colloid Interface Sci* 205, 323-330.

Lewis, K. (2007). Persister cells, dormancy and infectious disease. *Nat Rev Microbiol* 5, 48-56.

Limb Loss Research and Statistics Programme. (2006). People with amputation speak out. Amputee Coalition of America.

Limbless Statistics, United National Institute for Prosthetics & Orthotics Development. (Annual Report 2010-2011). University of Salford, Manchester.

Lopez-Santos, C., Fernandez-Gutierrez, M., Yubero, F., Vazquez-Lasa, B., Cotrino, J., Gonzalez-Elipe, A., and Roman, J. S. (2013). Effects of plasma surface treatments of diamond-like carbon and polymeric substrata on the cellular behavior of human fibroblasts. *J Biomater Appl* 27, 669-83.

Lu, X., Zhang, B., Wang, Y., Zhou, X., Weng, J., Qu, S., Feng, B., Watari, F., Ding, Y., and Leng, Y. (2011). Nano-Ag-loaded hydroxyapatite coatings on titanium surfaces by electrochemical deposition. *J R Soc Interface* 8, 529-39.

Lundborg, G., Brånemark, P. I., and Rosen, B. (1996). Osseointegrated thumb prostheses: a concept for fixation of digit prosthetic devices. *J Hand Surg Am* 21, 216-21.

Lydon, M. J., and Clay, C. S. (1985). Substratum topography and cell traction on sulphuric acid treated bacteriological-grade plastic. *Cell Biol Int Rep* 9, 911-21.

Maddikeri, R. R., Tosatti, S., Schuler, M., Chessari, S., Textor, M., Richards, R. G., and Harris, L. G. (2008). Reduced medical infection related bacterial strains

adhesion on bioactive RGD modified titanium surfaces: a first step toward cell selective surfaces. *J Biomed Mater Res A* 84, 425-35.

Mah, T. F. (2012). Biofilm-specific antibiotic resistance. *Future Microbiol* 7, 1061-72.

Manley, M. T., Capello, W. N., D'Antonio, J. A., Edidin, A. A., and Geesink, R. G. (1998). Fixation of acetabular cups without cement in total hip arthroplasty. A comparison of three different implant surfaces at a minimum duration of follow-up of five years. *J Bone Joint Surg Am* 80, 1175-85.

Manring, M.M., Hawk, A., Calhoun, J.H., Andersen, R.C. (2009). Treatment of War Wounds A Historical Review. *Clin Orthop Relat Res* 467, 2168-2191

Manurangsee, P., Isariyawut, C., Chatuthong, V., and Mekraksawanit, S. (2000). Osseointegrated finger prosthesis: An alternative method for finger reconstruction. *J Hand Surg Am* 25, 86-92.

Marinucci, L., Balloni, S., Becchetti, E., Belcastro, S., Guerra, M., Calvitti, M., Lilli, C., Calvi, E. M., and Locci, P. (2006). Effect of titanium surface roughness on human osteoblast proliferation and gene expression in vitro. *Int J Oral Maxillofac Implants* 21, 719-25.

Marks, L. J., and Michael, J. W. (2001). Science, medicine, and the future: Artificial limbs. *BMJ* 323, 732-5.

Masse, A., Bruno, A., Bosetti, M., Biasibetti, A., Cannas, M., and Gallinaro, P. (2000). Prevention of pin track infection in external fixation with silver coated pins: clinical and microbiological results. *J Biomed Mater Res* 53, 600-4.

Mathew, D., Bhardwaj, G., Wang, Q., Sun, L., Ercan, B., Geetha, M., and Webster, T. J. (2014). Decreased Staphylococcus aureus and increased osteoblast

density on nanostructured electrophoretic-deposited hydroxyapatite on titanium without the use of pharmaceuticals. *Int J Nanomedicine* 9, 1775-81.

Mavrogenis, A. F., Dimitriou, R., Parvizi, J., and Babis, G. C. (2009). Biology of implant osseointegration. *J Musculoskelet Neuronal Interact* 9, 61-71.

McBeath, R., Pirone, D.M., Nelson, C.M., Bhadriraju, K., and Chen, C.S. (2004). Cell shape, cytoskeletal tension, and RhoA regulate stem cell lineage commitment. *Dev Cell* 6, 483-95.

Mendonça, G., Mendonça, D.B., Simões, L.G., Araùjo, A.L., Leite, E.R., Duarte, W.R., Aragào, F.J., and Cooper, L.F. (2009). The effects of implant surface nanoscale features on osteoblast-specific gene expression. *Biomaterials* 30, 4053-4062.

Meulenbelt, H. E. J., Geertzen, J. H. B., Jonkman, M. F., and Dijkstra, P. U. (2011). Skin Problems of the Stump in Lower Limb Amputees: 1. A Clinical Study. *Acta Derm Venereol*, 173-177.

Middleton, C. A., Pendegrass, C. J., Gordon, D., Jacob, J., and Blunn, G. W. (2007). Fibronectin silanized titanium alloy: a bioinductive and durable coating to enhance fibroblast attachment in vitro. *J Biomed Mater Res A* 83, 1032-8.

Miller, P.D. and Holladay, J.W. (1958). Friction and Wear Properties of Titanium. *Wear* 2:133-140.

Modak, S. M., and Fox, C. L., Jr. (1973). Binding of silver sulfadiazine to the cellular components of Pseudomonas aeruginosa. *Biochem Pharmacol* 22, 2391-404.

Mohammad, S. F., Topham, N. S., Burns, G. L., and Olsen, D. B. (1988). Enhanced bacterial adhesion on surfaces pretreated with fibrinogen and fibronectin. *ASAIO Trans* 34, 573-7.

Moojen, D. J., Vogely, H. C., Fleer, A., Nikkels, P. G., Higham, P. A., Verbout, A. J., Castelein, R. M., and Dhert, W. J. (2009). Prophylaxis of infection and effects on osseointegration using a tobramycin-periapatite coating on titanium implants--an experimental study in the rabbit. *J Orthop Res* 27, 710-6.

Mooney, V., Schwartz, S. A., Roth, A. M., and Gorniowsky, M. J. (1977). Percutaneous implant devices. *Ann Biomed Eng* 5, 34-46.

Moran, E., Byren, I., and Atkins, B. L. (2010). The diagnosis and management of prosthetic joint infections. *J Antimicrob Chemother* 65 Suppl 3, iii45-54.

Moroni, A., Heikkila, J., Magyar, G., Toksvig-Larsen, S., and Giannini, S. (2001). Fixation strength and pin tract infection of hydroxyapatite-coated tapered pins. *Clin Orthop Relat Res*, 209-17.

Mortazavi, S. M., Schwartzenberger, J., Austin, M. S., Purtill, J. J., and Parvizi, J. (2010). Revision total knee arthroplasty infection: incidence and predictors. *Clin Orthop Relat Res* 468, 2052-9.

Mosher, D. F. (1984). Physiology of fibronectin. *Annu Rev Med* 35, 561-75.

Moskowitz, J. S., Blaisse, M. R., Samuel, R. E., Hsu, H. P., Harris, M. B., Martin, S. D., Lee, J. C., Spector, M., and Hammond, P. T. (2010). The effectiveness of the controlled release of gentamicin from polyelectrolyte multilayers in the treatment of Staphylococcus aureus infection in a rabbit bone model. *Biomaterials* 31, 6019-30.

Mudgal, C. S., and Jupiter, J. B. (2006). Plate and screw design in fractures of the hand and wrist. *Clin Orthop Relat Res* 445, 68-80.

Murakami, A., Arimoto, T., Suzuki, D., Iwai-Yoshida, M., Otsuka, F., Shibata, Y., Igarashi, T., Kamijo, R., and Miyazaki, T. (2012). Antimicrobial and

osteogenic properties of a hydrophilic-modified nanoscale hydroxyapatite coating on titanium. *Nanomedicine: Nanotechnology, Biology, and Medicine* 8, 374-382.

Murphy, C. M., and O'Brien, F. J. (2010). Understanding the effect of mean pore size on cell activity in collagen-glycosaminoglycan scaffolds. *Cell Adh Migr* 4, 377-81.

Murugan, R., and Ramakrishna, S. (2005). Development of nanocomposites for bone grafting. *Composites Science and Technology* 65, 2385-2406.

Muszanska, A. K., Rochford, E. T., Gruszka, A., Bastian, A. A., Busscher, H. J., Norde, W., van der Mei, H. C., and Herrmann, A. (2014). Antiadhesive polymer brush coating functionalized with antimicrobial and RGD peptides to reduce biofilm formation and enhance tissue integration. *Biomacromolecules* 15, 2019-26.

Myers, G. J., Abudu, A. T., Carter, S. R., Tillman, R. M., and Grimer, R. J. (2007). Endoprosthetic replacement of the distal femur for bone tumours: long-term results. *J Bone Joint Surg Br* 89, 521-6.

Nadell, C. D., Xavier, J. B., Levin, S. A., and Foster, K. R. (2008). The evolution of quorum sensing in bacterial biofilms. *PLoS Biol* 6, e14.

Navarro, M.I., Michiardi, A., Castaño, O., Planell, J.A. (2008). Biomaterials in orthopaedics. *J R Soc Interface* 5(27):1137-58.

Nebergall A, Bragdon C, Antonellis A, Kärrholm J, Brånemark R, and H., M. (2012). Stable fixation of an osseointegated implant system for above-the-knee amputees: titel RSA and radiographic evaluation of migration and bone remodeling in 55 cases. *Acta Orthop* 83, 121-8.

Neut, D., Dijkstra, R. J., Thompson, J. I., van der Mei, H. C., and Busscher, H. J. (2012). A gentamicin-releasing coating for cementless hip prostheses-Longitudinal

evaluation of efficacy using in vitro bio-optical imaging and its wide-spectrum antibacterial efficacy. *J Biomed Mater Res A* 100, 3220-6.

Neut, D., Hendriks, J. G., van Horn, J. R., van der Mei, H. C., and Busscher, H. J. (2005). Pseudomonas aeruginosa biofilm formation and slime excretion on antibiotic-loaded bone cement. *Acta Orthop* 76, 109-14.

Newcombe, L., Dewar, M., Blunn, G. W., and Fromme, P. (2013). Effect of amputation level on the stress transferred to the femur by an artificial limb directly attached to the bone. *Med Eng Phys* 35, 1744-53.

Niakan, M., Azimi, H. R., Jafarian, Z., Mohammadtaghi, G., Niakan, S., and Mostafavizade, S. M. (2013). Evaluation of Nanosilver Solution Stability against Streptococcus mutans, Staphylococcus aureus and Pseudomonas aeruginosa. *Jundishapur J Microbiol* 6, e8570.

Nishimura, R. D., Roumanas, E., Sugai, T., and Moy, P. K. (1995). Auricular prostheses and osseointegrated implants: UCLA experience. *J Prosthet Dent* 73, 553-8.

O'Brien, F. J., Harley, B. A., Waller, M. A., Yannas, I. V., Gibson, L. J., and Prendergast, P. J. (2007). The effect of pore size on permeability and cell attachment in collagen scaffolds for tissue engineering. *Technol Health Care* 15, 3-17.

O'Leary, M. (n.d.). ITAP. Amputee Adventures. http://www.amputee-adventures.org/about/itap.

Oddy, M. J., Pendegrass, C. J., Goodship, A. E., Cannon, S. R., Briggs, T. W., and Blunn, G. W. (2005). Extensor mechanism reconstruction after proximal tibial replacement. *J Bone Joint Surg Br* 87, 873-8.

Odermatt, E., Tamkun, J. W., and Hynes, R. O. (1985). Repeating modular structure of the fibronectin gene: relationship to protein structure and subunit variation. *Proc Natl Acad Sci U S A* 82, 6571-5.

Oei, J. D., Zhao, W. W., Chu, L., DeSilva, M. N., Ghimire, A., Rawls, H. R., and Whang, K. (2012). Antimicrobial acrylic materials with in situ generated silver nanoparticles. *J Biomed Mater Res B Appl Biomater* 100, 409-15.

Oga, M., Arizono, T., and Sugioka, Y. (1993). Bacterial adherence to bioinert and bioactive materials studied in vitro. *Acta Orthop Scand* 64, 273-6.

Okada, N., Nakamura, T., Ambo, Y., Takada, M., Nakamura, F., Kishida, A., and Kashimura, N. (2014). Triclosan-coated abdominal closure sutures reduce the incidence of surgical site infections after pancreaticoduodenectomy. *Surg Infect (Larchmt)* 15, 305-9.

Opalchenova, G., Dyulgerova, E., and Petrov, O. E. (1996a). Effect of calcium phosphate ceramics on gram-negative bacteria resistant to antibiotics. *J Biomed Mater Res* 32, 473-9.

Opalchenova, G., Dyulgerova, E., and Petrov, O. E. (1996b). A study of the influence of biphase calcium phosphate ceramics on bacterial strains: in vitro approach. *J Biomed Mater Res* 31, 219-26.

Osathanon, T., Bespinyowong, K., Arksornnukit, M., Takahashi, H., and Pavasant, P. (2011). Human osteoblast-like cell spreading and proliferation on Ti-6Al-7Nb surfaces of varying roughness. *J Oral Sci* 53, 23-30.

Overgaard, S., Bromose, U., Lind, M., Bunger, C., and Soballe, K. (1999). The influence of crystallinity of the hydroxyapatite coating on the fixation of implants. Mechanical and histomorphometric results. *J Bone Joint Surg Br* 81, 725-31.

Pankov, R., and Yamada, K. M. (2002). Fibronectin at a glance. *J Cell Sci* 115, 3861-3.

Parameswaran, A. D., Roberts, C. S., Seligson, D., and Voor, M. (2003). Pin tract infection with contemporary external fixation: how much of a problem? *J Orthop Trauma* 17, 503-7.

Parthasarathy, J., Starly, B., Raman, S., and Christensen, A. (2010). Mechanical evaluation of porous titanium (Ti6Al4V) structures with electron beam melting (EBM). *J Mech Behav Biomed Mater* 3, 249-59.

Pascual, A., Fleer, A., Westerdaal, N. A., and Verhoef, J. (1986). Modulation of adherence of coagulase-negative staphylococci to Teflon catheters in vitro. *Eur J Clin Microbiol* 5, 518-22.

Paulsson, M., Kober, M., Freij-Larsson, C., Stollenwerk, M., Wesslen, B., and Ljungh, A. (1993). Adhesion of staphylococci to chemically modified and native polymers, and the influence of preadsorbed fibronectin, vitronectin and fibrinogen. *Biomaterials* 14, 845-53.

Pendegrass, C. J., Goodship, A. E., and Blunn, G. W. (2006a). Development of a soft tissue seal around bone-anchored transcutaneous amputation prostheses. *Biomaterials* 27, 4183-91.

Pendegrass, C. J., Goodship, A. E., Price, J. S., and Blunn, G. W. (2006b). Nature's answer to breaching the skin barrier: an innovative development for amputees. *J Anat* 209, 59-67.

Pendegrass, C. J., Middleton, C., and Blunn, W. (2010a). Fibronectin Functionalized Hydroxyapatite Coatings: Improving Dermal Fibroblast Adhesion In Vitro and In Vivo. *Advanced Engineering Materials* 12, B365-B373.

Pendegrass, C. J., Middleton, C. A., Gordon, D., Jacob, J., and Blunn, G. W. (2010b). Measuring the strength of dermal fibroblast attachment to functionalized titanium alloys in vitro. *J Biomed Mater Res A* 92, 1028-37.

Pendegrass, C. J., Tucker, B., Patel, S., Dowling, R., and Blunn, G. W. (2012a). The effect of adherens junction components on keratinocyte adhesion in vitro: potential implications for sealing the skin-implant interface of intraosseous transcutaneous amputation prostheses. *J Biomed Mater Res A* 100, 3463-71.

Pendegrass, C. J., El-Husseiny, M., and Blunn, G. W. (2012b). The development of fibronectin-functionalised hydroxyapatite coatings to improve dermal fibroblast attachment in vitro. *J Bone Joint Surg Br* 94, 564-9.

Pendegrass, C. J., Lancashire, H. T., Fontaine, C., Chan, G., Hosseini, P., and Blunn, G. W. (2015). Intraosseous transcutaneous amputation prostheses versus dental implants: a comparison between keratinocyte and gingival epithelial cell adhesion in vitro. *Eur Cell Mater* 29, 237-49.

Pennisi, C. P., Dolatshahi-Pirouz, A., Foss, M., Chevallier, J., Fink, T., Zachar, V., Besenbacher, F., and Yoshida, K. (2011). Nanoscale topography reduces fibroblast growth, focal adhesion size and migration-related gene expression on platinum surfaces. *Colloids Surf B Biointerfaces* 85, 189-97.

Percival, S. L., Slone, W., Linton, S., Okel, T., Corum, L., and Thomas, J. G. (2011). The antimicrobial efficacy of a silver alginate dressing against a broad spectrum of clinically relevant wound isolates. *Int Wound J* 8, 237-43.

Perrelli, G., and Piolatto, G. (1992). Tentative reference values for gold, silver and platinum: literature data analysis. *Sci Total Environ* 120, 93-96.

Petering, H. (1976). Pharmacology and Toxicology of Heavy Metals: Silver. *Pharmac Ther* 1, 127-130.

Piatelli, A., Cordioli, G. P., Trisi, P., Passi, P., Favero, G. A., and Meffert, R. M. (1993). Light and Confocal Laser Scanning Microscopic Evaluation of Hydroxyapatite Resorption Patterns in Medullary and Cortical Bone. *Int J Oral Maxillofac Implants* 8, 309-315.

Pitkin, M. (2013). Design features of implants for direct skeletal attachment of limb prostheses. *J Biomed Mater Res A* 101, 3339-48.

Piza, G., Caja, V. L., Gonzalez-Viejo, M. A., and Navarro, A. (2004). Hydroxyapatite-coated external-fixation pins. The effect on pin loosening and pin-track infection in leg lengthening for short stature. *J Bone Joint Surg Br* 86, 892-7.

Plotkowski, M.-C., Filho, M. B., de Nazareth Meirelles, M., Tournier, J. M., and Puchelle, E. (1993). Pseudomonas aeruginosa Binds to Soluble Cellular Fibronectin. *Current Microbiology* 26, 91-95.

Pocock, G., and Richards, C. D. (2004). Human Physiology: The Basis of Medicine. 2nd Edition. Oxford University Press.

Politano, A. D., Campbell, K. T., Rosenberger, L. H., and Sawyer, R. G. (2013). Use of silver in the prevention and treatment of infections: silver review. *Surg Infect (Larchmt)* 14, 8-20.

Prigent-Combaret, C., Vidal, O., Dorel, C., and Lejeune, P. (1999). Abiotic surface sensing and biofilm-dependent regulation of gene expression in Escherichia coli. *J Bacteriol* 181, 5993-6002.

Proctor, R. A. (1987). Fibronectin: a brief overview of its structure, function, and physiology. *Rev Infect Dis* 9 Suppl 4, S317-21.

Prokopovich, P., Kobrick, M., Brousseau, E., and Perni, S. (2015). Potent antimicrobial activity of bone cement encapsulating silver nanoparticles capped with oleic acid. *J Biomed Mater Res B Appl Biomater* 103, 273-81.

Prokopovich, P., Leech, R., Carmalt, C. J., Parkin, I. P., and Perni, S. (2013). A novel bone cement impregnated with silver-tiopronin nanoparticles: its antimicrobial, cytotoxic, and mechanical properties. *Int J Nanomedicine* 8, 2227-37.

Prosser, B. L., Taylor, D., Dix, B. A., and Cleeland, R. (1987). Method of evaluating effects of antibiotics on bacterial biofilm. *Antimicrob Agents Chemother* 31, 1502-6.

Qu, J., Lu, X., Li, D., Ding, Y., Leng, Y., Weng, J., Qu, S., Feng, B., and Watari, F. (2011). Silver/hydroxyapatite composite coatings on porous titanium surfaces by sol-gel method. *J Biomed Mater Res B Appl Biomater* 97, 40-8.

Ranella, A., Barberoglou, M., Bakogianni, S., Fotakis, C., and Stratakis, E. (2010). Tuning cell adhesion by controlling the roughness and wettability of 3D micro/nano silicon structures. *Acta Biomater* 6, 2711-20.

Rathbone, C.R., Cross, J.D., Brown, K.V., Murray, C.K., and Wenke, J.C. (2011). Effect of Various Concentrations of Antibiotics on Osteogenic Cell Viability and Activity. *J Orthop Res* 29, 1070-1074.

Reach, J. S., Jr., Dickey, I. D., Zobitz, M. E., Adams, J. E., Scully, S. P., and Lewallen, D. G. (2007). Direct tendon attachment and healing to porous tantalum: an experimental animal study. *J Bone Joint Surg Am* 89, 1000-9.

Redepenning, J., Schlessinger, T., Burnham, S., Lippiello, L., and Miyano, J. (1996). Characterization of electrolytically prepared brushite and hydroxyapatite coatings on orthopedic alloys. *J Biomed Mater Res* 30, 287-94.

Reinke, J. M., and Sorg, H. (2012). Wound repair and regeneration. *Eur Surg Res* 49, 35-43.

Renner, L.D., and Weibel, D.B. (2011). Physicochemical regulation of biofilm formation. *MRS Bull* 36(5):347-355.

Ribeiro, M., Monteiro, F. J., and Ferraz, M. P. (2012). Infection of orthopedic implants with emphasis on bacterial adhesion process and techniques used in studying bacterial-material interactions. *Biomatter* 2, 176-194.

Rodemann, P. H., and Rennekampff, H.-O. (2011). Functional diversity of fibroblasts. *In* "Tumor-Associated Fibroblasts and their Matrix" (M. Mueller and N. Fusenig, eds.), pp. 22-36. Springer, New York.

Rosa, A.L., Kato, R.B., Castro Raucci, L.M., Teixeira, L.N., de Oliveira, F.S., Bellesini, L.S., de Oliveira, P.T., Hassan, M.Q., and Beloti, M.M. (2014). Nanotopography drives stem cell fate toward osteoblast differentiation through α1β1 integrin signaling pathway. *J Cell Biochem* 115, 540-548.

Ruoslahti, E., and Pierschbacher, M. D. (1987). New perspectives in cell adhesion: RGD and integrins. *Science* 238, 491-7.

Ryan, G., Pandit, A., and Apatsidis, D. P. (2006). Fabrication methods of porous metals for use in orthopaedic applications. *Biomaterials* 27, 2651-70.

Saijid, M. S., Craciunas, L., Sains, P., Singh, K. K., and Baig, M. K. (2013). Use of antibacterial sutures for skin closure in controlling surgical site infections: a systematic review of published randomized, controlled trials. *Gastroenterology Report* 1, 42-50.

Sandrucci, M. A., Nicolin, L., Casagrande, L., Biasotto, M., Breschi, L., Di Lenarda, R., Sancilio, S., and Grill, V. (2005). Preconditioning of dental alloys: Analysis of fibroblast proliferation and expression of fibronectin and chondroitin sulfate. *J Mater Sci Lett* 40, 6233-6240.

Sawyer, A. A., Hennessy, K. M., and Bellis, S. L. (2005). Regulation of mesenchymal stem cell attachment and spreading on hydroxyapatite by RGD peptides and adsorbed serum proteins. *Biomaterials* 26, 1467-75.

Schierholz, J. M., Lucas, L. J., Rump, A., and Pulverer, G. (1998). Efficacy of silver-coated medical devices. *J Hosp Infect* 40, 257-62.

Schonmeyr, B. H., Wong, A. K., Li, S., Gewalli, F., Cordiero, P. G., and Mehrara, B. J. (2008). Treatment of hydroxyapatite scaffolds with fibronectin and fetal calf serum increases osteoblast adhesion and proliferation in vitro. *Plast Reconstr Surg* 121, 751-62.

Schultz, G.S., Ladwig, G., Wysocki, A. (2005). Extracellular matrix: review of its roles in acute and chronic wounds. *World Wide Wounds*. www.worldwidewounds.com/2005/august/Schultz/Extrace-Matric-Acute-Chronic-Wounds.html

Seong, S., Younossi, O., Goldsmith, B.W., Lang, T. and Neumann, M.J. (2009). Titanium: Industrial Base, Price Trends, and Technology Initiatives. Santa Monica, CA: RAND Corporation. www.rand.org/pubs/monographs/MG789.

Serrano, C., Garcia-Fernandez, L., Fernandez-Blazquez, J. P., Barbeck, M., Ghanaati, S., Unger, R., Kirkpatrick, J., Arzt, E., Funk, L., Turon, P., and del Campo, A. (2015). Nanostructured medical sutures with antibacterial properties. *Biomaterials* 52, 291-300.

Shaw, W. J., Long, J. R., Dindot, J. L., Campbell, A. A., Stayton, P. S., and Drobny, G. P. (2000). Determination of Statherin N-Terminal Peptide Conformation on Hydroxyapatite Crystals. *J Am Chem Soc* 122, 1709-1716.

Sheehan, E., McKenna, J., Mulhall, K. J., Marks, P., and McCormack, D. (2004). Adhesion of Staphylococcus to orthopaedic metals, an in vivo study. *J Orthop Res* 22, 39-43.

Shen, J. W., Wu, T., Wang, Q., and Pan, H. H. (2008). Molecular simulation of protein adsorption and desorption on hydroxyapatite surfaces. *Biomaterials* 29, 513-32.

Shen, M., and Horbett, T. A. (2001). The effects of surface chemistry and adsorbed proteins on monocyte/macrophage adhesion to chemically modified polystyrene surfaces. *J Biomed Mater Res* 57, 336-45.

Shi, Z., Neoh, K. G., Kang, E. T., Poh, C., and Wang, W. (2008). Bacterial adhesion and osteoblast function on titanium with surface-grafted chitosan and immobilized RGD peptide. *J Biomed Mater Res A* 86, 865-72.

Shimazaki, T., Miyamoto, H., Ando, Y., Noda, I., Yonekura, Y., Kawano, S., Miyazaki, M., Mawatari, M., and Hotokebuchi, T. (2010). In vivo antibacterial and silver-releasing properties of novel thermal sprayed silver-containing hydroxyapatite coating. *J Biomed Mater Res B Appl Biomater* 92, 386-9.

Shin, Y., and Akao, M. (1997). Tissue Reactions to Various Percutaneous Materials with Different Surface Properties and Structures. *Artificial Organs* 21, 995-1001.

Sierakowski, A., Watts, C., Thomas, K., and Elliot, D. (2011). Long-term outcomes of osseointegrated digital prostheses for proximal amputations. *J Hand Surg Eur Vol* 36, 116-25.

Silver, S. (2003). Bacterial silver resistance: molecular biology and uses and misuses of silver compounds. *FEMS Microbiol Rev* 27, 341-53.

Simonet, W. S., Lacey, D. L., Dunstan, C. R., Kelley, M., Chang, M.-S., R. Lu ̈thy, R., Nguyen, H. Q., Wooden, S., Bennett, L., and Boyle, W. J. (1997). Osteoprotegerin: A Novel Secreted Protein Involved in the Regulation of Bone Density. *Cell* 89, 309-319.

Simpson, W. A., Hasty, D. L., and Beachey, E. H. (1985). Binding of fibronectin to human buccal epithelial cells inhibits the binding of type 1 fimbriated Escherichia coli. *Infect Immun* 48, 318-23.

Sinclair, K. D., Pham, T. X., Williams, D. L., Farnsworth, R. W., Loc-Carrillo, C. M., and Bloebaum, R. D. (2013). Model development for determining the efficacy of a combination coating for the prevention of perioperative device related infections: a pilot study. *J Biomed Mater Res B Appl Biomater* 101, 1143-53.

Singh, R., Ray, P., Das, A., and Sharma, M. (2009). Role of persisters and small-colony variants in antibiotic resistance of planktonic and biofilm-associated Staphylococcus aureus: an in vitro study. *J Med Microbiol* 58, 1067-73.

Singh, R., Ray, P., Das, A., and Sharma, M. (2010). Penetration of antibiotics through Staphylococcus aureus and Staphylococcus epidermidis biofilms. *J Antimicrob Chemother* 65, 1955-8.

Slomianka, L. (2009). Integumentary System: Dermis. In: Blue Histology Histology. School of Anatomy and Human Biology – The University of Western Australia. www.lab.anhb.uwa.edu.au.

Smith, J. L., Fratamico, P. M., and Novak, J. S. (2004). Quorum sensing: a primer for food microbiologists. *J Food Prot* 67, 1053-70.

Smith, T. J., Galm, A., Chatterjee, S., Wells, R., Pedersen, S., Parizi, A. M., Goodship, A. E., and Blunn, G. W. (2006). Modulation of the soft tissue reactions to percutaneous orthopaedic implants. *J Orthop Res* 24, 1377-83.

Sogo, Y., Ito, A., Matsuno, T., Oyane, A., Tamazawa, G., Satoh, T., Yamazaki, A., Uchimura, E., and Ohno, T. (2007). Fibronectin-calcium phosphate composite layer on hydroxyapatite to enhance adhesion, cell spread and osteogenic differentiation of human mesenchymal stem cells in vitro. *Biomed Mater* 2, 116-23.

Sonmez, K., Bahar, B., Karabulut, R., Gulbahar, O., Poyraz, A., Turkyilmaz, Z., Sancak, B., and Basaklar, A. C. (2009). Effects of different suture materials on wound healing and infection in subcutaneous closure techniques. *B-ENT* 5, 149-52.

Sonmez, S., Aksakal, B., and Dikici, B. (2014). Influence of hydroxyapatite coating thickness and powder particle size on corrosion performance of MA8M magnesium alloy. *J Alloys and Compounds* 596, 125-131.

Sorrell, J. M., and Caplan, A. I. (2004). Fibroblast heterogeneity: more than skin deep. *J Cell Sci* 117, 667-75.

Sousa, S. R., Moradas-Ferreira, P., and Barbosa, M. A. (2005). TiO2 type influences fibronectin adsorption. *J Mater Sci Mater Med* 16, 1173-8.

Spiegelberg, B. G., Sewell, M. D., Aston, W. J., Blunn, G. W., Pollock, R., Cannon, S. R., and Briggs, T. W. (2009). The early results of joint-sparing proximal tibial replacement for primary bone tumours, using extracortical plate fixation. *J Bone Joint Surg Br* 91, 1373-7.

Sridharan, G., and Shankar, A. A. (2012). Toluidine blue: A review of its chemistry and clinical utility. *J Oral Maxillofac Pathol* 16, 251-5.

Stanford, C. M., and Keller, J. C. (1991). The concept of osseointegration and bone matrix expression. *Crit Rev Oral Biol Med* 2, 83-101.

Stayton, P. S., Drobny, G. P., Shaw, W. J., Long, J. R., and Gilbert, M. (2003). Molecular recognition at the protein-hydroxyapatite interface. *Crit Rev Oral Biol Med* 14, 370-6.

Stephens, P., Davies, K. J., Occleston, N., Pleass, R. D., Kon, C., Daniels, J., Khaw, P. T., and Thomas, D. W. (2001). Skin and oral fibroblasts exhibit phenotypic differences in extracellular matrix reorganization and matrix metalloproteinase activity. *Br J Dermatology* 144, 229-237.

Stewart, P. S. (2002). Mechanisms of antibiotic resistance in bacterial biofilms. *Int J Med Microbiol* 292, 107-13.

Stewart, P. S., and Costerton, J. W. (2001). Antibiotic resistance of bacteria in biofilms. *Lancet* 358, 135-8.

Story, B. J., Wagner, W. R., Gaisser, D. M., Cook, S. D., and Rust-Dawicki, A. M. (1998). In vivo performance of a modified CSTi dental implant coating. *Int J Oral Maxillofac Implants* 13, 749-57.

Suarez, J., Griffin, W., Springer, B., Fehring, T., Mason, J. B., and Odum, S. (2008). Why do revision knee arthroplasties fail? *J Arthroplasty* 23, 99-103.

Subbiahdoss, G., Pidhatika, B., Coullerez, G., Charnley, M., Kuijer, R., van der Mei, H. C., Textor, M., and Busscher, H. J. (2010a). Bacterial biofilm formation versus mammalian cell growth on titanium-based mono- and bi-functional coating. *Eur Cell Mater* 19, 205-13.

Subbiahdoss, G., Grijpma, D. W., van der Mei, H. C., Busscher, H. J., and Kuijer, R. (2010b). Microbial biofilm growth versus tissue integration on

biomaterials with different wettabilities and a polymer-brush coating. *J Biomed Mater Res A* 94, 533-8.

Suci, P. A., Mittelman, M. W., Yu, F. P., and Geesey, G. G. (1994). Investigation of ciprofloxacin penetration into Pseudomonas aeruginosa biofilms. *Antimicrob Agents Chemother* 38, 2125-33.

Sullivan, J., Uden, M., Robinson, K. P., and Sooriakumaran, S. (2003). Rehabilitation of the trans-femoral amputee with an osseointegrated prosthesis: the United Kingdom experience. *Prosthet Orthot Int* 27, 114-20.

Sullivan, T. P., Eaglstein, W. H., Davis, S. C., and Mertz, P. (2001). The pig as a model for human wound healing. *Wound Repair Regen* 9, 66-76.

Sumner, D.R., Turner, T.M., Igloria, R., Urban, R.M., Galante, J.O. (1998). Functional adaptation and ingrowth of bone vary as a function of hip implant stiffness. *J Biomech* 31(10): 909-17.

Svehla, M., Morberg, P., Bruce, W., Zicat, B., and Walsh, W. R. (2002). The effect of substrate roughness and hydroxyapatite coating thickness on implant shear strength. *J Arthroplasty* 17, 304-11.

Swindle, M. M., Makin, A., Herron, A. J., Clubb, F. J., Jr., and Frazier, K. S. (2012). Swine as models in biomedical research and toxicology testing. *Vet Pathol* 49, 344-56.

Tack, K. J., and Sabath, L. D. (1985). Increased minimum inhibitory concentrations with anaerobiasis for tobramycin, gentamicin, and amikacin, compared to latamoxef, piperacillin, chloramphenicol, and clindamycin. *Chemotherapy* 31, 204-10.

Tamada, Y., and Ikada, Y. (1993). Effect of Preadsorbed Proteins in Cell Adhesion to Polymer Surfaces. *J Colloid and Interface Science* 155, 334-339.

Tan, G., Tan, Y., Ni, G., Lan, G., Zhou, L., Yu, P., Liao, J., Zhang, Y., Yin, Z., Wang, H., and Ning, C. (2014). Controlled oxidative nanopatterning of microrough titanium surfaces for improving osteogenic activity *J Mater Sci Mater Med* 25, 1875-1884.

Teare, D. O. H., Emmison, N., Ton-That, C., and Bradley, R. H. (2000). Cellular Attachment to Ultraviolet Ozone Modified Polystyrene Surfaces. *Langmuir* 16, 2818-2824.

Teng, F. Y., Ko, C. L., Kuo, H. N., Hu, J. J., Lin, J. H., Lou, C. W., Hung, C. C., Wang, Y. L., Cheng, C. Y., and Chen, W. C. (2012). A comparison of epithelial cells, fibroblasts, and osteoblasts in dental implant titanium topographies. *Bioinorg Chem Appl* 2012, 687291.

Thanni, L. O., and Tade, A. O. (2007). Extremity amputation in Nigeria--a review of indications and mortality. *Surgeon* 5, 213-7.

Tillander, J., Hagberg, K., Hagberg, L., and Brånemark, R. (2010). Osseointegrated titanium implants for limb prostheses attachments: infectious complications. *Clin Orthop Relat Res* 468, 2781-8.

Trampuz, A., and Widmer, A. F. (2006). Infections associated with orthopedic implants. *Curr Opin Infect Dis* 19, 349-56.

Trop, M., Novak, M., Rodl, S., Hellbom, B., Kroell, W., and Goessler, W. (2006). Silver-coated dressing acticoat caused raised liver enzymes and argyria-like symptoms in burn patient. *J Trauma* 60, 648-52.

Tsimbouri, P., Gadegaard, N., Burgess, K,, White, K., Reynolds, P., Herzyk, P., Oreffo, R., and Dalby, M.J. (2014). Nanotopographical Effects on Mesenchymal Stem Cell Morphology and Phenotype. *J Cellular Biochem* 115, 380-390.

Tuomanen, E., Cozens, R., Tosch, W., Zak, O., and Tomasz, A. (1986). The rate of killing of Escherichia coli by beta-lactam antibiotics is strictly proportional to the rate of bacterial growth. *J Gen Microbiol* 132, 1297-304.

Väänänen, H. K., Zhao, H., Mulari, M., and Halleen, J. M. (2000). The cell biology of osteoclast function. *J Cell Sci* 113 (Pt 3), 377-81.

Vamos, E. P., Bottle, A., Edmonds, M. E., Valabhji, J., Majeed, A., and Millett, C. (2010). Changes in the incidence of lower extremity amputations in individuals with and without diabetes in England between 2004 and 2008. *Diabetes Care* 33, 2592-7.

van Wachem, P. B., Hogt, A. H., Beugeling, T., Feijen, J., Bantjes, A., Detmers, J. P., and van Aken, W. G. (1987). Adhesion of cultured human endothelial cells onto methacrylate polymers with varying surface wettability and charge. *Biomaterials* 8, 323-8.

Verkkala, K., Eklund, A., Ojajarvi, J., Tiittanen, L., Hoborn, J., and Makela, P. (1998). The conventionally ventilated operating theatre and air contamination control during cardiac surgery--bacteriological and particulate matter control garment options for low level contamination. *Eur J Cardiothorac Surg* 14, 206-10.

Vogely, H. C., Oosterbos, C. J., Puts, E. W., Nijhof, M. W., Nikkels, P. G., Fleer, A., Tonino, A. J., Dhert, W. J., and Verbout, A. J. (2000). Effects of hydrosyapatite coating on Ti-6A1-4V implant-site infection in a rabbit tibial model. *J Orthop Res* 18, 485-93.

von Recum, A. F. (1984). Applications and failure modes of percutaneous devices: a review. *J Biomed Mater Res* 18, 323-36.

Vydyanath, A., Gurnett, C. A., Marston, S., and Luther, P. K. (2012). Axial distribution of myosin binding protein-C is unaffected by mutations in human cardiac and skeletal muscle. *J Muscle Res Cell Motil* 33, 61-74.

Wafa, H., Grimer, R. J., Reddy, K., Jeys, L., Abudu, A., Carter, S. R., and Tillman, R. M. (2015). Retrospective evaluation of the incidence of early periprosthetic infection with silver-treated endoprostheses in high-risk patients: case-control study. *Bone Joint J* 97-B, 252-7.

Walker, J. (2010). Preventing infections caused by the pinning of broken bones. Arthritis Research UK http://www.arthritisresearchuk.org/research/grant-tracker-items/2010/preventing-infections-caused-by-the-pinning-of-broken-bones.aspx.

Walters, M. C., 3rd, Roe, F., Bugnicourt, A., Franklin, M. J., and Stewart, P. S. (2003). Contributions of antibiotic penetration, oxygen limitation, and low metabolic activity to tolerance of Pseudomonas aeruginosa biofilms to ciprofloxacin and tobramycin. *Antimicrob Agents Chemother* 47, 317-23.

Wang, C. C., Hsu, Y. C., Su, F. C., Lu, S. C., and Lee, T. M. (2009). Effects of passivation treatments on titanium alloy with nanometric scale roughness and induced changes in fibroblast initial adhesion evaluated by a cytodetacher. *J Biomed Mater Res A* 88, 370-83.

Wang, R., Neoh, K. G., Kang, E. T., Tambyah, P. A., and Chiong, E. (2015). Antifouling coating with controllable and sustained silver release for long-term inhibition of infection and encrustation in urinary catheters. *J Biomed Mater Res B Appl Biomater* 103, 519-28.

Wang, R. C., Hsieh, M. C., and Lee, T. M. (2011). Effects of nanometric roughness on surface properties and fibroblast's initial cytocompatibilities of Ti6Al4V. *Biointerphases* 6, 87.

Wang, S., and Jain, H. (2010). High Surface Area Nanomacroporous Bioactive Glass Scaffold for Hard Tissue Engineering. *J Am Ceram Soc* 93, 3002-3005.

Wassall, M. A., Santin, M., Isalberti, C., Cannas, M., and Denyer, S. P. (1997). Adhesion of bacteria to stainless steel and silver-coated orthopedic external fixation pins. *J Biomed Mater Res* 36, 325-30.

Wei, Q., Tarighi, S., Dotsch, A., Haussler, S., Musken, M., Wright, V. J., Camara, M., Williams, P., Haenen, S., Boerjan, B., Bogaerts, A., Vierstraete, E., Verleyen, P., Schoofs, L., Willaert, R., De Groote, V. N., Michiels, J., Vercammen, K., Crabbe, A., and Cornelis, P. (2011). Phenotypic and genome-wide analysis of an antibiotic-resistant small colony variant (SCV) of Pseudomonas aeruginosa. *PLoS One* 6, e29276.

Wenzel, R. N. (1936). Resistance of solid surfaces to wetting by water. *Industrial and Engineering Chemistry* 28, 988-994.

Wilke, A., Orth, J., Kraft, M., and Griss, P. (1993). Bone ingrowth behaviour of hydroxyapatite- coated, polyethylene-intruded and uncoated, sandblasted pure titanium implants in an in- fected implantation site: an experimental study in miniature pigs. *J Mater Sci: Mater Med* 4.

Wilson, C. J., Clegg, R. E., Leavesley, D. I., and Pearcy, M. J. (2005). Mediation of biomaterial-cell interactions by adsorbed proteins: a review. *Tissue Eng* 11, 1-18.

Winter, G. D. (1974). Transcutaneous implants: reactions of the skin-implant interface. *J Biomed Mater Res* 8, 99-113.

Woods, D. E. (1987). Role of fibronectin in the pathogenesis of gram-negative bacillary pneumonia. *Rev Infect Dis* 9 Suppl 4, S386-90.

Woods, D. E., Bass, J. A., Johanson, W. G., Jr., and Straus, D. C. (1980). Role of adherence in the pathogenesis of Pseudomonas aeruginosa lung infection in cystic fibrosis patients. *Infect Immun* 30, 694-9.

Woods, D. E., Straus, D. C., Johanson, W. G., Jr., and Bass, J. A. (1981). Role of fibronectin in the prevention of adherence of Pseudomonas aeruginosa to buccal cells. *J Infect Dis* 143, 784-90.

Woolf, N. (1998). "Pathology: Basic and Systemic," Saunders, London.

Wright, J. B., Lam, K., and Burrell, R. E. (1998). Wound management in an era of increasing bacterial antibiotic resistance: a role for topical silver treatment. *Am J Infect Control* 26, 572-7.

Wu, M., He, J., Ren, X., Cai, W. S., Fang, Y. C., and Feng, X. Z. (2014). Development of functional biointerfaces by surface modification of polydimethylsiloxane with bioactive chlorogenic acid. *Colloids Surf B Biointerfaces* 116, 700-6.

Xue, W., Tao, S., Liu, X., Zheng, X., and Ding, C. (2004). In vivo evaluation of plasma sprayed hydroxyapatite coatings having different crystallinity. *Biomaterials* 25, 415-21.

Yannas, I. V. (1992). Tissue regeneration by use of collagen-glycosaminoglycan copolymers. *Clin Mater* 9, 179-87.

Yinusa, W., and Ugbeye, M. E. (2003). Problems of amputation surgery in a developing country. *Int Orthop* 27, 121-4.

Yoshimura, T., Imai, H., Threrujirapapong. T., and Kondoh, K. (2009). Cost Effective Pure Titanium with High Mechanical Response by Oxide Dispersion Strengthening. *Materials Transactions* 50 (12): 2751-2756.

Zegers, M. M., Forget, M. A., Chernoff, J., Mostov, K. E., ter Beest, M. B., and Hansen, S. H. (2003). Pak1 and PIX regulate contact inhibition during epithelial wound healing. *EMBO J* 22, 4155-65.

Zhang, L., Fritsch, M., Hammond, L., Landreville, R., Slatculescu, C., Colavita, A., and Mah, T. F. (2013). Identification of genes involved in Pseudomonas aeruginosa biofilm-specific resistance to antibiotics. *PLoS One* 8, e61625.

Zhang, L., Hinz, A. J., Nadeau, J. P., and Mah, T. F. (2011). Pseudomonas aeruginosa tssC1 links type VI secretion and biofilm-specific antibiotic resistance. *J Bacteriol* 193, 5510-3.

Zhang, Q., Chen, J., Feng, J., Cao, Y., Deng, C., and Zhang, X. (2003). Dissolution and mineralization behaviors of HA coatings. *Biomaterials* 24, 4741-8.

Zhao, L., Chu, P. K., Zhang, Y., and Wu, Z. (2009). Antibacterial coatings on titanium implants. *J Biomed Mater Res B Appl Biomater* 91, 470-80.

Zhou, F., Li, D., Wu, Z., Song, B., Yuan, L., and Chen, H. (2012). Enhancing specific binding of L929 fibroblasts: effects of multi-scale topography of GRGDY peptide modified surfaces. *Macromol Biosci* 12, 1391-400.

Ziegler-Graham, K., MacKenzie, E. J., Ephraim, P. L., Travison, T. G., and Brookmeyer, R. (2008). Estimating the prevalence of limb loss in the United States: 2005 to 2050. *Arch Phys Med Rehabil* 89, 422-9.

Zink, C., Hall, H., Brunette, D. M., and Spencer, N. D. (2012). Orthogonal nanometer-micrometer roughness gradients probe morphological influences on cell behavior. *Biomaterials* 33, 8055-61.

Zitzmann, N. U., Abrahamsson, I., Berglundh, T., and Lindhe, J. (2002). Soft tissue reactions to plaque formation at implant abutments with different surface topography. An experimental study in dogs. *J Clin Periodontol* 29, 456-61.

Zografos, G. C., Martis, K., and Morris, D. L. (1992). Laser Doppler flowmetry in evaluation of cutaneous wound blood flow using various suturing techniques. *Ann Surg* 215, 266-8.